Accounting for Viscous Fingering in Relative Permeability Estimation of Special Core Analysis Measurements

By:

BRUNO MIGUEL FERREIRA PEREIRA
BSc., MSc.

Submitted for the Degree of Doctor of Philosophy
In Petroleum Engineering

Department of Petroleum Engineering
Heriot-Watt University
Edinburgh, UK

2017

Abstract

Relative permeability (k_r) is a critical input data for any calculation involving multiphase flow in petroleum reservoirs. Normally, kr curves are obtained by performing coreflood experiments as part of SCAL measurements or EOR studies. The results of the experiments are then used to obtain kr values often by either analytical models (e.g. JBN) or history matching techniques. Most of these models are based on the Buckley-Leverett displacement theory and are not applicable to unstable displacements. Therefore, using these models to describe a core flood experiment involving viscous fingering will result in potentially large errors in the estimation of kr curves.

This study focused on the estimation of relative permeability curves for unstable experiments, more specifically in unfavourable mobility corefloods with a tendency to develop viscous fingering. Refined 2D coreflood simulations were used to evaluate the effect of viscous fingering in kr estimation methods. The simulations were performed as immiscible corefloods in homogeneous cores using a Black-oil model in a commercial simulator.

The first part of this study, describes the methodology used to generate viscous fingering in numerical corefloods. Instability triggering methods were used with high resolution simulation to generate the viscous fingering. This methodology was then used to generate different numerical experiments with viscous fingering formation.

In the second part, the currently widely used oil industry approaches for relative permeability estimation (1D history matching and JBN method) were evaluated for cases with unfavourable mobility. The errors were quantified in order to understand the effect of fingering on these methods and the amount of error one can incur when using them for these cases.

In the latter part of the thesis, two novel methods are proposed for estimating relative permeabilities for unfavourable mobility coreflood experiments, namely viscous fingering. These methods are based on the proposed model called ‘stable equivalent model’. This model proposes a correction to the velocity of the fluids in a coreflood affected by viscous fingering, allowing to account for viscous fingering in relative permeability estimation. The model is used to modify the JBN method and 1D history matching, allowing these methods to tackle viscous instability. The integrity of these techniques was validated against published experimental data and numerical data.

Dedication

I dedicate this thesis to Science and my family; without both I wouldn’t be who I am today.

Acknowledgments

I would like to express the earnest gratitude and respect to my dear supervisor Professor Mehran Sohrabi who provided an outstanding technical guidance and moral support, helping me focus on the vital parts of this work. My second supervisor Dr. Hamid Shahverdi for his incredible support and guidance, pointing me in the right direction, especially at the beginning of my thesis. My special thanks go to Professor Dabir Tehrani for his prominent practical comments and constructive assistance throughout this project and for his outstanding scientific mind who serves as inspiration for the younger generations.

Much appreciation to GALP Energia for the financial support, the opportunity and for inviting me to their open days allowing me to contact with real petroleum engineering companies and present my work.

Special thanks to Dr. Amir Jahanbakhsh for supporting me in numerous occasions with vital technical consultation and theoretical knowledge. To Dr. Mojtaba Seyyedi, my 'office mate', for the many insightful conversations. To Ms. Juliana Facanha and Dr. Heron Gachuz for the enjoyable and memorable time we had in Edinburgh. To Mr. Duarte Silva and Dr. Luis Pereira, both fellow Portuguese colleagues, with whom I shared great moments.

I would like to also thanks my dear colleges on the WAG group, Dr. Amir Jahanbakhsh, Dr. Pedram Mahzari, Dr. Omid Shahrokhi, Dr. Mobeen Fatemi, Ms. Shokoufeh Aghabozorgi, Mr. Bashir Alkhazmi and Mr. Hassan Alzayer.

Last but not least, I would like to thank my dear boyfriend for the support during all my thesis and patience which was vital for the completion of my work. Also would like to thanks my parents for providing me with the necessary conditions to pursue my dreams, working hard so that I would have the necessary financial support.

ACADEMIC REGISTRY
Research Thesis Submission

Name*:*	Bruno Miguel Ferreira Pereira		
School/PGI:	The School of Energy, Geoscience, Infrastructure and Society (EGIS)		
Version: *(i.e. First, Resubmission, Final)*	Final	Degree Sought (Award **and** Subject area)	PhD in Petroleum Engineering

Declaration

In accordance with the appropriate regulations I hereby submit my thesis and I declare that:

1) the thesis embodies the results of my own work and has been composed by myself
2) where appropriate, I have made acknowledgement of the work of others and have made reference to work carried out in collaboration with other persons
3) the thesis is the correct version of the thesis for submission and is the same version as any electronic versions submitted*.
4) my thesis for the award referred to, deposited in the Heriot-Watt University Library, should be made available for loan or photocopying and be available via the Institutional Repository, subject to such conditions as the Librarian may require
5) I understand that as a student of the University I am required to abide by the Regulations of the University and to conform to its discipline.

* *Please note that it is the responsibility of the candidate to ensure that the correct version of the thesis is submitted.*

Signature of Candidate*:*		Date:	

Submission

Submitted By *(name in capitals):*	
Signature of Individual Submitting:	
Date Submitted:	

For Completion in the Student Service Centre (SSC)

Received in the SSC by *(name in capitals):*			
3) Method of Submission *(Handed in to SSC; posted through internal/external mail):*			
*4) E-thesis Submitted (**mandatory for final theses)***			
Signature:		Date:	

Table of Contents

Publications

- Pereira, B.M.F., Shahverdi, H. & Sohrabi, M., 2014. Refinement of Relative Permeability Measurements by Accounting for Viscous Fingering in Coreflood Experiments. SPE Annual Technical Conference and Exhibition Proceedings, SPE-170717-MS.

- Pereira, B.M.F., Sohrabi, M. & Shahverdi, H., 2014. IMPACT OF VISCOUS FINGERING ON OIL PRODUCTION AND RELATIVE PERMEABILITY MEASUREMENTS. Rio Oil & Gas Expo and Conference 2014 Proceedings, pp.1–10.

Chapter 1: Introduction

1.1 Relative Permeability Estimation

In an oil reservoir it is possible to have more than one fluid moving simultaneously. For example, when injecting water into an oil filled reservoir, both water and oil move together. It is then impossible to describe their movement with a single absolute permeability, instead, the relative permeability is used. The relative permeability is one of the most important parameters in the oil industry. Its precise estimation is very important for the analysis of the nature of flow inside the reservoir and a considerable amount of money is used in order to correctly estimate its value.

The standard approach to estimate the relative permeability is to do core analysis. Several pieces of rock (cores) are extracted from the reservoir and brought to a laboratory. The relative permeability for each fluid can then be determined by either "steady-state" or "unsteady-state" methods (Honarpour et al. 1986).

1.1.1 Steady-State Methods

Steady state methods are reported (Mohammed A. Mian 1992; Abaci et al. 1992) as being the most reliable way to obtain the relative permeability of a fluid system in porous media and may be used in heterogeneous cores or unstable flow. For imbibition relative permeability measurement, the test starts with the core initially saturated with irreducible wetting phase saturation and a non-wetting phase saturation. Then both phases are co-injected in the inlet face of the core at a fixed rate until steady-state is achieved (Peters 2012). The steady-state is reached when the differential pressure across the core no longer changes with time and the ratio of the injected fluids and the ratio of the production fluids are the same. The relative permeability may then be calculated using the Darcy's law of flow. This methodology is performed for several ratios of injected fluids. Each ratio will correspond to a different saturation and for each saturation a relative permeability value will be calculated.

Nevertheless, steady-state method has a big disadvantage: it is very time consuming (Virnovsky et al. 1995; Lucia 2007; Dandekar 2013). For each ratio of injection only 1 point of the relative permeability is calculated, meaning that in order to have the full curve

it is necessary to vary this ratio many times until several values of the relative permeability can be used to plot the correct curvature of the parameter. Also, for each ratio of injection the equilibrium must be reached; when the oil is very viscous this may imply very long amounts of time. For these reasons, a steady-state estimation may take months to perform, being a very expensive procedure. In an industry environment where, sometimes, many core samples are needed in order to characterize a section of the reservoir, it becomes inpractical to use this method of relative permeability estimation. Thus, these methods are used less commonly than unsteady-state methods (Chen & Ewing 2002).

1.1.2 Unsteady-State Methods

The unsteady-state method for relative permeability estimation is much faster than the steady-state. The method consists in the injection of one fluid (e.g. water) into a porous media with a known quantity of another fluid (e.g. oil filled core). During this injection the production data (amount of fluids leaving the core) along with other parameters (saturation profiles, differential pressure, etc) may be obtained in order to mathematically estimate the relative permeability curves. The theory developed by Buckley & Leverett (1942) and extended by (Welge 1952) is generally used for the measurement of the relative permeability under unsteady-state conditions (Honarpour et al. 1986).

There are several methods to estimate the relative permeability from unsteady-state experiments. The most common methods are Johnson, Bossler and Naumann's method (known as JBN) and 1D history matching. The JBN method got its name from its authors (Johnson et al. 1959) and was developed with a modification to the Welge 1952 equations. The exact equations of this method are going to be throughly analysed further in this work. There is also a graphical calculation methodology for this method, created by Jones & Roszelle 1978. The usefulness of the graphical JBN is the minimization of error from experimental artifacts, for example, the smootheness of the production or differential pressure curves. JBN method is very sensitive to varition of values of pressure and in experimental environment it is possible to have some values of pressure that are above or below the general trend, resulting in error. The great disavantage of JBN is that the method cannot handle, in theory, cases where gravity an important effect in the fluid flow. Also, since it is based on Welge 1952 equations, it cannot tackle any form of deviation to flow stability. Another basic assumption of this method is that the capillary pressure and hence the capillary pressure end effects can be ignored. This is realized in practice by

conducting experiments at sufficiently high flow rates. However, for many field scale calculations the flow rates are such that the inclusion of the capillary pressure is necessary (Firoozabadi & Aziz 1991). Nevertheless, JBN is a very fast and simple method that can be performed easily using a spreadsheet. This fact made JBN one of the most widely used methods in relative permeability estimation.

Another method for relative permeability estimation with unsteady-state experiments is the 1D history matching (1D HM) method. This method uses coreflood simulators capable of capturing the dynamics of the flow inside the core by inputting the parameters (like core and fluid data) of the experiment. Then, relative permeability curves are generated using a standard correlation like Corey (Brooks & Corey 1966) and used in the simulation. Each relative permeability will result in production and differential pressure. The result of the estimation is found when the error between the production and the differential presure of the simulation and the experiment is smaller than the minimum acceptable error, corresponding to a certain set of relative permeability curves. The advantage of this method in comparison with JBN, is that 1D HM is capable of handling capillary pressure in the estimation. The disadvantage is that 1D HM is an implicit method, while JBN is an explicit method, meaning that it is possible to run easily into non-uniqueness problems in the 1D HM. The non-uniqueness of the relative permeability is many times associated with the viscosity ratio of capillary number (Dou & Zhou 2013; Tsakiroglou et al. 2007).

Although JBN and 1D HM are simple and, normally, fast methods to use for Special Core Analysis (SCAL), they are based on stable flow models. This means that neither of the 2 methods can correctly handle instability of any type, including gravity segregation, viscous fingering or heterogeneity-driven flow. Nevertheless, that (very important) fact is ignored by many laboratories, the reason for this is the considerably higher difficulty and time needed when the estimation is performed with steady-state methods or advanced simulation.

It is possible to account for certain instability effects in a multidimensional history matching (2D or 3D) if the correct set and experiment data is gathered (e.g. proper saturation profile data matching, using CT scan for the data gathering). Nevertheless, it is essential to have an extra experimental parameter measured during coreflood injection, the saturation profile along the core at different times of injection. By matching both the production and differential pressure with the saturation profiles at any point in the injection time, the flow is guaranteed to be following the instability pattern developed in the experiment, leading to a correct relative permeability estimation. There are in

literature some examples of this procedure (Brock & Orr Jr 1991; Peters 1994), but its use is very rare and normally only used in scientific investigation mainly because it involves specific experimental data (core imaging, CT scans, etc) and case specific simulation setup, which results in a very time consuming process to be applied to industry.

1.2 Flow Stability

The distinction between different states of fluid flow may be analysed by how the flow reacts to a disturbance in the initial state (Chandrasekhar 1981). These disturbances will relate to the initial properties of the system, such as velocity, pressure and density. James Clerk Maxwell described the qualitative concept of stability as (Drazin & Crepeau 2003): "When an infinitely small variation of the present state will alter only by an infinitely small quantity the state at some future time, the condition of the system, whether at rest or in motion, is said to be stable but when an infinitely small variation in the present state may bring about a finite difference in the state of the system in a finite time, the system is said to be unstable."

This means that for a stable flow, an infinitely small variation or perturbation, will not result in a significant effect on the initial state of the system and it will eventually wear-off with time. In an unstable flow, any perturbations will affect the state of the system, causing that disturbance to grow larger with time, in a way that it progressively departs from the initial state and never returns to it.

Perturbation in the flow may be created from a number of sources. In porous media, as reservoirs, there are 3 main types of instability precursors, gravity, heterogeneity and viscous differences.

1.2.1 Gravity Segregation

Gravity influences every aspect of fluid flow in planet Earth, it also has an important effect in the movement of fluids. When two or more different fluids are in contact with each other, gravity will have a stronger effect on the fluid with higher density. If two fluids are moving in a porous media (through its interstitial pores), the fluid with higher density will be pushed (gradually) downwards. If the diameter and length of the medium are big enough, the fluid with higher density will flow in the lower part of the medium, while the lightest will travel in the top of the medium. This effect is called 'gravity segregation' and it happens frequently in petroleum engineering (Wyckoff et al. 1932; Funk 1956). Gravity segregation is the cause poor sweep efficiency and it is well known

in WAG (water and gas) injections because the gas has the tendency to go through the top of the reservoir while the water goes through the bottom, creating big unswept regions (Speight 2013; Ho & Webb 2006), Figure 1-1. In Special Core Analysis (SCAL), gravity segregation results in early breakthrough of the injected fluids and less oil recovery (Spivak 1974; Moortgat 2016). This, obviously, has an important influence in the estimation parameters, like the relative permeability, and analysis of mechanism of flow in SCAL.

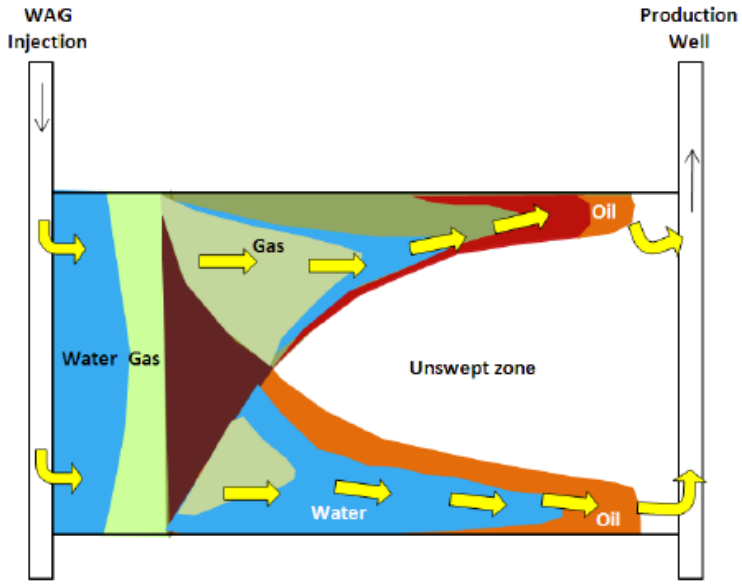

Figure 1-1: Gravity Segregation in WAG (water and gas) injection (adapted from Shahverdi 2012).

1.2.2 Heterogeneity

A medium is called hetegeneous when its absolute permeability is not approximately constant through whole volume. A simple example is the geological fractures that are very common in reservoirs, especially in carbonate rocks (Palaz & Marfurt 1997; Dominguez & V 1992), with fractures where huge gaps in the rock formation exist and obviously, this facilitates the movement of fluids, resulting in a much higher absolute permeability than in the rest of the porous medium. Then high permeability parts make the fluids move preferentially through those spaces, resulting in poor sweep efficiency and less oil recovery. Figure 1-2 shows an example of heterogeneity preferential flow paths, in this case flow through layers (layer flow).

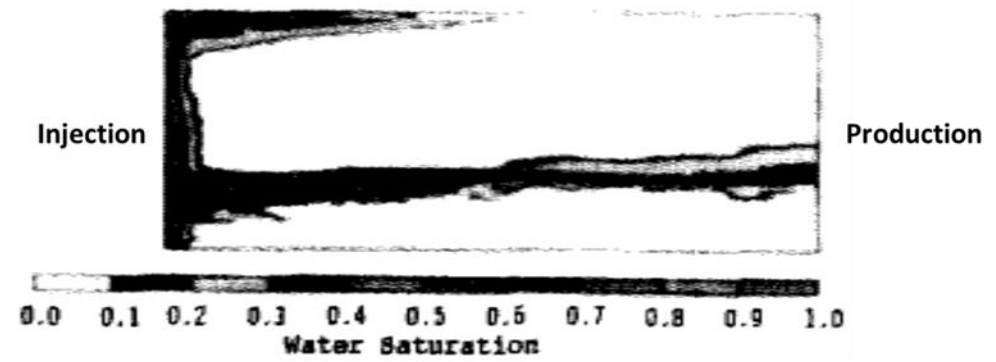

Figure 1-2: Example of heterogeneity influence in fluid flow (layer flow). White represents unsweep areas of the core, while the injection fluid black coloured. (from Peters 1994)

The degree of heterogeneity of a porous medium may be evaluated using the Dykstra Parsons Coefficient. The Dykstra Parsons Coefficient evaluates the heterogeneity of a core by looking at the Gaussian permeability distribution; the bigger the value of the coefficient the more heterogeneous a core is (Willhite 1986). It is very important to have information about the degree of heterogeneity in a core or reservoir since it can seriously influence the fluid flow.

1.2.3 Viscous Fingering

Viscous fingering or viscous instability may occur in displacement processes when the displacing fluid has a higher mobility than the displaced fluid (Stalkup et al. 1990). The mobility ratio is defined as the ratio of the endpoint mobility of the displacing fluid over the end point mobility of the displaced fluid as in the following equation:

$$M = \frac{k_{rd}^0/\mu_d}{k_{ro}^0/\mu_o} \quad \text{.....1-1}$$

Where k_{rd}^0 is the relative permeability of the displacing fluid, k_{ro}^0 is the relative permeability of the oil, μ_d is the viscosity of the displacing fluid and μ_o is the viscosity of the oil. At an unfavorable mobility ratio, i.e., M > 1, the displacement is considered to be potentially unstable and the displacing fluid (e.g., gas) may finger through the displaced fluid (e.g., oil). Viscous fingering can have a dramatic effect on the sweep efficiency of a displacement process. Viscous unstable flows are often associated with early breakthrough of the displacing fluid and less cumulative displaced fluid recovery. Figure 1-3 shows an example of viscous fingering generated using simulation.

For more than half a century handling of the fluid flow with viscous fingering has challenged the oil industry, resulting in a large number of studies investigating the factors that influence the development of viscous fingers in experimental and theoretical scenarios.

Figure 1-3: Viscous fingering pattern generated using simulation. The colour pattern is distributed from black for 0% injection fluid in place and white for 100%, resulting in different shades of grey for the various saturations.

1.3 Review on Viscous Fingering Modelling and Simulation

1.3.1 Review on Stability Indicators

1.3.1.1 Mobility Ratio

When talking about viscous fingering, mobility ratio is probably the biggest indicator of a flow stability, but there have been many definitions for this parameter. Generally, 3 different mobility ratio definitions have been reported (Craig 1993; Dake 1978; Willhite 1986). All definitions are similar in nature, but use different relative permeability values. The first, and probably most common, is the endpoint mobility ratio, presented previously in equation 1-1. In this definition, the endpoint relative permeability value (for a water injection, the water relative permeability is at the residual oil saturation and the oil at irreducible water saturation) of each fluid is used to calculate the mobility ratio between them. However, this definition raises pertinent questions relative to the saturation at which both fluids are in contact. For example at the displacement front (where the most advanced parts of the displacing fluid and the unswept section are in contact) the most probable scenario is that in the displacing fluid side, the saturation of oil is not equal to the residual oil saturation. The second definition, was proposed by Dake (1978) who addresses this by defining a shock mobility ratio, *Ms*, which includes both the water and oil mobility at the front of the displacement:

$$M_s = \frac{{k_{rdf}}/{\mu_d} + {k_{rof}}/{\mu_o}}{{k_{ro}}/{\mu_o}} \quad \text{.....1-2}$$

Where k_{rdf} is the relative permeability of the displacing fluid at the shock front saturation, k_{rof} is the relative permeability of the oil at the shock front saturation, μ_d is the viscosity of the displacing fluid and μ_o is the viscosity of the oil.

Craig (1993) proposed the third mobility-ratio definition, $M_{<S>}$. This definition includes water mobility at average water saturation behind the shock front:

$$M_{\langle s\rangle} = \frac{k_{rda}/\mu_d}{k_{ro}/\mu_o} \qquad \text{.....1-3}$$

The k_{rda} is the displacing fluid relative permeability at the average water saturation behind the shock front, which can be determined from fraction-flow analysis. Kumar et al. (2008) has analysed the three mobility ratio definitions and have argued that the first definition used the endpoint relative permeability assuming that the oil is at residual conditions just before the shock front, which is unreal for high viscosity ratio injections. On the other hand, both the second and third definitions take into account the proper saturation behind the front. Kumar et al. concluded that Dake's definition is more in line with high mobility ratio flooding, since, different to Craig's definition, it takes into account both the oil and displacing fluid saturation behind the shock front.

1.3.1.2 Stability Numbers

Early studies demonstrated that the stability problem may depend on various parameters like mobility ratio, displacement velocity, system permeability and wettability (Engelberts & Klinkenberg 1951; van Meurs & van der Poel 1958; Saffman & Taylor 1958; Chuoke et al. 1959; Scheidegger 1960; Scheidegger & Limited 1960; Outmans 1962; Rachford 1964; Hagoort 1974). However, none of these studies combine all the variable into one parameter that can serve as a measure of prediction of the flow stability during an injection into a porous medium. The first authors to derive a parameter with a critical value for stability were Peters & Flock (1979). They suggested a stability number, I_{sc}, and that flow is stable if the following condition is met:

$$I_{sc} = \frac{(M-1)(v-v_c)\mu_w D^2}{C^*\sigma k_{wor}} < 13.56 \qquad \text{.....1-4}$$

Where M is the endpoint mobility ratio, v is the superficial velocity, v_c is the characteristic velocity, μ_w is the water viscosity, D is the core diameter, C^* is the wettability number, σ is the interfacial tension and k_{wor} is the permeability to water at residual oil saturation. The work of Peters & Flock (1979) was also able to show that the dimensions were the most critical parameters, since they are raised to the second power, whereas all others are raised to the first power. Nevertheless, the work of Peters & Flock (1979) failed to take into account how the variations in rock and fluid properties would affect the stability boundary. This was because they based their derivation on velocity potential. Bentsen (1985) corrected this by basing his derivation in the force potential, correctly taking into account the effect of the rock and fluid properties on the stability. This version of the stability number was, however, inappropriately analysed (Coskuner & Bentsen 1985). This problem was then solved in Sarma & Bentsen (1987), resulting in the stability number, I_{sr}, as following:

$$I_{sr} = \frac{\mu_d v\left(M - 1 - N_g\right)}{k_{dor}\sigma_e} \frac{M^{5/3} + 1}{(M+1)\left(M^{1/3} + 1\right)^2} \frac{4h^2b^2}{h^2 + b^2} \leq \pi^2 \quad \text{.....1-5}$$

$$\sigma_e = \frac{A_c\phi(1 - S_{wi} - S_{or})}{2/\bar{r}_m} \quad \text{.....1-6}$$

$$N_g = \frac{\Delta\rho\ g\ k_{dor}\ cos\ \alpha}{\mu_d v} \quad \text{.....1-7}$$

Where μ_d is the displacing fluid viscosity, v the superficial velocity, M the mobility ratio, N_g the gravitational number, k_{dor} the relative permeability of the displacing fluid at residual oil saturation, σ_e the pseudo interfacial tension, h the thickness of the porous medium, b the width of porous medium, A_c the area under capillary pressure vs saturation curve, S_{wi} the initial water saturation, S_{or} the residual oil saturation, $2/\bar{r}_m$ the average macroscopic mean radius, Δ_ρ the difference of densities between oil and the displacing fluid, g the gravity acceleration and α the angle core makes with vertical. The value of $2/\bar{r}_m$ is 1 by definition (Sarma & Bentsen 1987).

In addition to proposing a stability number, Sarma & Bentsen (1987) showed the close relationship between the stability (or instability) number with the breakthrough recovery, Figure 1-4.

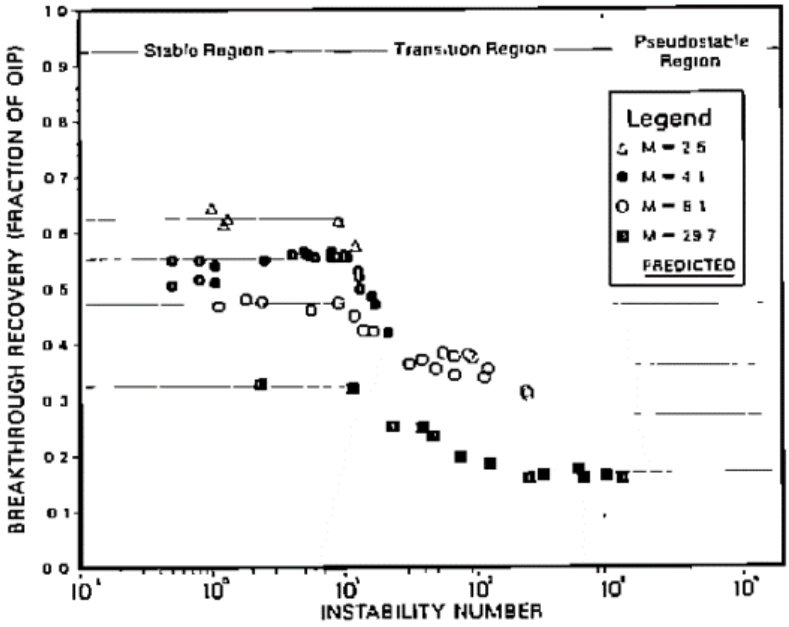

Figure 1-4: Breakthrough recovery as a function of the instability number (Sarma & Bentsen 1987, bad quality due to the state of the original paper).

The breakthrough recovery is closely related to the flow stability, since any deviation to stable flow results in early breakthrough and less breakthrough recovery of oil. Sarma & Bentsen (1987) experimental results showed that it is possible to separate the nature of flow stability into 3 main regions: stable region, transient region and pseudostable region. They were also successful into showing that the stability thresholder is around their predicted value of $I_{sr} = \pi^2$.

Sarma & Bentsen (1987) work provided a very valuable tool to identify the stability of a coreflood injection using a simple equation.

1.3.2 Review and Modelling/Simulation

1.3.2.1 Flow Visualization

There are several studies published in literature showing experimental flow visualization of viscous fingering in unfavourable mobility experiments. These types of studies are important to show the mechanisms that influence the pattern of formation of viscous fingering.

The first scientific investigation and experimental observation of the fingering phenomenon was in the work of Hill (1952). The author studied the displacement of sugar by water in columns of granular bone charcoal.

Hele-Shaw (1898) became famous for introducing a simple system to study the flow of water around various objects for low Reynold´s number (Vicsek 1992). Hele-Shaw

designed a cell consisting of 2 transparent plates of linear size (around 30cm) separated by a small distance (around 1 mm). The viscous fluids were then placed between the 2 plates and pressure was applied either at one of the edges (longitudinal version, Figure 1-5) or at the centre of the upper plate (radial version, Figure 1-6).

Figure 1-5: Viscous fingering formation in longitudinal Hele-Shaw cell (Xu 1997).

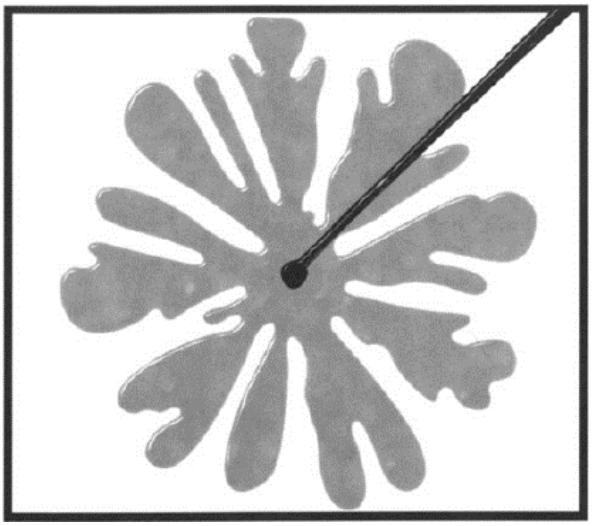

Figure 1-6: Viscous fingering formation in radial Hele-Shaw cell (Xu 1997).

The viscous fingering may also be driven by surface tension at the interface and by differences in the viscosity of 2 immiscible fluids. These cases were studied by Chuoke et al. (1959) and Saffman & Taylor (1958). These investigators performed linear analysis for a flat interface. The mechanism became known as the 'Saffman-Taylor instability', although it should be called 'Chuoke-Saffman-Taylor instability' (Xu 1997). Saffman & Taylor (1958) investigated the viscous fingering using Hele-Shaw cells to make systematic observations.

Several years after Saffman-Taylor the viscous fingering phenomenon visualization and qualitative analysis continued to be of interest, especially in the oil industry. Examples of this are the works of Brock & Orr Jr (1991), Pavone (1992), Cuthiell et al. (2006) and Malhotra et al. (2015).

Brock & Orr Jr (1991) have done an extensive study of viscous fingering in homogeneous and heterogeneous core floods. They have also compared the experimental patterns with their own simulations. They showed that in homogeneous media, viscous fingering grows by spreading and splitting at their tips. Also, fingers shield nearby fingers from further growth when they outpace them and some are eliminated by coalescence. This resulted, in rectilinear flow, in a decline of the number of fingers as the flow progressed.

Pavone (1992) used a molding technique to observe and measure 2-phase viscous fingering. The author concluded that viscous fingering patterns have a great dependence on the flow rate and the viscosity ratio. Likewise, he showed that the fingering patterns in coreflooding are different from those seen in Hele-Shaw cells. In coreflooding, the fingering was always composed of a stable and a fingering zone.

Cuthiell et al. (2006) have performed unstable experiments and matched the saturation patterns using simulation. They have showed that it possible to correctly simulate viscous fingering patterns with the use of a permeability distribution triggering method, Figure 1-7.

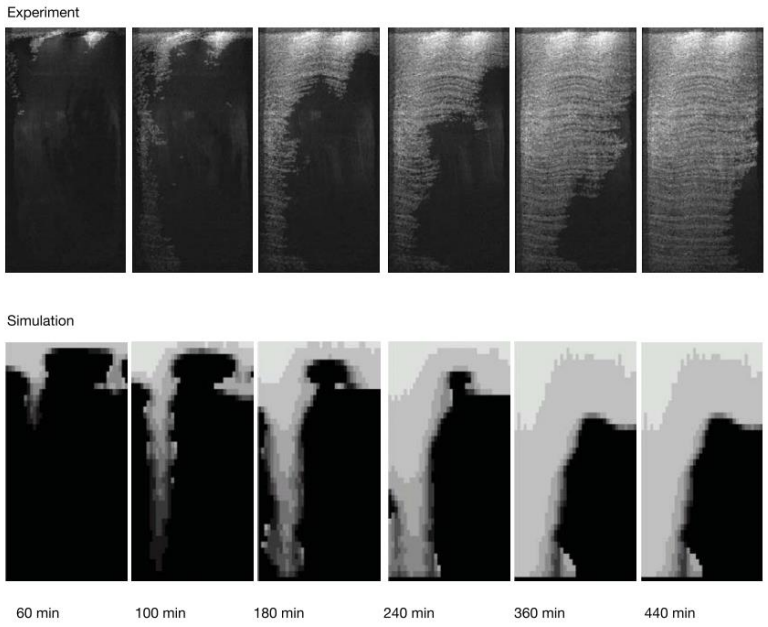

Figure 1-7: Simulation (bottom) matching experimental (top) general fingering pattern (Cuthiell et al. 2006).

In a more recent study by Malhotra et al. (2015) the growth of viscous fingering was investigated in experimental setups. The authors observed that at low viscosity ratios, the shield effect is less pronounced and multiple fingers grow parallel to each other. However, at higher viscosity ratios, merging coalescence and shielding are prominent as fingering mechanisms. Tip splitting was seen to be more pronounced at higher viscosity ratios. They also concluded that the fingertip/front velocities increase with the viscosity ratio up to a certain viscosity ratio, remaining in a 'plateau' after that.

1.3.2.2 Viscous Fingering Modelling

Viscous fingering can only occur in a multidimensional scenario that allows for interface instabilities to develop. There are 2 modelling approaches for this phenomenon: (1) high-resolution numerical simulations that capture the details of the viscous fingering flow (Christie & Jones 1987; Tan & Homsy 1988; Christie 1989; Zimmerman & Homsy 1991; Christie et al. 1993; Tchelepi & Orr Jr 1994; Chen & Meiburg 1998; Ruith & Meiburg 2000) and (2) macroscopic models which capture the relevant average behaviour of these displacements, e.g. breakthrough time and production data (Juanes & Blunt 2006).

In order to generate viscous fingering in high-resolution numerical simulations, it is necessary to trigger this phenomenon by adding dynamics in the flow. Some early studies on viscous fingering used truncation and round-off errors to trigger the instability. However, these attempts were unsuccessful, except for very adverse viscosity ratios (Peaceman & Rachford Jr 1962; Claridge 1972). Much simpler and reliable methods have been used by other authors to trigger the small perturbations leading to viscous fingering pattern formation (Christie 1989; Blunt & Christie 1994; Cuthiell et al. 2006).

The first approach is to have a finite-amplitude perturbation of the front at $t=0$ with a homogeneous permeability field. This type of perturbation corresponds to a disturbance caused by inlet conditions in a homogeneous medium.

The second approach is to create a random permeability field. In a real core there are differences between the absolute permeability of a certain position in relation to another one. This differences appear even in homogeneous cores. The flow instability is then propagated in such cores due to these tiny differences that create variations in the flow velocities, causing a 'domino' effect that leads to completely unstable fronts. Then, it is possible to use a log-normal distribution to attribute, in simulation, a different value of absolute permeability for each grid block. If the variance is small enough, the simulation continues to ensure that the core is homogenous, however, these differences allow the formation of viscous fingering. Both these approaches were tested by Christie (1989) and

found to have similar results. The same author in a different work proposed the use of 5% variance in the permeability distribution triggering method (Blunt & Christie 1994) so that the differences in permeability are small enough to guarantee homogeneity and sufficient to initiate fingering.

Cuthiell et al. (2006) was amongst the authors that used this technique to trigger fingering in simulation. The author compared their simulation saturation profiles with experimental results and obtained a very good agreement, using this triggering method.

1.3.3 Review on Viscous Fingering Influence on Relative Permeability Estimation

There is a lack of literature on the effect of viscous fingering in the relative permeability estimation. However, there are some studies on the effect of the viscosity ratio on the relative permeability. This parameter is strongly correlated to the viscous fingering, so it is possible to have some clue about the effect of fingering in the relative permesbility estimation from this parameter. In literature, the influence of the viscosity ratio on relative permeability has been studied by several authors. From the survey performed in this work, only two studies concluded that the viscosity ratio has no effect on relative permeability; these were papers by Croes and Shwarz (1955) and Johnson, Bossler and Naumann (1959). Johnson et al. reported that the effect of viscosity ratio was only to delineate different segments of the same set of relative permeability curves. In other studies, the authors reported a definitive effect of viscosity ratio on calculated relative permeability; these include works by Lefebvre du Prey (1973), Singhal et al. (1976) and Islam and Bentsen (1986). Islam and Bentsen's work compared relative permeability curves obtained by their proposed method against JBN method, to find decreases in the effective permeability of water and increases in the effective permeability of oil curves, with the increase in the viscosity ratio (oil to water). Common to many of the published experimental investigations is the lack of a sufficient quantity of evidence to support or deny the claims that high values of the viscosity ratio can adversely affect the JBN calculated relative permeability curves. Perhaps the most important literature work on this subject is the one from Maini et al. (1990). The author performed unsteady-state experiments with unfavourable viscosity ratio and compared them with the steady-state version of the same experiments. The results show that the relative permeability estimated by the unsteady state methods has considerable error for the oil curve, but almost no error for the displacing fluid curve. These results are very important because

they are comparing the real relative permeability curves (steady-state) with the unsteady-state experiments.

1.4 Scope of Work

1.4.1 What is the Problem?

Viscous fingering has been an object of study for a long time, but properly accounting for it in special core analysis (SCAL) measurements remains a challenge. Currently available flow equations and correlations can predict stable/ideal flow with good precision, however, when moving from stable to unstable flow most of them fail to do so. Viscous instability is characterized by the displacing fluid moving faster than the displaced fluid, resulting in a discontinuous and irregular front of displacement known as viscous fingering. Viscous fingering may happen when the mobility of the displacing fluid is higher than that of the displaced fluid (Stalkup, 1990). It is generally considered that for mobility ratio higher than 1, the flow has tendency to instability. Some authors like Blunt et al. (1994) use the shock mobility ratio instead of endpoint mobility ratio, which has more physical meaning since it is measured at the front of the displacement, where the fingering is formed. The phenomenon results in early breakthrough and poor sweep efficiency.

While significant amount of work has been done on viscous fingering modelling, there is a lack of work in predicting the real relative permeability of a core/fluid system in which viscous fingering takes place.

The relative permeability is one of the most important parameters in the study of fluid flow. While other parameters like porosity, absolute permeability, velocity and relative permeability have a significant role in fluid flow. Currently, a lot of resources are spent in laboratory experiments worldwide to determine the relative permeability (k_r) that can better represent the experimental results for a given core. These relative permeabilities are then used for reservoir simulation, which are crucial for making various decisions by petroleum engineers. Most laboratories use 1D history matching (1D HM) or analytical methods based on the Buckley-Leverett theory to estimate k_r from production data like Johnson, Bossler and Naumann (1958) proposed the JBN method.

In the presence of viscous fingering JBN and 1D HM (and all methods based in Buckley & Leverett 1942 equations) can produce erroneous results. 1D history matching obviously cannot capture differences of the saturation in the front, because viscous fingering is a multidimensional phenomenon, and the Buckley-Leverett's theory is only applicable for

stable flows with constant velocity, as emphatically pointed out by Sarma et al. (1994). There are, nevertheless, methods that can numerically simulate apparent viscous fingering, like high resolution 2D and 3D history matching in association with methods that can trigger this phenomenon (for example, using permeability distribution functions or particular viscous fingering models, Juanes and Blunt 2006). The problem of using 2D or 3D matching is the very time consuming simulations involved with this type of analysis and the higher degree of complex set up needed to create the simulations. The non-uniqueness of results of history matching is also a challenge when using 2D/3D history matching because it is possible to find different relative permeabilities that match the production data and differential pressure but have different saturation profiles. Experimental CT scans may have to be used in order to input the experimental saturation profiles in the history matching to deal with the non-uniqueness issue. This can be potentially problematic for many laboratories who do not have CT equipment.

This problem has not passed unnoticed in the work of Sarma et al. (1994). The author used 1D history matching in unstable coreflood experiments with viscous fingering and estimated the k_r curves. The authors called these k_r curves, pseudo-relative permeabilities due to the fact that they do not represent the real relative permeability. The authors highlighted the importance of developing a method for estimation of the real k_r.

As part of this work, a procedure for simulating viscous fingering in commercial simulators has been developed (unstable numerical experiments). This methodology comprises the steps necessary to avoid numerical dispersion, along with the necessary triggering method to cause flow instability. The capability of creating unstable numerical experiments allowed the author to develop a novel methodology for evaluating the precision of relative permeability estimation methods. This methodology was used to quantify the error of estimation when using methods based in Buckley-Leverett's theory to calculate the relative permeability of cases with viscous fingering formation.

As another outcome of this work, a model was proposed to modify the standard JBN and 1D history matching methods in order to enable them to account for viscous fingering in special core analysis (SCAL) measurements. These methods have a great potential value for the industry. They offer a fast and simple method to account for viscous fingering in the relative permeability estimation. Also, it is possible to use them as first guess for multi-dimensional history matching, reducing (considerably) the matching time.

1.4.2 Thesis Content

The viscous fingering simulation methodology and validation is presented in Chapter 2. This chapter starts by the definition of Numerical Coreflood Experiments (NCFEs), which were used throughout this work. Then, the methodology for the NCFE simulation and viscous fingering formation using the proper finger triggering method is shown. Subsequently, a sensitivity analysis was performed for the degree of perturbation initiated by the triggering method (permeability distribution) and another for the dispersion of simulation using varying numbers of total grid blocks in unstable experiments. Subsequently, the simulated viscous fingering patterns were compared with viscous fingering pattern observed in literature and a qualitative analysis was performed. In the final part of Chapter 2, synthetic viscous fingering generated in NCFEs were compared against stability models, to assess if the synthetic fingering obeys the known physics of the one observed in experiments described in literature.

Chapter 3 includes all the NCFEs used in this work. Using the methodologies developed in Chapter 2, a number of NCFEs were created to be used in validation throughout the work. The NCFEs were divided into 2 groups, the 'independent' and the 'sets'. All the parameters of the NCFEs are presented in this chapter, along with some qualitative analysis of the fingering patterns generated.

The evaluation of existing relative permeability estimation models is presented in Chapter 4. The chapter starts with a novel methodology to evaluate the precision of existing methods of relative permeability estimation. This methodology uses the NCFE definition in order to establish a comparison target for these methods, by providing the relative permeability curves as a known parameter, enabling error estimation. Then, JBN's precision in relative permeability estimation is evaluated against unfavourable mobility NCFEs. Firstly, the 'independent NCFEs' group is used in order to show JBN's precision in cases that have completely different parameters between each other. After, JBN is evaluated against the 'NCFE sets' group of simulations, to evaluate, its precision as a function of the gradual increase in instability. The error between JBN relative permeability estimations and the real values is calculated for both simulation groups. The same methodology is performed to assess the 1D HM precision.

In Chapter 5, 2 novel methods are presented to account for viscous fingering in relative permeability estimation. The chapter starts with the formulation of the theory behind the methods. Form this theory, a model called 'Stable Equivalent Model' is proposed. This model is used to convert the unstable experimental data into a stable equivalent that can

be used in mathematical formulations of fluid flow based on stable displacement. Then, the modified JBN method (MJBN) is derived using the Stable Equivalent Model applied to the standard JBN method. This modification to the standard JBN method allows it to account for viscous fingering in coreflood experiments. Following this work, the limitations and applications of MJBN are presented. In the same manner, a modification to the standard 1D HM (SEM) is proposed using the Stable Equivalent model. The SEM (stable equivalent matching) is derived as a method based on 1D HM, but with the advantage to account for viscous fingering.

The validation of MJBN and SEM is performed in Chapter 6. Firstly, MJBN and SEM precision is evaluated against NCFEs. The 2 groups of NCFEs presented in Chapter 3 are used: "independent NCFEs" and "NCFE sets". The two methods are then used to estimate the relative permeability from each NCFE and the error between the estimated curves and the real ones is calculated. In addition, a comparison between the production data obtained when using the estimated relative permeability curves instead of the real is provided. Next, the validation of SEM and MJBN is executed in actual unstable experiments provided by a literature reference. The experiments and every important parameter necessary for the calculations are documented. Then, the standard JBN and 1D HM are used to access the precision of the relative permeability estimations in these unstable experiments. Afterwards, the MJBN and SEM methods are used and their results are compared with the standard methods to show the improvement in accuracy resultant of the modifications. Finally, a discussion of the results observed is provided.

Finally, in Chapter 7, the highlights of results and points concluded in this study are given as well as some recommendation for future studies.

Chapter 2: Viscous Fingering Simulation

2.1 Numerical Coreflood Experiments (NCFEs)

Numerical CoreFlood Experiments (NCFEs) are defined as coreflood simulations using fluid and core properties similar to the ones performed in laboratory core flood experiments.

The major reason for the use data from a Numerical CoreFlood Experiment (NCFE) instead of Actual Experimental Data (AED) is the advantage for the user to know with certainty the conditions at which the injection and production data were generated. For example, the relative permeability (k_r) curves are very difficult to obtain experimentally, except when using steady-state methods, but these methods require long time to produce reliable data for this study (getting a single relative permeability curve, using steady-state method can take several months). Unsteady-state methods are faster but the k_r curves obtained can be very inaccurate, especially when fluids with adverse viscosity ratios are used, which could easily lead to wrong conclusions. Using NCFEs, the relative permeability will be input by the user and therefore it is a known parameter. It is also possible to capture the effect of a single parameter on the flow, for example, the effect of viscosity ratio, by maintaining all parameters the same changing only the viscosities of the fluids, while in AED, different viscosity ratios would lead to different relative permeability curves. Using NCFEs it is possible to apply the same set of k_r curves in an experiment, while changing the viscosity ratio. This allows, for example, to study how increasing viscous instability can affect the estimation of k_r. NCFEs will be treated as a real experiment for discussion proposes in this work.

2.2 NCFEs Simulation

In this work, a commercial software (CMG-IMEX) was used in order to generate the NCFEs. The objective was to 'create' unstable flow data that could be used to study the viscous fingering phenomenon in conditions similar to those encountered in a coreflood injection in a laboratory. Also, the precise definition of different parameters (e.g. *kr* curves) in NCFEs allowed the study of the influence of viscous fingering formation in each one of them, something that would be impossible to do with AED, due to uncertainty of those same parameters.

All the NCFEs created are in resemblance of typical laboratory experiments. Viscous fingering can be influenced by several factors in a real experiment, many (if not all) of these factors would also impact the estimation of the *kr* curves. So, in order to isolate the effect of fingering on the relative permeability estimation, simplifications were made allowing a better study of the phenomenon.

Firstly, black-oil simulation was used instead of compositional. Black-oil simulation does not account for mass transfer between the fluids, which will greatly simplify the simulation. Compositional simulation may take a very long time to finish, especially when viscous fingering is being triggered in a very refined grid. In this work a great number of simulations were produced and resulted in a very time consuming process even using black-oil simulation, so a compositional version would most probably be impractical with the computer power available (hundreds of simulations were performed during this thesis).

Secondly, all the simulations performed, were done in immiscible conditions. This was a necessary condition for 2 main reasons: simulation time and lack of literature work in immiscible scenarios. Immiscible simulations are faster and easier for the computer to run, which, due to the high number of simulations necessary for this work, translates into an advantage in relation to the counterpart. Also, there have been a lot of studies in literature performed in miscible fingering scenarios but very little work was published in immiscible. The use of immiscible simulation in this work would, therefore, result in a higher novelty for this thesis and also produce data that can be used by future authors on the subject.

In addition to these conditions, some other simplifications were made depending on the subject in study and will be described in the respective part of this work; they are mainly concerning the capillary pressure (P_c) and gravity effects.

2.2.1 Triggering Viscous Fingering in Simulation

NCFEs are a very valuable tool when studying viscous fingering. The major question is how to trigger the viscous fingering in a simulator that uses the Darcy law based equations. It is impossible from these equations alone to trigger viscous fingering without using a perturbation method. A perturbation method, as the name implies, is a way to introduce small differences in the flow velocity so that, when in an unfavourable mobility experiment, they can grow into unstable patterns like viscous fingering. Some early studies on the subject (Claridge 1972; Peaceman & Rachford Jr 1962) have attempted to

trigger viscous fingering by truncation and round-off error, though they proved to be generally unsuccessful, except for very adverse viscosity ratios (Christie 1989). Christie (1989) had better results using the following two approaches to trigger numerical viscous fingering:

1. A finite-amplitude perturbation of the front at t = 0 within a homogeneous permeability field, corresponding to a disturbance caused by inlet conditions in a homogeneous medium.
2. A random permeability field, where the cell permeabilities were chosen from a log-normal distribution with a specified variance.

Christie obtained similar results from both approaches in his work. For the simulations stated in this work, the second approach was used to trigger fingering, because it is the approach that resembles a real core more closely, since in an actual experiment the absolute permeability is not constant along and across the core. Also there is published literature with good agreement between fingering generated from this method in comparison to experiments (Cuthiell et al. 2006; Cuthiell et al. 2001).

A random permeability field or permeability distribution was used throughout this thesis as the perturbation method to trigger viscous fingering. This method consists of assigning a different value of absolute permeability to each grid block in the system following a normal or Gaussian distribution profile. A Gaussian distribution can be produced using the mean and the desired variance (or standard deviation) in relation to it. A Gaussian distribution can be described by a probability density function as follows:

$$f(x) = \frac{1}{\sqrt{2\upsilon\pi}} e^{-\frac{(x-\mu)^2}{2\upsilon}} \qquad \text{.....2-1}$$

Where, x is the value of absolute permeability, $f(x)$ is the probability of the value x to exist in the gird blocks of the simulation, μ is the mean value of absolute permeability and υ is the variance (which is the squared root of the standard deviation). From this equation is possible to draw a probability density function plot as in Figure 2-1.

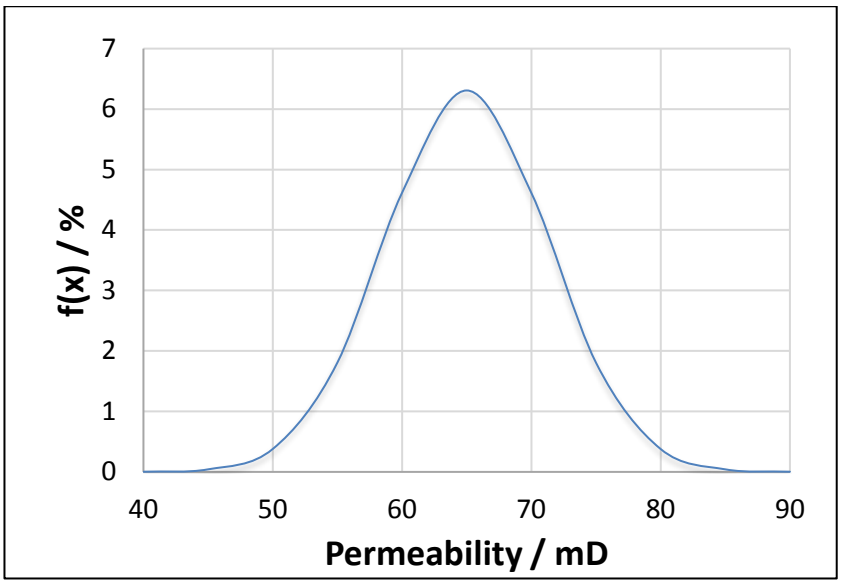

Figure 2-1: Example Gaussian probability density function for a 65 mD core with a variance of 40.

From the figure is possible to see that there is a higher probability for the values closer to 65 mD (the mean in this example) than those away from it. Depending on the variance is possible to increase the probability for values farther away from the mean.

2.2.2 Permeability Distribution - Sensitivity Analysis

It is very important to choose a good permeability distribution variance for the case in study. It is the variance that describes the degree of heterogeneity of the core. For this thesis, the cores in study are considered homogeneous, this means that the differences in permeability are small enough that they will not have an impact on the flow. To ensure that this is true in the NCFEs, the variance must be low enough to ensure homogeneity, but big enough to result in fingering formation.

The difference between a simulation running in a constant absolute permeability core and a simulation running in a core with a permeability field is the small differences in velocity that will happen in each grid block. If the flow mobility is unfavourable these differences will accumulate to generate the fingering. It was then important to conduct a sensitivity analysis to find the ideal variance that would result in viscous fingering formation, while avoiding heterogeneity driven flow.

2.2.2.1 Methodology

In order to examine the impact of the permeability distribution in the flow, a statistical study was carried out. For this study a NCFE was created (codename PDV) with

unfavourable mobility characteristics, the core properties and coreflood condition can be seen in Table 2-1 and
Table 2-2.

Table 2-1: NCFE PDV Core properties.

NCFE	*Length / cm*	*Diameter / cm*	*Porosity / %*	*Permeability / mD*	*S_{oi} / frac*
PDV	60.5	5.08	18.2	2500	1

Table 2-2: NCFE PDV Coreflood Conditions.

NCFE	*Injection Rate / $cm^3.min^{-1}$*	*Pressure / kPa*	*Oil Viscosity / mPa.s*	*Gas Viscosity / mPa.s*	*Viscosity Ratio*
PDV	0.375	10300	30	0.05	600

The viscosity ratio for this case was around 600 to ensure an unfavourable mobility coreflood. The relative permeability curves were created using Sigmund & McCaffery (1979) equations and are presented in Figure 2-2 for oil (k_{ro}) and gas (k_{rg}).

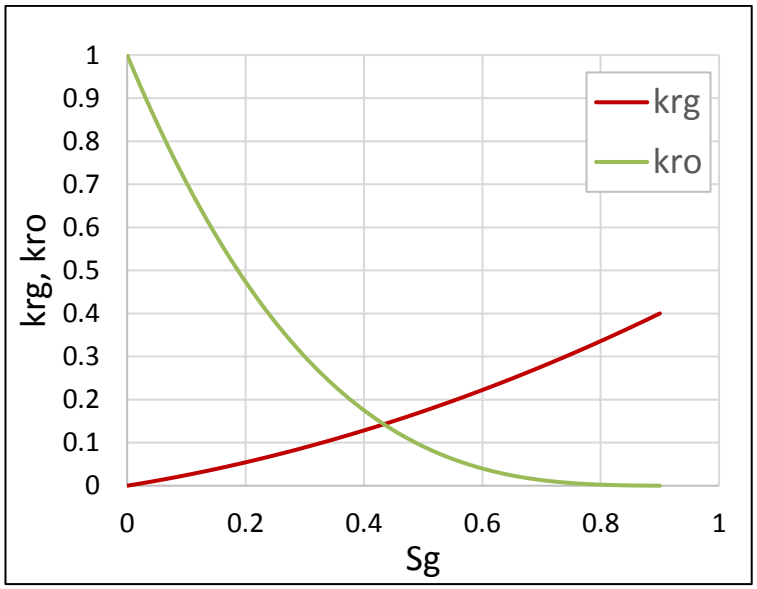

Figure 2-2: Relative permeability curves for oil and gas used in PVD.

This relative permeability was chosen in order to ensure instability formation due to its high mobility ratio at the small gas saturation range. While normally the endpoint mobility ratio is used to define the instability of a coreflood, several authors use the shock mobility ratio instead (e.g. Christie et al. 1993). The shock mobility ratio is the mobility difference at the front of the displacing fluid. In this relative permeability it is possible to see that for the gas the values start very high from the beginning of the displacement, this means that the shock mobility ratio (which will be around that saturation range) will, very probably, be higher, especially since the viscosity ratio is very high. With such a relative permeability it was expected a very early breakthrough, because of its unfavourable nature.

The input data presented was then used to create 2D NCFEs in CMG-IMEX, using different degrees of permeability distribution, with a coefficient of variation of 0%, 10%, 20%, 30% and 40% and codename PDV 0, PDV 1, PDV 2, PDV 3 and PDV 4, respectively. The coefficient of variation is a standardized measure of dispersion of a probabilistic distribution and can be defined as:

$$c_v(\%) = \frac{\sigma}{\mu} \times 100 \quad \text{.....2-2}$$

Where, c_v is the coefficient of variation, σ is the standard deviation and μ is the mean permeability. A c_v of 0% corresponds to a constant absolute permeability throughout the core (no Gaussian permeability distribution). For PDV 1, PDV 2, PDV 3 and PDV 4 the permeability fields were created in a tool included in CMG, by the introduction of the mean absolute permeability (2500 mD) and the respective variability for each case in order to obtain the different coefficient of variation values. The permeability fields for all the 2D NCFEs were performed in a very refined grid of 55296 grid blocks (864 x 64 x 1, length x diameter x thickness). The grid blocks were squared shaped to ensure the same contribution in the vertical and horizontal direction, reducing their influence in the fingering pattern, although for this case (with high number of grid blocks per unit area) the effect of grid averaging should be low. In addition to the 2D simulations, an 1D simulation was also created using the same input data and constant mean absolute permeability throughout the core with the codename PDV 1D. For each permeability distribution scenario (PDV 1, PDV 2, PDV 3 and PDV 4) 7 different simulation were performed by changing the permeability field generated but maintaining the coefficient of variability of each case in order to build a statistical evaluation. In order to perform a

proper statistical study, it would be necessary many more values than 7, although these simulations take a very long time, so 7 was chosen as reasonable for this case. The CMG software also allows the user to generate 'clusters' of permeability values, by aggregating similar permeability values together to create high and low zones. However, permeability was assigned randomly to avoid unnecessary heterogeneities problems. For PDV 1D and PDV 0 only 1 simulation was performed, since the permeability was constant and no variations could be made.

2.2.2.2 Results

Figure 2-3 and Figure 2-4 show the results of the simulations in terms of breakthrough recovery versus permeability distribution range in 'box and whiskers' plots. Figure 2-3 presents the results for all the simulations together, but due to the high difference between the 1D and 0% in comparison with the rest, it is not possible to distinguish differences between 10%, 20%, 30% and 40% c_v NCFEs. The breakthrough time was chosen for this comparison study, because of its tight relation with viscous fingering formation and recovery problems that come with it. Several authors (Koval 1963; Peters & Flock 1979; Tchelepi & Jr. 1994; Araktingi & Orr Jr 1993) have measured the intensity of the instability by comparing the breakthrough time in different experiments, making this parameter the standard way to measure instability in a coreflood experiment.

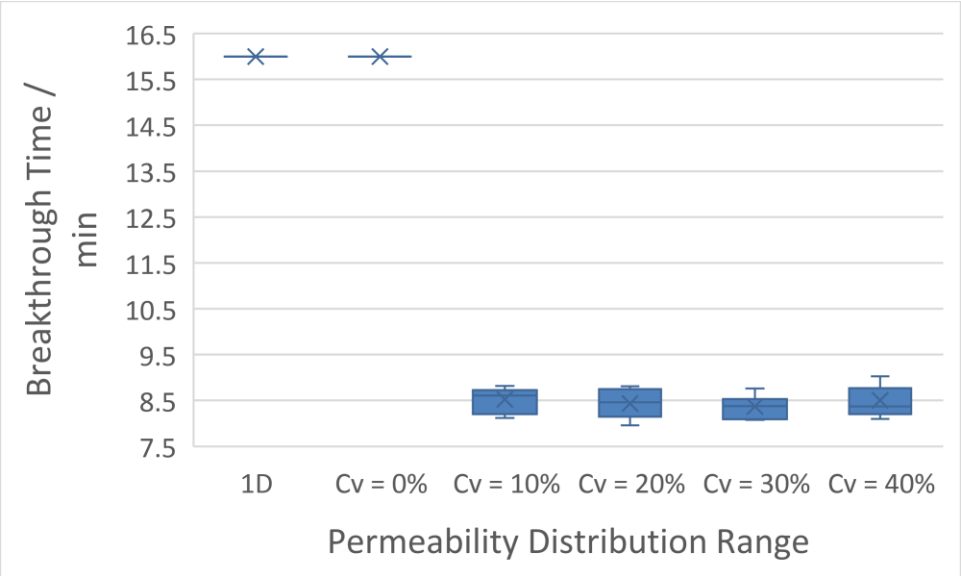

Figure 2-3: Breakthrough time result for different 2D simulation permeability distribution variabilities (0%, 10%, 20%, 30% and 40%) and 1D simulation.

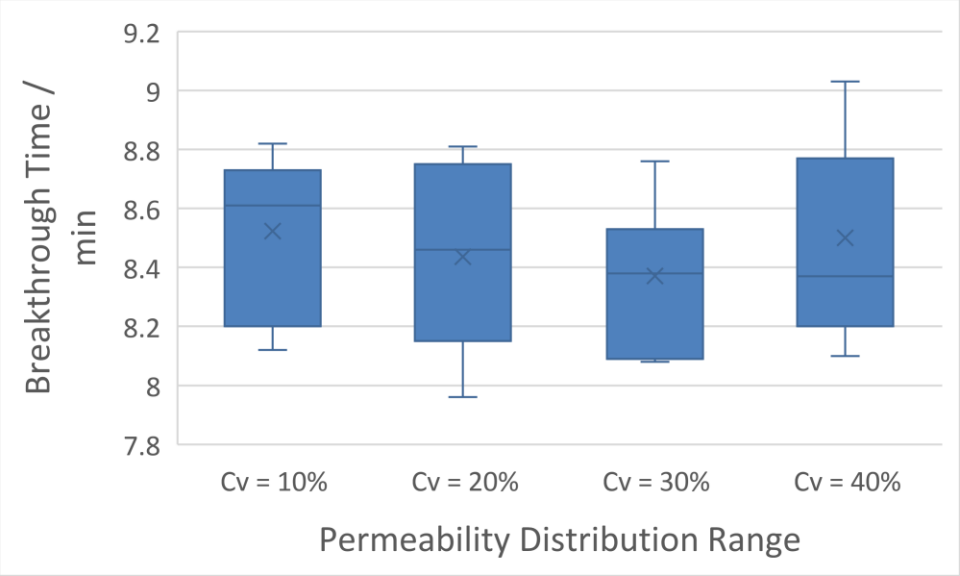

Figure 2-4: Breakthrough time result for different 2D simulation permeability distribution variabilities (10%, 20%, 30% and 40%).

From the figures the effect of introducing permeability distribution in simulation in comparison with the use of a constant absolute permeability throughout the core is clear. The breakthrough times for the PDV 1D and PDV 0 cases were around 16 min while for PDV 1, 2, 3 and 4, it was around 8 min. The conditions used for these NCFEs were very unfavourable meaning that a 16 min breakthrough corresponded to only around 3% of the total pore volume of gas injected. Also, it is important to understand that these results are different than what would be obtained in a laboratory experiment comparing 2 cases of injection one with fingering suppression (using for example gravity stabilization methods) and another with fingering formation. The reason for this is the relative permeability. In these NCFEs the relative permeability is maintained constant for all the experiments in order to evaluate the solo effect of permeability distribution in the breakthrough time by allowing fingering formation. In a laboratory experiment, even using the same core and fluid properties, the change from stable flow to unstable would inevitably result in different relative permeabilities and very probably the difference between breakthrough times should be even higher, because the mobility ratio would change. Blackwell et al. (1959) has clearly shown the effect of mobility alteration in the breakthrough recovery. In his experiments, a mobility ratio of 1 produced around 90% of IOIP (initial oil in place) at breakthrough in comparison with around 20% IOIP for a mobility ratio of 86. This highlights one of the advantages of using NCFEs, because it is possible to separate the effect of viscosity ratio in the flow with changing the effect of the

relative permeability, allowing a better study of the underlying effects of viscosity in viscous fingering.

Furthermore from Figure 2-3 is possible to realise that there is no apparent, or significant, difference between the breakthrough times of PDV 1, 2, 3 and 4. Meaning, that only a small variability in the permeability distribution is necessary to trigger the fingering formation. Using a high variability permeability distribution may result in preferential flow paths for the displacing fluid in the core (typically called heterogeneity effect). Although, for this case, no significant difference is seen in the breakthrough recovery results when increasing the coefficient of variation from 10% to 40% (Figure 2-4). There are small differences in terms of mean (represented by X in the plot) and the median (represented by the line) that seem to indicate some degree of reduction in the breakthrough time when the coefficient of variation increases, although the 1st and 3rd quartiles are within the range of each other for this case. This behaviour has been seen elsewhere (Djabbarov et al. 2016) in literature and means that there is not enough variability in the permeability distribution values to affect the viscous fingering formation due to heterogeneity.

2.2.3 Number of Grid Blocks - Sensitivity Analysis

Viscous fingering is a multidimensional phenomenon where fingers of the displacing fluid move through the displaced fluid. In simulation, fingering can be represented in many forms, either by mathematical equations that directly generate fingering patterns (several mathematical expressions have been proposed for dendritic growth and fingering (Xu 1997)) or by triggering methods (as in the previous section). However, whatever the method chosen fingering needs the use of a very refined grid to avoid any misrepresentation by averaging. For example, if the grid block numbers are small, there may be only 2 fingers in a coreflood simulation, but in fact those 2 fingers may be 4, but since the grid is too coarse they are not dissociated from each other leading to wrong conclusions. Defining precisely the number of grid blocks necessary to correctly represent viscous fingering, or at least reduce the amount of possible error to an insignificant value, may be done by sensitivity analysis. Sensitivity analysis, in this case, is essentially a study in production data to see how the number of grid blocks influences the results and when that number is great enough to avoid significant error.

2.2.3.1 Methodology

In this work, finding the correct number of grid blocks is paramount for a good scientific study on viscous fingering. To find the best grid block number to be used in simulations several gas injections into oil filled core NCFEs were created (with the codename GBN, to distinguish from other NCFEs in this thesis) to develop a statistical study in the same manner as presented in the previous section for the permeability distribution. The NCFEs were separated into 7 sets, each set corresponding to a number of grid blocks in simulation: 200, 1600, 3500, 6500, 11300, 24900, 55300 grid blocks. The reason for the grid blocks numbers to be so specific instead of round numbers is because the grid was created with the almost perfect squared shaped blocks. Excel solver was used in order to achieve this, for a certain 2D area it was calculated how many grid blocks were necessary in order to have blocks with aspect ratio close to 1. Squared blocks were important to avoid privileged averaging in one direction in relation to another, of course for a very fine grid this problem is negligible, but it may have considerable influence in the coarse grid cases. All the GBN NCFEs had the same fluid and core properties presented in Table 2-3.

Table 2-3: Core and fluid properties used in the GBN NCFEs.

Parameter	***Value***	***Units***
S_{oi}	1	frac.
S_{wc}	0	frac.
Length	60.5	cm
Diameter	5.08	cm
Porosity	0.1818	frac
Pore Volume	222.7	cm^3
Injection Rate	0.375	cm^3/min
Oil Viscosity	30	mPa.s
Gas Viscosity	0.05	mPa.s
Pressure	10.300	kPa
Permeability	2500	mD

Then for each GBN set, 7 NCFEs with different permeability distributions were created with the same mean absolute permeability. From the previous section, it was seen that permeability distributions with a variation coefficient of 10% would be sufficient to create

viscous fingering and low enough to avoid heterogeneity, so a permeability distribution with c_v = 10% was used in GBN NCFEs also. Different permeability distributions were essential to evaluate the effect of grid blocks number in viscous fingering formation, since in simulation that is the differentiating factor between each simulation. In other words, if the same permeability distribution was used, the statistical error within the same number of grid blocks would not be possible to be evaluated. The relative permeability used for GBN NCFEs was created using Sigmund & McCaffery 1979 and is presented in Figure 2-5. The endpoint mobility ratio for this NCFEs is around 240, which is high enough for instability to occur in the core.

2.2.3.2 Results/Discussion

Figure 2-6 presents the breakthrough versus the grid block number for the different NCFE GBN sets in the form of a "box and whiskers" type plot. It is clear from the figure that higher number of blocks leads to more accuracy of results as expected. However, the spreading of the results is abruptly reduced after 11300 blocks. For 200, 1600, 3500 and 6500 blocks there is considerable spread of the breakthrough times, this means that using any number of grid block within the range of 200 to 6500 could result in considerable error due to the effect of gridding in simulation, not only in terms of accuracy and also precision. In fact, if it is assumed that the breakthrough times range in the simulations with 55300 blocks is most accurate result, then the simulations with 200 and 1600 block don't even have any value that is included in the 55300 block breakthrough time range.

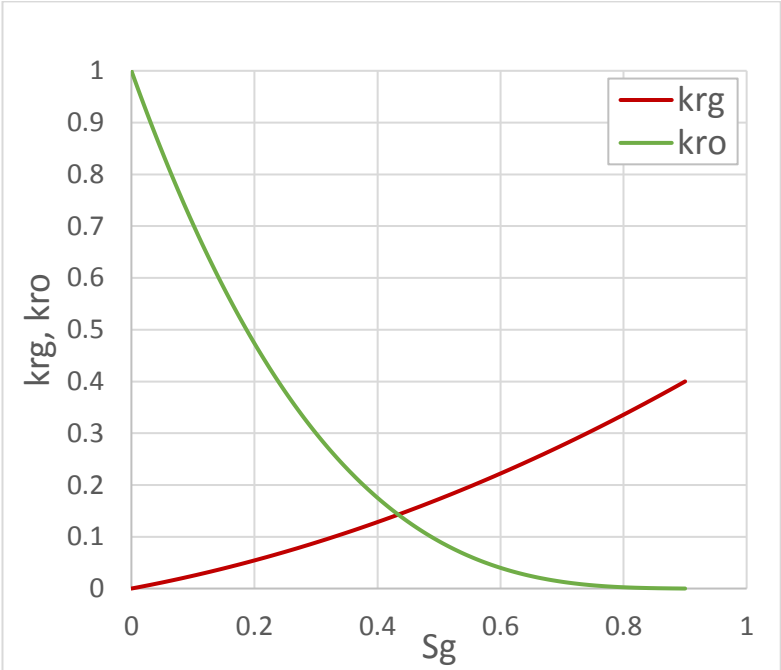

Figure 2-5: Relative permeability curves for gas (k_{rg}) and oil (k_{ro}) used in GBN NCFEs.

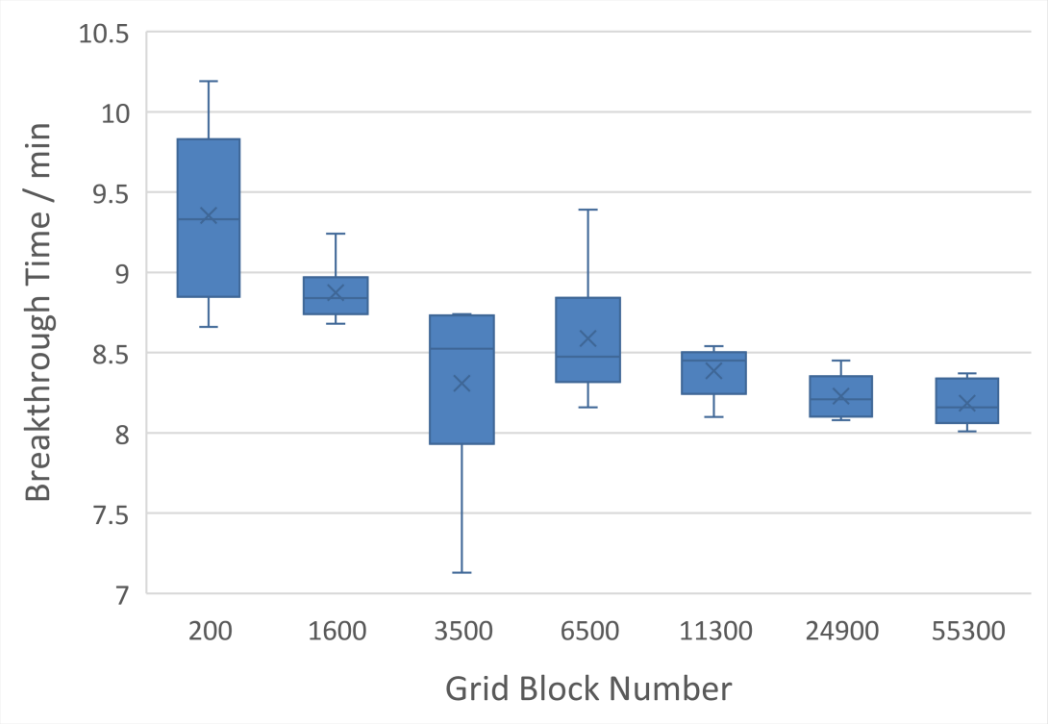

Figure 2-6: Breakthrough time result for different 2D simulation grid block numbers (200, 1600, 3500, 6500, 11300, 24900 and 55300).

In terms of fingering simulation, the best range of grid block number to be used in simulation would be that between 24900 and 55300. The 24900 blocks breakthrough time range is almost the same as in 55300, meaning that the best accuracy (assuming that accuracy improves with number of blocks) was reached and a higher number of blocks will not lead to more accurate results.

The reasons for these differences in breakthrough time tie up with the representation of the saturation profiles inside the core in simulation. Refined grids (with more grid blocks) have the ability to represent a higher number of fingering. 1 GBN NCFE of each set was selected and the respective oil saturation profile at 9 min of injection (near breakthrough) was extracted to view the difference in fingering formation for each grid block number, Figure 2-7.

For the coarser grid (200) the flow front is essentially divided by 1 finger that stands out from the rest of the gas moving through the oil close to the wall. When more refined grid is inputted in the simulation more detail is given to the front and more fingers start to appear. It is almost possible to see from the first saturation profile to the last (top to bottom) an incremental improvement in the resolution (and number of secondary fingers) of the saturation patterns. In the last 2 saturations (for 24900 and 55300 grid blocks) the fingers patterns have close resemblance for the 2 cases, which produces similar results.

The results shown in Figure 2-6 are the result of these differences in the saturation profiles. As the grid gets more refined, viscous fingering gets more complex and a higher number of secondary fingers are possible to be generated. There is, however, a limit after which further complexity/refinement of the fingering will not affect the results of the simulation, because the differences in saturation are very small and turn out to be insignificant, as seen for the NCFEs with 24900 and 55300 grid blocks.

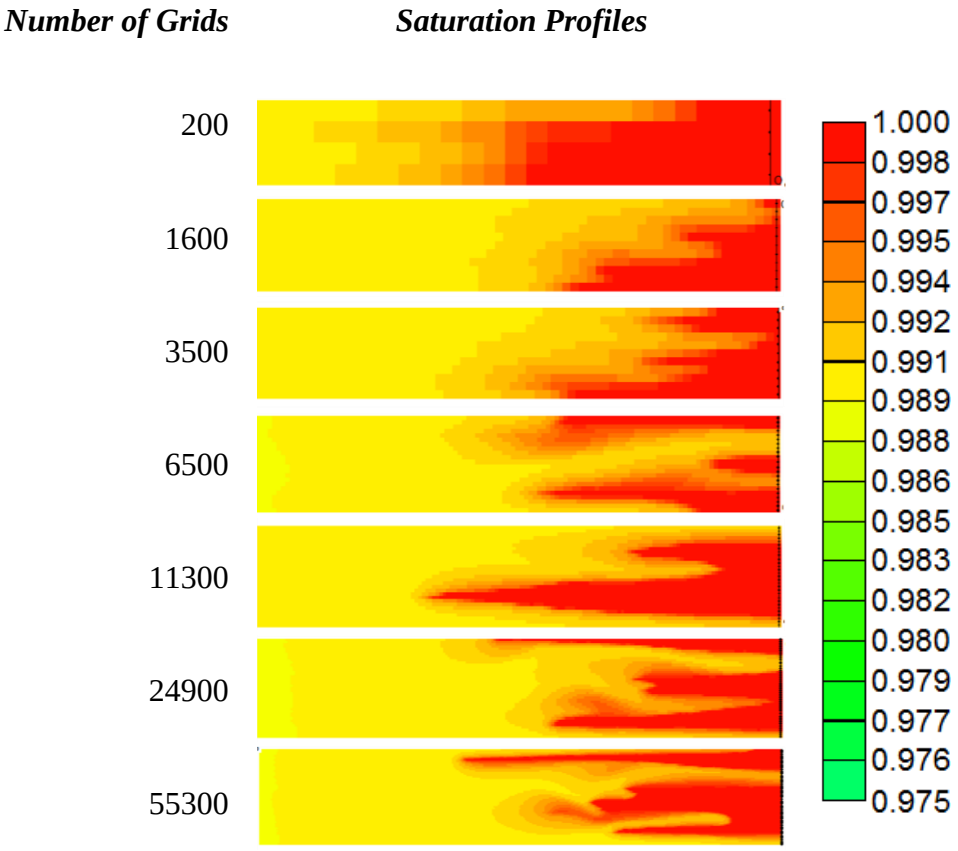

Figure 2-7: Oil saturation profiles when using different number of grid blocks in simulation, after 9 min of injection.

These results how that the 2D NCFEs between 24900 and 55300 grid blocks have enough accuracy to represent fingering. Since the simulations were performed in a 60.5 cm of length and 5.08 cm diameter, it can be concluded that the density of blocks in simulation should be in the range 20.31 to 45.10 blocks/cm^2. This derives directly from 24900 and 55300 divided by the total core area in simulation for this statistical study. Therefore, all simulations performed in this thesis respect this density of blocks in 2D simulation when there is a wish to generate viscous fingering patterns.

2.3 Viscous Fingering Pattern Analysis

The previous sections of this chapter represent the foundations for the work in viscous fingering simulations. Using the correct grid block number with appropriate permeability distribution in a 2D simulation environment should be enough to generate viscous fingering. In this section of the thesis, the procedures developed previously will be used to assess the capability of the simulator to generate fingering when the flow is unstable.

2.3.1 Methodology

To evaluate the fingering generation capability of simulators a set of 7 NCFEs was created beginning with a stable displacement and incrementally instability was imposed in successive displacements. The NCFEs represented an experiment where gas is injected into an oil filled core with connate water. This was done by changing the viscosity ratio in the coreflood experiments. Gas viscosity was maintained constant at 0.05 and the oil viscosity was changed to 0.05, 0.25, 0.5, 2.5, 5, 15 and 35 mPa.s, resulting in viscosity ratios 1, 5, 10, 50, 100, 300 and 700, respectively. The oil viscosities for the lower viscosity ratios are very low and not probable to happen in a real coreflood experiment, however they were necessary to have low mobility ratios.

CMG – IMEX was used as simulator software to perform the 2D NCFEs. The cores were defined as 60.5 cm length and 5.08 cm diameter. The simulation used a quadratic representation of the cylindrical core, changing it to a prism with 60.5x4.5x4.5 (length, width and thickness) dimensions. Width and thickness were chosen keeping the same cross area as in the original cylindrical core. The cores were rendered with 55,296 grid blocks distributed in 864x64x1: length, width and thickness respectively. To represent a coreflood experiment with rotating core (where the core rotates during the coreflood experiment at a certain velocity in order to remove gravity effect using the centrifugal force), the cores were created in a XY Cartesian coordinate grid, instead of XZ, X being the direction of the flow.

Gas injection was fixed at 0.375 cm^3/min and the initial pressure of the experiments at 12,000 kPa. The cores were initially saturated with 82% oil and 18% of connate water and the average absolute permeability of the core was 65 mD. Permeability distribution was used, using a Gaussian distribution with a variance of 42 and mean of 65 mD. This distribution was created within the software using a specific tool.

The relative permeability used in the NCFEs was created using Sigmund & McCaffery 1979 equations with parameters No = 2.5, Ng = 2.5, A = 0.01, B = 0.01, k_{ro}^{0} = 0.6, k_{rg}^{0} = 0.8, resulting the relative permeability in Figure 2-8.

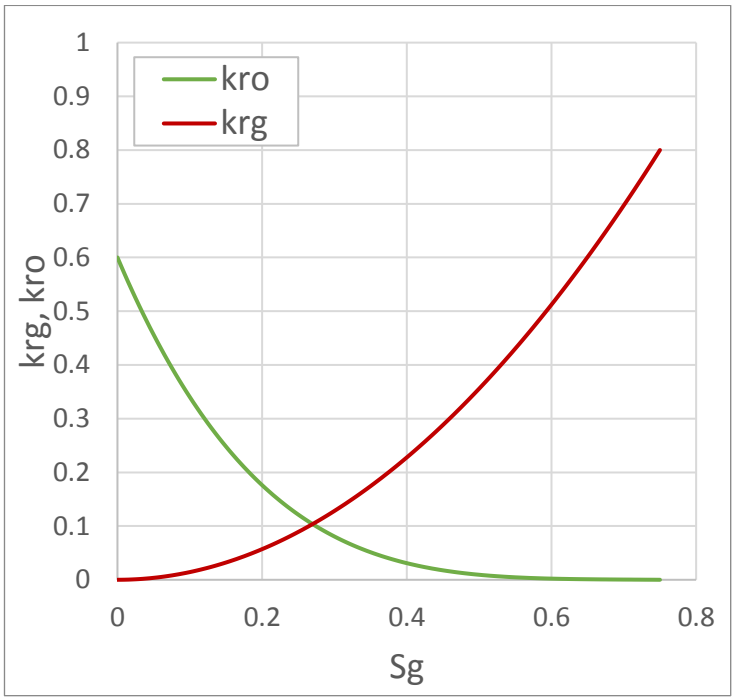

Figure 2-8:Relative Permeability used in the NCFEs.

The main core and fluid properties used in the NCFEs are presented in Table 2-4.

Table 2-4: Core and Fluid Properties used in the Numerical Coreflood Experiments (NCFEs).

Parameter	***Value***	***Units***
S_{oi}	0.82	frac.
S_{wc}	0.18	frac.
Length	60.5	cm
Diameter	5.08	cm
Porosity	0.2	frac
Pore Volume	245	cm^3
Injection Rate	0.375	cm^3/min
Gas Viscosity	0.05	mPa.s
Pressure	12.000	kPa
Permeability	65	mD

2.3.2 Results/Discussion

In order to evaluate the fingering formation in the different NCFEs, the gas saturation profile was gathered to see the stability of the oil-gas front, the results are presented in Figure 2-9 for the respective viscosity ratio. Note that a dichromatic scheme was used with black for oil (parts of the core untouched by gas) and shades of grey for different saturation of gas (lighter colour means more gas in that zone of the core). The colour scale was different between each of the NCFEs in order to highlight the differences in the front. Also, the core length was cut, in the images, to show the fingering zone more clearly, since the NCFE was performed in a relatively long core. For low viscosity ratios there is a high saturation shock at the front, which is not seen for high viscosity ratios due to the difference in mobility (e.g. high viscosity differences lead to lower mobility of the fluid and less saturation displacement inside the core), therefore if the same colour gradient scale was used the front profile would not be visible in all cases. It was then decided to use a colour scale that would fit each experiment best. Also, the pictures of the saturation profiles were not captured at the same point in time, neither at the same amount of pore volume injected, such action would be useless for the evaluation of the results since the experiments were performed at different mobility, which would result in different breakthrough times. Every image was then captured at a point where the front is fully visible but close to the gas breakthrough time. It is known that viscous fingers coalesce into a few 'main' fingers while going through the total length of the core (Slobod & Thomas 1963; Zimmerman & Homsy 1991), so by capturing the front image near the breakthrough time, the effect of fingering in production is better captured, since that will be the final aspect of the fingering before leaving the core.

Figure 2-9 shows the NCFEs with low viscosity ratio (1 and 5) with the same saturation of gas for the whole width of the core at the front of the displacement, making them stable displacement. However, it is visible that from viscosity ratio of 1 to 5 the front goes from a perfect homogeneous saturation of gas at the frontal width to small perturbations at the very tip of the gas front. These perturbations are created because the mobility favourability was reduced.

For viscosity ratio of 10, it is noticeable that viscous fingering is present at the front of the displacement. The fingering zone (the length between the tip of the further gas finger to the place where no part of the core is touched by gas or where no black is found) however is small and the oil zones untouched by the gas are small in it, which means that

the influence of fingering in this case should be small and the threshold of stability was just crossed.

Comparing the saturation profile for viscosity ratio of 10 with 50, the oil banks remaining after the fingers have considerably increased. Although the fingering density (number and width of fingers) remains practically the same the fingering zone is longer.

For viscosity ratios 100, 300 and 700 the same trend is followed. With the increase in viscosity ratio the fingering zone increases considerably and fingers become longer and thinner, resulting in more oil banks after breakthrough and less oil recovery. Shielding is the process by which the growth of a finger retards the growth of adjacent trailing fingers(Zimmerman & Homsy 1991; Li et al. 2006; Malhotra et al. 2015). At low viscosity ratios the fingers were observed to be growing parallel to each other, meaning that the effect of shielding was low, however for these viscosity ratios (100+) shielding takes place, resulting in a bigger upswept area before breakthrough. It is noticeable that between viscosity ratio of 300 and 700 there are very small differences in the fingering pattern, even though the difference in viscosity ratio between the 2 cases is of 400. This is in agreement with other studies of viscous flow instability (Sarma & Bentsen 1987), where it is stated that after a certain degree of instability a state of pseudo stability is reached. Pseudo stability means that even though the experiment is unstable and the front shows considerable degree of deformation, increases in the instability factors for that case will result in no change in terms of production data. In other words, the front has reached the maximum deformation due to instability. In accordance with that theory, there are 3 zones of flow stability: stable, transient and pseudo stable, where stable zone corresponds to the case where no influence of frontal dysmorphia is seen in the production data and transient corresponds to the zone where incremental increase of instability will translate in successive less oil recovery. In the results of Figure 2-9, the cases with viscosity ratio of 1 and 5 would be in the stable zone; 10, 50 and 100 in the transient; 300 and 700 in the pseudo stable zone.

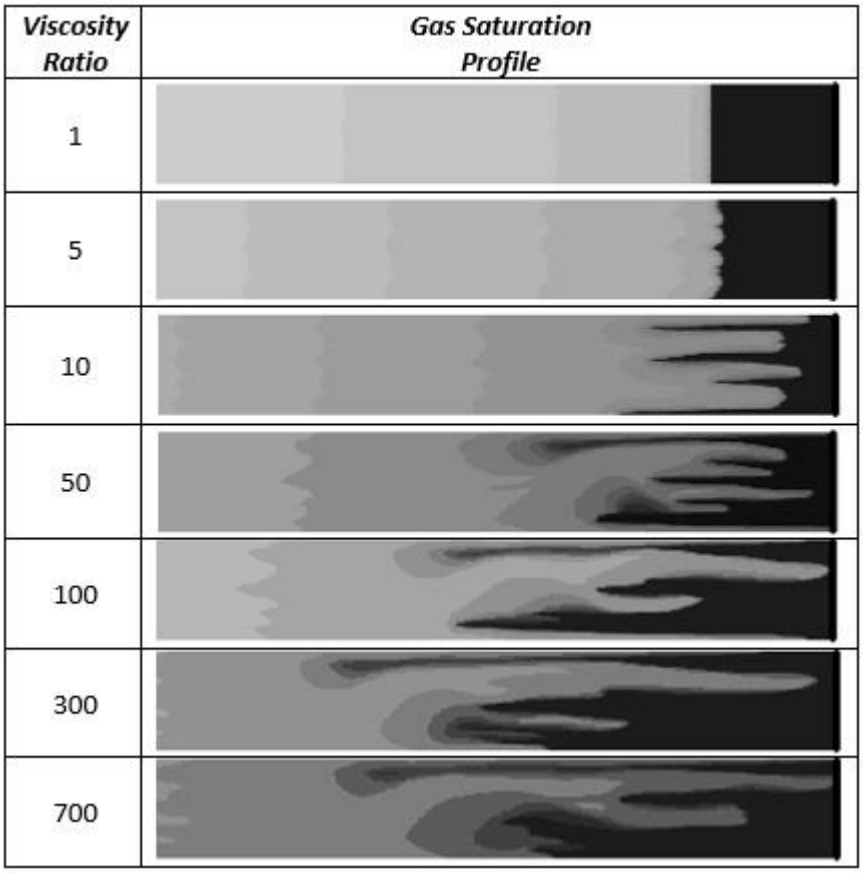

Figure 2-9: Gas saturation profiles inside the core for different viscosity ratios, using the same core and fluid properties, showing differences in the frontal stability and formation of fingering for unfavourable viscosity ratios (Black = oil, different shades of grey correspond to different gas saturations).

2.3.2.1 Viscous Fingering Mechanisms

During formation of viscous fingering there are 4 main mechanisms that take place depending on the mobility contrast between the fluid: Shielding, Spreading, Coalescence and Tip Splitting (Wooding 1969; Homsy 1987; Manickam & Homsy 1993; Manickam & Homsy 1994; Manickam & Homsy 1995; Li et al. 2006; Sesini et al. 2010; Malhotra et al. 2015). Shielding is the process where the growth of one finger inhibits the growth of the adjacent fingers, causing it to grow faster in length than them. Spreading is the mechanism by which the finger becomes larger as the flow progresses through the core. Coalescence happens when fingers get together to form a bigger (wider) one; or when small fingers join with a larger one, either by connecting the tip to the body of the other finger or by complete merge. Tip Splitting is the process by which the tip of a finger splits itself into 2 or more fingers.

These 4 mechanisms are observed in this study. The evidence of this mechanism is evaluated using 2 of the 7 cases described previously, one with viscosity ratio of 10 and another with 700, representing the cases with low and high viscosity ratios, respectively. For low viscosity ratios, Tip Splitting and Shielding are almost non-existent because the mobility difference of the fluids is not sufficient to make them manifest. For these viscosities, coalescence and spreading are the main mechanisms of fingering growth.

Figure 2-10 shows the sequential evolution of the gas oil interface from the NCFE with viscosity ratio of 10. In the beginning many, very short and thin, fingers form at the front of the displacement. As time advances this high number of fingers decrease from more than 10 to only 4 up to 141 min, due to merge of the smaller fingers together. The resulting fingers are longer and wider, and they grow parallel to each other resulting in no shielding effect. For later times, 186 and 216 min, in the displacement spreading is also observed although very slightly.

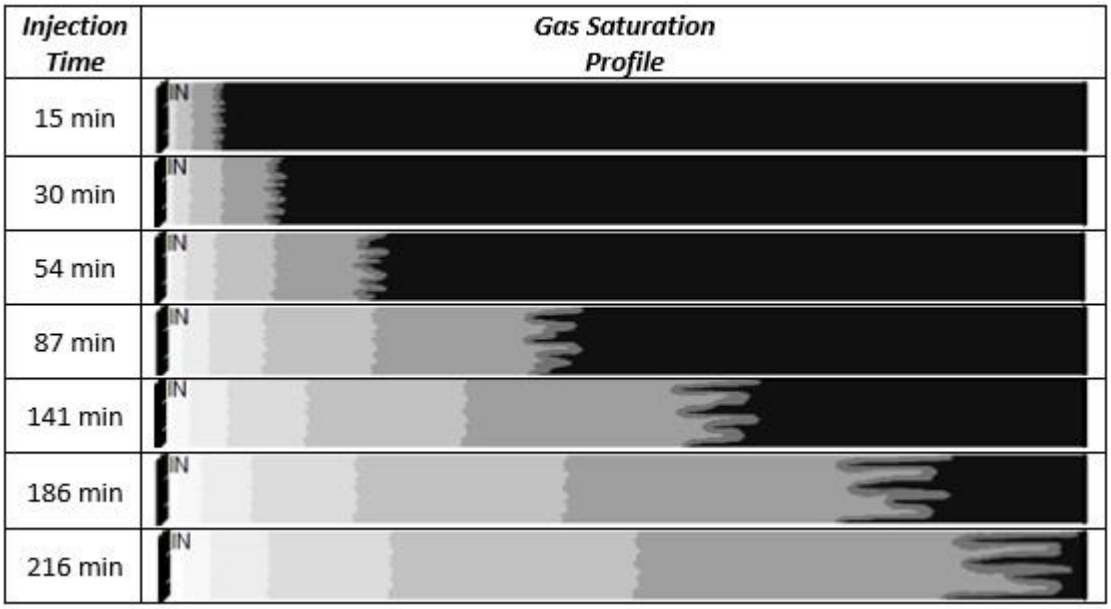

Figure 2-10: Gas saturation profiles showing the sequential evolution of the interface between gas and oil from the NCFE with viscosity ratio = 10.

In Figure 2-11 the sequential evolution of the front oil-gas in seen for the case with viscosity ratio of 700. Due to the viscosity difference, in this case the 4 mechanism of fingering happen during the beginning of injection up to the breakthrough. In the first moments of injection a high number of fingers are formed, but these fingers are longer than in the previous case. Immediately, fingering coalescence takes place and fingers merge to form wider fingers, which is specially seen from 15 to 24 min, where the number

of fingers considerably reduces. Also, at the same time shielding effect starts to happen, making the main fingers grow at enhanced rate in comparison with the other fingers next to them. From minute 24 to 39 the shielding effect and the coalescence are responsible for reducing the oil-gas front to 2 main fingers. During this time some tip splitting happens for the smaller fingers, especially the ones closer to the main fingers, resulting in further coalescence. In the final moments of the displacement, there is also fingering spreading mostly on the 2 main fingers.

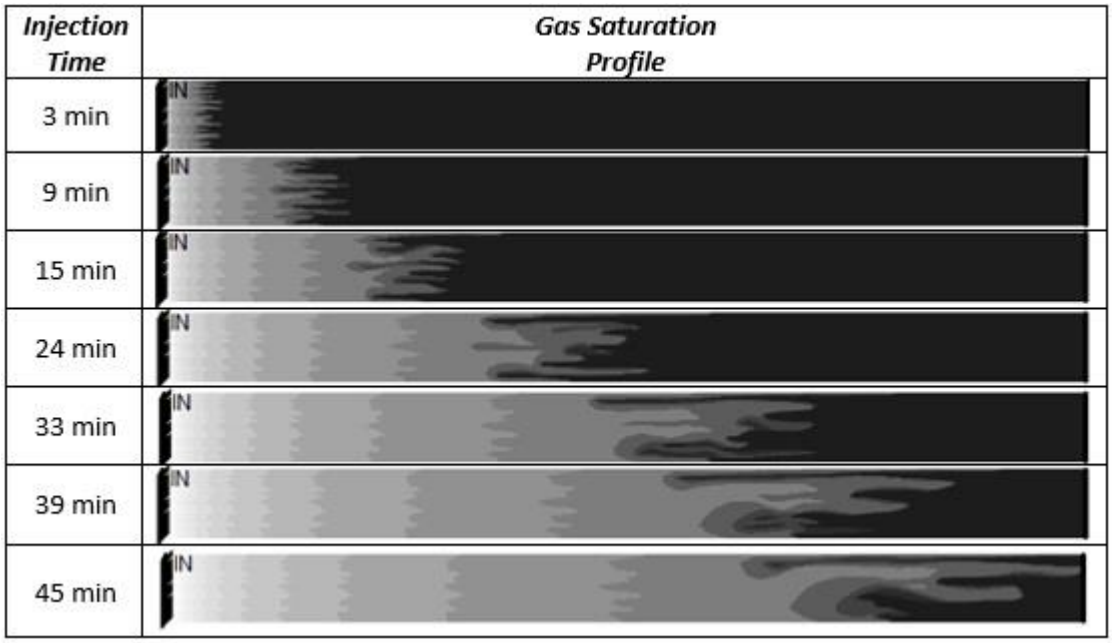

Figure 2-11: Gas saturation profiles showing the sequential evolution of the interface between gas and oil from the NCFE with viscosity ratio = 700.

The viscous fingering resulting from the simulations performed in this study show the 4 mechanisms of viscous fingering as enunciated before. The simulation of fingering using permeability distribution in standard reservoir simulators can be used to reproduce viscous instabilities for the standard core flood injections (Cuthiell et al. 2001; Cuthiell et al. 2006; Christie 1989). There are also other types of viscous fingering resulting from very high injection velocities, resulting in very complex dendritic patterns. Such type of experiments cannot be reproduced in simulators without proper mathematical equations to generate them. In this work, viscous fingering is being created in order to represent the typical coreflood conditions. The patterns created represent well the typical fronts seen by several other authors.

Figure 2-12 shows some examples of viscous fingering seen in core experiments by Pavone 1992, Brock & Orr Jr 1991, Malhotra et al. 2015 and the NCFE produced for viscosity ratio 700. It is clear that the simulated patterns have the same degree of complexity as the ones seen in their experiments.

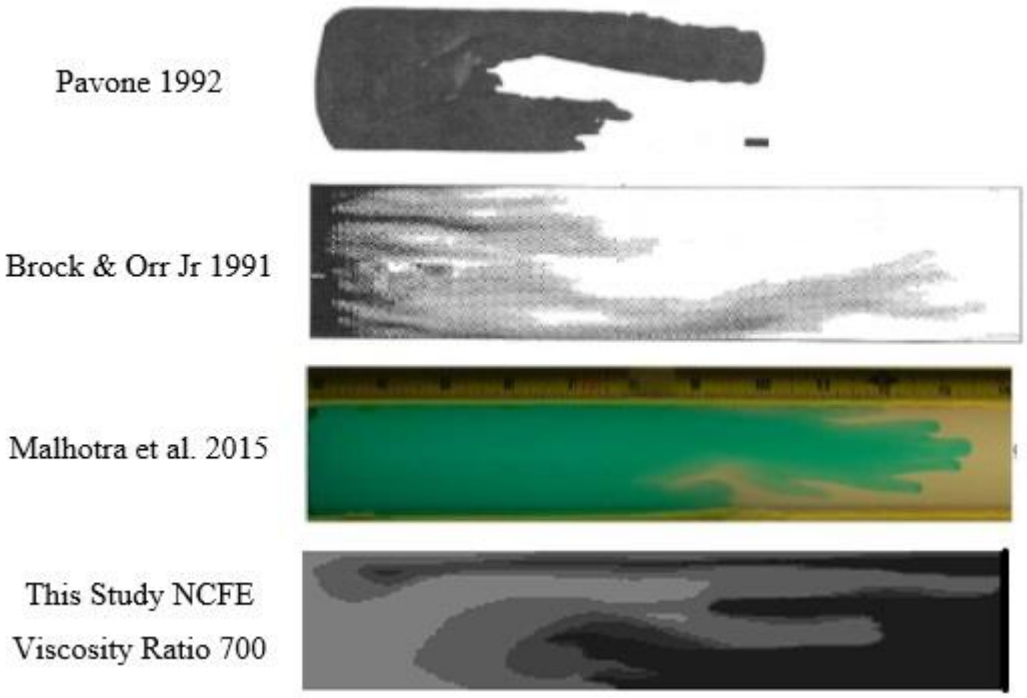

Figure 2-12:Comparison between experimental produced viscous fingering patterns from literature and the NCFE results from this study, showing the same type and complexity in the front.

The results of these NCFEs demonstrate that viscous fingering can be produced in typical simulators using the methods presented in the previous sections of this chapter. Also, it shows that the viscous fingering formation only occurs when the mobility is unfavourable.

2.4 Comparison of Synthetic Viscous Fingering Generation with Stability Models

In this Chapter, the general methodology for simulation of viscous fingering in common reservoir simulators was presented and it was shown that such simulations could generate stable or unstable patterns depending on the viscosity ratio of the experiment. However, to show that these NCFEs represent well the viscous instability formation, it is necessary to show that the viscous fingering formation obeys the laws of stability proposed by other authors. It has been proposed, in literature, a dimensionless number to predict the stability of the flow using several parameters like endpoint mobility ratio or the flow velocity. This

stability number was firstly proposed by Peters & Flock 1979 and later modified (and corrected) in Sarma & Bentsen 1987 work, and it consists in the comparison of the calculated stability number, I_{sr}, value with a thresholder value, which separates stable flows from unstable ones. In Sarma & Bentsen 1987 work, the stability threshold was defined as being equal to π^2, if I_{sr} is lower that this number then the flow is considered stable and unstable if I_{sr} is higher than π^2.

In this section, using the comparison of the value of I_{sr} with the saturation profiles generated in NCFEs, it will be shown that the threshold for viscous fingering formation obey very well the stability number proposed by Sarma & Bentsen 1987.

2.4.1 Methodology

For this section the same data as in Table 2-4 and the relative permeability from Figure 2-8 were used to produce different NCFEs. The stability number as defined by Sarma & Bentsen 1987 uses a parameter that requires the existence of a capillary pressure versus saturation curve. Since in the previous NCFEs capillary pressure was ignored, a curve had to be generated. Here, a Corey-Brooks correlation (Brooks & Corey 1966) was used to create a capillary pressure, by the following equation:

$$P_{cog} = \frac{c_o}{\left(\frac{S_o - S_{or}}{1 - S_{or}}\right)^{a_o}} \qquad \text{.....2-3}$$

Where P_{cog} is the gas-oil capillary pressure, c_o and a_o are constants, S_o is the oil saturation and S_{or} is the residual oil saturation. The capillary pressure versus saturation curve was generated using c_o = 0.1 kPa and a_o = 0.7, resulting in the curve presented in Figure 2-13.

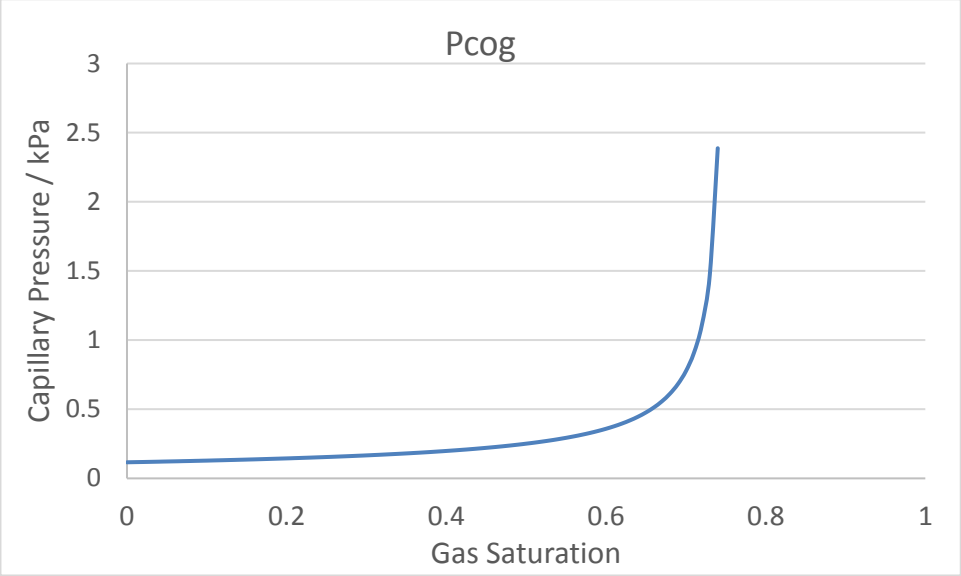

Figure 2-13: Gas-oil capillary pressure versus gas saturation curve used in the gas injection NCFEs.

In order to generate increasing instability from each subsequent NCFE, the gas viscosity was maintained at constant 0.05 mPa.s while the oil viscosity was changed in order to get a viscosity ratio (oil viscosity divided by gas viscosity) of 5, 10, 20, 50, 100, 300 and 700, totalizing 7 different NCFEs. Due to the difference in viscosity, it is expected some of the NCFEs will generate viscous fingering while others are stable.

Using this input data, the saturation profiles of the NCFEs were collected in order to visually access the stability of the front. The stability of each NCFE was compared with the prediction of stability using the stability number.

The stability number by Sarma & Bentsen 1987 is defined as I_{sr} in the following equations (presented in the Introduction Chapter):

$$I_{sr} = \frac{\mu_d v\left(M - 1 - N_g\right)}{k_{dor}\sigma_e} \frac{M^{5/3} + 1}{(M+1)\left(M^{1/3}+1\right)^2} \frac{4h^2b^2}{h^2+b^2} \leq \pi^2 \quad \text{.....1-5}$$

$$\sigma_e = \frac{A_c\phi(1 - S_{wi} - S_{or})}{2/\bar{r}_m} \quad \text{.....1-6}$$

$$N_g = \frac{\Delta\rho\ g\ k_{dor}\ Cos\ \alpha}{\mu_d v} \quad \text{.....1-7}$$

These equations were derived for a water/oil case and so it was adapted in this work for the general case ‘displacing fluid/oil’ so that it could represented both water and gas injections.

2.4.2 Results/Discussion

The value of the stability number for each NCFE was calculated using the input data and is presented in Table 2-5 with the stability prediction (flow is stable for $I_{sr} < \pi^2$), the NCFEs codename was generated by 'VR_' (meaning viscosity ratio) and the viscosity ratio value for that NCFE (e.g. for the NCFE with viscosity ratio of 100, the code name is VR_100). From Sarma & Bentsen 1987 I_{sr}, it is possible to say that up until viscosity ratio of 20 is expected a stable front for the NCFEs in study and for higher viscosity ratios fingering should form. For viscosity ratio of 20 the calculated value of I_{sr} is very close to the stability threshold, so it is predicted that small perturbation may be visible at the front of the displacement.

Table 2-5: Value of stability number estimated for each NCFE in study.

NCFE	*Isr*	*Stability Prediction*
VR_5	1.2	Stable
VR_10	3.5	Stable
VR_20	9.3	Stable (Near Threshold)
VR_50	32.5	Unstable
VR_100	82.2	Unstable
VR_300	350.5	Unstable
VR_700	1062.6	Unstable

The predictions from the stability number were compared with the gas saturation profiles from each NCFE in Figure 2-15. The core saturation profiles show the end-half of the core to facilitate comparison and all images were taken near the breakthrough time, where the fingering pattern is completely formed. Since different saturation ranges are presented depending on the viscosity ratio of the NCFE, the colour gradient was defined specifically to evaluate the front of the displacement, so the same shade of grey in different NCFEs may represent a different saturation range.

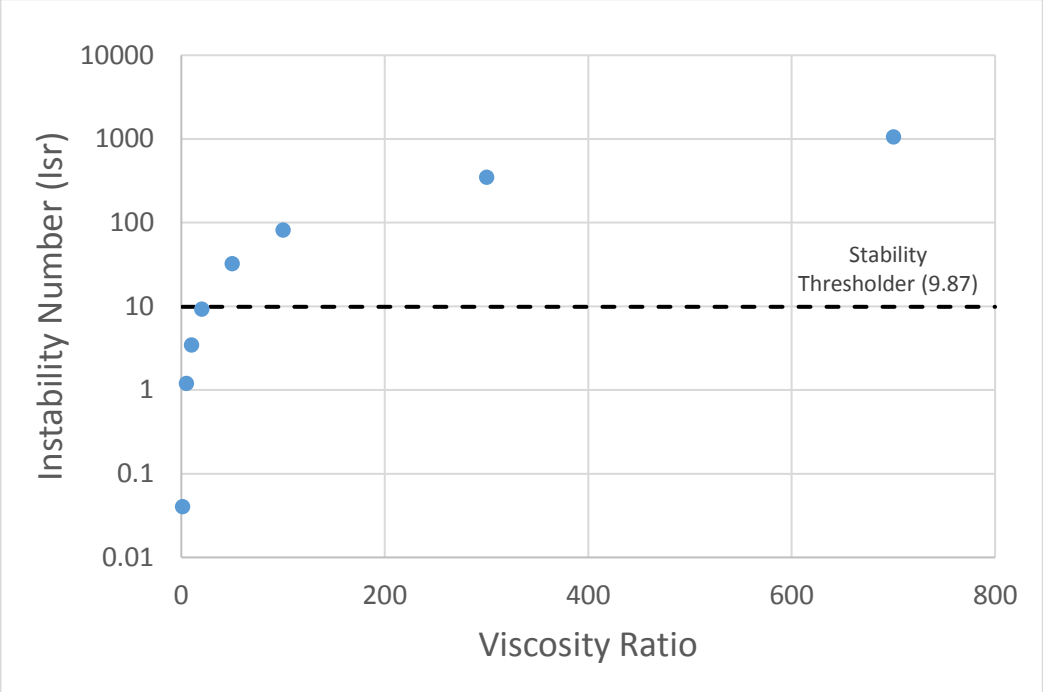

Figure 2-14: Variation of the stability number values with the viscosity ratio for the NCFEs in study, showing the cases with viscosity ratio of 50, 100, 300 and 700 above the stability threshold and therefore prone to have an unstable front.

NCFE	I_{sr}	*Gas Saturation Profile*
VR_5	1.2	
VR_10	3.4	
VR_20	9.3	
VR_50	32.5	
VR_100	82.2	
VR_300	350.5	
VR_700	1062.6	

Figure 2-15: Gas saturation profiles as obtained in the NCFEs against the calculated stability number, I_{sr}.

Figure 2-15 shows that the estimation from the stability number correlates very well with the results obtained in simulation. The NCFEs with low stability number (VR_5 and VR_10) present finger-free stable front. For viscosity ratio of 20 the calculated stability number was very close to the stability threshold (I_{sr} = 9.87), this fact resulted in some small perturbation at the front, where it can be seen two small and wide portions of gas progress faster than the rest. These portions are, nevertheless, very small and clearly mark the beginning of the fingering formation for subsequent NCFEs (with higher viscosity ratios), as is the case of VR_50, VR_100, VR_300 and VR_700. For these 4 cases viscous fingering forms at the front of displacement and the patterns get more complex as the viscosity ratio increases, resulting in thinner and longer fingers, consistent with more unstable flows.

From these results it seems acceptable to assume that the procedures to generate viscous fingering used in the NCFEs are in agreement with the stability models proposed by other authors in the literature. Since the work developed in this thesis was very focused in the use of numerical simulation (in the form of NCFE) to the viscous fingering phenomenon, this conclusion is very significant because it shows that the generated viscous instabilities respect the models validated against experimental data by other authors.

2.5 Conclusions

The following conclusion can be drawn for the methodology used to generate viscous fingering in simulation:

- In this thesis, Numerical Coreflood Experiments (NCFEs) were defined as coreflood experiments numerically generated using commercial simulators, using similar input data as the one used in the Centre for Enhanced Oil Recovery & CO_2 Solutions at Heriot-Watt University. These NCFEs have a big advantage against laboratory experiments, because it is possible to precisely define the uncertain parameters like relative permeability or capillary pressure, allowing the user to study the direct effect of these parameters in the production results. Also, NCFEs enable the production of a high amount of synthetic coreflood data in minimal time in comparison with laboratory corefloods that may take months to complete.
- Typical commercial simulators are not able to generate viscous fingering even in unfavourable mobility conditions. Triggering methods are then used to create enough differences between each grid block in order to generate viscous fingering. In this thesis permeability distribution was used in order to trigger the fingering

formation. Permeability distribution methodology consists in assigning a different value of absolute permeability to each grid block in the simulation following a Gaussian distribution. The degree of variance is very important to be able to generate viscous fingering while avoiding heterogeneity effects (which are undesirable because they would mask the viscous fingering influence in the flow). It was found that using a coefficient of variation of 10% is sufficient to generate viscous fingering and low enough to ensure homogeneity.

- Viscous fingering simulation results in very complex patterns. These patterns can only be fully captured using a high number of grid blocks (high resolution simulation) to avoid the effect of dispersion. Using a higher number of grids may result in more fingers generated, especially for very unstable flows. Nevertheless, there is a limit where the use of more grid blocks will not have significant impact in the production results, meaning that increasing the number of block after this limit only results in a higher simulation time. It was concluded that the optimal number of grid blocks was around 20.31 blocks/cm^2, so in all simulations performed throughout this thesis the number of grid blocks is always bigger than this value.
- The viscous fingering patterns generated by simulation were compared with those from experimental observation made by other authors. The simulation results present some of the main mechanisms of viscous fingering in coreflood: shielding, spreading, coalescence and tip splitting, representing well observations made by other authors. Some of this mechanism only happen when the mobility is very unfavourable, being completely non-existent in low viscosity ratio cases. This behaviour means that the physics of the fingering formation is being correctly captured by using the permeability distribution triggering method. Also the patterns generated in simulation were compared with patterns captured by core imaging in literature, concluding that they were very similar. In conclusion, using the methodology presented to generate fingering (with the appropriate triggering and simulation parameters like high resolution gridding) allows the complex patterns in simulation to be represented.
- Viscous fingering generation was evaluated to determine if the instability was being generated only in cases where the conditions were favourable for their formation. Using a stability model from literature called stability number, I_{sr}, developed by Sarma & Bentsen 1987, it was proved that fingering only forms, in

these work simulations, if the value of I_{sr} is beyond the stability threshold, obeying their stability model. This gives validity to the methodology used to simulate viscous fingering, proving that viscous fingering will only form if the conditions are just right.

Chapter 3: Created Unstable Numerical Coreflood Experiments

3.1 Simulation Software

This chapter presents the numerical coreflood experiments (NCFEs) used through this thesis, along with an analysis of the data obtained. The NCFEs were performed using commercially available software from Computer Modelling Group, CMG. All results were produced using either CMG-IMEX (black-oil simulator) or CMOST (history matching tool). IMEX was used to produce all the NCFEs, while CMOST was used to produce 2D history matching.

Additionally, in-house software, 3RPSim, was used to do 1D history matching, for its simplicity and matching speed. 3RPSim is a tool which uses a genetic algorithm in order to estimate the relative permeability. Using ECLIPSE software, it recreates the experimental observed data until the error between simulation and experimental data is smaller than the defined objective function.

3.2 NCFEs Description

3.2.1 Independent Numerical Coreflood Experiments

A series of unfavourable mobility numerical coreflood experiments were created in order to be used in relative permeability estimation methods later in this work. For these simulations it was important to have a high variety of core proprieties (like different absolute permeability, porosity, connate water), fluid proprieties (viscosities) and injection scenarios (injection rate, injection fluid, etc), in order to be able to validate relative permeability estimation methods in different conditions, showing that they are not case dependent. These NCFEs cannot be used for comparison between each other, (for example, for comparison of instability formation) because many variables are changed from simulation to simulation.

A set of 9 independent NCFEs were created for this propose. This 9 NCFEs were produced in 2 hypothetical cores that mimic the core dimensions used at Heriot Watt's 'Centre for Enhanced Oil Recovery and CO_2', 1 core with 60.5 cm length and another with 30.25 cm. The diameter in both cores was the same: 5.08 cm. From these 2 cores, 6 NCFEs were created to represent gas injections into oil filled cores and 3 NCFEs representing water injections into oil filled cores. Various properties were then changed in order to create the different NCFEs. Table 3-1 and Table 3-2 show the core and fluid

proprieties used for each NCFE, where *Soi* is the initial oil saturation, *Swc* the connate (immobile) water, *L* the length of the core, *PV* the total pore volume and *Kabs* the mean absolute permeability of the core.

Table 3-1: Core properties used in each for the 9 NCFEs.

NCFE Name	Soi	Swc	L (cm)	Porosity (frac)	PV (cm3)	Pressure (KPa)	Kabs (mD)
NCFE_1	0.82	0.18	60.50	0.20	245	12000	65
NCFE_2	1.00	0.00	30.25	0.20	122	10300	80
NCFE_3	0.80	0.20	60.50	0.19	233	10300	125
NCFE_4	0.85	0.15	60.50	0.15	184	10300	40
NCFE_5	0.85	0.15	30.25	0.15	92	10300	5000
NCFE_6	0.70	0.30	30.25	0.40	245	9700	300
NCFE_7	0.85	0.15	60.50	0.18	220	11000	60
NCFE_8	0.87	0.13	30.25	0.40	245	10340	4500
NCFE_9	1.00	0.00	30.25	0.15	92	10300	80

Table 3-2: Fluid properties and injection scheme for the 9 NCFEs.

NCFE Name	Inj. Scheme	Qi (cm/min)	oil visc (mPa.s)	gas visc (mPa.s)	water visc (mPa.s)
NCFE_1	Gas-Oil	0.10	35	0.05	-
NCFE_2	Gas-Oil	0.30	40	0.04	-
NCFE_3	Gas-Oil	0.20	21	0.07	-
NCFE_4	Gas-Oil	0.20	15	0.06	-
NCFE_5	Gas-Oil	0.20	5	0.05	-
NCFE_6	Gas-Oil	0.30	100	0.06	-
NCFE_7	Water-Oil	0.20	300	-	0.5
NCFE_8	Water-Oil	0.17	200	-	0.7
NCFE_9	Water-Oil	0.30	500	-	0.5

Capillary pressure was ignored (Pc = 0) for all the NCFEs and mass transfer was also defined as not occurring. For each NCFE a relative permeability was created using the method by Sigmund & McCaffery 1979. Figure 3-1 to Figure 3-9 show the relative permeability curves produced, by their method, for NCFE 1 to 9, respectively. The relative permeability curves vary in a different array of curvature and endpoints in order to make these NCFEs as widely different as possible from each other in order to be representative of completely different experiments that could have been performed in a laboratory. These *kr* curves will be accepted from here on as the 'real' curves for the corresponding NCFE. In this way, error from relative permeability estimation methods may be quantified with certainty, instead of using production data and differential

pressure (as it is used in laboratories) to evaluate the precision of estimation (which may be erroneous, due to the impossibility to account for every possible aspect of a laboratory coreflood experiment).

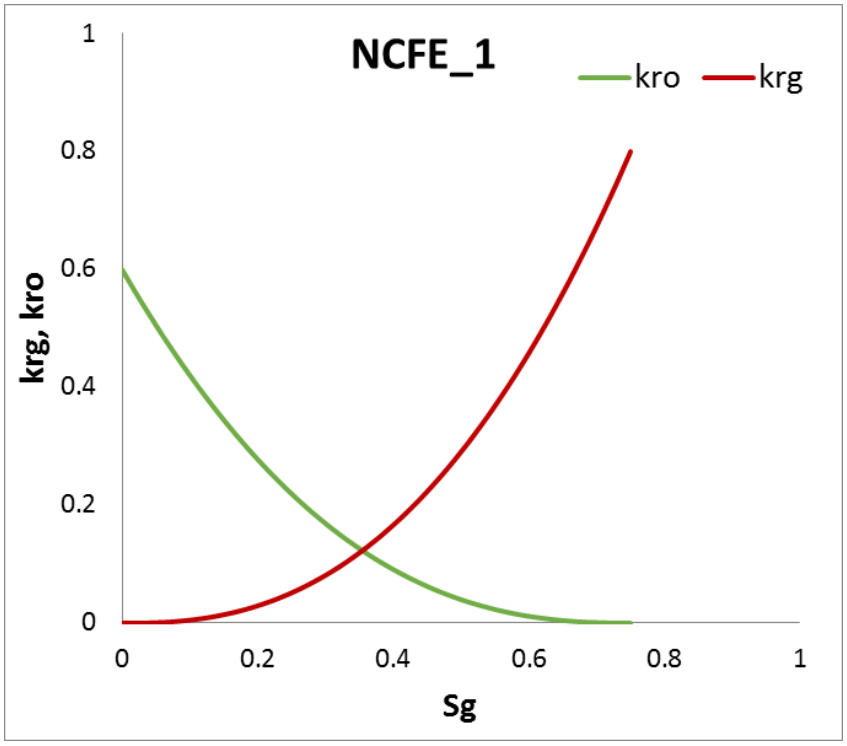

Figure 3-1: Relative Permeability as generated using Sigmund & McCaffery 1979 *method for NCFE_1.*

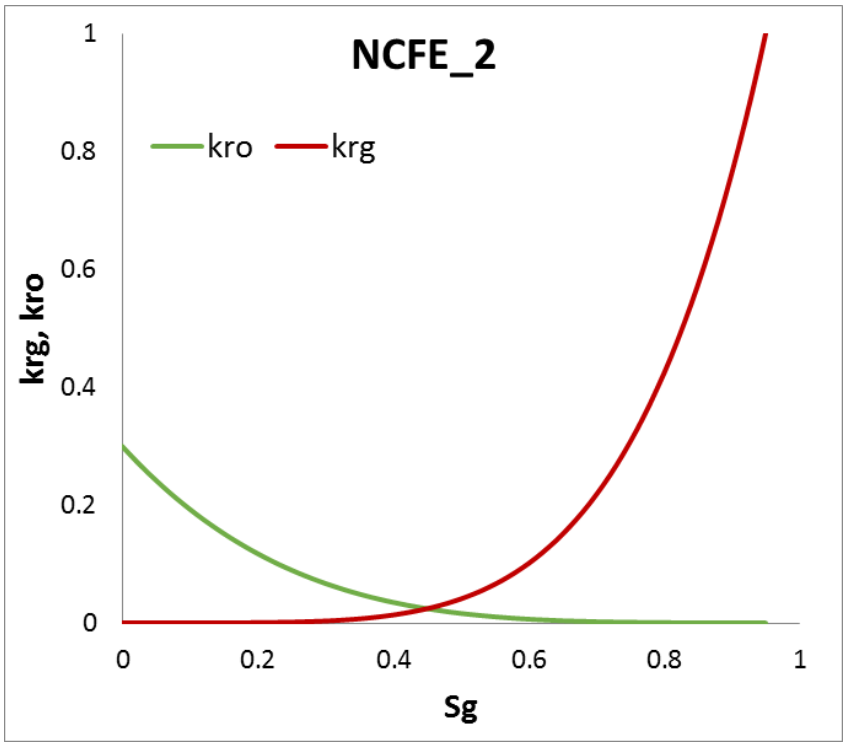

Figure 3-2: Relative Permeability as generated using Sigmund & McCaffery 1979 *method for NCFE_2.*

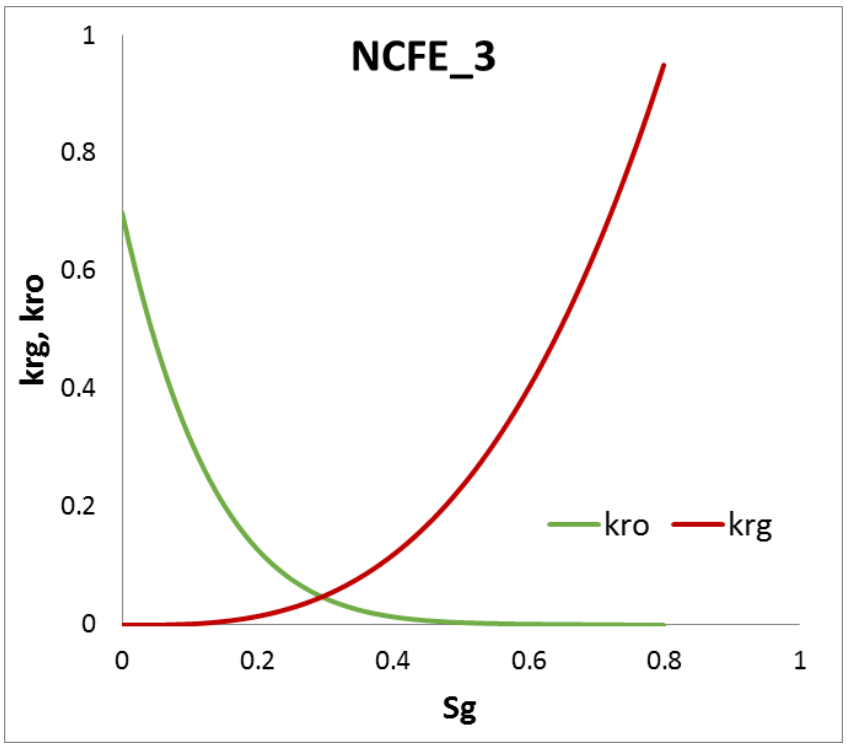

Figure 3-3: Relative Permeability as generated using Sigmund & McCaffery 1979 *method for NCFE_3.*

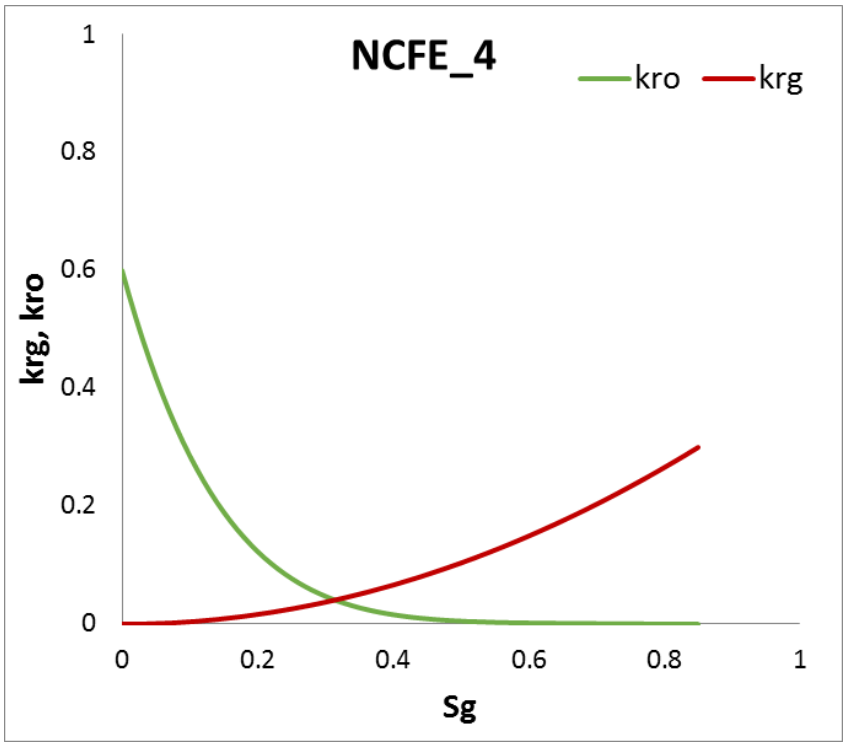

Figure 3-4: Relative Permeability as generated using Sigmund & McCaffery 1979 *method for NCFE_4.*

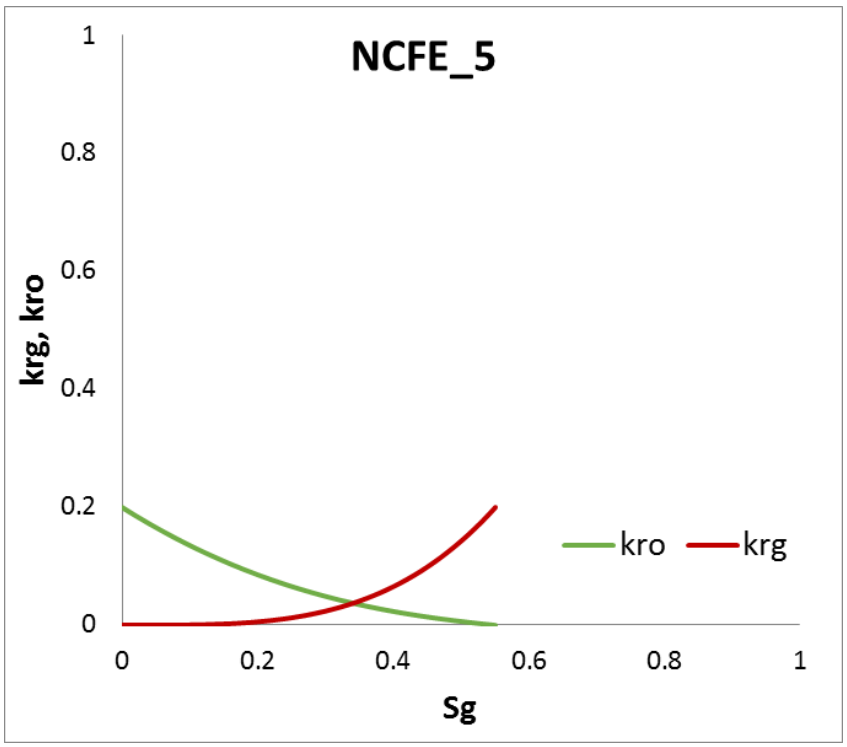

Figure 3-5: Relative Permeability as generated using Sigmund & McCaffery 1979 *method for NCFE_5.*

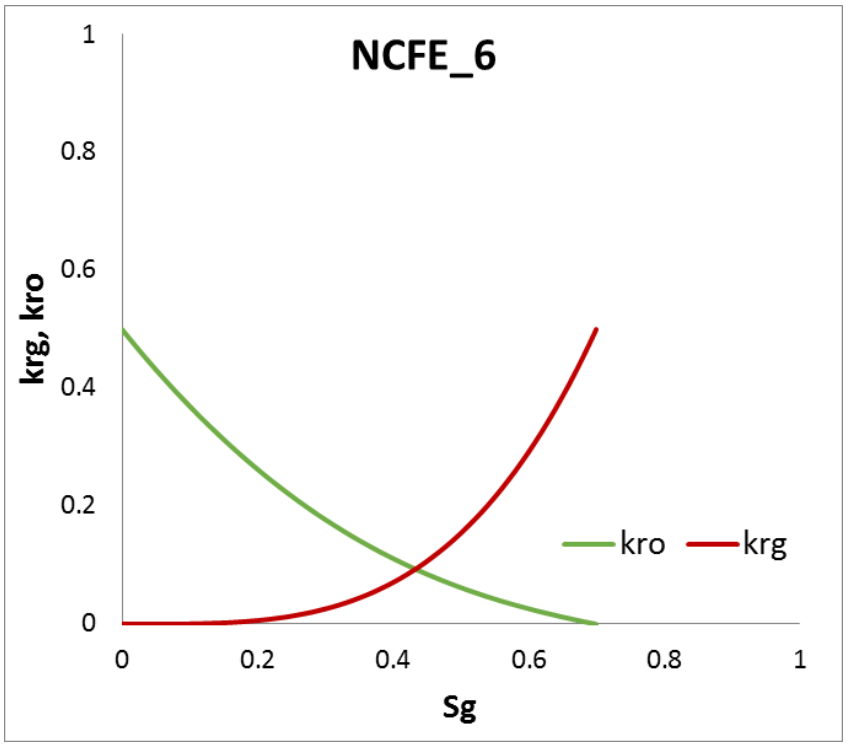

Figure 3-6: Relative Permeability as generated using Sigmund & McCaffery 1979 *method for NCFE_6.*

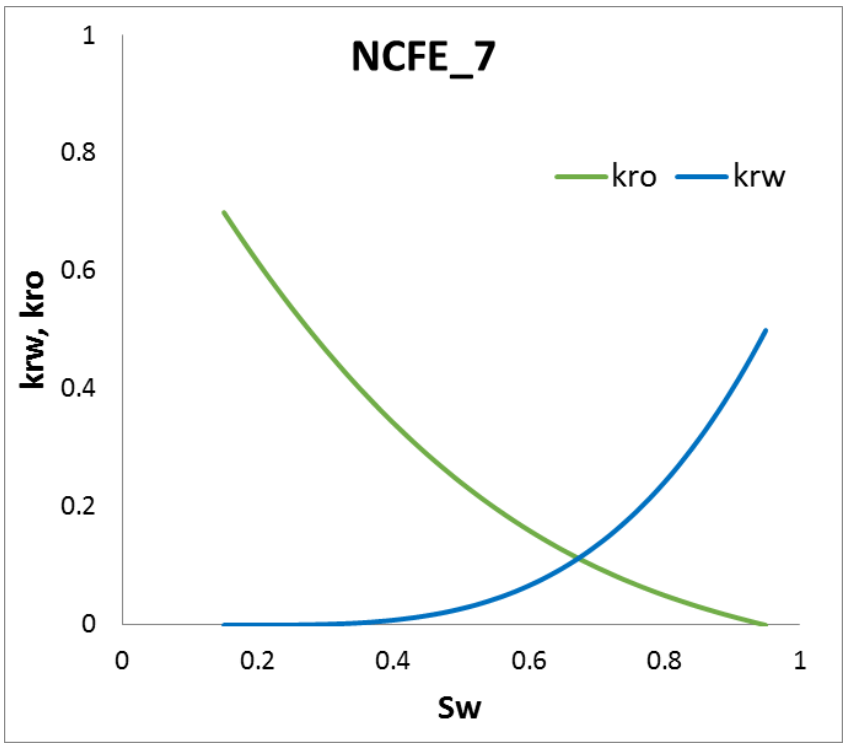

Figure 3-7: Relative Permeability as generated using Sigmund & McCaffery 1979 *method for NCFE_7.*

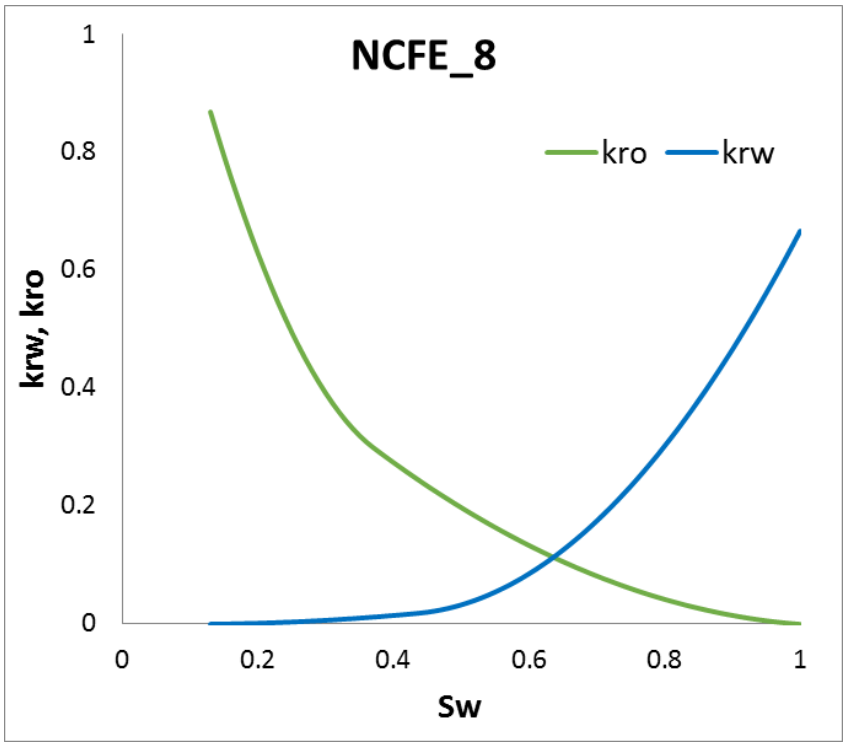

Figure 3-8: Relative Permeability as generated using Sigmund & McCaffery 1979 *method for NCFE_8.*

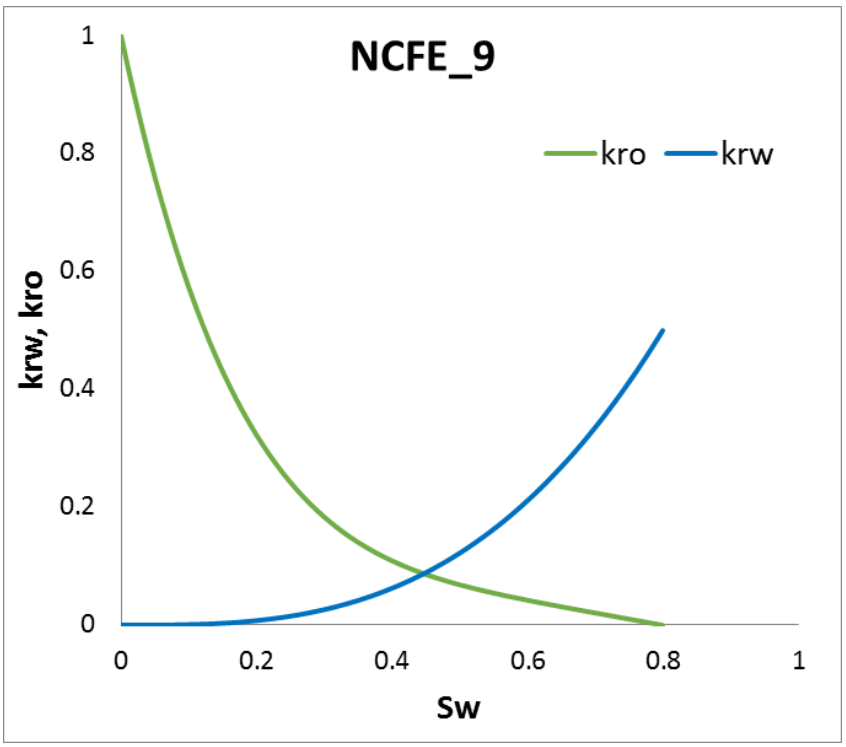

Figure 3-9: Relative Permeability as generated using Sigmund & McCaffery 1979 *method for NCFE_9.*

These 9 NCFEs were then used in CMG-IMEX (black-oil) simulator, using all the necessary alterations and options needed to correctly generate viscous fingering, presented in Chapter 2 (permeability distribution, number of grid blocks, etc). Since this work focus on the estimation of relative permeability curves, the most important parameters to the estimation of these curves were gathered: cumulative oil production, differential pressure and saturation profiles.

In Figure 3-10 are presented the oil saturation profiles gathered from each simulation of the 9 NCFEs. All saturation images were taken near the breakthrough time, where the fingering pattern is completely formed. Also, different saturation ranges are presented, since, depending on the viscosity ratio of the NCFE, the colour gradient was defined specifically to evaluate the front of the displacement, so the same colour in different NCFEs may represent a different saturation range.

From the oil saturation images is undoubtedly noticed that viscous fingering happens for all NCFE with exception of NCFE_8. Although the viscosity ratio of NCFE_8 is unfavourable for a stable displacement, the relative permeability that was imposed plays a major role and does not allow fingering to form. Since each NCFE was created from different parameters it is not possible to compare the degree of instability between

experiments, but it can be safely concluded that each experiment has generated completely different patterns at the front of displacement.

Sim.	***Oil Saturation Profile***
NCFE_1	
NCFE_2	
NCFE_3	
NCFE_4	
NCFE_5	
NCFE_6	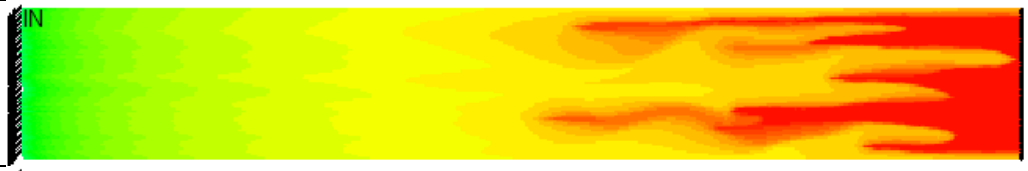
NCFE_7	
NCFE_8	
NCFE_9	

Figure 3-10: Oil saturation profiles resulting of each NCFE simulation.

3.2.2 Effect of Increasing Viscous Instability in Relative Permeability Estimation

In the previous section, independent unstable NCFEs were created in order to investigate the precision of relative permeability estimation methods in terms of case specificity. Nevertheless, it is important to study the precision of such methods in terms of stability severity. In other words, the objective is to maintain all parameters the same except the mobility of the fluids in order to have incremental increase in instability.

Viscosity ratio has a very important role in the formation of viscous fingering. Normally viscous fingering have a tendency to form when the endpoint mobility ratio is higher than 1:

$$\frac{k_{rd}/\mu_d}{k_{ro}/\mu_o} > 1 \qquad 3\text{-}1$$

Where k_{rd} is the relative permeability of the displacing fluid, k_{ro} the relative permeability of the oil, μ_d and μ_o the viscosity of the displacing fluid and the oil, respectively. This means that the mobility of the displacing fluid is higher than the mobility of the oil and there will be a tendency for the displacing fluid to finger through the more viscous displaced fluid. Rearranging the above equation to separate the viscosities from the permeabilities the following equation is obtained:

$$\frac{k_{rd}}{k_{ro}}\frac{\mu_d}{\mu_d} > 1 \qquad 3\text{-}2$$

The term 'viscosity ratio' is normally referred to the ratio of the viscosity of the displaced fluid over the viscosity of the displacing fluid. As the viscosity ratio increases the mobility ratio also increases in a directly proportional way, it is then expected for the fingering severity to increase with higher viscosity ratios.

Consequently, it was decided to perform a number of Numerical Core Flood Experiments (NCFE) which will be used later in this thesis to study the influence of increasing viscosity ratio in the different k_r estimation methods. By performing NCFE using a set of fixed rock properties but different viscosity ratios, the direct influence of fingering in the estimated k_r curves may be studied, by comparing the input k_r in simulation with the one obtained from estimation. It is expected that for a method based in and deduced with the presumption of stable flow, it will have increasing error on the relative permeability curves when the viscosity ratio increases.

Two of the previously presented numerical experiments, NCFE_1 and NCFE_2, were chosen to create the new sets of experiments. NCFE_1_VR is the name of the set based on the properties of NCFE_1. This set consists of 8 NCFEs with the same properties as NCFE_1 except the viscosity of the oil, which was changed in other to establish different viscosity ratios (and mobility) for the fluids in the coreflood. The oil viscosity was

changed in order to achieve 1500, 700, 300, 100, 50, 20, 10 and 5 viscosity ratios, one attributed to each NCFE within the set.

NCFE_2_VR is the name of the set of numerical experiments based on NCFE_2. This set consists of 9 NCFEs with the same properties as NCFE_1, except the oil viscosity, obtaining viscosity ratios of 1000, 800, 500, 300, 250, 200, 150, 100 and 20.

All NCFEs were then simulated using the CMG – IMEX Black-oil simulator in 2D models using the methodology described in Chapter 2 to trigger the viscous fingering (high resolution grid, permeability distribution). Capillary pressure, gravity and mass transfer were ignored for all the NCFEs.

Figure 3-11 and Figure 3-12 show the saturation profiles from the simulation of each the NCFEs from NCFE_1_VR and NCFE_2_VR sets, respectively. Figure 3-11 core images were cut in half in other to facilitate the comparison between each case, since the core was 2 feet long and it would be difficult to compare the results maintaining the same aspect ratio.

The oil saturation profiles show a clear evolution of the viscous fingering from case with lower viscosity ratio to the higher one. The viscous fingering number, thickness, length and shape (wave or straight) change with mobility difference of the flow. Both sets start with a stable coreflood, which is important because it helps to mark the limit of stability of the flows. Then viscous fingering forms, initially in low number of wide fingers, all travelling together towards the outlet. As the flow progresses the shielding mechanism appears and some fingers start to travel faster than adjacent fingers, leaving considerably more oil behind. Also, fingers become narrower and longer. At the higher viscosity ratio cases (especially for NCFE_1_VR set) the 4 main mechanism of viscous fingering are present: Shielding, Spreading, Coalescence and Tip Splitting, resulting in a full developed fingering profile.

These two sets of NCFEs will be extremely valuable for the subsequent sections of this thesis, since they show the progress from stability to full grown fingers in the same base case. They also have the advantage of being comparable within the same set, which allows the study of possible correlations between instability and relative permeability estimation precision.

Viscosity Ratio	***Oil Saturation Profile NCFE_1_VR***
5	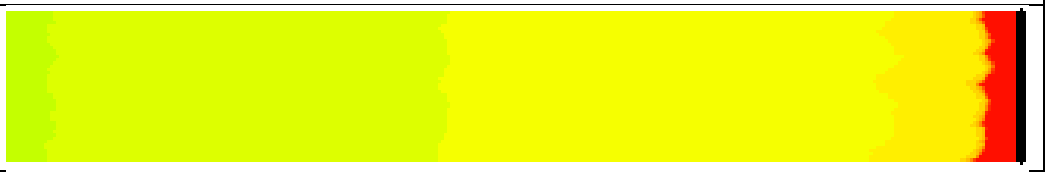
10	
20	
50	
100	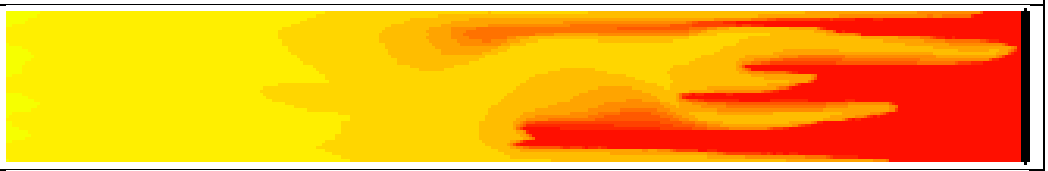
300	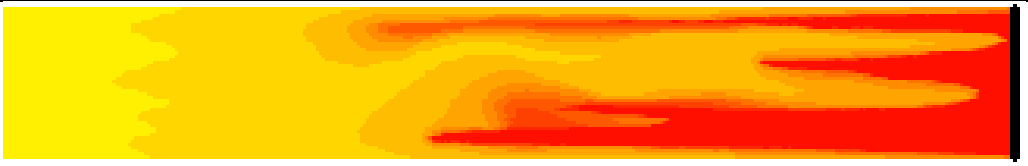
700	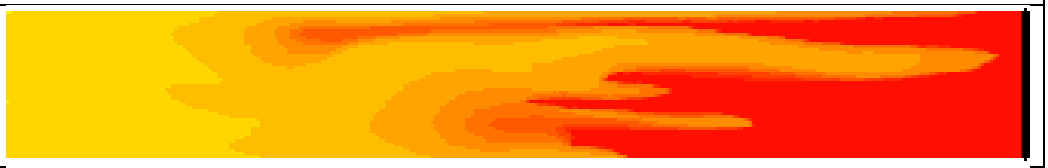
1500	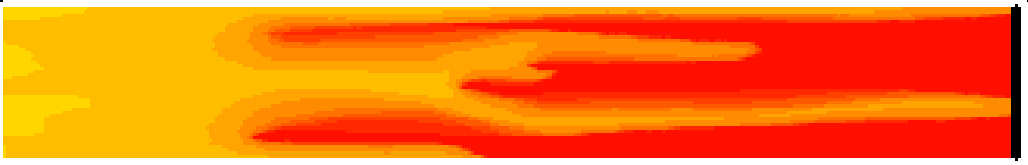

Figure 3-11: Oil saturation profiles resulting of each NCFE simulation in NCFE_1_VR set.

Viscosity Ratio	Oil Saturation Profile NCFE_2_VR
20	
100	
150	
200	
250	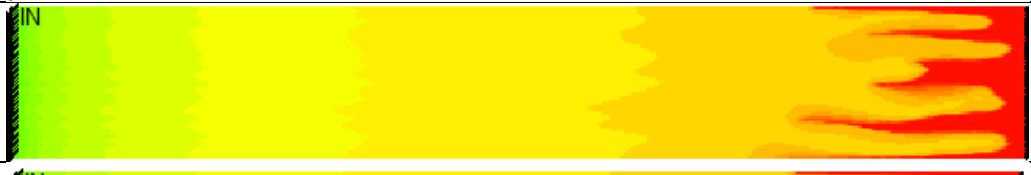
300	
500	
800	
1000	

Figure 3-12: Oil saturation profiles resulting of each NCFE simulation in NCFE_2_VR set.

Chapter 4: Evaluation of Existing Relative Permeability Estimation Methods for Unfavourable Mobility Corefloods

4.1 Introduction

The two main methods to calculate the relative permeability in laboratory experiments are the steady-state and unsteady-state methods.

The steady-state method, consists in the injection of all the fluids, at given proportions, until the equilibrium is obtained (i.e. the fluids inflow and outflow are the same). At that point, the relative permeability of each fluid for the corresponding saturation can be estimated, using Darcy's law in the following manner:

$$k_{ri} = \frac{q_i \mu_i L}{kA\Delta P} \quad \text{..... 4-1}$$

Where k_{ri} is the relative permeability, μ_i the viscosity and q_i the flow rate for phase i; ΔP is the differential pressure, A the cross-sectional area and L the length of the core. To estimate another value of relative permeability for another saturation, a new injection must be performed (e.g. the inflow proportions of each fluid are changed). Steady-state method may take a very long time to perform and have a higher cost than unsteady-state methods.

In the unsteady-state methods, one fluid is injected into a core, displacing the resident fluid phases. In these methods, the relative permeability may be obtained by either explicit or implicit methods. JBN method (Johnson et al. 1959) is the most common of the explicit methods. JBN uses the production data and differential pressure along with the core and fluid data from the experiment to estimate the relative permeability. The biggest disadvantage of JBN is that it cannot take capillary pressure into account. In implicit or parameter estimation computations (Bard 1974), the relative permeability is estimated by optimization so that the difference between the measured values and the simulated values is below the appointed acceptable error. This optimization is performed by changing certain tuning parameters, that will result in relative permeability at each iteration. These relative permeabilities are then tested against the measured production data and differential pressure of the experiment, until one result in an error that is less the acceptable minimum.

In this section, implicit (1D history matching) and explicit (JBN method) relative permeability estimation methods are going to be evaluated in coreflood experiments with unfavourable mobility. Evaluation of relative permeability methods is commonly done by using the estimated relative permeability curves in simulators to compare the production data (e.g. oil production, differential pressure, etc) resulted from these estimated curves with the experimental observations. However, such comparisons may lead to wrong conclusions if the simulations cannot depict correctly the experimental cases. This is especially important when instability occurs. Describing the patterns of flow in simulation may be very challenging if the flow does not have a perfectly stable front, so in cases with viscous fingering, for example, it would be necessary the use of extra laboratory equipment (saturation pattern measuring, like core imaging) and the inclusion of such information in multidimensional simulation, 2D or 3D, instead of simple one-dimension simulation.

In this chapter the use of NCFEs is proposed, where the relative permeability curves may be very well defined, since the user may choose which relative permeability curve to use in each experiment. Using this numerical experiments, analytical JBN and 1D history matching estimation relative permeability methods were evaluated against the 'real' relative permeability curves, giving insight on the amount of error instabilities may produce in the standard methods. The objectives for this Chapter are summarized below:

- Quantify the amount of error involved in using JBN or 1D history matching methods applied in viscous unstable flows.
- Enhance the understanding of viscous fingering influence in relative permeability estimation, identifying key parameters that could be used to reduce error.

4.2 Novel Methodology for Determination of k_r Estimation Methods' Precision

The error produced by a certain relative permeability estimation method may be easily obtained by comparison of the calculated with the reliable relative permeability for the same coreflood experiment. However, obtaining a reliable relative permeability curve is very challenging. The majority of relative permeability curves produced from unsteady-state methods do not consider instability, since it is mathematically challenging to reproduce the patterns, most laboratories use 1D history matching or analytical methods like JBN.

Getting a reliable relative permeability from an unsteady-state experiment involves the use of specific laboratory equipment, in this case core imaging. Core imaging will output

the saturation profiles along the core at different points in time. Using such profiles in history matching (in conjunction with the typical production data and differential pressure) may tackle the viscous fingering issue, if the simulator has an appropriate triggering method and enough grid blocks to avoid numerical dispersion. Also, 1D is (obviously) not enough and 2D or 3D simulation must be used. This type of analysis is very complex and it may take considerable time to set up the appropriate simulation and find an acceptable result.

Steady-state experiments may be used to find very reliable relative permeability curves, but they take a very long time to run, especially in cases with high viscosity contrast where the amount of time necessary to reach equilibrium is significant, curiously, these are exactly the experiments that are more 'vulnerable' to viscous fingering.

In this work a novel methodology was devised in order to investigate the precision of relative permeability estimation methods. NCFEs are numerically generated coreflood experiments that were constructed using typical core and fluid properties. The relative permeability curves of these experiments were created using known relative permeability correlations, consisting of the real relative permeability curves for those experiments. This enables the use of these curves for error estimation. Also, in NCFEs it is possible to have control over effects that could influence the results and lead to the wrong conclusions, like gravity segregation and capillary pressure.

Figure 4-1 summarizes the methodology steps followed in order to evaluate the precision of JBN and 1D history matching (1D HM) in cases with viscous fingering formation. The first steps of the methodology used are the selection of the desired core, fluid data and the creation of the relative permeability curve. The relative permeability is created using a standard correlation from the literature like Brooks & Corey 1966 or Sigmund & McCaffery 1979, in this work the latter was chosen because it has more degrees of freedom (additional constants allow a wider range of curvatures of the relative permeabilities). This relative permeability is the 'real' result for error estimation purposes. Then, a commercial simulator (in this case CMG-IMEX) is used to obtain the production data and differential pressure from the respective NCFE. It is important to select the appropriate simulation conditions in this step depending on what is the objective. For example, in order to trigger viscous fingering high resolution gridding and triggering methods have to be used as explained previously in Chapter 2. The simulation results are then used in the method of study, e.g. JBN or 1D HM, resulting in the estimated relative permeability curves for that NCFE: 'Calculated Relative Permeability Curves'.

The last step is to calculate the precision of the method of study by calculation of the error. In the case of JBN, this method is very sensitive to pressure differences in the simulation/experiment, so the resulting relative permeability will be formed of various points that will not perfectly fit a curve. The standard practice is to fit a relative permeability correlation to the results of the JBN estimation. In this work Sigmund & McCaffery 1979 correlation was chosen for consistency proposes, since the same correlation was used to create the relative permeabilities for the NCFEs. Figure 4-2 is an example of the fitting curves used to match the relative permeability curves calculated from JBN. 1D HM does not need such fitting, since the history matching software has rules in order to have smooth curve fitting with a polynomial equation.

Another common problem of unsteady-state estimation method is that the valid saturation range of the resulting relative permeability curves is limited to the time after breakthrough until the end of the experiment. The example in Figure 4-2 had an early breakthrough with 0.09 gas saturation at the outlet surface and the experiment finished at approximately 0.26 gas saturation at the outlet, so for this case the valid range of estimation is between 0.09 and 0.26. Inside the valid saturation range is the relative permeability points that are reliable in the method used. There is no unsteady-state method that would give relative permeability curves before the breakthrough, because 2-phase flow is only happening at the outlet of the core (where the permeabilities are measured) after this time.

Using a correlation like the one from Sigmund & McCaffery 1979 allows extrapolation of the curve beyond the valid range, allowing it to have some prediction of what the values are. This is visible in Figure 4-2 where the curves where extrapolated for before the breakthrough, using the known oil endpoint. In the case of a laboratory experiment the endpoint of oil may be determined at the very beginning of the displacement, where almost all the moving fluid inside the core is oil. At that point in time, using Darcy equation for oil flow and solving it in order to the relative permeability of oil will give a good approximation of the oil endpoint k_r. In this work the use of NCFEs allows finding the oil k_r endpoint, just by looking at the relative permeability used.

The error calculation between the JBN or 1D HM predictions and the 'real' k_r curves is calculated using the mean absolute percentage error (MAPE) in the valid saturation zone:

$$Mean\ Percentage\ Absolute\ Error\ (MAPE) = \sum_{i=1}^{n} \left| \frac{y_i - \hat{y}_i}{\hat{y}_i} \right| \times \frac{100}{n} \qquad 4\text{-}2$$

Where:

y_i = estimated (calculated) k_r value for sample displacing fluid saturation,

$\hat{y}_i$ = real k_r value for sample displacing fluid saturation,

i = current sample (each sample corresponds to a displacing fluid saturation value),

n = total number of samples.

The described methodology was used in the NCFEs presented (in detail) in Chapter 3, namely NCFE_1 to NCFE_9. The core and fluid properties are presented in Table 3-1 and Table 3-2 and the respective relative permeability curves in Figure 3-1 to Figure 3-9.

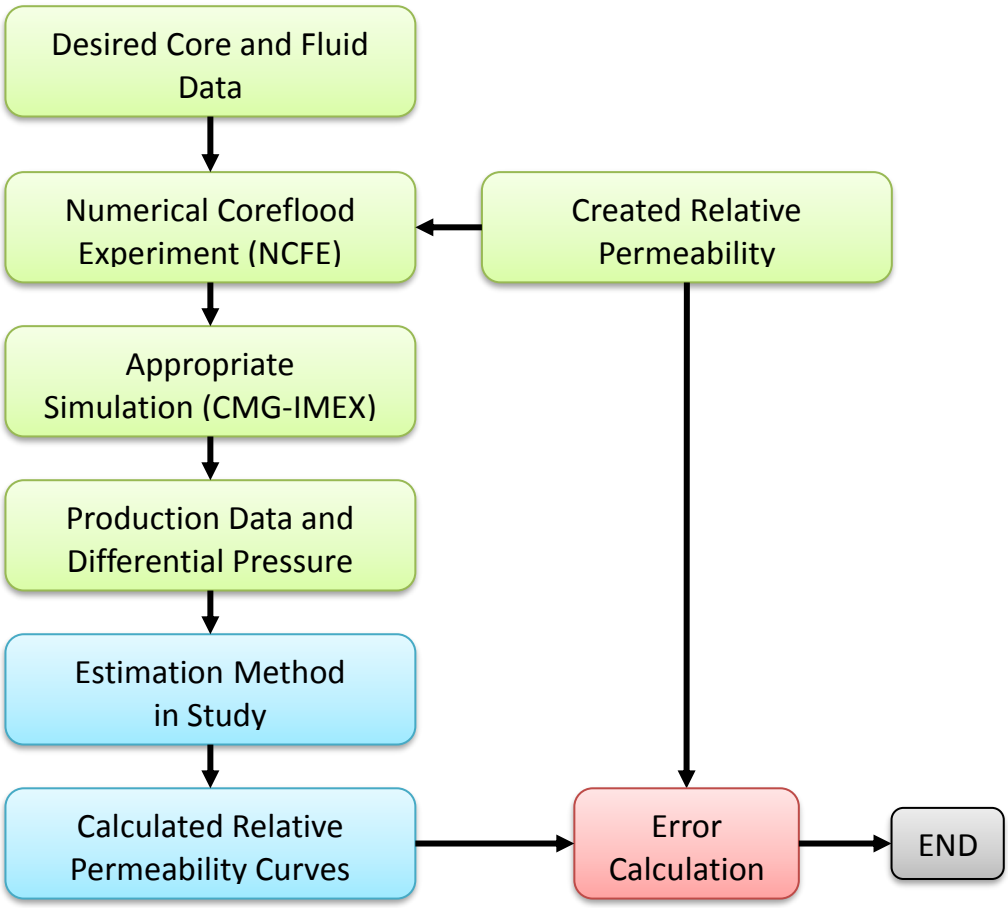

Figure 4-1: Algorithm of the methodology used to evaluate the precision of k_r estimation methods.

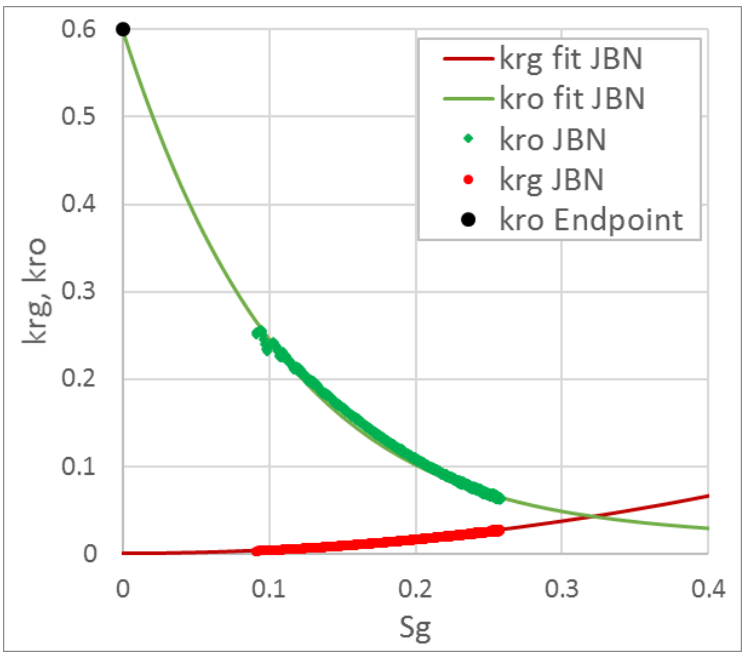

Figure 4-2: Example of fitting curves for the JBN method using Sigmund and McCaffery correlation for the fit.

4.3 JBN Method

In 1957 E. F. Johnson, D. P. Bossler and V. O. Naumann proposed an analytical method for estimating the relative permeability curves using the injection and production data of a core flood experiment (Johnson et al. 1959). This method (known as JBN method) used the Welge (1952) mathematically derived equations to find a relationship between the fractional flow of oil, and the k_{ro} and k_{rd} equations, Equations 4-3 to 4-8.

$$S_{d,avg} = S_{d,i} + \frac{N_p}{PV} \quad 4\text{-}3$$

$$f_o = \frac{dS_{d,avg}}{dD_i} \quad 4\text{-}4$$

$$S_{d,out} = S_{d,avg} - D_i \times f_o \quad 4\text{-}5$$

$$I_r = \frac{\Delta P}{\Delta P_i} \quad 4\text{-}6$$

$$k_{ro\ JBN} = k_{ro}^0 \frac{f_o \times d\left(\frac{1}{D_i}\right)}{d\left(\frac{1}{D_i I_r}\right)} \quad 4\text{-}7$$

$$k_{rd\ JBN} = \frac{(1-f_o)}{f_o}\frac{\mu_d}{\mu_o}k_{ro} \quad 4\text{-}8$$

Where:

f_o = fractional flow of oil, at the outlet of the core,

$S_{d,avg}$= average saturation of the displacing fluid inside the core,

N_p = cumulative oil produced,

PV = core pore volume,

Di = cumulative displacing fluid injected (fractional of total pore volume),

$S_{d,out}$= saturation of displacing fluid leaving the core (in the outlet face of the core),

I_r = relative injectivity, as defined by Eq. 4-6,

u = average velocity of the fluid entering the core (Flowrate / Area),

ΔP = differential pressure across the core,

ΔP_i = initial differential pressure (at the start of injection),

$k_{ro\ JBN}$ = relative permeability to oil by JBN method,

$k_{rd\ JBN}$ = relative permeability of the displacing fluid by JBN method.

μ_d = displacing fluid viscosity,

μ_o = oil viscosity.

In the original paper by Johnson et al. 1959 the relative permeabilities are relative to the total permeability defined by the authors as the relative permeability to oil at initial conditions, with initial water saturation (irreducible water) present in the core $k_{ro} = k_o/k_{o@Swirr}$, rather than the current standard method of dividing k_o by the absolute permeability i.e., $k_{ro} = k_o/k$. Jones & Roszelle 1978 pointed to this fact and suggested to divide JBN's k_{ro} by the factor $k/k_{o@Swirr}$ to represent the relative permeability to oil making the resulting k_{ro} values comparable, both on the basis of the JBN method.

When the displacing fluid is injected in the core, the initial water saturation is equal to its irreducible saturation, $S_{wi} = S_{wirr}$. Following Jones & Roszelle 1978 suggestion, the k_{ro} derived by the JBN method, i.e. k_{roJBN}, is multiplied by the term $k_{o@Swirr}/k$ to obtain the standard k_{ro} as in this work. Here $k_{o@Swirr}/k$ is the permeability to oil at irreducible water saturation. This value is obtained using the very initial oil flow-rate at the core outlet (when a very small amount of displacing fluid is injected). In this report, the term '$k_{o@Swirr}/k$' is referred to as the 'end-point k_{ro}', and is denoted by k_{ro}^0, as in Equation 4-7. In this study, $S_{wirr} = 0$ is sometimes used and other times a small positive value. When $S_{wirr} = 0$, the term k_{ro}^0 will be equal to 1.

The method provides convenient means for calculating the relative permeability curves from oil production and total fluid production data. The method also requires other data such as the measured flow rates of each fluid and the pressure drop across the core sample or sand-pack; this data must be smooth and continuous in its overall trend because the JBN method requires differentiation of the pressure drop.

The JBN method, however, has certain limitations: the capillary pressure, gravity influence, and fluid segregation (fingering) due to viscosity differences are ignored. The equations are applicable only to stable flow displacement.

4.3.1 JBN Method's Precision in Case of Stable Flows

Before testing the precision of the JBN method in unstable cases it was important to validate this estimation method in stable cases. It would be unwise to evaluate JBN in unstable cases without knowing precisely the standard amount of error, otherwise it would be impossible to distinguish the error created by viscous fingering's action in the method, from the error created by the application of the method itself.

JBN was evaluated against 9 independent NCFEs presented previously in Chapter 3, NCFE_1 to NCFE_9. All these experiments have a high viscosity contrast used to promote the instabilities in the front. Appraisal of JBN method in a stable scenario needed to be performed in coreflood experiments with completely stable front, but at the same time it was important to perform this evaluation on the same experiments in which JBN would be tested for its accuracy in presence of instability. The way around this problem, was to simulate NCFE_1 to NCFE_9 in 1D simulation. One dimensional simulation guarantees the same exact properties of the flow but completely eradicates the possibility of unstable front formation. This way it was possible to evaluate JBN precision in a stable scenario for the same experiments where it would be tested when viscous fingering forms. Following the methodology workflow presented in Figure 4-1, the error in estimated k_r curves by JBN for these stable NCFEs was calculated and is presented in Figure 4-3.

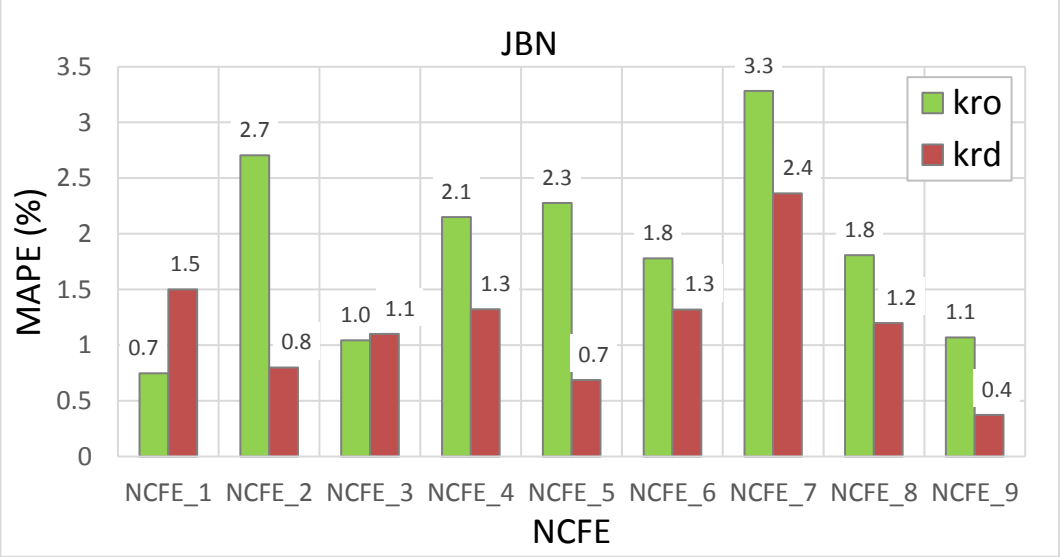

Figure 4-3: Mean absolute percentage error between JBN's relative permeability curves and the real ones, showing very small error in k_{ro} and k_{rd} (below 3.5%).

The results show that JBN has small errors in estimation of k_{ro} and k_{rd} when the flow is stable, with errors between 0.40 and 3.30 % and a mean of 1.53%. This small errors point to a very good precision of JBN when the NCFEs are stable. This results will serve as base to compare the performance of JBN in unstable flows.

In addition to these 9 independent experiments, a new set of NCFEs was constructed with incremental increase in viscous instability. These numerical experiments have the base data of NCFE_1 and NCFE_2, but the viscosity of the oil was changed in order to have different instability scenarios, the viscosity of the gas was maintained the same as the original NCFEs. NCFE_1_VR is the set of simulations based on NCFE_1 with viscosity ratios of 1500, 700, 300, 100, 50, 20, 10 and 5. NCFE_2_VR is the set of simulations based on NCFE_2 with viscosity ratios of 1000, 800, 500, 300, 250, 200, 150, 100 and 20. Further detail in the experiments is presented in Chapter 3. The importance of these new sets of NCFEs for this study is the fact that each simulation belonging to the same set is comparable in terms of instability, because all the properties are the same, except the viscosities. This way it is possible to assess if the error from estimation methods have a correlation to the variance in stability of the flow.

Before evaluating the JBN method in unstable flow it was important to know how much was the 'base error' of the method for stable displacements of these new sets of NCFEs. So, an analogous manner to what was done with the independent NCFEs, all the cases in the sets NCFE_1_VR and NCFE_2_VR were simulated in one dimension (1D) for this purpose. Then the workflow presented in Figure 4-1 was followed to obtain the error of each simulation, presented in Figure 4-4 and Figure 4-5, for NCFE_1_VR and NCFE_2_VR sets, respectively.

The scale of these figures was chosen to facilitate the comparison of the error range between stable and the unstable results, which will be presented in the subsequent section. These results show the same conclusion as the independent NCFEs set: the error of estimation for stable displacements is low (below 3%). It is also possible to say that no pattern (or tendency) was revealed from these results, in other words, there is no visible correlation between the change in viscosity ratio and the errors observed. From these remarks, it is possible to say that these errors are the 'base errors' for the JBN estimations and are result of the direct application of the method. Therefore, when analysing the JBN precision for unstable experiments all errors below 3% will be considered as good estimations, inside the confidence range.

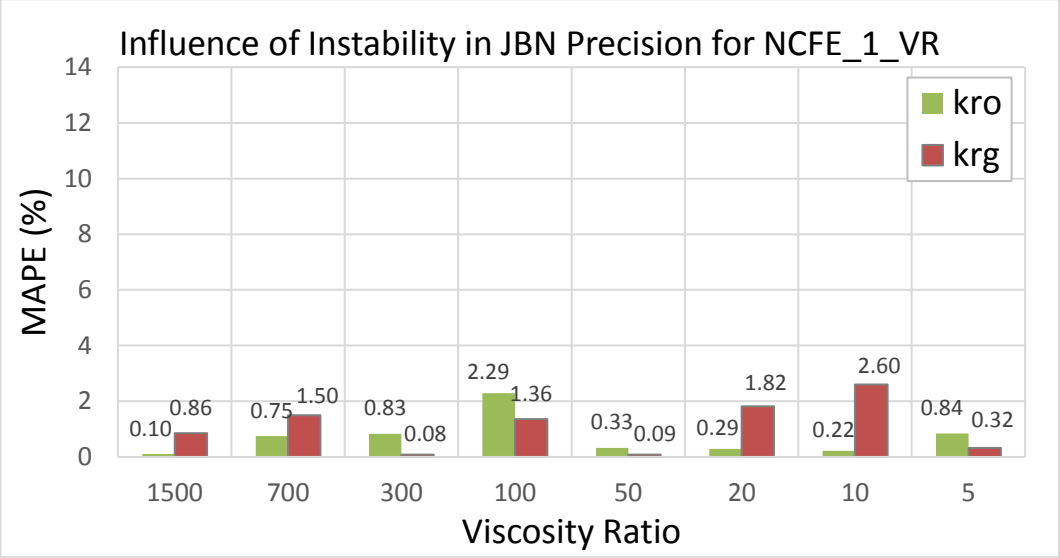

Figure 4-4:Mean absolute percentage error for JBN estimations at different viscosity ratios of simulation set NCFE_1_VR, stable displacement (1D simulation)

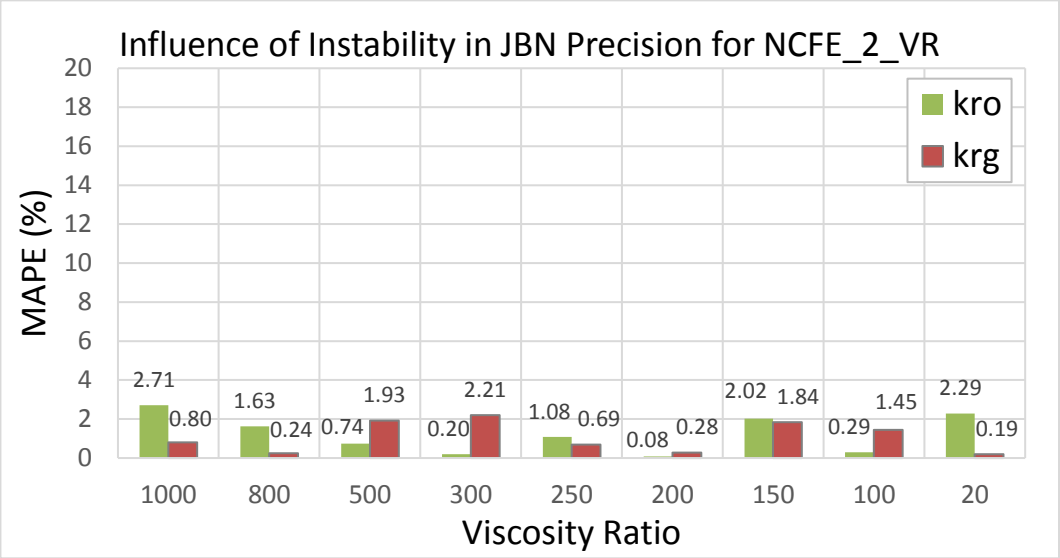

Figure 4-5: Mean absolute percentage error for JBN estimations at different viscosity ratios of simulation set NCFE_2_VR, stable displacement (1D simulation).

4.3.2 JBN Method's Precision in Case of Viscous Unstable Flows

The methodology for the calculation of JBN precision in viscous unstable flows followed the workflow from Figure 4-1. The NCFE_1 to NCFE_9 results from 2D high resolution simulation with permeability distribution as the triggering method for viscous fingering, presented in Chapter 3, were used for this purpose. Oil production and differential pressure, along with some pertinent core and fluid data, were gathered and used in JBN method. The relative permeability curves estimated by JBN for the NCFE_1 to NCFE_9,

were calculated and compared with the relative permeabilities used originally in the NCFEs simulation with the mean average percentage error. The results for NCFE_1 are presented in Figure 4-6 and Figure 4-7.

NCFE_1 has clear formation of viscous fingering as seen in Figure 3-10. Such unstable formation will result in an earlier breakthrough and different saturation profiles, which will be translated into different production than if the experiment was stable. This affected negatively the prediction of JBN method as it is seen in Figure 4-6 for k_{ro}. Since JBN averages all the production results in a stable model, it will 'see' the oil leaving the core earlier and assume that the gas has sweept through the whole outlet surface, resulting in an underestimation of the oil flow, which in turn results in a lower relative permeability. These results are very consistent with the viscous fingering nature. For the gas relative permeability, the results seem more surprising (at first). JBN prediction for the gas falls right on top of the real relative permeability, leading to the question: why is the gas not being affected by fingering? This fact has been observed in Maini et al. (1990) experimental data. The author performed unsteady-state experiments with unfavourable viscosity ratio and compared them with the steady-state version of the same experiments. The results show that the relative permeability estimated by the unsteady state methods has considerable error for the oil curve, but almost no error for the displacing fluid curve. This work proposed the theory for this behaviour is as the gas is behaving according to the basic equations and laws of flow. It may seem like the gas is the one behaving differently by forming fingering, but what makes the gas finger is the inability of the oil to accompany the gas velocity. The oil may act as a 'brake' to the gas movement, but since the flow of gas is maintained constant at the inlet, the oil will reach its 'breaking point' and allow the gas to flow past it in channels. The gas will develop its velocity accordingly to the laws of flow (Darcy's equation) even inside these channels. So, in fact it is the oil that is 'giving up' its standard mobility to let the gas move at the intended velocity. The concept will be later developed in order to serve as a model to relative permeability estimation methods that can tackle viscous fingering.

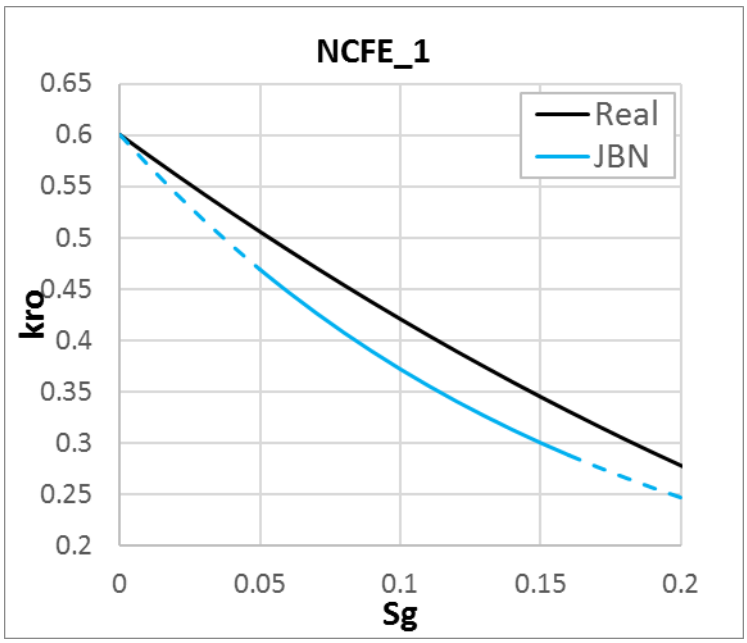

Figure 4-6: Relative permeability to oil as estimated by JBN compared with the real relative permeability (used in the NCFE) for NCFE_1, the solid lines represent the valid saturation range.

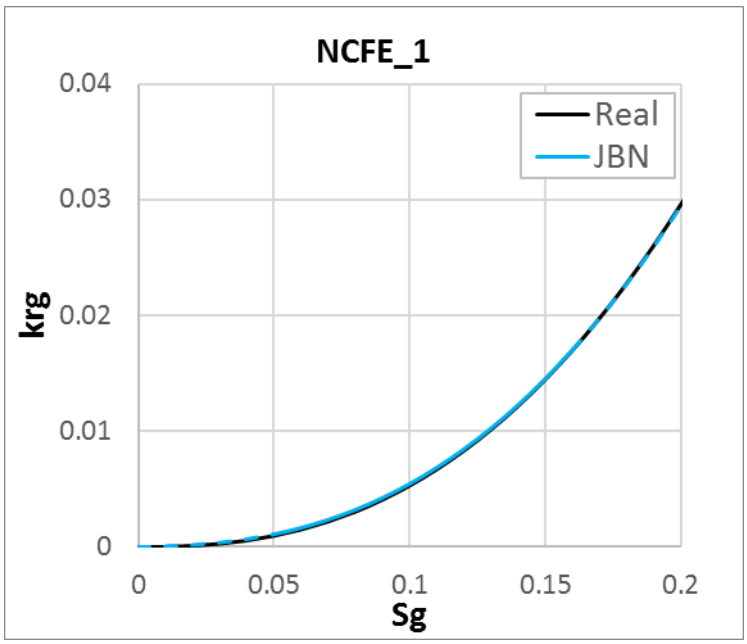

Figure 4-7: Relative permeability to gas as estimated by JBN compared with the real relative permeability (used in the NCFE) for NCFE_1, the solid lines represent the valid saturation range.

The same conclusions may be drawn from the rest of the NCFEs, presented in Figure 4-8 to Figure 4-23. It is important to note that in some of this cases, there is not only a shift in the oil k_r to lower values and the curvature does not remain the same. This is especially important if the JBN trend is used to predict the residual oil saturation. In the laboratory, some of this coreflood experiment may be stopped before the oil recovery is low enough to assume the residual oil saturation was reached, using JBN to extrapolate the value may

lead to considerable error if such is the case. All of these NCFEs were also extended up until an oil fractional flow of 0.001, meaning that for every 1 pore volume of gas injected, only 0.001 of oil is produced, at this point it was assumed irreducible oil saturation. In simulation, of course, it would be possible to reduce the oil to its 'true' residual oil, however such procedure would be unrealistic and drove purely on the mathematic equations. As an example, if the coreflood reaches 0.001 oil fractional flow in 2 days, it would take months to reach the 'true' residual oil. Also, the 'true' residual oil saturation is completely driven by the relative permeability that was chosen for that experiment which (especially in very viscous cases) is unrealistic at best. Even in laboratory experiments, when the viscosity contrast is high, the residual oil saturation obtained in 1D history matching is many times less than the one obtained in the experiment. Residual oil saturation in this context is different to 'immobile' oil and therefore k_{ro} (S_{or}) is not necessarily 0.

From these 9 NCFEs two are very important and need to be discussed in comparison with the results in JBN. NCFE_8 is the only case where viscous fingering has not formed or, at least, the deformation of the front is very small, resulting in very little difference between this case and a stable displacement, Figure 3-10. JBN result for NCFE_8 shows that in the absence of viscous fingering formation the method correctly predicts the real curves, even if the viscosity contrast of the fluids is high.

NCFE_9 is also one of the cases where less error is observed from JBN estimation. Figure 3-10 shows that the type of fingering formed in this case is very different from all the other cases, travelling together and not leaving so much oil behind, this may be the reason for a better estimation by JBN.

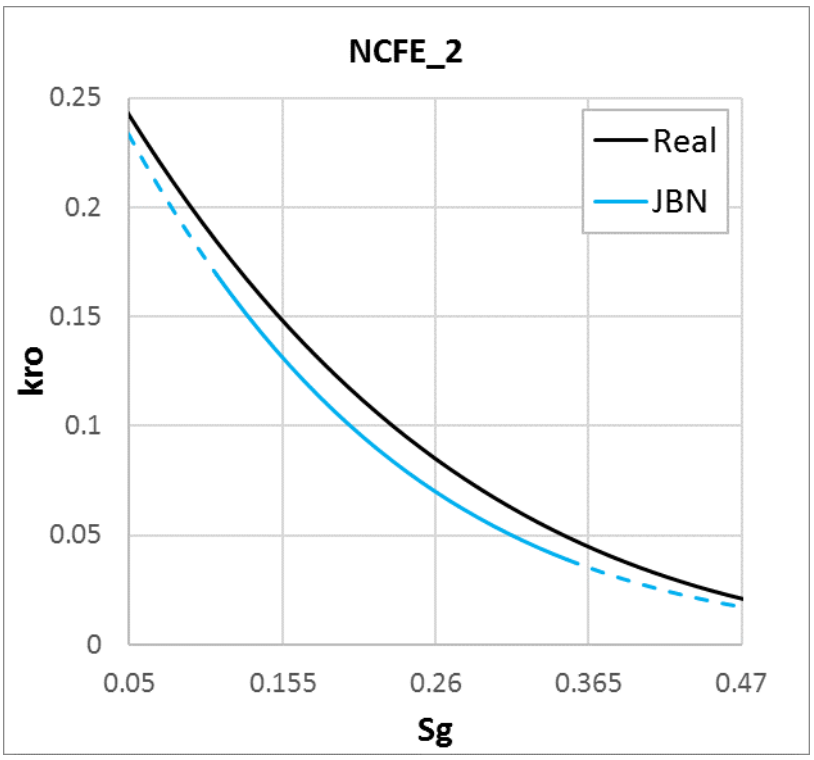

Figure 4-8: Relative permeability to oil as estimated by JBN compared with the real relative permeability (used in the NCFE) for NCFE_2, the solid lines represent the valid saturation range.

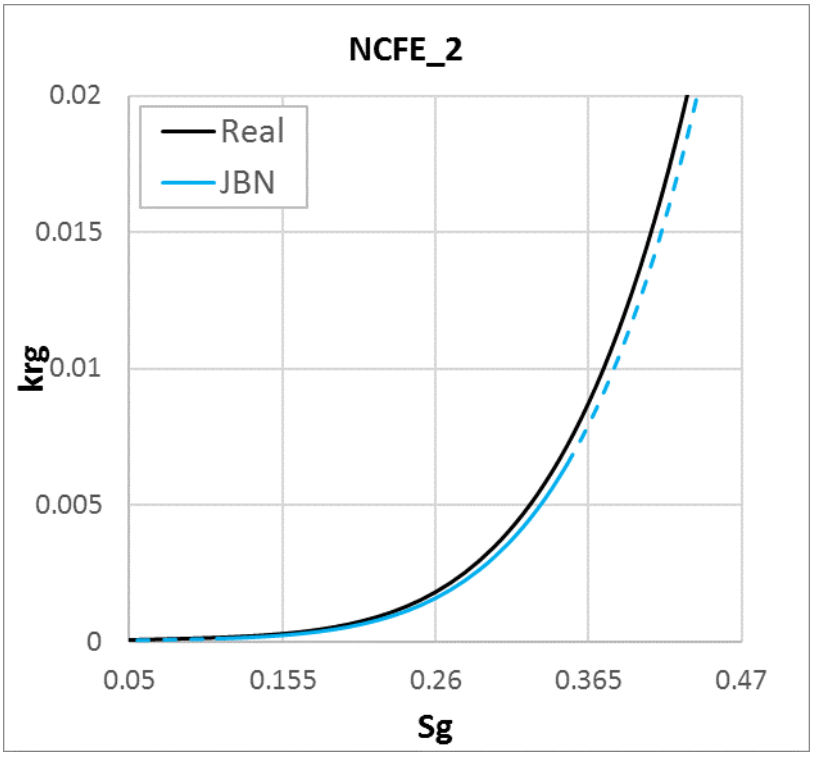

Figure 4-9: Relative permeability to gas as estimated by JBN compared with the real relative permeability (used in the NCFE) for NCFE_2, the solid lines represent the valid saturation range.

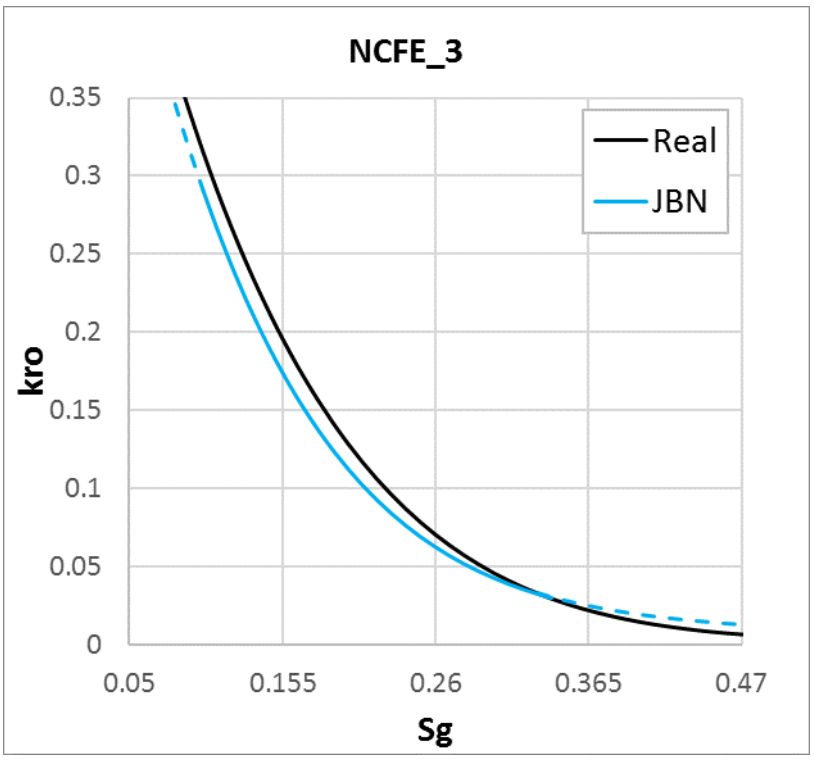

Figure 4-10: Relative permeability to oil as estimated by JBN compared with the real relative permeability (used in the NCFE) for NCFE_3, the solid lines represent the valid saturation range.

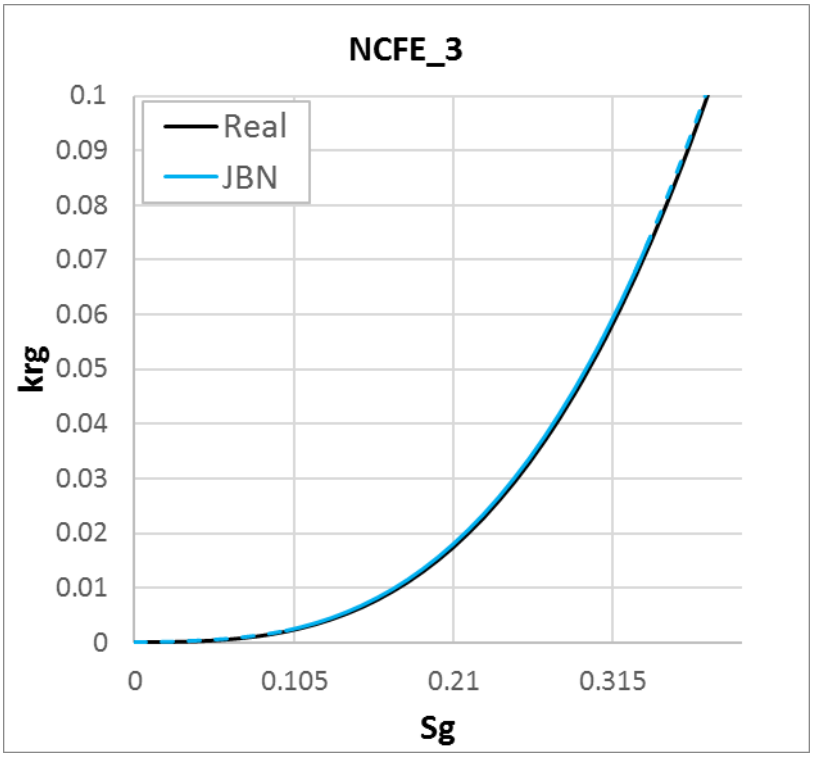

Figure 4-11: Relative permeability to gas as estimated by JBN compared with the real relative permeability (used in the NCFE) for NCFE_3, the solid lines represent the valid saturation range.

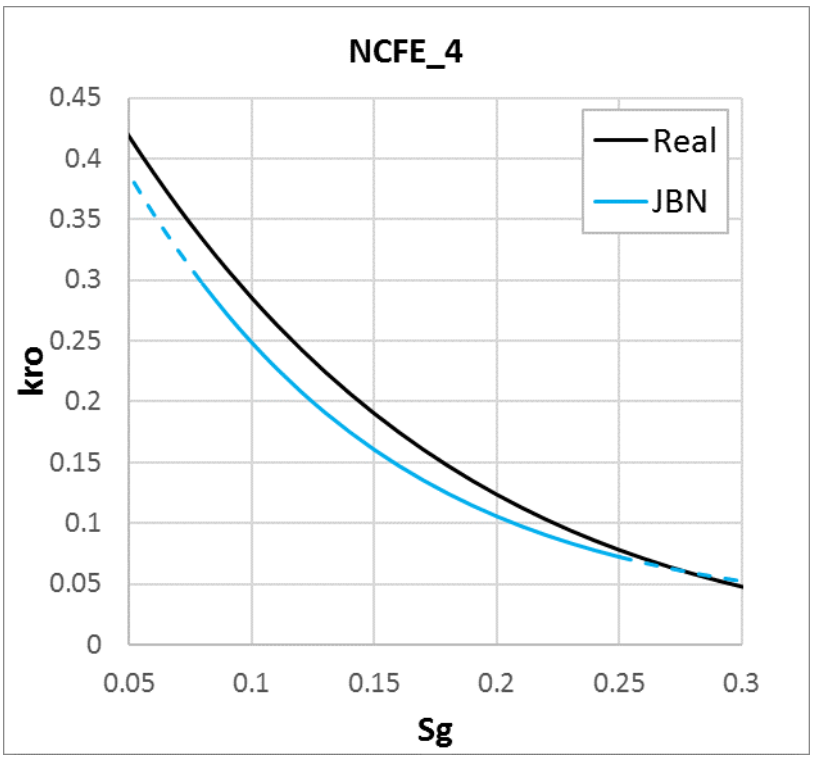

Figure 4-12: Relative permeability to oil as estimated by JBN compared with the real relative permeability (used in the NCFE) for NCFE_4, the solid lines represent the valid saturation range.

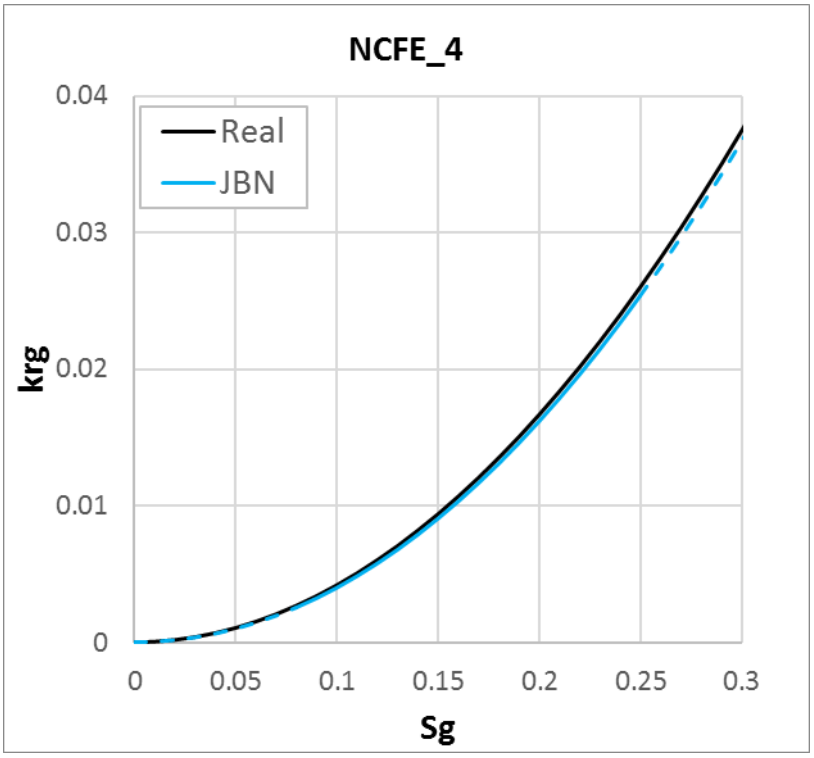

Figure 4-13: Relative permeability to gas as estimated by JBN compared with the real relative permeability (used in the NCFE) for NCFE_4, the solid lines represent the valid saturation range.

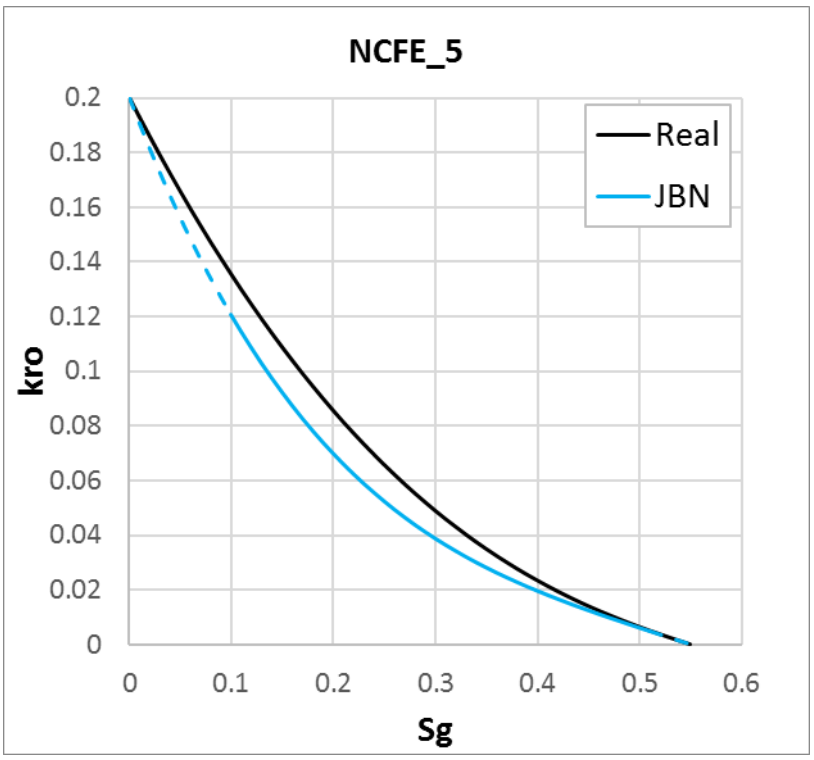

Figure 4-14: Relative permeability to oil as estimated by JBN compared with the real relative permeability (used in the NCFE) for NCFE_5, the solid lines represent the valid saturation range.

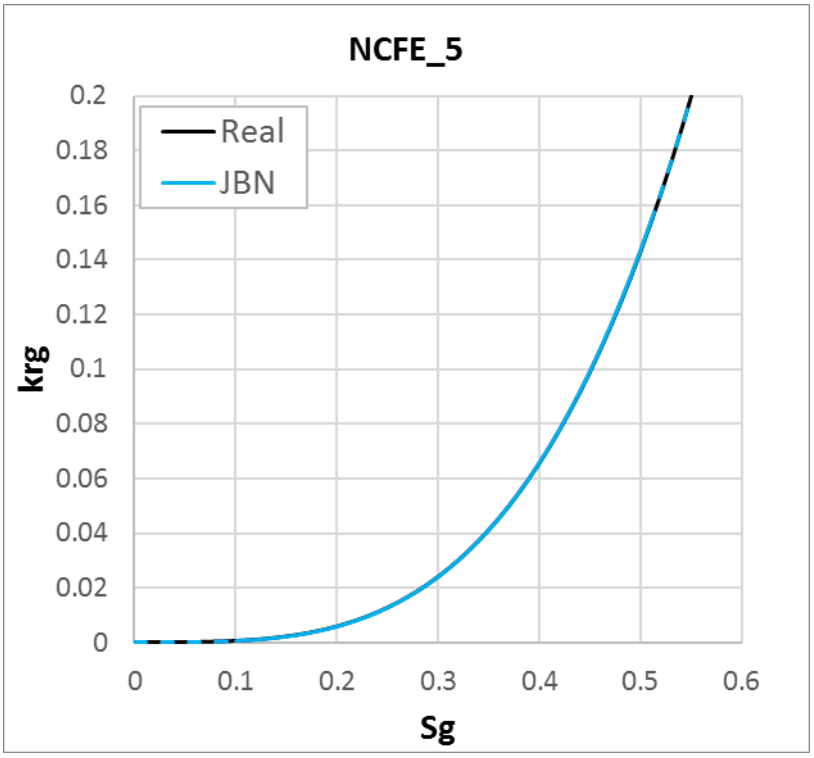

Figure 4-15: Relative permeability to gas as estimated by JBN compared with the real relative permeability (used in the NCFE) for NCFE_5, the solid lines represent the valid saturation range.

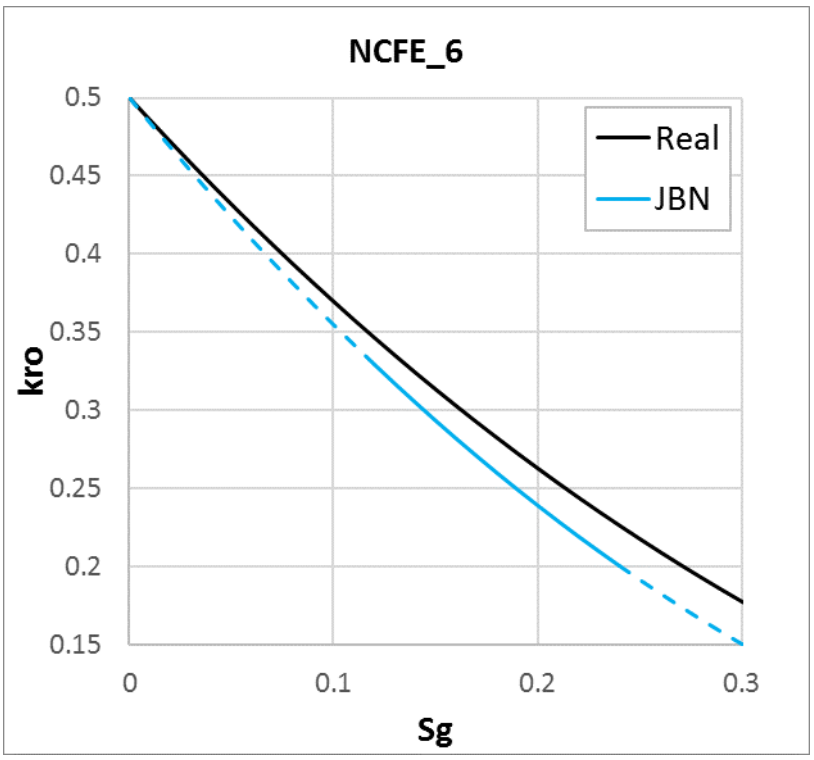

Figure 4-16: Relative permeability to oil as estimated by JBN compared with the real relative permeability (used in the NCFE) for NCFE_6, the solid lines represent the valid saturation range.

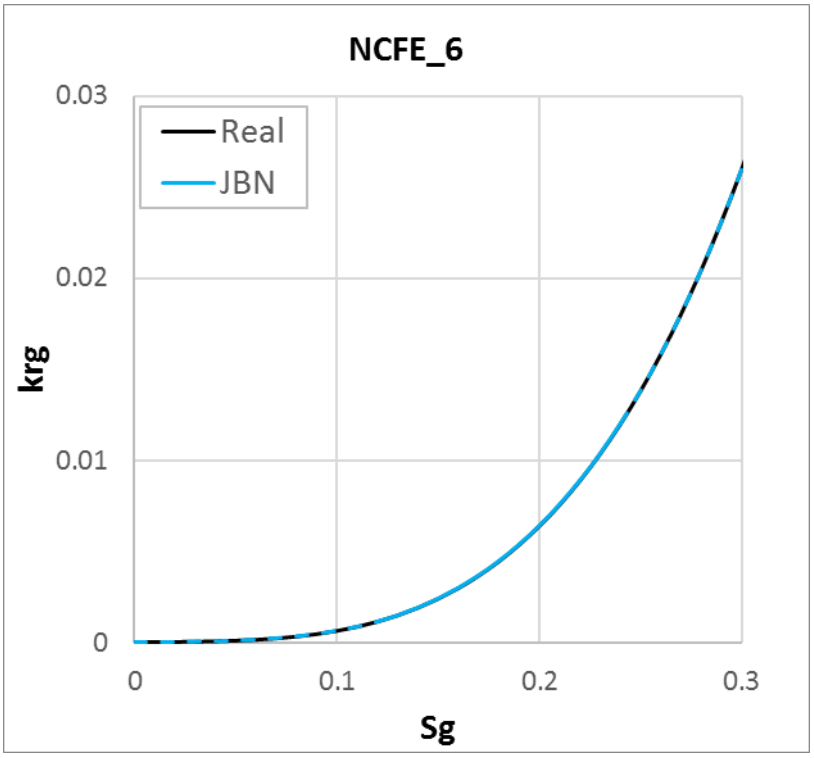

Figure 4-17: Relative permeability to gas as estimated by JBN compared with the real relative permeability (used in the NCFE) for NCFE_6, the solid lines represent the valid saturation range.

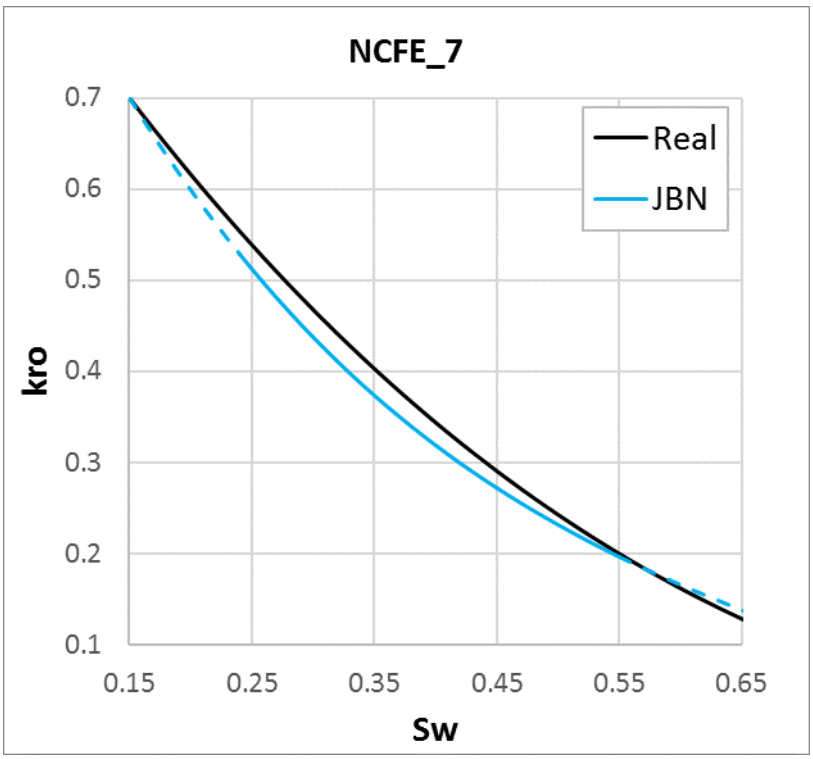

Figure 4-18: Relative permeability to oil as estimated by JBN compared with the real relative permeability (used in the NCFE) for NCFE_7, the solid lines represent the valid saturation range.

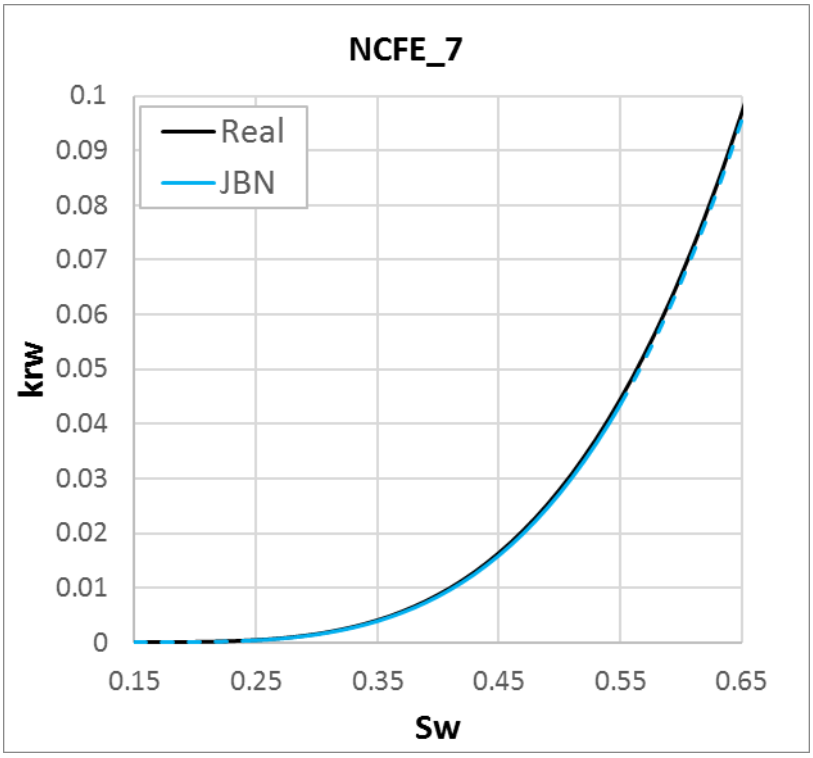

Figure 4-19: Relative permeability to water as estimated by JBN compared with the real relative permeability (used in the NCFE) for NCFE_7, the solid lines represent the valid saturation range.

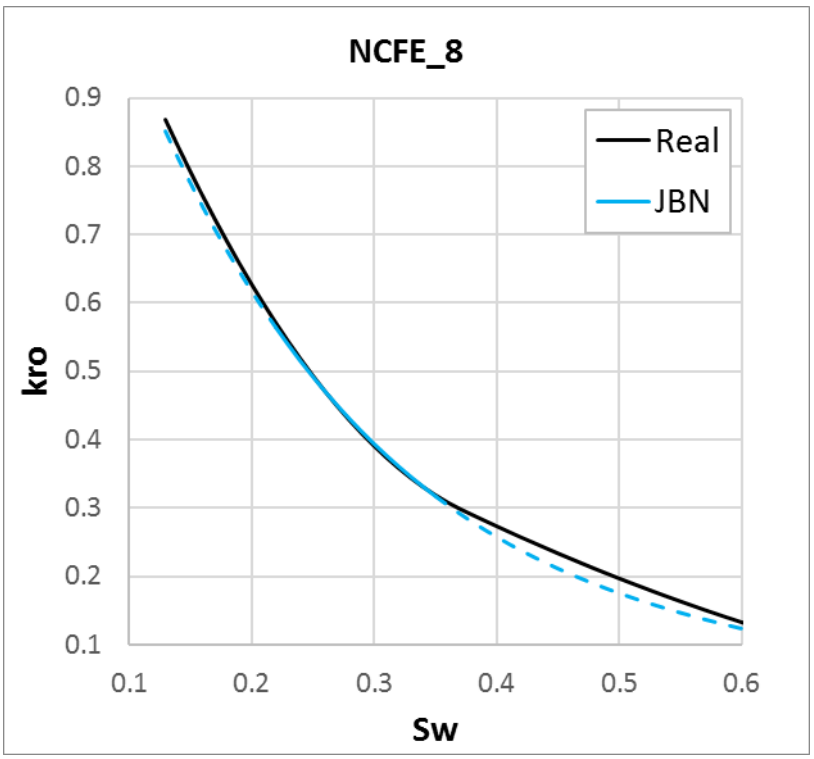

Figure 4-20: Relative permeability to oil as estimated by JBN compared with the real relative permeability (used in the NCFE) for NCFE_8, the solid lines represent the valid saturation range.

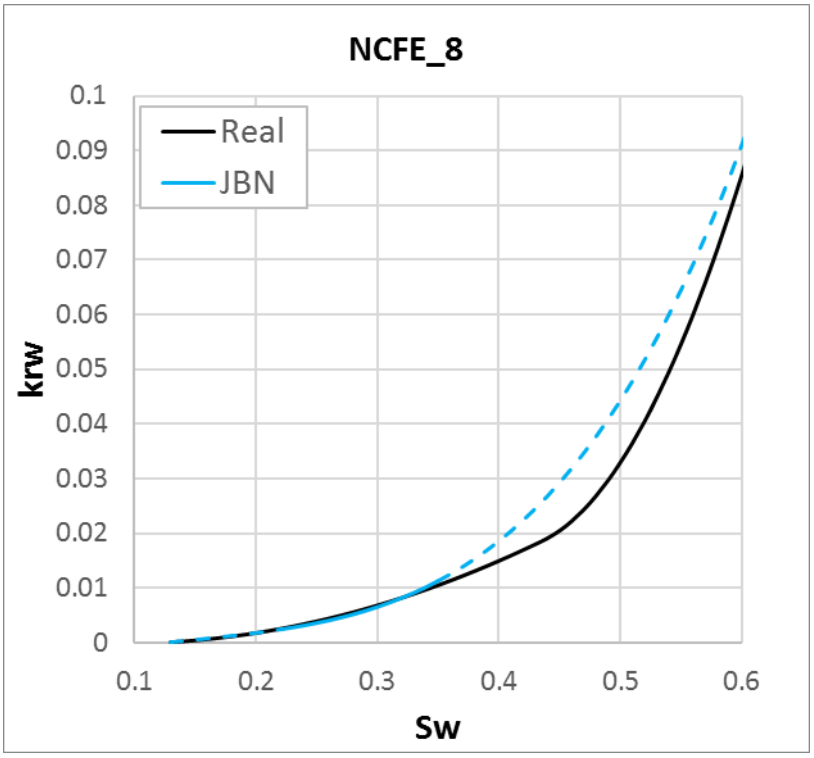

Figure 4-21: Relative permeability to water as estimated by JBN compared with the real relative permeability (used in the NCFE) for NCFE_8, the solid lines represent the valid saturation range.

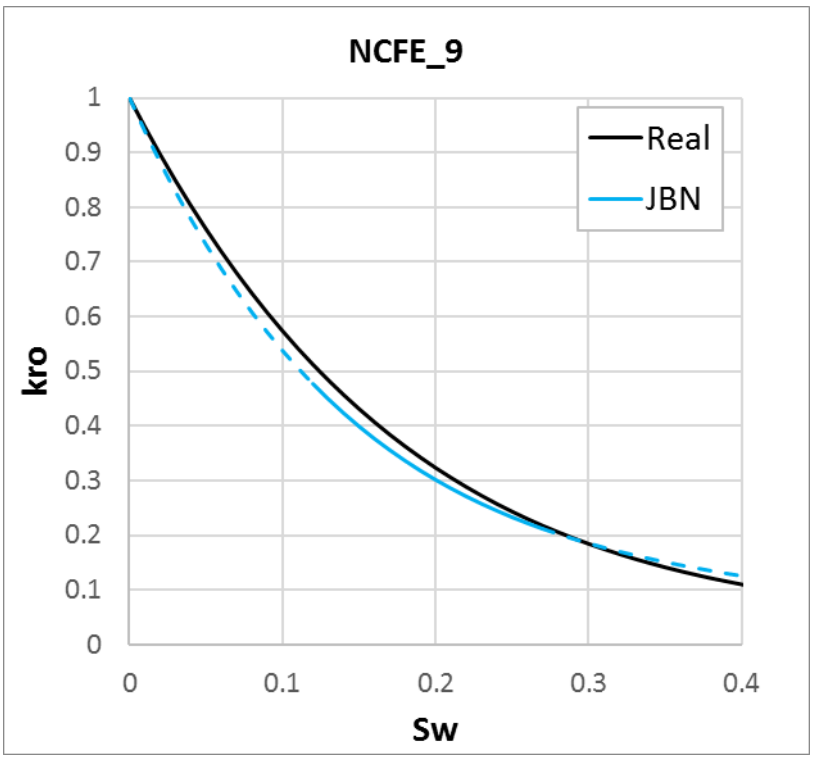

Figure 4-22: Relative permeability to oil as estimated by JBN compared with the real relative permeability (used in the NCFE) for NCFE_9, the solid lines represent the valid saturation range.

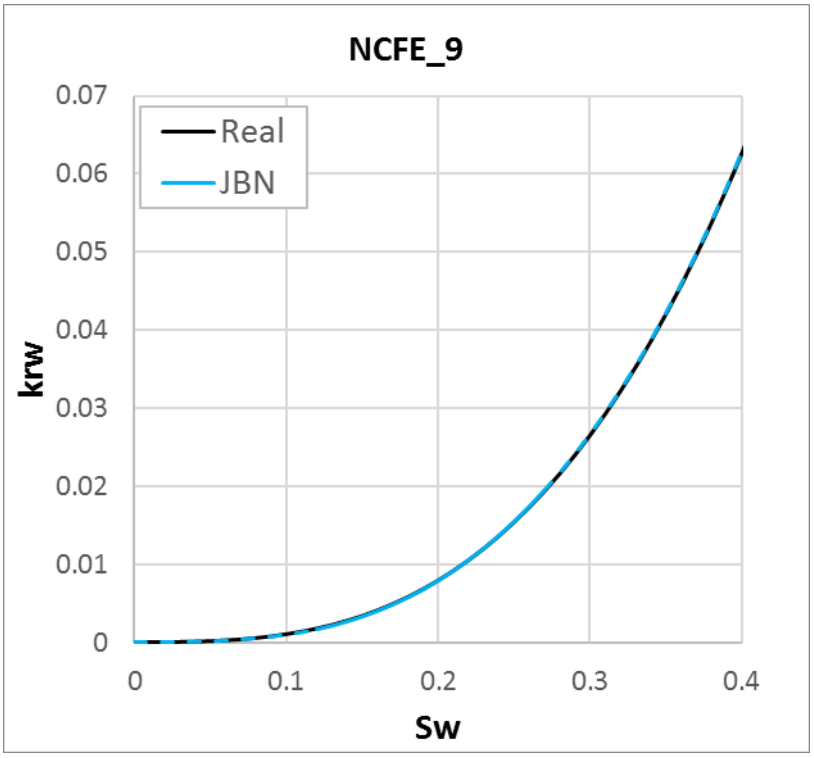

Figure 4-23: Relative permeability to water as estimated by JBN compared with the real relative permeability (used in the NCFE) for NCFE_9, the solid lines represent the valid saturation range.

The error between the JBN and real k_r curves was calculated, using the MAPE (%) equation. Figure 4-24 presents the mean absolute percentage error for both k_{ro} and k_{rd} in each NCFE. The quantitative analysis allows a more objective analysis to the visible errors from Figure 4-6 to Figure 4-23. Errors for k_{ro} are undoubtedly much higher than for k_{rd}, reaching in some cases more than 15%. Considering that these experiments were performed under controlled conditions, meaning that gravity effect and heterogeneity had no effect in the corefloods, it is safe to assume that this error results from the viscous instabilities, which created the frontal patterns observed in Figure 3-10 and Figure 2-15. Additionally, comparison of these errors with the ones for the same NCFEs but under stable conditions, leaves small room for doubt about the origin of this error, Figure 4-25.

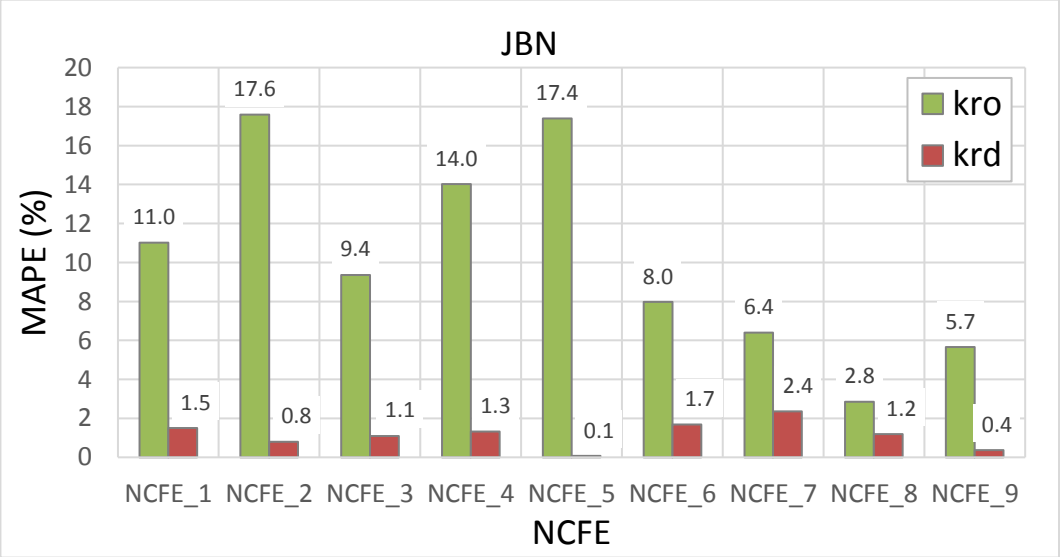

Figure 4-24:Mean absolute percentage error between JBN's relative permeability curves and the real ones, showing error in the oil relative permeability curves between 2.8 and 15.8 %.

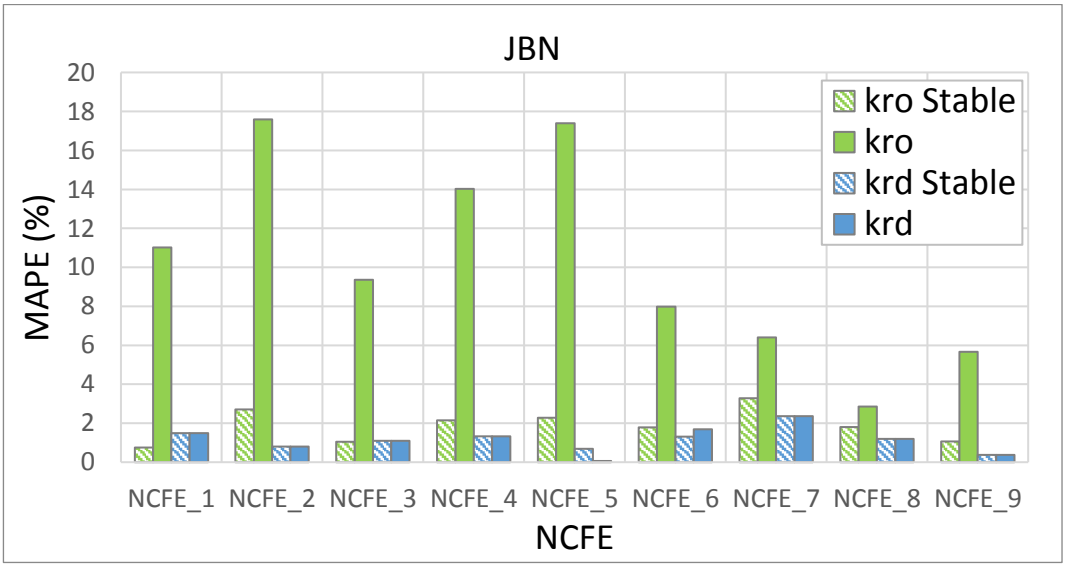

Figure 4-25: Mean absolute percentage error for JBN estimation in Stable and Unstable experiments.

Figure 4-25 shows the overwhelming difference in error between JBN's estimated k_{ro} of stable and unstable NCFEs. Is imaginable how such error would affect laboratories who perform SCAL analysis and relative permeability estimation of core plugs. Precise measuring of relative permeabilities is essential, not only to draw conclusions from the flow performance but, also, for reservoir simulation. In reservoir simulation it is very common to estimate the relative permeability of a certain reservoir section from the aggregate results of several corefloods of plugs cut from that reservoir section. This may lead to a 'snowball' effect, where the error gets added with each erroneous estimation.

In addition to the independent NCFEs, sets NCFE_1_VR and NCFE_2_VR were also used in JBN method in order to evaluate its precision. Similar to the other independent cases, these sets of NCFEs were simulated in 2D high resolution gridding with permeability distribution in order to allow the generation of viscous fingering. Then the methodology present in Figure 4-1 was used to quantify the error of the estimations, Figure 4-26 and Figure 4-27.

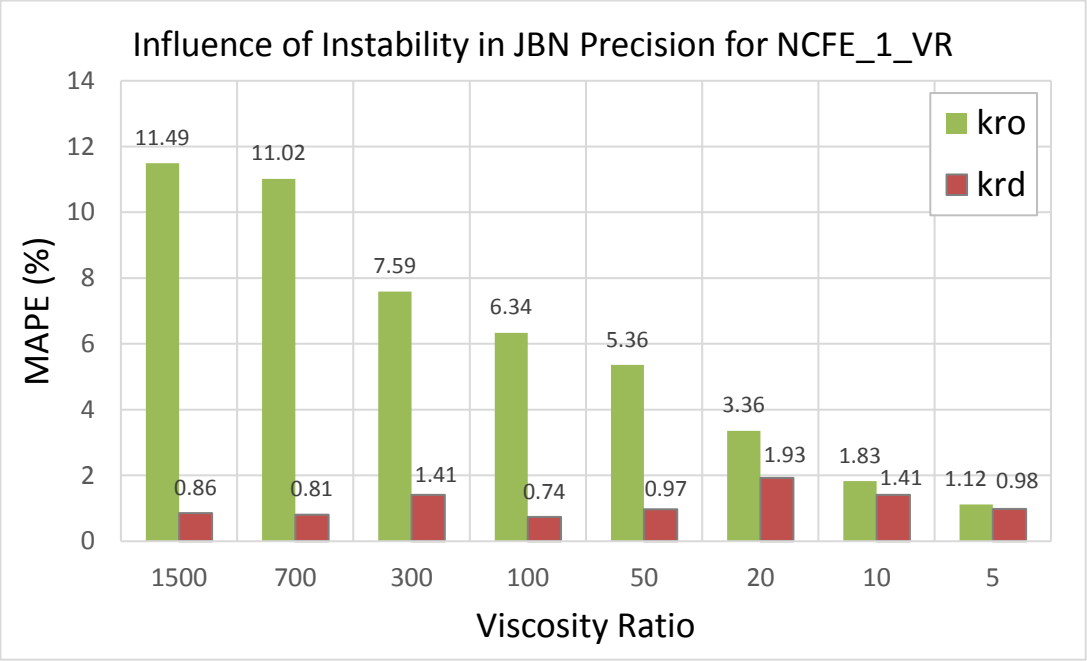

Figure 4-26:Influence of instability (produced by viscosity ratio) in JBN's estimation of relative permeability for the NCFE_1_VR set, showing a direct correlation between instability and error.

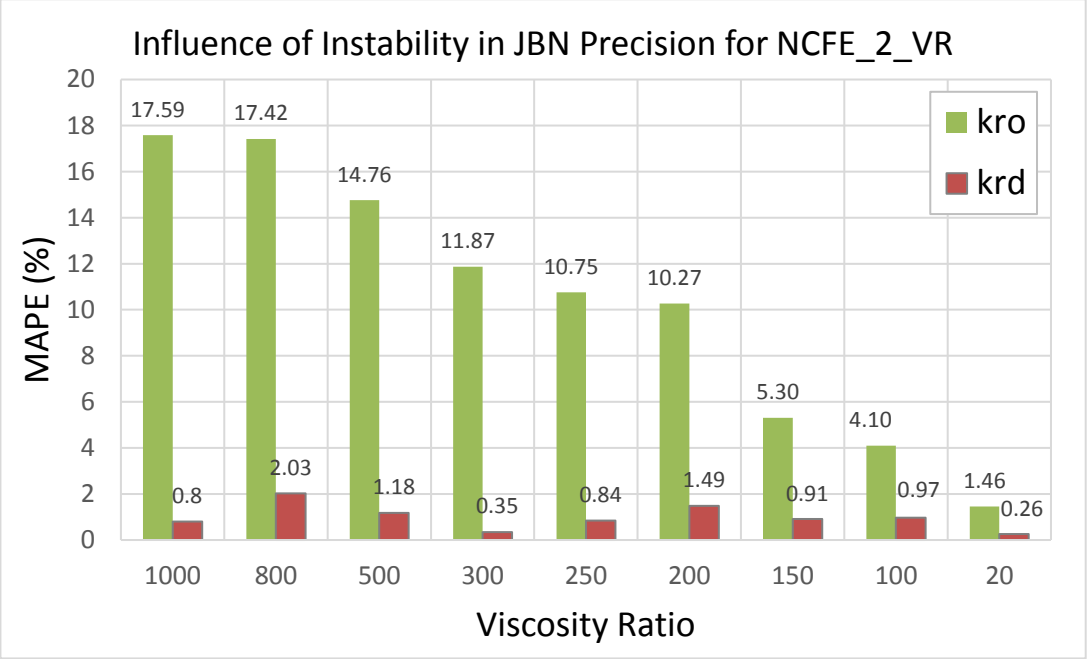

Figure 4-27: Influence of instability (produced by viscosity ratio) in JBN's estimation of relative permeability for the NCFE_2_VR set, showing a direct correlation between instability and error.

As in the independent experiments k_{rg} is below the base error, meaning that no significant error was added to it due to viscous fingering. For the k_{ro} curve, though, Figure 4-26 and Figure 4-27 show a completely different scenario than in Figure 4-4 and Figure 4-5. Many of the simulations, especially those with high viscosity ratio, are above the base error for k_{ro} observed for the same NCFEs in stable condition. Also, and bearing in mind that the results are comparable for all NCFEs within the same set, there is clearly a correlation between the error of estimation and the viscosity ratio. As explained in Chapter 3, the variable degree of instability was achieved by changing the viscosity ratio of each NCFEs within the same set. This allowed (for the same experiment) cases with incrementally higher instability, due to the difference in the mobility of the gas and the oil, promoted by the viscosity. Knowing that higher viscosity ratio translates to more instability in the flow, it is easy to correlate that the JBN error increases with the instability. Another point worth notice is the fact that the error is reduced to below the tolerance error at the same viscosity ratios where viscous fingering is ceasing to exist. For example, in NCFE_1_VR set the saturation profiles Figure 3-11 show that the severity of viscous fingering is reduced drastically bellow viscosity ratio of 50, following the trend of the JBN estimation error. The same can be concluded in Figure 3-12 the saturation clearly shows that from viscosity ratio of 100 to viscosity ratio of 20 (for NCFE_2_VR set), the viscous fingering is eliminated, and that fact is shown in the JBN results as well. These points allow to conclude without a doubt that viscous fingering

was a considerable influence in the JBN method precision and that the error of estimation increases with the increase in instability of the flow.

From these results it is possible to claim that the JBN method is not an acceptable method to perform relative permeability estimation in the presence of viscous fingering and using such a method may result in considerable error.

4.4 1D History Matching

Originally, parameter estimation computation methods (history matching) was used to estimate 2-phase relative permeability curves by (Kerig & Watson 1986).

In history matching, the core and fluid data is used to produce a coreflood simulation with a first guess of a relative permeability and capillary pressure. The result of this simulation (e.g. production data and differential pressure) is then compared with the experimental measured results via quantification of error (misfit). If the misfit is higher than the defined tolerance, an optimization algorithm is used to generate the second guess of the relative permeability, which, in turn, will be used in a new simulation and from the result of that simulation, the misfit will be calculated, completing the cycle. When the misfit is less than the tolerance, the relative permeability will be the estimation result of the history matching method. Figure 4-28 shows the methodology followed by the typical 2-phase relative permeability history matching.

Unlike JBN method, it is possible to take into account capillary pressure and gravity in one dimensional history matching as long as there are equations that can describe those forces in the coreflood simulation.

For this work, an in-house software, 3RPSim, was used to perform the 1D history matching. 3RPSim uses the Genetic Algorithm as optimization algorithm for the relative permeability. Although, 3RPSim is capable of directly estimating 3-phase relative permeabilities, for this work it will be used to perform 2-phase estimations only, since these are the type of corefloods under study.

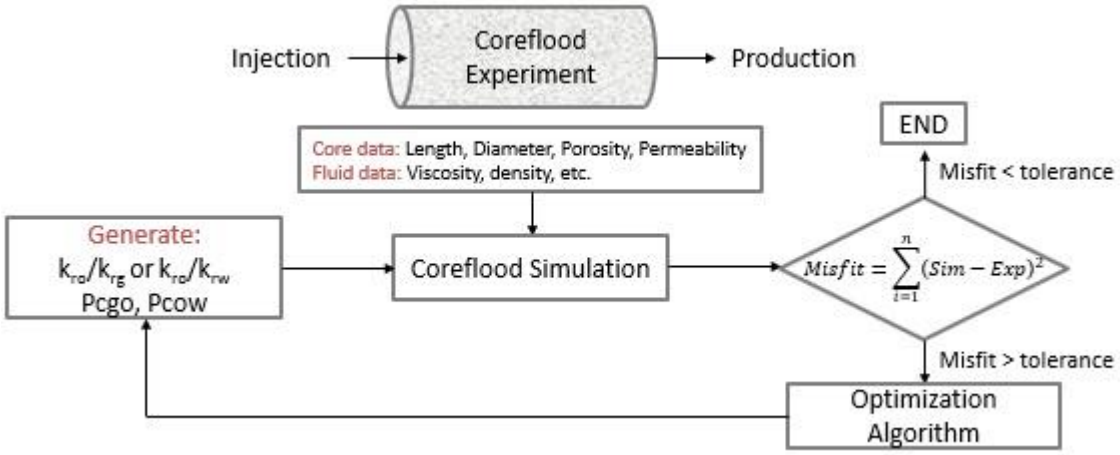

Figure 4-28: Workflow for determination of two phase k_r values from unsteady state coreflood experiment.

4.4.1 1D History Matching's Relative Permeability Estimation Precision in Case of Stable Flows

In a similar manner to the JBN method analysis, it was important to evaluate the validity of the HWU (Heriot-Watt University) research group's in-house 1D history matching (1D HM) software as a suitable relative permeability estimation method for stable cases.

1D HM was evaluated against 9 NCFEs presented previously in Chapter 3, NCFE_1 to NCFE_9. All these experiments have a high viscosity contrast used to promote the instabilities in the front. For this section, the 9 numerical experiments were simulated in one dimension, to ensure a stable front and at the same time make them comparable to the unstable experiments as explained before. These are the same NCFEs used in the JBN analysis, so it is possible to compare 1D history matching with the explicit one.

The methodology as presented in Figure 4-1 was followed to calculate the error between the estimated 1D HM relative permeability and the real one. Figure 4-29 shows the MAPE (%) for each phase and NCFE. The results show that all estimations have less than 3% error, which makes the 1D HM method a reliable method to estimate the relative permeability curves in stable experiments.

The comparison between 1D HM and JBN methods precision is plotted in Figure 4-30. From these results, it is possible to conclude that both methods have very small errors when the front is stable.

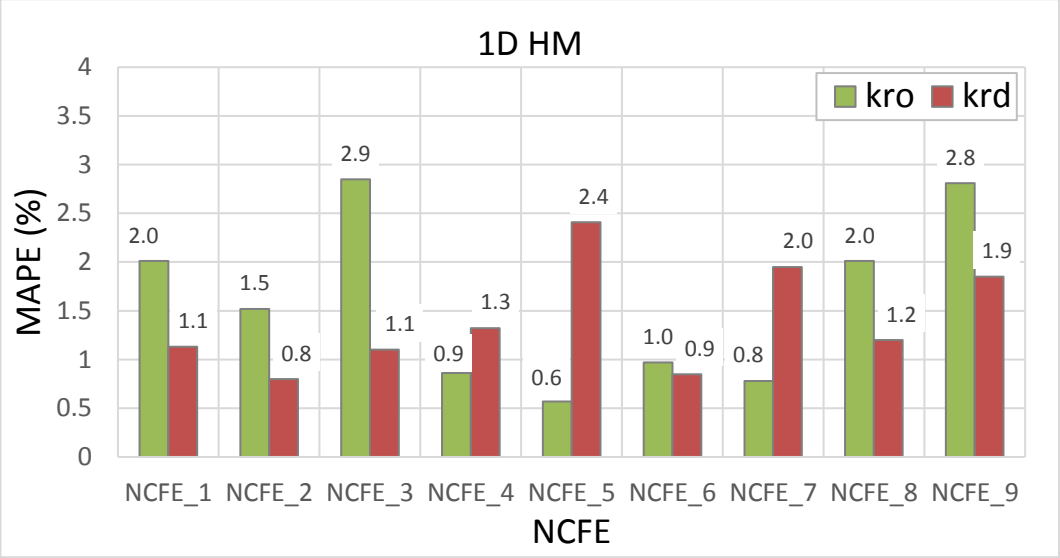

Figure 4-29: Mean absolute percentage error between 1D HM relative permeability curves and the real ones, showing very small error in k_{ro} and k_{rd} (below 2.9%).

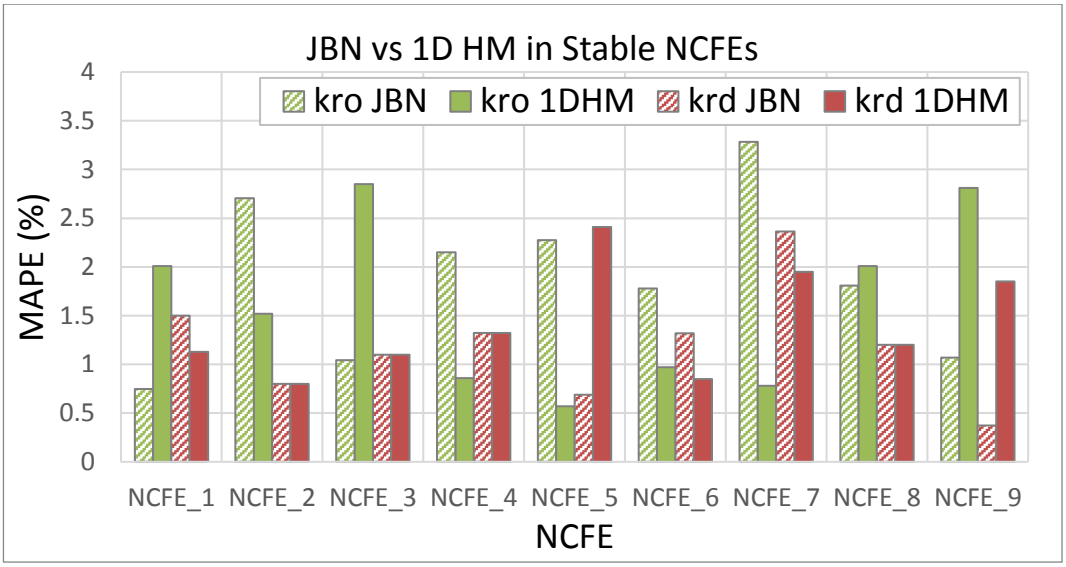

Figure 4-30:Comparison between the error of kr estimation by 1D HM and JBN in stable NCFEs.

In addition to these 9 independent experiments, a new set of NCFEs was constructed with incremental increase in viscous instability. These numerical experiments have the base data of NCFE_1 and NCFE_2, but the viscosity of the oil was changed in order to have different instability scenarios, the viscosity of the gas was maintained the same as the original NCFEs. NCFE_1_VR is the set simulations based on NCFE_1 with viscosity ratios of 1500, 700, 300, 100, 50, 20, 10 and 5. NCFE_2_VR is the set simulations based on NCFE_2 with viscosity ratios of 1000, 800, 500, 300, 250, 200, 150, 100 and 20. Further detail in the experiments are presented in Chapter 3.

Before evaluating the 1D HM method in unstable flow it was important to know how much was the 'base error' of the method for stable displacements of these new sets of NCFEs. So, in a similar manner to what was done with the independent NCFEs, all the

cases in the sets NCFE_1_VR and NCFE_2_VR were simulated in one dimension (1D) for this purpose. Then the workflow present in Figure 4-1 was followed to obtain the error of each simulation set, which can be seen in Figure 4-31 and Figure 4-32, for NCFE_1_VR and NCFE_2_VR sets, respectively. The scale of these figures was chosen to facilitate the comparison of the error range between stable and the unstable results, which will be presented in the subsequent section.

These results show the same conclusion as the independent NCFEs set: the error of estimation for stable displacements is low (below 3%). It is also possible to say that no visible correlation between the change in viscosity ratio and the error of estimation was observed. From these remarks, it is possible to say that the tolerance for 1D HM error is 3%, anything below this value is taken as a good estimate for the method.

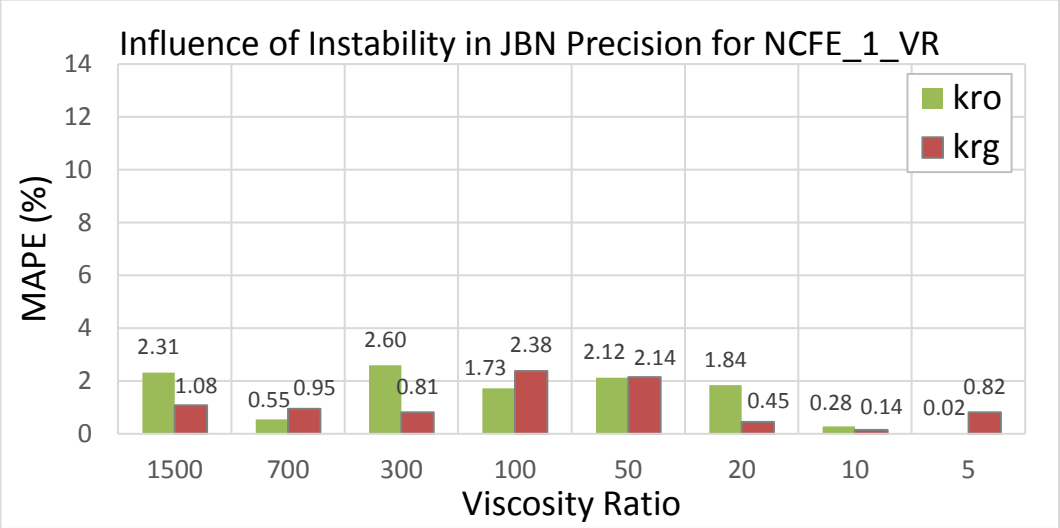

Figure 4-31: Mean absolute percentage error for 1D HM estimations at different viscosity ratios of simulation set NCFE_1_VR, stable displacement (1D simulation).

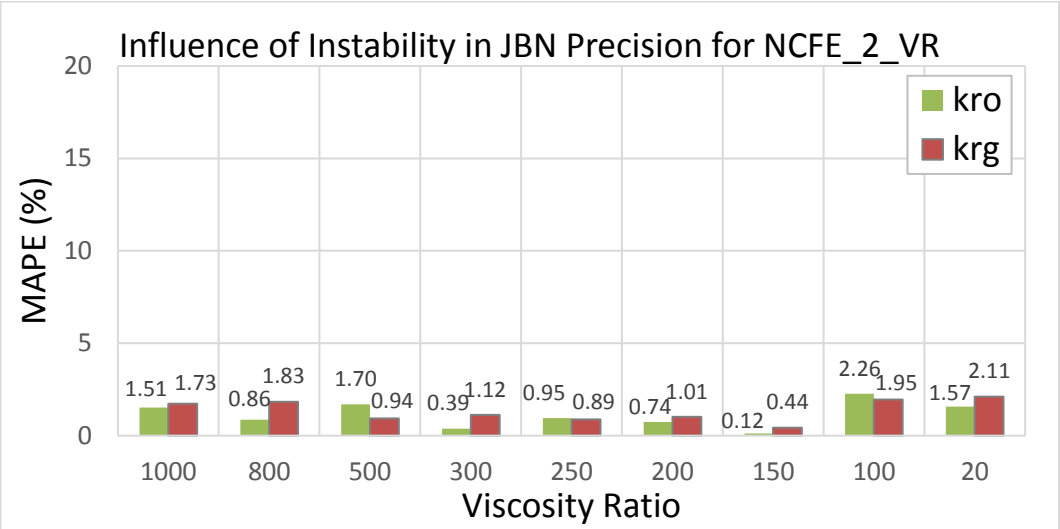

Figure 4-32: Mean absolute percentage error for 1D HM estimations at different viscosity ratios of simulation set NCFE_2_VR, stable displacement (1D simulation).

4.4.2 1D History Matching's Relative Permeability Estimation Precision in Case of Viscous Unstable Flows

The methodology presented in Figure 4-1 was followed in order to analyse the precision of 1D HM in cases with viscous unstable flows. The NCFE_1 to NCFE_9 results from 2D high resolution simulation with permeability distribution as triggering method for viscous fingering (presented in Chapter 3), were used in this section as input for the 1D HM workflow shown in Figure 4-28. Oil endpoint, $k_{ro}(S_{gi}$ or $S_{wi})$, was also introduced as a known parameter in the software to accelerate the matching. The error between the method estimated k_r and the real was then calculated. Figure 4-33 to Figure 4-50 show the relative permeability curves as calculated by 1D HM in comparison to the real ones for NCFE_1 to NCFE_9.

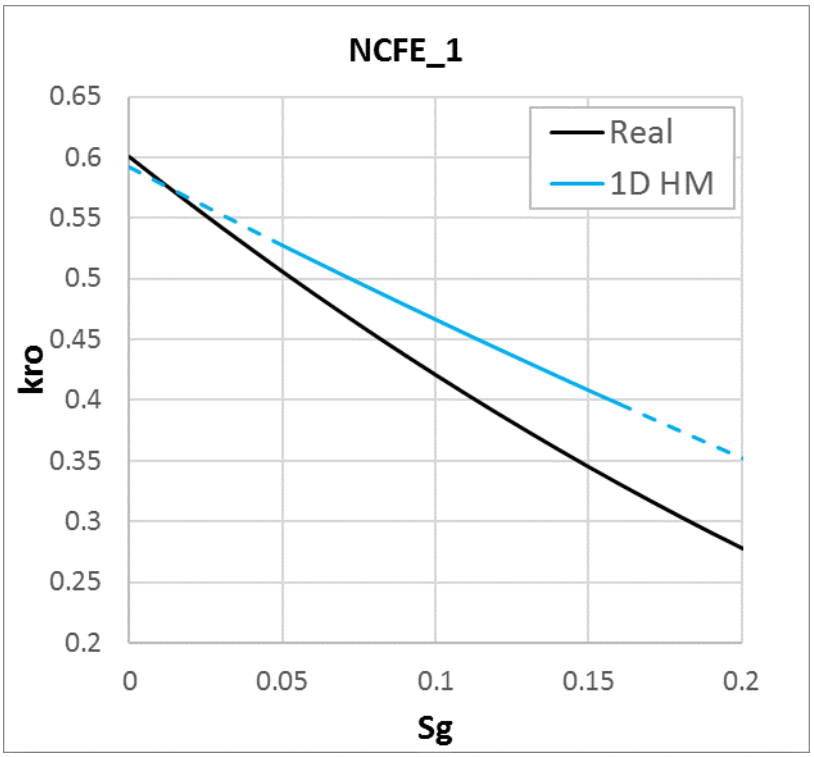

Figure 4-33: Relative permeability to oil as estimated by 1D HM compared with the real relative permeability (used in the NCFE) for NCFE_1, the solid lines represent the valid saturation range.

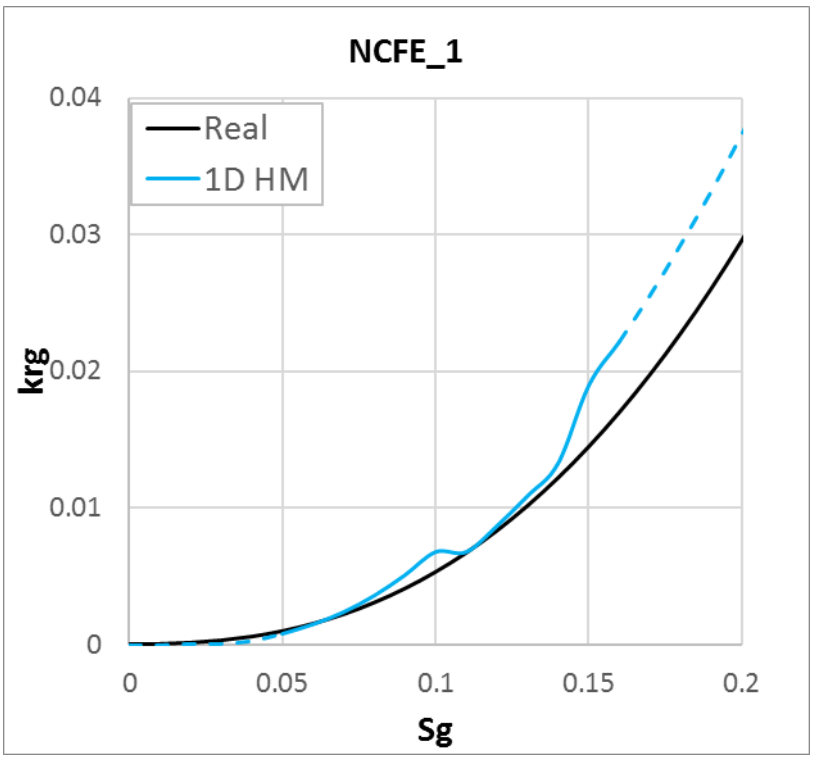

Figure 4-34: Relative permeability to gas as estimated by 1D HM compared with the real relative permeability (used in the NCFE) for NCFE_1, the solid lines represent the valid saturation range.

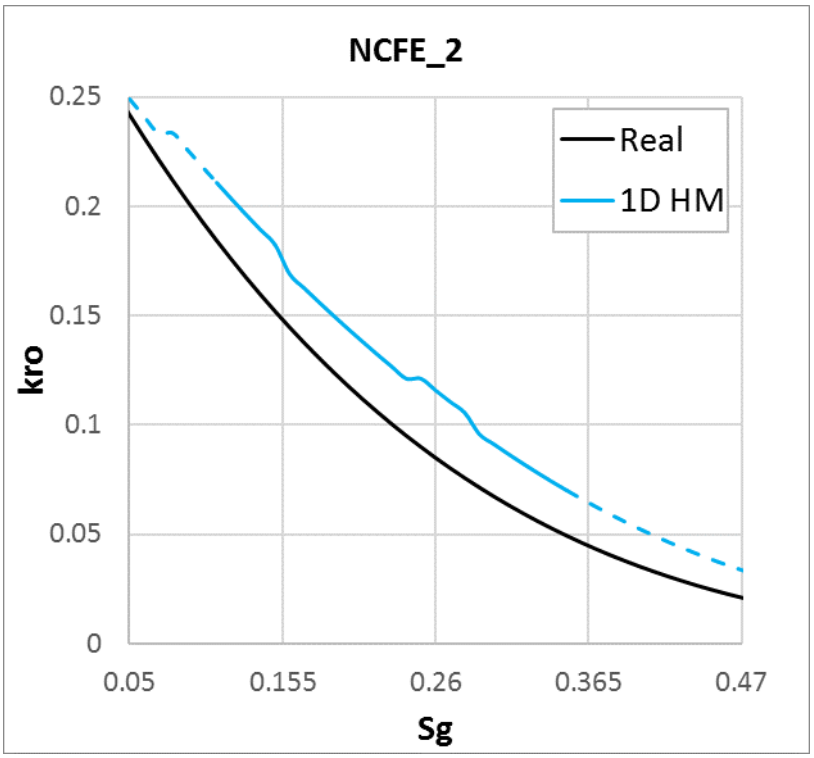

Figure 4-35: Relative permeability to oil as estimated by 1D HM compared with the real relative permeability (used in the NCFE) for NCFE_2, the solid lines represent the valid saturation range.

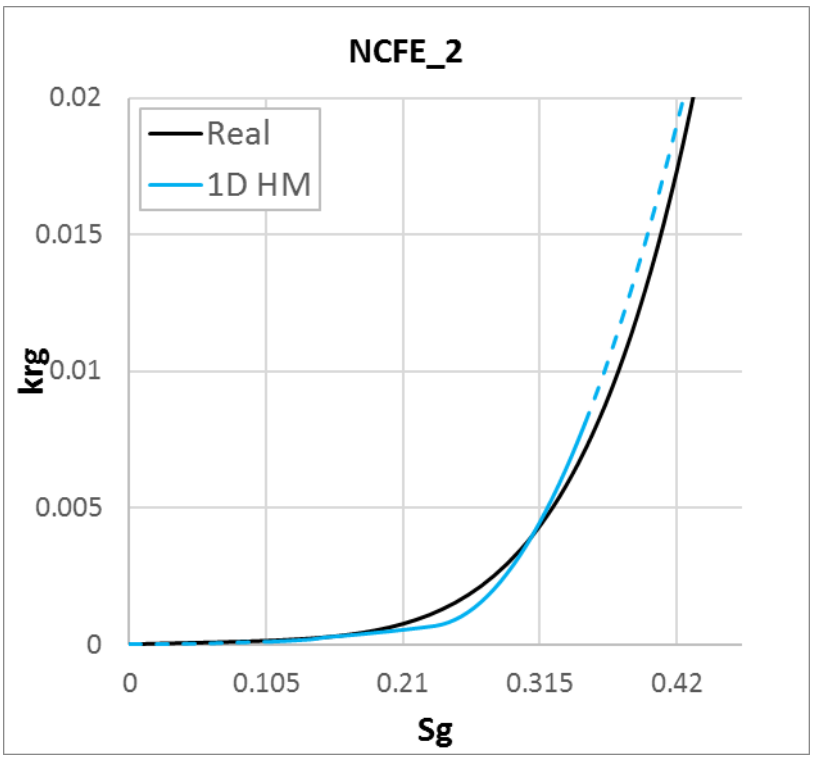

Figure 4-36: Relative permeability to gas as estimated by 1D HM compared with the real relative permeability (used in the NCFE) for NCFE_2, the solid lines represent the valid saturation range.

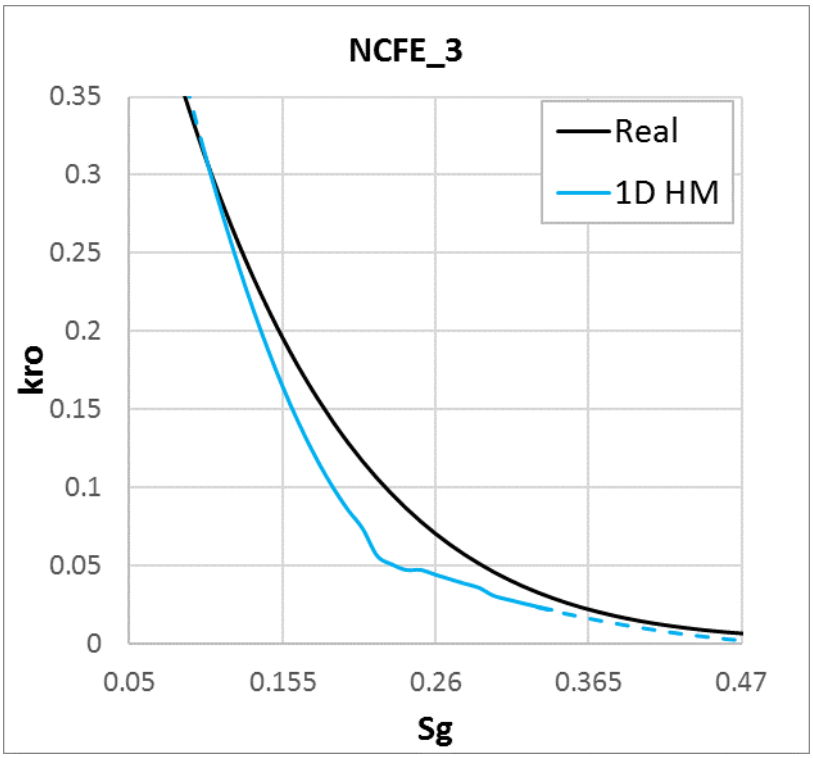

Figure 4-37: Relative permeability to oil as estimated by 1D HM compared with the real relative permeability (used in the NCFE) for NCFE_3, the solid lines represent the valid saturation range.

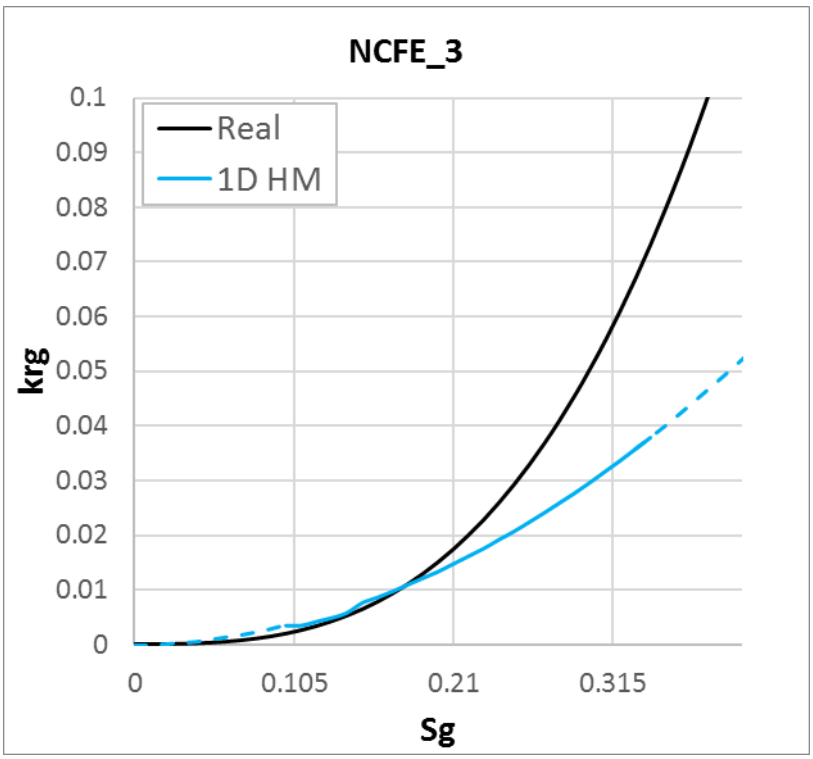

Figure 4-38: Relative permeability to gas as estimated by 1D HM compared with the real relative permeability (used in the NCFE) for NCFE_3, the solid lines represent the valid saturation range.

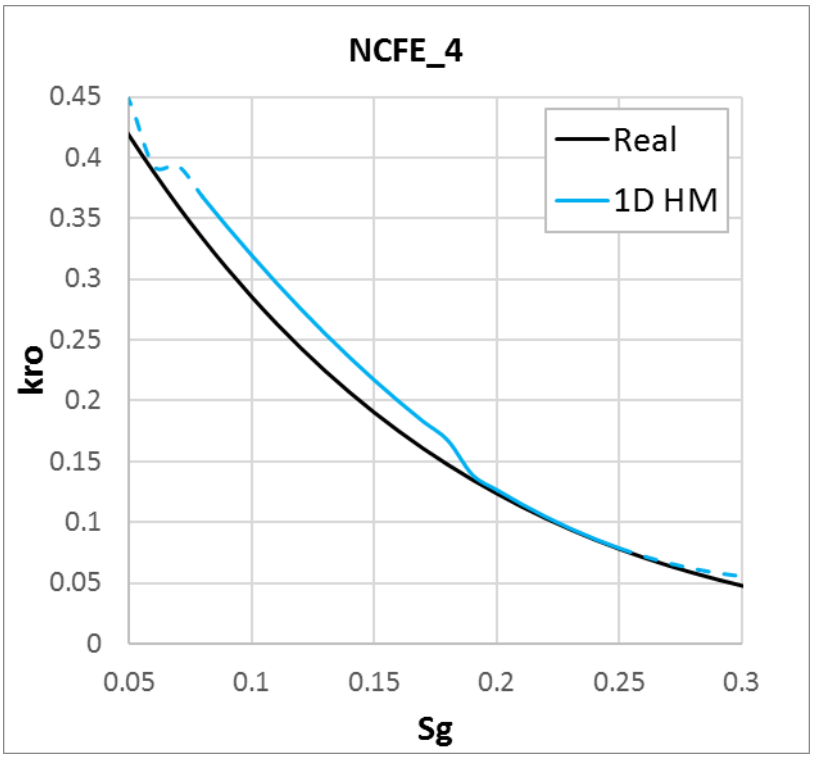

Figure 4-39: Relative permeability to oil as estimated by 1D HM compared with the real relative permeability (used in the NCFE) for NCFE_4, the solid lines represent the valid saturation range.

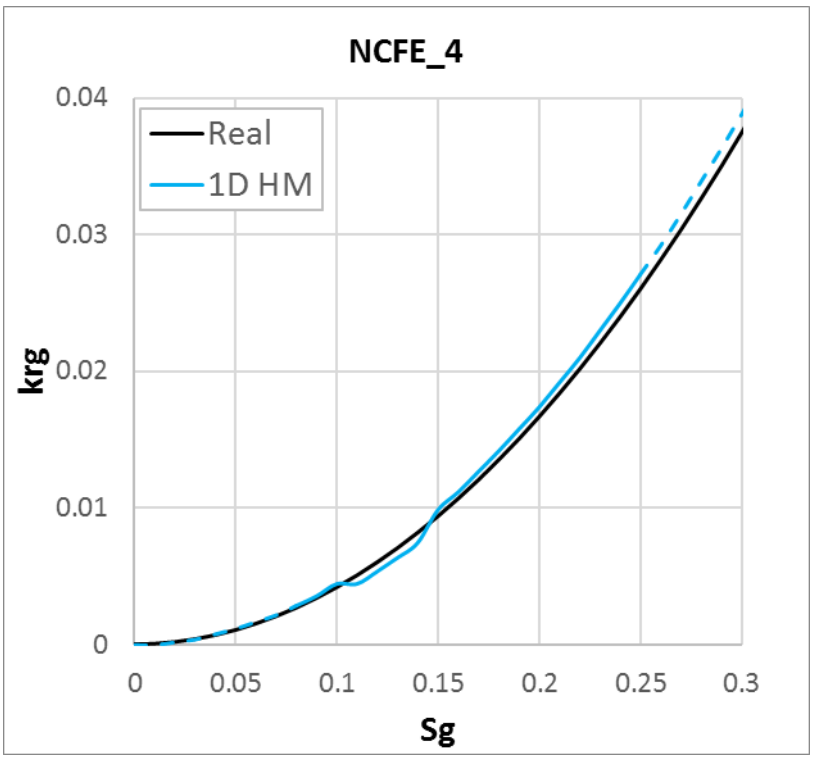

Figure 4-40: Relative permeability to gas as estimated by 1D HM compared with the real relative permeability (used in the NCFE) for NCFE_4, the solid lines represent the valid saturation range.

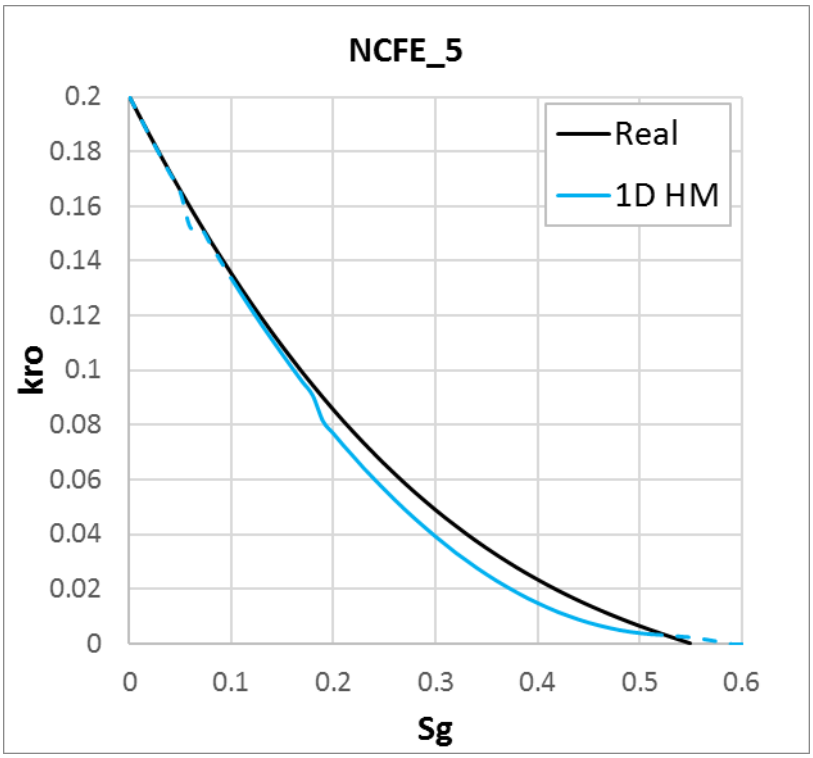

Figure 4-41: Relative permeability to oil as estimated by 1D HM compared with the real relative permeability (used in the NCFE) for NCFE_5, the solid lines represent the valid saturation range.

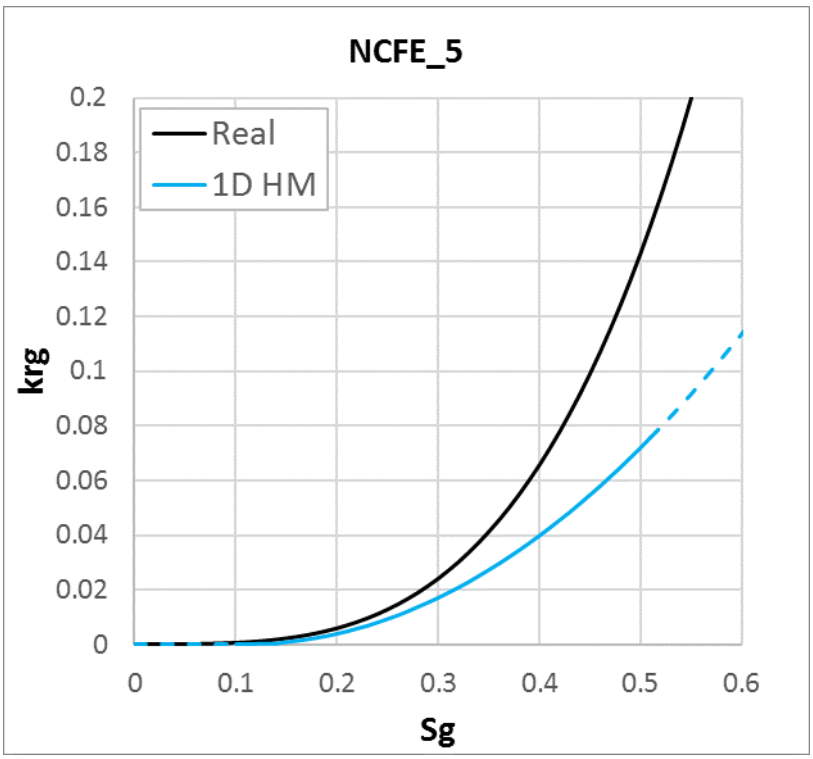

Figure 4-42: Relative permeability to gas as estimated by 1D HM compared with the real relative permeability (used in the NCFE) for NCFE_5, the solid lines represent the valid saturation range.

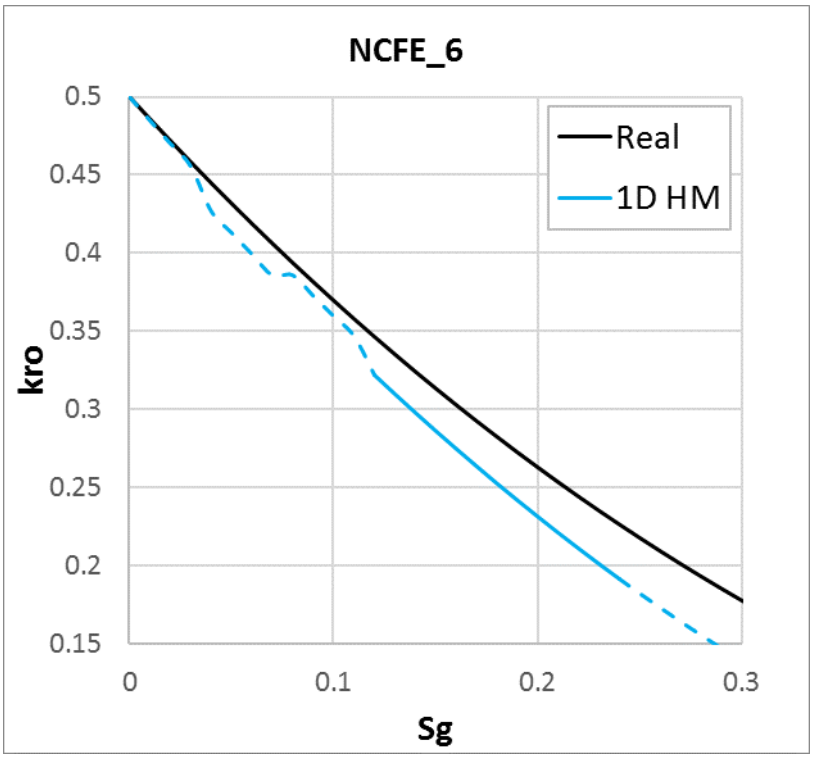

Figure 4-43: Relative permeability to oil as estimated by 1D HM compared with the real relative permeability (used in the NCFE) for NCFE_6, the solid lines represent the valid saturation range.

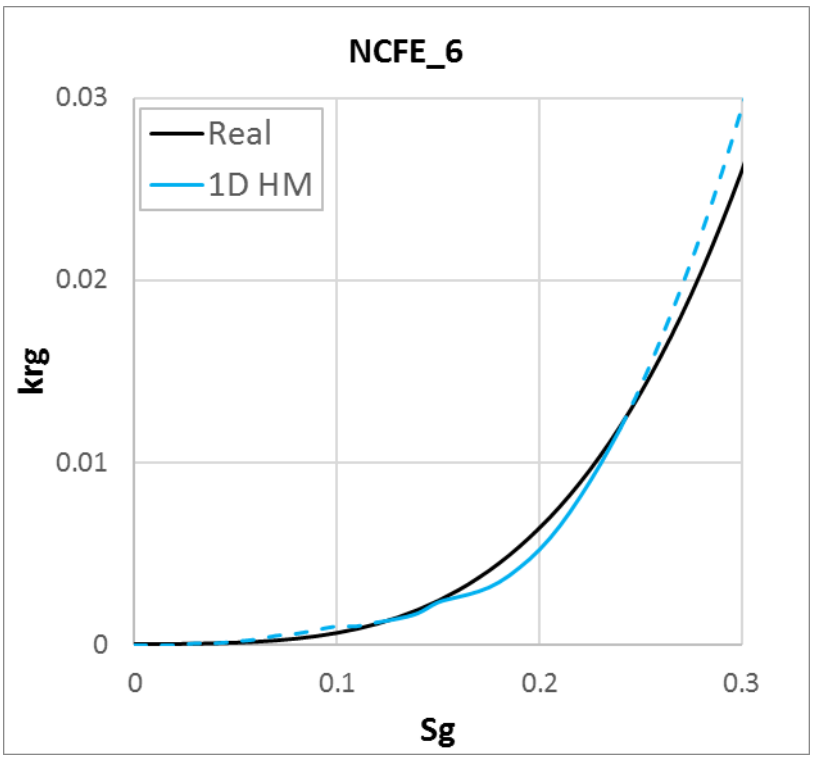

Figure 4-44: Relative permeability to gas as estimated by 1D HM compared with the real relative permeability (used in the NCFE) for NCFE_6, the solid lines represent the valid saturation range.

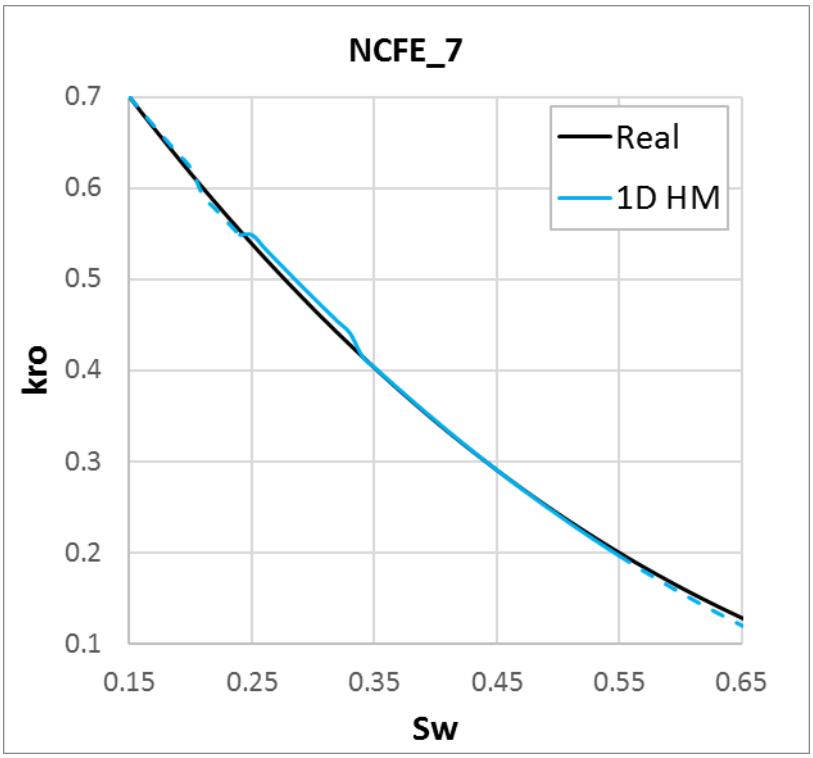

Figure 4-45: Relative permeability to oil as estimated by 1D HM compared with the real relative permeability (used in the NCFE) for NCFE_7, the solid lines represent the valid saturation range.

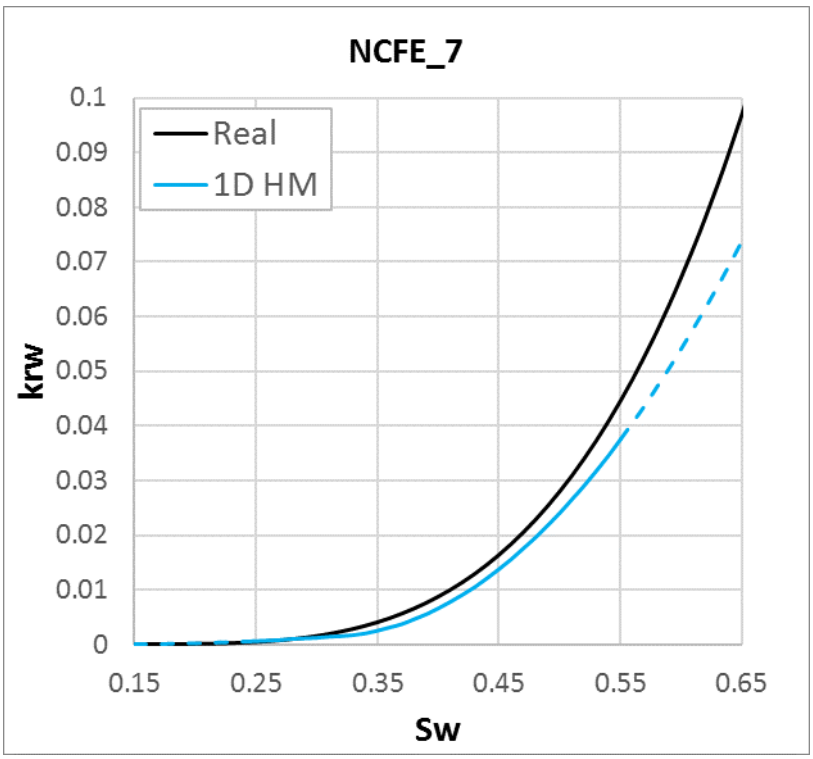

Figure 4-46: Relative permeability to water as estimated by 1D HM compared with the real relative permeability (used in the NCFE) for NCFE_7, the solid lines represent the valid saturation range.

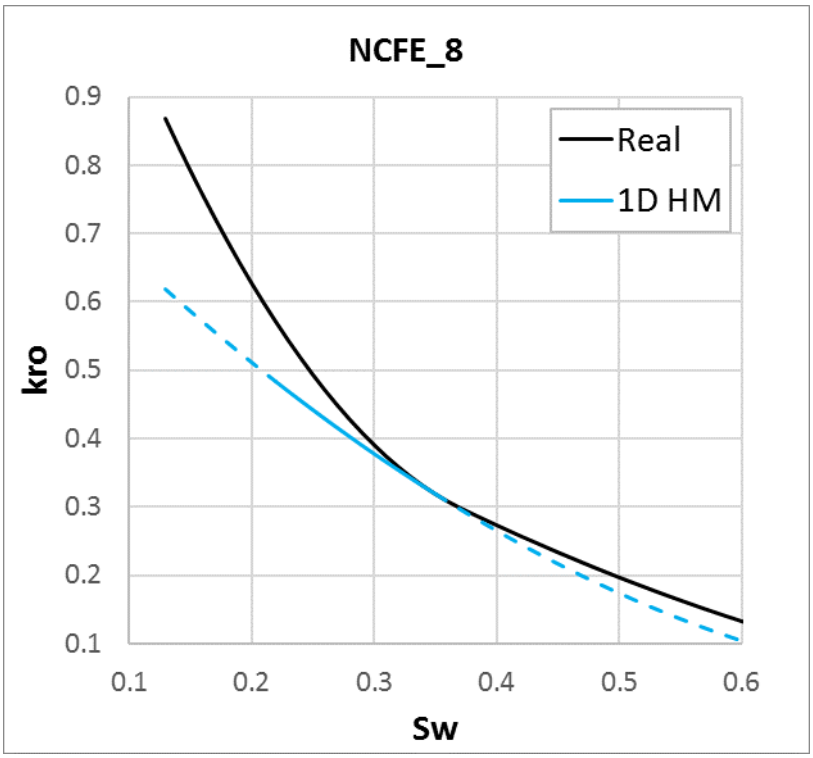

Figure 4-47: Relative permeability to oil as estimated by 1D HM compared with the real relative permeability (used in the NCFE) for NCFE_8, the solid lines represent the valid saturation range.

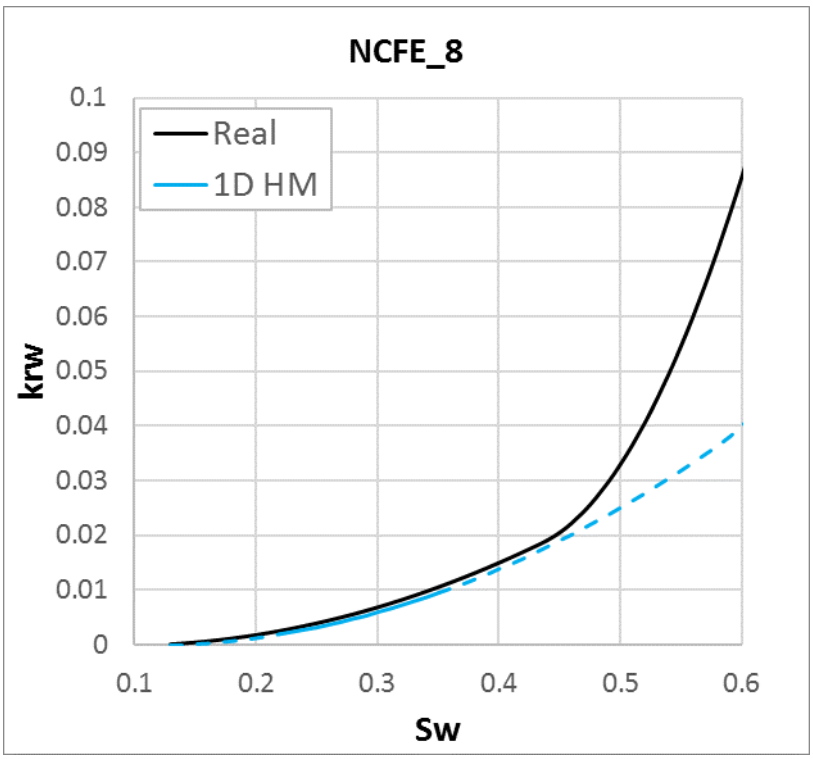

Figure 4-48: Relative permeability to water as estimated by 1D HM compared with the real relative permeability (used in the NCFE) for NCFE_8, the solid lines represent the valid saturation range.

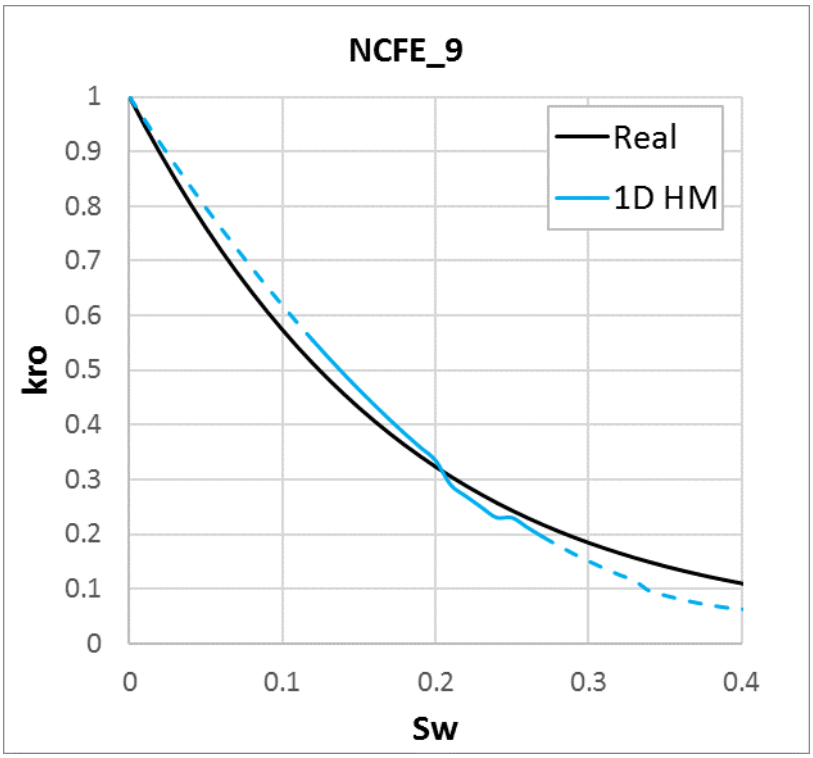

Figure 4-49: Relative permeability to oil as estimated by 1D HM compared with the real relative permeability (used in the NCFE) for NCFE_9, the solid lines represent the valid saturation range.

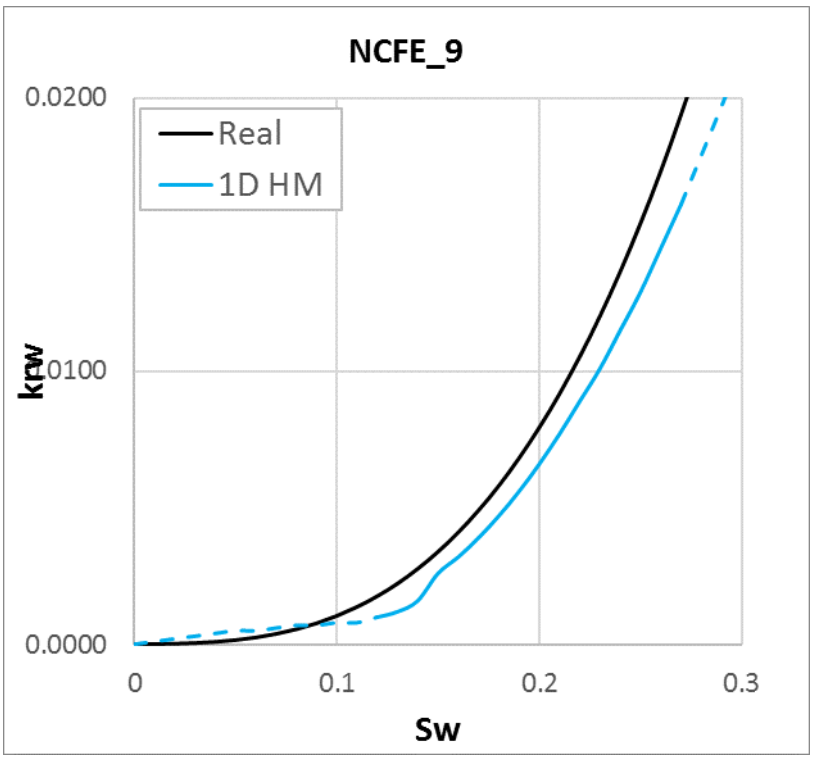

Figure 4-50: Relative permeability to water as estimated by 1D HM compared with the real relative permeability (used in the NCFE) for NCFE_9, the solid lines represent the valid saturation range.

The calculated mean absolute percentage error (MAPE) for each case is presented in Figure 4-51.

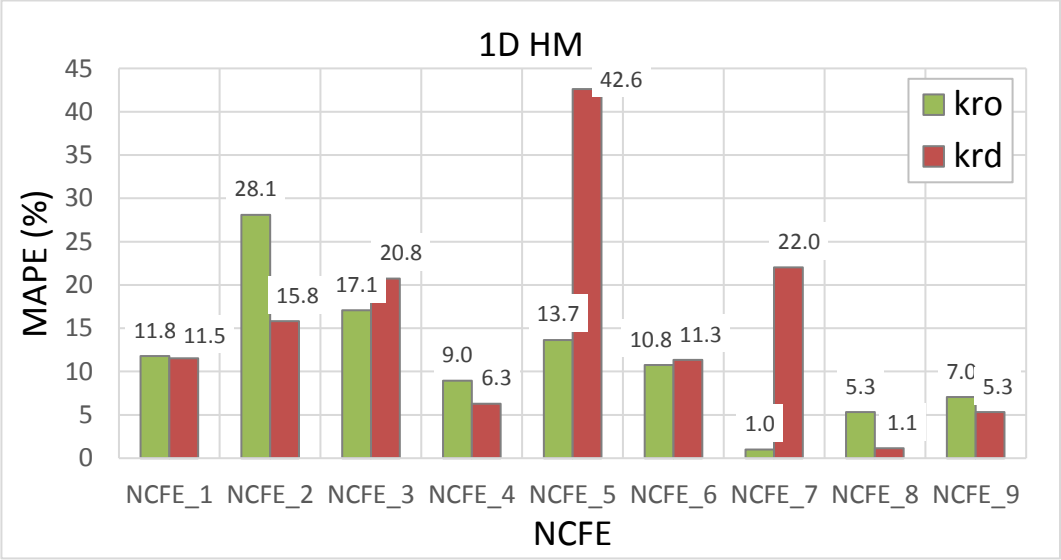

Figure 4-51:Mean absolute percentage error for the results of 1D HM estimation of k_{ro} and k_{rd}.

These results show that 1D HM has considerable error when estimating relative permeabilities for unstable cases. However, unlike JBN method, 1D HM seems not to be 'able' to tackle the phenomenon for the displacing fluid relative permeability, this fact may be due to the way 1D HM does the estimation.

Previously, a theory was developed from the results observed stating that in the case of viscous fingering formation, the displacing fluid is moving at its intended velocity, only the oil loses its capability to keep up with the displacing fluid letting it finger through and therefore not obeying the same mathematical laws developed in stability. In JBN method, being an explicit method, uses stable models to estimate directly the relative permeability. According to the theory, this fact allows the JBN to estimate correctly the displacing fluid relative permeability, since the gas moves in agreement with such models, but it fails to estimate the relative permeability to oil. 1D HM uses flow equations (Darcy's law) just as JBN does, however, it does not fit the complex results into stable models, it forces the results into a 1D simulation. In other words, it creates a 1D scenario where the same results (as the experiment) are seen. The difference between 1D HM and JBN is that, in JBN there is a certain model which translates the production data into relative permeabilities connecting all the physical properties and converging into an answer, while in the implicit method (1D HM) there is no such connection. For example, the key factor of this viscous fingering theory (the change in the oil velocity to let the displacing fluid through), is completely ignored, because in 1D simulation oil and displacing fluid must travel 'together'. It is possible to say that JBN has more 'physical meaning' than 1D HM. Another important result that can be drawn from this study is the difference of errors between JBN method and 1D HM, Figure 4-52. If it is considered 3% as a base error (error resulting from the method itself and not the fingering as seen in Figure 4-3 and Figure 4-29), the MAPE for the relative permeability to oil from both methods is within the same range of values, except for NCFE_2 and NCFE_3. This means that the results are consistent between both methods. However, in terms of displacing fluid, the error can, sometimes, be much higher than for the oil in the 1D HM. NCFE_5 and NCFE_7 are clear examples of this fact. It is then possible to say that it is preferable to use JBN method in cases with viscous fingering, since the very considerable error may be avoided in the estimation of the displacing fluid relative permeability.

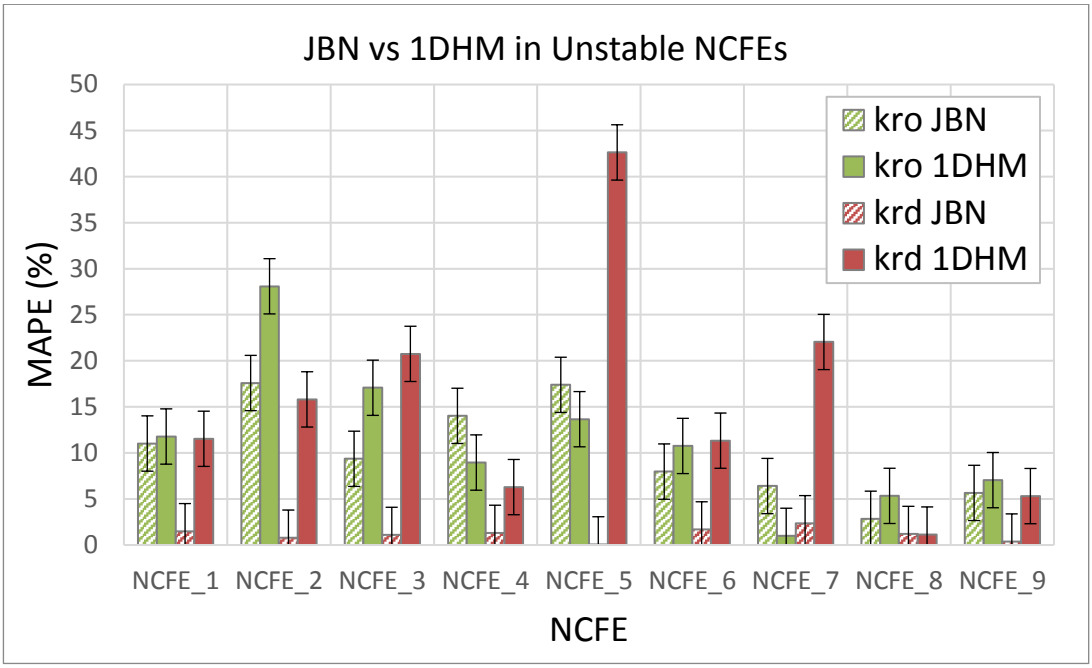

Figure 4-52:Mean absolute percentage errors for k_{ro} and k_{rd} as estimated by JBN and 1D HM. The base error is shown in black.

Similarly, to the JBN precision study, 1D HM was evaluated in NCFE_1_VR and NCFE_2_VR sets. These sets of NCFEs allow the establishment of correlations, since simulations are comparable if belonging to the same set. Figure 4-53 and Figure 4-54 show the errors of estimation using 1D HM for NCFE_1_VR and NCFE_2_VR sets of numerical coreflood experiments (NCFEs).

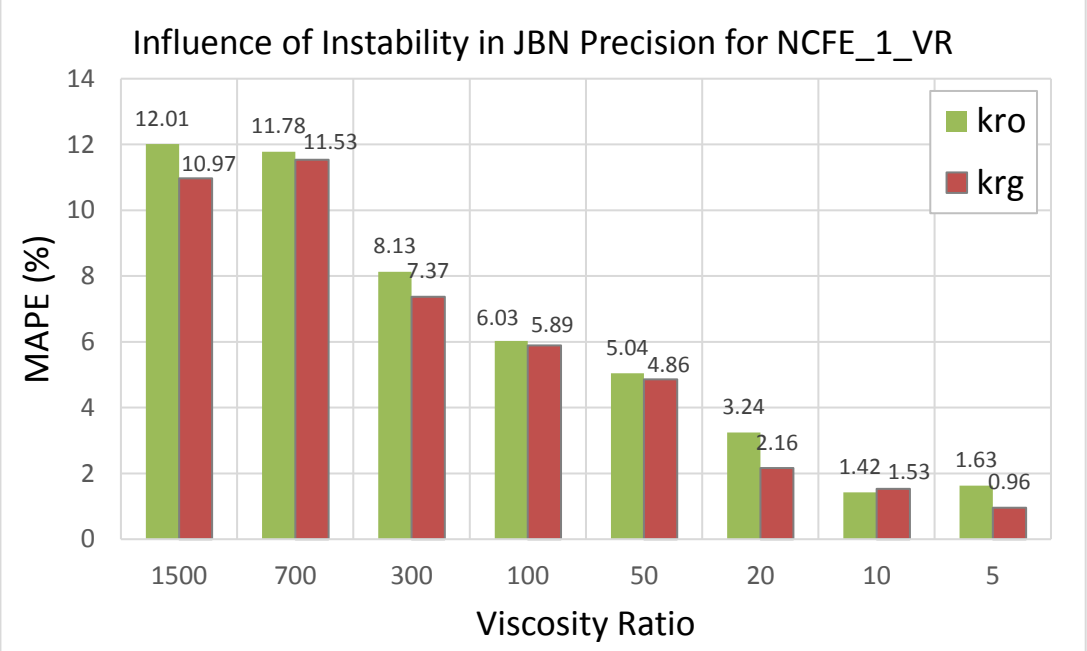

Figure 4-53: Influence of instability (produced by viscosity ratio) in 1D HM estimation of relative permeability for the NCFE_1_VR set, showing a direct correlation between instability and error.

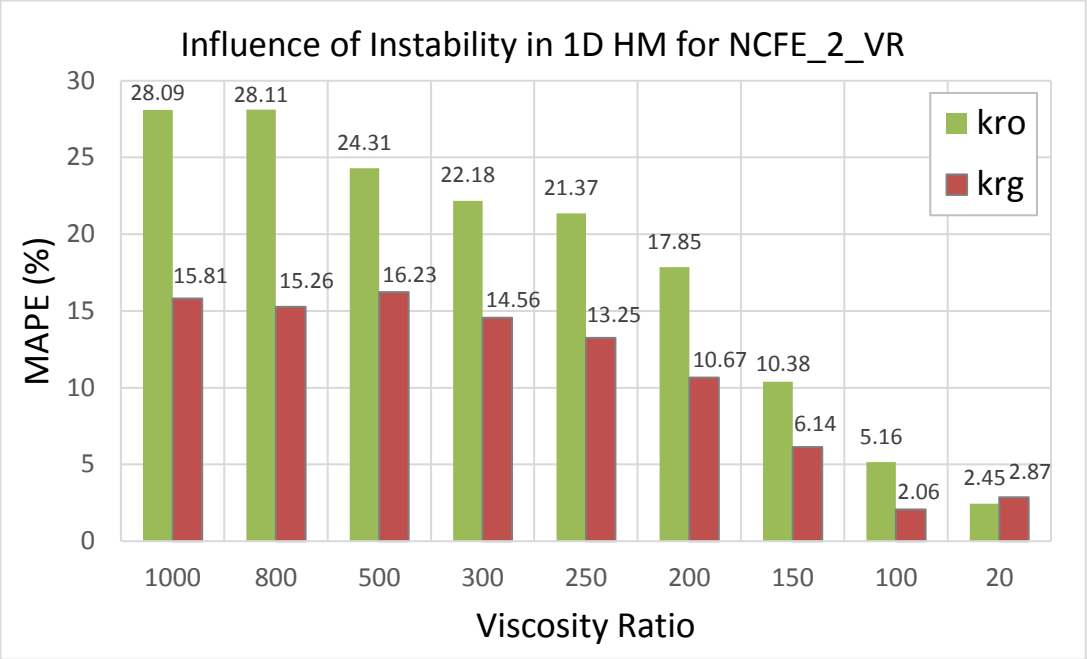

Figure 4-54: Influence of instability (produced by viscosity ratio) in 1D HM estimation of relative permeability for the NCFE_2_VR set, showing a direct correlation between instability and error.

These results show the direct correlation between the increase in instability (high viscosity ratio) and the error of estimation when using 1D HM. The more unfavourable the flow is the higher the error from the estimation method. This behaviour is very similar to what was seen for the JBN method. Nevertheless, as in the independent NCFEs, the error of the k_{rg} is not ignorable as in the JBN method results and it changes in a similar faction as the relative permeability of the oil, meaning that both the oil and gas k_r error is being influence by the stability of the flow. Such a conclusion is further supported by Figure 4-31 and Figure 4-32, since in stable displacement the errors of estimation are all below 3%, meaning that all the errors above this value are due to viscous fingering.
The 1D HM errors are consistent with the saturation profiles from Figure 3-11 and Figure 3-12, for both sets the error is reduced as the fingering gets less severe.

4.5 Conclusions

The following conclusion may be drawn from the evaluation of existing relative permeability estimation methods for unfavourable mobility corefloods:

- In this chapter, a novel methodology was proposed to evaluate the precision of 1D HM and JBN method in coreflood experiments with viscous fingering. The methodology uses numerical coreflood experiments (NCFEs) in other to allow a precise definition of the relative permeability curves, so that the estimation

methods' results could be conclusively compared. These NCFEs were treated as real laboratory experiments and the relative permeability used as the real curves for that experiment. The error of each method could be easily calculated by comparison of the estimated k_r and the real k_r curves.

- JBN method exhibited good precision on the stable version of the NCFEs, with all errors below 3%, deeming the method appropriate for relative permeability estimation of stable corefloods. For the unstable version of the NCFEs, JBN estimation of k_{ro} showed to be highly dependent on the viscous fingering severity. Differently, for k_{rd}, the results did not reveal any correlation with the instability of the flow and all errors were within the range of the error observed in the stable version of the NCFEs. This fact implies that JBN is correctly capturing the physics of flow for the displacing fluid but not the displaced fluid.
- One dimensional history matching had similar results to JBN method in the stable version of the NCFEs, with all the errors below 3%. For unstable version of the NCFEs, 1D HM estimation resulted in high error for both oil and displacing fluid relative permeability curves. The precision of the method followed a good correlation with viscous fingering formation, resulting in much higher errors than the ones observed in the stable version of these corefloods.
- This chapter results suggests 1D HM and JBN methods as unfit for the estimation of relative permeability curves of unstable coreflood experiments. Both methods showed a great dependency on the stability of the flow. Nevertheless, from these results, JBN seems to be a better choice to deal with instability when gravity and capillary pressure are ignorable, since the method showed good precision for the displacing fluid relative permeability. It is also possible to advise caution for the industry when using any of these methods to estimate the relative permeability for potentially unfavourable coreflood experiments.

Chapter 5: Accounting for Viscous Fingering in Relative Permeability Estimation Methods Based in Stable Displacement

5.1 Introduction

In the previous chapter it was demonstrated that the main relative permeability estimation methods cannot adequately account for viscous fingering, resulting in considerable error. The essential questions will therefore be: how should the relative permeability be estimated when viscous fingering is disturbing the flow in a coreflood experiment? This chapter addresses this question, by proposing a theory that helps explain the error occurring in relative permeability methods that are based in stable models. From that theory a model will be proposed which will allow modification of the JBN and 1D HM methods to take into account the viscous fingering and therefore reducing the error of such estimations.

5.2 Theory

To properly take viscous fingering into account in relative permeability estimation were initially quantitatively investigated the differences between a stable flow displacement and an unstable one.

Consider experiment 'A' as a homogenous porous medium displacement, which is characterized with a constant permeability K. In this experiment, a fluid with viscosity μ_1 and density ρ_1 will be displaced by a second fluid with viscosity μ_2 and density ρ_2. In this experiment the fluids are immiscible and no mass transfer will occur. The Darcy's laws describing each fluid, under suitable continuum assumptions, are:

$$\frac{dp_1}{dx} = \frac{-\mu_1 U}{k_{r1} K} + \rho_1 g \qquad 5\text{-}1$$

$$\frac{dp_2}{dx} = \frac{-\mu_2 U}{k_{r2} K} + \rho_2 g \qquad 5\text{-}2$$

Where p is the pressure of each fluid, k_r is the relative permeability, x is the distance travelled, U is the velocity and g is the acceleration of gravity. Now consider the front of displacement, where both fluids meet. The pressure force (p_2-p_1) on the displacing fluid

as a result of a virtual displacement δx of the interface from its simple convected location is (adapted from Homsy 1987):

$$\delta p = (p_2 - p_1) = \left[\left(\frac{\left(\frac{\mu_1}{k_{r1}} - \frac{\mu_2}{k_{r2}}\right)U}{K}\right) + (\rho_1 - \rho_2)g\right]\delta x \qquad 5\text{-}3$$

If the pressure force is positive, then any small displacement will be amplified and result in instability. Figure 5-1 a) shows an example where instability formed and Figure 5-1 b) an example where the flow is stable. For this work, the focus of study was the viscous fingering therefore, gravity was ignored to isolate the effect of the viscous forces (viscous fingering) in the relative permeability estimation, since it is clearly visible from equation 5-3 that the densities may reduce of increase the severity of the instability. Viscous fingering is characterized by varying saturation values along the z-axis with the progressing of the flow in the core (z-axis being the direction perpendicular to the flow), as presented in Figure 5-1 for experiment 'A'.

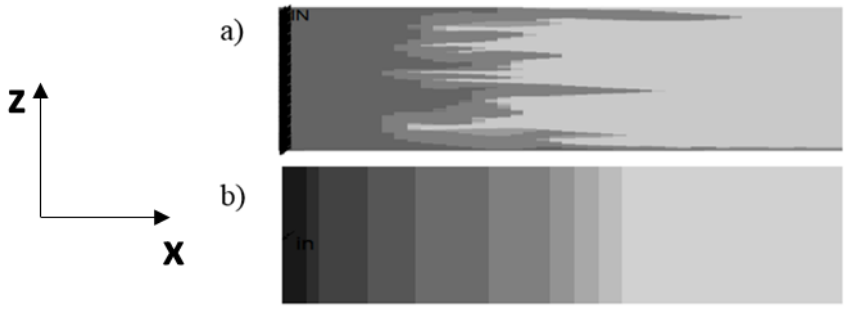

Figure 5-1: Experiment's 'A' Oil Saturation Profile for a) unstable flow with viscous fingering and b) stable/ideal displacement. Injection from the left.

Viscous fingering may lead to various problems, like early breakthrough and less ultimate recovery (Juanes & Blunt 2006; Sarma & Bentsen 1987). This phenomenon is also responsible for errors in standard relative permeability estimation method that are based on stable models. The Buckley-Leverett equations (Buckley & Leverett 1942), which are widely used in various kr estimation methods (e.g. JBN), and 1D history matching are only suitable for stable flow displacement experiments. Due to their simplicity, these methods are widely used in laboratories which perform special core analysis (SCAL) to estimate the relative permeability.

There are, nevertheless, methods that can numerically simulate apparent viscous fingering, like 2D and 3D history matching in association with methods that can trigger this phenomenon (for example, using permeability distribution functions, Cuthiell et al. 2006, or analytical viscous fingering models, Juanes & Blunt 2006) or, with more

physically based CT scans that can give some approximate pictures of the saturation profiles inside the core, only with fluids of high density contrast, like gas and water. The main disadvantage of these methods is the long time that 2D and 3D history matching takes, which can make them impractical. Also, most laboratories do not have access to saturation profile measurement methods, which are inefficient in most gas oil systems, anyway.

Although, for decades, the viscous fingering has been studied and several authors have tried to predict their patterns and develop models (Scott & Read 1959; Blackwell & Pozzi 1963; Maher 1985; Paterson 1985; Craig et al. 1957; Blackwell et al. 1959; Bacri et al. 1992) only very few studies have been reported on prediction of kr in presence of viscous fingering, making it impossible to draw conclusions by comparison, because there is no reliable relative permeability to make the comparison. The novel methodology developed in the previous chapter gives a unique opportunity to quantify and understand the error of prediction of relative permeability estimation models based on stability, by allowing the comparison between estimated and real relative permeability curves (something that to the best of the author's knowledge was never reported elsewhere).

From the results of Chapter 4, it was concluded that JBN equations can correctly estimate the displacing fluid relative permeability, but not the displaced fluid one. This seems to imply that the displacing fluid is behaving according to the equations of flow developed for stability.

Returning to experiment 'A' and if viscous fingering is happening in that displacement, from equation 5-3, it is known that (if gravity is ignored) the pressure force is positive because the mobility (relative permeability divided by the viscosity) of the displacing fluid is higher than the mobility of the displaced fluid. If the medium is not perfectly homogeneous (e.g. in a real porous medium the absolute permeability is not the same in any point of the medium, instead it follows a distribution of permeabilities), the differences in pressure will develop (because of small differences in the permeability of the medium which lead to the development of higher pressures in some zones of the front) and cause certain sections of the front to flow faster than others, resulting in the fingering of displacing fluid. Also, from the previous Chapter, it was seen that JBN equations were able to predict the relative permeability of the displacing fluid very well for cases with viscous fingering. The error promoted by the instabilities was all in the relative permeability of the oil. Based on these observations it is possible to suggest a theory with the following propositions:

- the displacing fluid will develop viscous fingering, but the its average flow obeys the stable models.
- the oil, being less mobile than the displacing fluid, has its 'intended' mobility (the one calculated from stable models) disrupted and, therefore, the mobility cannot be predicted by the models based on stability, resulting in error. This disrupted mobility will be lower than the one predicted by the stable models and will be a function of the degree of instability.

These propositions mean that, in fact, what is causing the error of estimation when applying stable models into flows with viscous fingering is the incorrect account for the oil flow, due to changes provoked by fingering.

With this theory, it is possible to explain why the JBN method can predict the relative permeability of the displacing fluid, but not the displaced fluid. The method is not able to predict that the oil mobility is different because the displacing fluid is bypassing most of the oil and that the oil flow is being reduced by this fact. Because JBN is based in stable models, the method sees the overall mobility of the oil as being lower, because it assumes that the front moves all at the same velocity and that the saturations are the same for the whole front, leading to the results of Chapter 4, where the relative permeability to oil is always lower than the real one. In other words, the relative permeability of the oil is not only a function of the displacing fluid saturation but also a function of a new parameter related with the degree of disruption provoked by the fingering displacing fluid.

As explained previously, the 1D HM has different conclusions for the displacing fluid /oil interaction and, differently than JBN, it has considerable error on the relative permeability of the displacing fluid. This derives from the fact that the 1D HM is trying to fit an unstable case into a 1D coreflood simulation. While the JBN uses the production data from the unstable experiment to calculate directly the relative permeability, 1D HM guesses relative permeabilities that can see comparable results to those in the experiment in 1D simulation. In other words, it can be said that JBN 'sees' the unstable problem but does an averaging of the results, while the 1D HM cannot even 'see' the unstable problem.

Using this theory proposed from the observation of Chapter 4 results it was possible to create a model in order to correct the methods based on stable flow to account for viscous fingering.

5.3 Stable Equivalent Model

In order to transform stable based methods to take viscous fingering into account a model had to be developed from the proposed theory. As explained in a previous section, the problem of methods like JBN is that they fit an unstable displacement into a stable model, which results in wrong relative permeability estimations.

In order to modify these methods to account for viscous fingering the concept of 'stable equivalent displacement' was introduced. A stable equivalent displacement is defined as transformation of an unstable coreflood experiment into ideal/stable flow, which when used in stable models of k_r estimation will result in the correct relative permeability curves.

For example, consider an unstable experiment where viscous fingering was formed during flooding. For this experiment it is assumed that the relative permeability is known with zero error. Using that relative permeability, two numerical corefloods are created with all the properties from the experiment. One of those numerical corefloods is performed in a 1D simulation and another in a 2D simulation (this 2D simulation uses the saturation profiles along the core observed during the experiment, to recreate the exact saturation patterns observed in the experiment). If the production data and differential pressure of both simulation (1D and 2D) were evaluated, it would be seen that the they would be different (assuming that the instability was substantial) and that the 2D simulation was much closer to the real experiment than the 1D simulation. Now, if both simulation results were used in JBN and 1D HM to calculate the relative permeability, the estimation would have less error when using the 1D simulation than the 2D simulation. In this example the 1D simulation may be called the stable equivalent representation of the experiment.

The usefulness of this approach is that (Buckley & Leverett 1942) based methods (e.g. JBN method) and 1D history matching methods would be completely applicable to the stable equivalent case and could be used to estimate the kr curves tackling the viscous fingering problem, since a multidimensional problem was converted into a one dimensional equivalent. This approach is different than using directly the relative permeability estimation methods on the production data of the experiment. In the later approach, the results from a multidimensional problem are 'fitted' into a stable model and will result in pseudo relative permeability curves that may not necessarily be representative of the reality and may result in considerable error, especially if this relative permeability curve will then be used for reservoir simulation.

The objective is then use propositions of the theory suggested in the previous section to develop a way to transform an unstable experiment data into a stable equivalent data that can then be used in JBN or 1D HM methods to obtain reliable relative permeability estimations. A summary of this idea may be found in Figure 5-2. The figure shows, schematically, that applying estimation methods like 1D history matching and JBN directly into the unstable coreflood production data will result in an unrealistic relative permeability curve (pseudo relative permeability curves). Although, by transforming this unfavourable mobility experiment into stable equivalent, 1D history matching and JBN can reach the real relative permeability.

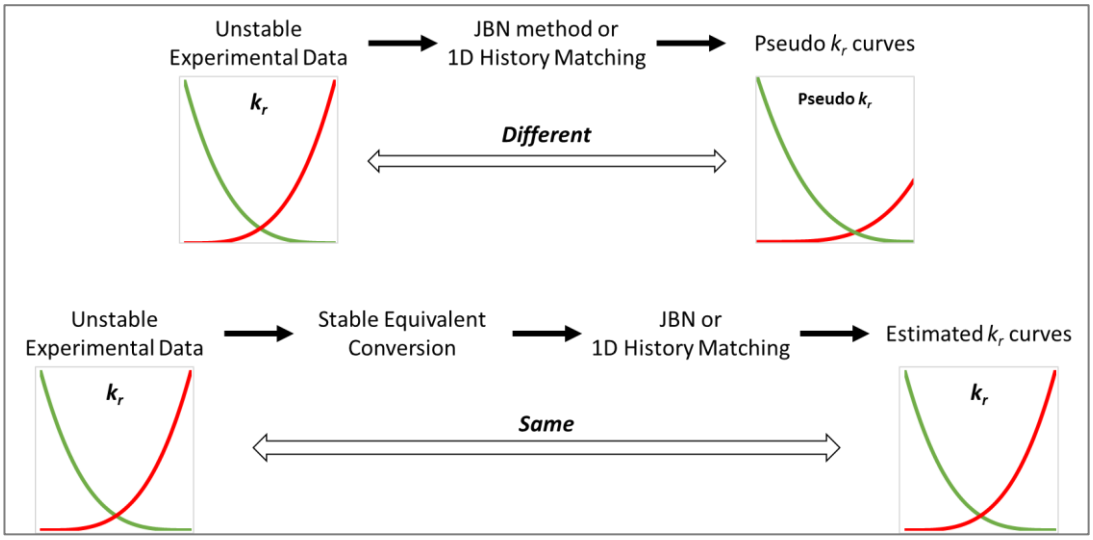

Figure 5-2: Appling ideal/stable flow based methods to unstable experimental data leads to error in relative permeability estimation, converting the data to a stable equivalent before using such methods (e.g. JBN or 1D history matching) can in theory supress that error.

5.3.1 Conversion of Unstable Corefloods into Stable Equivalents

The theory suggested in Chapter 5.2 proposes that only the error seen in stable kr estimation methods derives from the fact that the oil flow was disrupted by the displacing fluid fingering. The model was developed to treat oil (displaced fluid) and displacing fluid separately because of this fact.

5.3.1.1 Derivation of the Flow Equation for the Displacing Fluid

Traditionally, it was considered the displaced fluid as being oil, however this model may be used for any other displaced fluid. The displacing fluid was considered to be displacing fluid for the whole derivation process, but it may be any fluid.

The equations for fluid flow in porous media are basically described by the Darcy's Law. Assuming a typical coreflood experiment, the Darcy's Law describing the displacing fluid velocity is:

$$v_{d\,ex} = \frac{-Kk_{rd}}{\mu_d}\frac{dP_d}{dx} \quad \text{.....5-4}$$

Where $v_{d\,ex}$ is the displacing fluid superficial velocity, k_{rd} is the relative permeability to displacing fluid, μ_d is the displacing fluid viscosity, K is the absolute permeability, P_d is the displacing fluid pressure and x is the position in the flow direction. Viscous fingering is characterized by an increase in average velocity of the displacing fluid, due to differences in viscosity of the two fluids in the system, causing it to finger through the displaced fluid. Assuming that the experiment is unstable and viscous fingering forms, the velocity of displacing fluid will increase due to fingering in comparison to the ideal/stable scenario. This will make the flow of oil decrease proportionally to the increase of the velocity due to fingering. Therefore, in order to convert the experiment to its stable equivalent, the increase in velocity produced from fingering has to be compensated. In this way it is possible to say that the stable equivalent will have a lower velocity of displacing fluid than the actual velocity of the displacing fluid in the experiment. Mathematically this may be expressed as follows:

$$v_{ds} = \eta \times v_{d\,ex} \quad \text{.....5-5}$$

Where v_{ds} is the displacing fluid superficial velocity for the stable equivalent flow and η is the factor that measures how much the flow was accelerated by fingering. In other words, $v_{d\,ex}$ is higher (displacing fluid flows faster) due to fingering, by a factor of η (values from 0 to 1) than that of the stable equivalent flow. If η is 1 then the experiment has ideal/stable front and there is no difference in the velocities (experimental and stable equivalent are the same).

Since these displacing fluid velocities are superficial velocities and the area is the same for both:

$$q_{ds} = \eta \times q_{d\,ex} \quad \text{.....5-6}$$

Where q_{ds} and $q_{d\,ex}$ are the displacing fluid flow rate for the stable equivalent and the experiment, respectively.

From this perspective the whole influence of the fingering formation is taken into account in the displacing fluid flow equation, meaning that no modification will be done to the oil

flow equation. The Darcy equations for flow of oil and displacing fluid can be described as following:

$$q_{o\,ex} = q_o = \frac{-Kk_{ro}A}{\mu_o}\frac{dP_o}{dx} \quad \text{..... 5-7}$$

$$q_{d\,ex} = \frac{-Kk_{rd}A}{\mu_d}\frac{dP_d}{dx} \quad \text{..... 5-8}$$

Where $q_{o\,ex}$ and q_o are the oil flow rate for the experiment, k_{ro} is the relative permeability to oil, μ_o is the oil viscosity, P_o is the oil pressure, $q_{d\,ex}$ is the displacing fluid flow rate for the experiment and A is the cross sectional area. Substituting equation 5-8 in equation 5-6 gives:

$$q_{ds} = \frac{-Kk_{rd}A}{\mu_d}\frac{dP_d}{dx}\eta \quad \text{..... 5-9}$$

5.3.1.2 Derivation of the η Factor

By rearranging equation 5-5 it is possible to obtain equation 5-10, which allows the calculation of η. Since the value of $v_{d\,ex}$ is known (the superficial velocity can be calculated by dividing the displacing fluid injection rate by the cross sectional area) from the experiment, to calculate η, using equation 5-10, we only need to estimate the value of v_{ds} , i.e., the stable velocity of displacing fluid. Here the Sarma and Bentsen's (Sarma & Bentsen 1987) equation is used. Their equation was theoretically derived for water injection into a medium bearing viscous oil, so it was adapted here for displacing fluid injection, equation 5-11. It calculates the actual velocity of the displacing fluid, $v_{d,fa}$, in a stable displacement in terms of end-point mobility ratio, M, equations 5-11 to 5-13:

$$\eta = \frac{v_{ds}}{v_{d\,ex}} \quad \text{.....5-10}$$

$$v_{d,fa} = v_{ads} = \frac{v_{d\,ex}}{\phi(1 - S_{wirr} - S_{or})}\left[1 + \frac{M - 1 - N_g}{M + 1}\frac{M^{2/3} - 1}{M^{2/3}}\right] \quad \text{.....5-11}$$

$$M = \frac{k_{rd}^0/\mu_d}{k_{ro}^0/\mu_o} \quad \text{.....5-12}$$

$$N_G = \frac{\Delta\rho g k_{dor} Cos\alpha}{v_{d\,ex}\mu_d} \quad \text{.....5-13}$$

Where $v_{d,fa}$ is the actual velocity of displacing fluid as if the displacement was stable, N_g the gravitational number, ϕ the porosity, S_{wirr} the irreducible water saturation, S_{or} the

residual oil saturation, k_{rd}^0 the displacing fluid endpoint relative permeability (relative permeability to displacing fluid at residual oil saturation), k_{ro}^0 the oil endpoint relative permeability (relative permeability to oil at the very start of displacing fluid injection, when there is only oil and irreducible water in the core), $\Delta\rho$ the difference between the fluid densities, g the gravitational constant and K the absolute permeability of the core.

It is important to note the difference between v_{ds} and v_{ads}. The term v_{ds} is the superficial velocity for the stable equivalent experiment this means the velocity without accounting for the interstitial spaces in the core and is calculated by dividing the flow-rate of displacing fluid by the cross sectional area of the core. On the other hand, the addition of the subscript 'a' in the velocity (e.g. v_{ads}) means that this is an actual velocity, which is the velocity of the displacing fluid inside the core accounting for the flow paths and pores where the displacing fluid passes by. It can be calculated by measuring the time it takes the displacing fluid to go from the point of injection to the end of the core (total core length divided by breakthrough time). The idealized displacement model that serves as the basis for the instability theory proposed by Sarma and Bentsen is based on the assumption that the displacing and displaced fluids will remain separated by a saturation discontinuity, if the displacement is stable (Sarma & Bentsen 1987). However, in the real porous media this discontinuity doesn't exist and a distribution of the fluids will evolve to separate the two sections where only one fluid is following. The authors resolved this issue by assuming that only half of a water finger was propagating. They assumed that this approximation reflects the real saturation distribution in porous media. They showed that this approximation was very well supported by their experimental data.

Also worth mentioning is that the oil residual saturation, S_{or}, is the saturation at which the recovery of oil is almost zero. Since in this work numerical simulation was used, this point is very important to take note. In simulation the S_{or} is defined by the relative permeability used, meaning that, even if the oil cannot be recovered realistically, the simulation will continue to remove oil at a very low rate that in a very long time would reach the S_{or} defined in relative permeability. So it was defined that when the fractional flow of oil is less than 0.1% of the injected fluid (for each 1 pore volume of injected displacing fluid only 0.001 pore volumes of oil is recovered), the oil residual saturation is reached, since the simulations were performed with zero capillary pressure.

To calculate $v_{d,fa}$ first the endpoint mobility, M, and the gravitational number, N_g, are calculated using equations 5-12 and 5-13. The endpoint mobility calculation needs the endpoint relative permeabilities for displacing fluid and oil, both of which may be

obtained from experimental data. At the very beginning of the experiment the differential pressure, *dP/dx*, will be equal to the differential pressure of oil (dP_o/dx) and $q_{o\ ex}$ will be equal to the injection rate, because only oil is flowing, therefore, using Darcy's law, equation 5-7, it is possible to calculate k_{ro}. Since this value of k_{ro} is at the maximum saturation of oil it corresponds to the endpoint relative permeability, k_{ro}^0. In the same manner, for displacing fluid, the endpoint can be calculated by measuring the differential pressure when the oil saturation is minimum, i.e., very close to the residual oil saturation, when only displacing fluid in flowing inside the core. For those conditions the differential pressure is equal to the differential pressure of displacing fluid (dP_d/dx) and $q_{d\ ex}$ is equal to the injection rate, so equation 5-7 may be used to obtain k_{rd}, which will be equal to k_{rd}^0. Alternatively, (if at the end of experiment) S_o is not close to the residual oil saturation, it may be estimated using an extrapolation of the JBN k_r curves.

Sarma & Bentsen 1987 called $v_{d,fa}$ the actual velocity for the displacing fluid of an experiment if the flow was stable, which is the same as saying that this velocity is the actual velocity of the denominated stable equivalent flow, v_{ads}. This means that their $v_{d,fa}$ is equal to v_{ads}. It is important to notice here that Sarma & Bentsen 1987 used the actual velocity equation, v_{ads}, instead of the superficial velocity, v_{ds}. Therefore, to use this definition of velocity to calculate η, equation 5-10 has to be re-written in terms of actual velocity. Since the area and porosity are the same for the experiment and its stable equivalent, the relationship between the superficial and actual velocities is the same and can be written as in equation 5-14:

$$\eta = \frac{v_{ads}}{v_{ad\ ex}} \qquad \text{.....5-14}$$

Where $v_{ad\ ex}$, the actual displacing fluid velocity of the experiment, can be calculated using the breakthrough time obtained from the experiment:

$$v_{ad\ ex} = \frac{L}{t_{BT}} \qquad \text{.....5-15}$$

Where L is the core length and t_{BT} is the time that the displacing fluid takes to breakthrough from the core outlet, after the start of the injection.

One may say that if η is calculated using the velocities of the experiment, different injection rates would result in different values of η, because the breakthrough time is different. This is not true, since η is the ratio of the experimental and stable equivalent velocities, which 'cancels out' the effect of the change of injection rate at breakthrough time, i.e. η is independent of injection rates. However, the effect of the injection rate in the fingering formation is still considered by equation 5-11. But it is possible that η is

different for different injection rate, not because of the breakthrough times changes, but only when the higher injection rates influence fingering. Nevertheless, for the range of injection rates typically used in the experiments this difference should be negligible.

The η factor is a direct measure of how much the velocity of the displacing fluid changed from stable to unstable and may be used to determine if the relative permeability estimation by stable method will have considerable error or not. For example, if the calculated factor for a case is close to 1 then low error is expected by using stable methods to calculate the relative permeability to that specific case.

The relative permeability of the oil may, then, be calculated using this proposed model to generate a case with stable displacing fluid velocity. However, the same is not true for the displacing fluid relative permeability estimation. In order to reduce the velocity of the fingering to a stable scenario the velocity of the displacing fluid was altered and as it was proposed by the theory, the displacing fluid flow is correctly estimated by stable models. To 'revert' the alteration of the displacing fluid flow, one can simply correct the saturation at which the relative permeability of the displacing fluid is measured. This step is only necessary in the 1D history matching method since in JBN the k_{rd} may be found from the standard methodology and only the k_{ro} estimation needs to follow these proposed modifications. More details on how the saturation was corrected for the displacing fluid will be given in the section dedicated to the modification of the 1D HM to account for viscous fingering.

5.4 Modified JBN Method (MJBN) Derivation

5.4.1 Derivation of Modified Oil Fractional Flow

In the previous section it was theoretically proposed that one could tackle viscous fingering in coreflood relative permeability estimation, by converting the experimental data into a stable equivalent. The MJBN method focuses on the modification of the interpretation of fractional flow of oil in the original JBN method. In this section the fractional flow equation for the stable equivalent case will be deduced.

Subtracting equation 5-9 to equation 5-7 results in:

$$-\frac{1}{KA}\left(q_o\frac{\mu_o}{k_{ro}}-q_{ds}\frac{\mu_d}{k_{rd}}\frac{1}{\eta}\right)=-\frac{dP_c}{dx} \quad \text{..... 5-16}$$

Where P_c is the capillary oil-displacing fluid pressure. Knowing that $q_{ds} = q_s - q_o$ (where q_s is the total flow in the stable equivalent):

$$-\frac{1}{KA}\left(q_o\frac{\mu_o}{k_{ro}} - q_s\frac{\mu_d}{k_{rd}}\frac{1}{\eta} + q_o\frac{\mu_d}{k_{rd}}\frac{1}{\eta}\right) = -\frac{dP_c}{dx} \quad \text{..... 5-17}$$

Which can be rearranged to:

$$q_o\left(\frac{\mu_o}{k_{ro}} + \frac{\mu_d}{k_{rd}}\frac{1}{\eta}\right) = KA\frac{dP_c}{dx} + q_s\frac{\mu_d}{k_{rd}}\frac{1}{\eta} \quad \text{..... 5-18}$$

Dividing everything by q and knowing that oil fractional flow is defined as $f_{os} = q_o/q_s$:

$$f_{os}\left(\frac{\mu_o}{k_{ro}} + \frac{\mu_d}{k_{rd}}\frac{1}{\eta}\right) = \frac{KA}{q}\frac{dP_c}{dx} + \frac{\mu_d}{k_{rd}}\frac{1}{\eta} \quad \text{..... 5-19}$$

Which can be rearranged to:

$$f_{os} = \frac{\frac{KA}{q}\frac{dP_c}{dx} + \frac{\mu_d}{k_{rd}}\frac{1}{\eta}}{\left(\frac{\mu_o}{k_{ro}} + \frac{\mu_d}{k_{rd}}\frac{1}{\eta}\right)} \quad \text{..... 5-20}$$

Multiplying by k_{rd}/μ_d in both numerator and denominator:

$$f_{os} = \frac{\frac{KA}{q}\frac{k_{rd}}{\mu_d}\frac{dP_c}{dx} + \frac{1}{\eta}}{\left(\frac{\mu_o}{\mu_d}\frac{k_{rg}}{k_{ro}} + \frac{1}{\eta}\right)} \quad \text{..... 5-21}$$

Ignoring capillary pressure, $P_c = 0$:

$$f_{os} = \frac{\frac{1}{\eta}}{\left(\frac{1}{\eta} + \frac{\mu_o}{\mu_d}\frac{k_{rd}}{k_{ro}}\right)} \quad \text{..... 5-22}$$

The fractional flow of oil, f_{os}, is for the stable equivalent experiment (the unstable experiment is being 'transformed' into an equivalent stable one, by accounting for the increasing displacing fluid velocity in the fractional flow equation, so that the JBN method can be applied). This fractional flow will be higher (after breakthrough) than the one calculated directly from experiment data, since the velocity was reduced by a factor η, to account for fingering.

In f_{os} equation, k_{rd} and k_{ro} are the relative permeabilities estimated using the standard JBN method. So, one may calculate f_{os} by calculating the relative permeability curves values with the standard JBN method, so that f_{os} may be then used in the MJBN method.

The modified fractional flow equation will lead to change in some of the original JBN equations, namely $S_{d,out}$ and k_{ro}, equations 4-5 and 4-7, respectively.

The JBN method would calculate $S_{d,out}$, i. e. the displacing fluid saturation at the outlet face of the core (ignoring the displacing fluid fingering effect), as in equation 4-5. To account for the displacing fluid fingering, in the MJBN formulation, the term f_o is replaced by its stable equivalent value $f_{o\ stable}$, as obtained from Equation 5-22, to obtain the modified displacing fluid saturation at the outlet face using Equation 5-23, and the corresponding oil relative permeability, $k_{ro\ MJBN}$, from Equation 5-24 as follows:

$$S_{d,out\ stable} = S_{\mathrm{d,avg}} - D_i \times f_{os} \quad \text{.....5-23}$$

$$k_{ro\ MJBN} = k_{ro}^{0} \frac{f_{os} \times d\left(\frac{1}{D_i}\right)}{d\left(\frac{1}{D_i I_r}\right)} \quad \text{..... 5-24}$$

Where $S_{d,out\ stable}$ is the displacing fluid saturation at the outlet surface calculated for the stable equivalent, $S_{d,avg}$ the average saturation of displacing fluid inside the core, *Di* the cumulative displacing fluid injected expressed as a fraction of total pore volume and $k_{ro\ MJBN}$ the relative permeability to oil calculated from MJBN method for the displacing fluid saturation at the outlet of the core.

5.4.2 Derivation of Displacing Fluid's Relative Permeability

As seen from the results of Chapter 4 and proposed by the theory in which this model is based on, the relative permeability of the displacing fluid does not need any correction, so it may be simply calculated as in equation 4-8 as a function of $S_{d,out}$, so it follows that:

$$k_{rd\ MJBN} = k_{rd\ JBN} \quad \text{..... 5-25}$$

Alternatively, it is possible to estimate the relative permeability of the displacing fluid using the stable equivalent case. This approach, although unnecessary in the MJBN was very important to develop the 1D HM correction, which will be presented further in the Chapter. To estimate the displacing fluid's relative permeability from the stable equivalent experiment it is necessary to 'revert' the reduction in the displacing fluid flow that was necessary to eliminate the influence of viscous fingering in the oil flow. This can be simply done by correcting the saturation of displacing fluid at the outlet for each the k_{rd} is a function of, as it is explained below. When in the stable equivalent the velocity of the displacing fluid is reduced the fractional flow of oil is increased in response as seen in 5-22, which in turn reduced the saturation of displacing fluid at the outlet surface as in equation 5-23. In order to eliminate this effect on the displacing fluid relative permeability only, the $k_{rd\ MJBN}$ is plotted as a function of $S_{d,out}$ (calculated using f_o, equation 4-5) instead of $S_{d,out\ stable}$ (calculated using f_{os}, equation 5-23 and 5-22):

$$k_{rd\ MJBN}(S_d) = k_{rd\ JBN}(S_d) = k_{rd\ stable}(s_{d,out}) \quad \text{.....5-26}$$

$$k_{rd\ MJBN}(S_d = S_{d,out}) = \frac{(1-f_{os})}{f_{os}}\frac{\mu_d}{\mu_o}k_{ro\ MJBN} \quad \text{.....5-27}$$

This change mimics the mobility difference produced by the fingering velocity in the original experiment and therefore allows the calculation of the relative permeability of the displacing fluid by attributing a higher value of saturation corresponding to the mobility of the displacing fluid in fingering.

In the next section, it will be explained how to use all these equations in the MJBN method to produce the relative permeability of displacing fluid. As explained before this is an optional methodology to find the k_{rd} in JBN but, as will be shown, it was fundamental to correct the 1D HM where the method is not explicit and k_{rd} is not correctly calculated in the standard version of the method as it is in JBN.

5.4.3 Method Algorithm

An algorithm was created to correctly use MJBN method for coreflood relative permeability estimation, Figure 5-3. Described in detail in the following steps:

1. Initially all the necessary experimental data is gathered, this includes the core and fluid data and, also, the production and differential pressure results.

2. With the experimental data it is possible to calculate η factor using equation 5-14, this factor is constant and specific for a certain experiment.
3. Then, an iterative process starts for the calculation of each point of relative permeability curves versus the displacing fluid saturation. Each iteration, t_i, corresponds to an injection time were the experiment results were gathered, where i counts sequentially the number of values registered during the experiment. Between each time step, the value of i increases by 1 (i=i+1), until the count reach the total number of values measured, i = n.
4. For the time $t = t_i$, the corresponding experimental data is gathered and used to calculate the fractional flow of oil f_o as in equation 4-4.
5. From this oil fractional flow, the saturation of the displacing fluid at the outlet surface is calculated from equation 4-5.
6. Then equations 4-6, 4-7, 4-8 are used to calculate the relative permeability curves estimated by the standard JBN method for oil and displacing fluid, $k_{ro\ JBN}$ and $k_{rd\ JBN}$, respectively, at the injection time $t = t_i$.
7. The values of $k_{ro\ JBN}$ and $k_{rd\ JBN}$ are used to calculate the stable equivalent fractional flow of oil, f_{os}, for the correspondently time step using equation 5-22.
8. The relative permeability to oil, $k_{ro\ MJBN}$, as estimated by the modified JBN method (MJBN) is calculated using equation 5-24 and the relative permeability of the displacing fluid, $k_{rd\ MJBN}$, using equation 5-27. The value of $k_{ro\ MJBN}$ is corresponds to the displacing fluid saturation calculated by equation 5-23, $S_{d,out\ stable}$. The value of $k_{rd\ MJBN}$ corresponds to the displacing fluid saturation calculated by equation 4-5, $S_{d,out}$.
9. These relative permeabilities may be plotted as a function of the corresponding saturations in addition to any values calculated in previous iterations in order to have curves as a function of different saturation values.
10. If the count, i, is different than n, then the process is repeated for the next time step doing i=i+1 and returning to point 4 of this description.
11. If the i corresponds to the last measured value, the relative permeability curves are completed for that experiment.

Being an unsteady-state method, the relative permeably curves resulting from MJBN are only valid after the breakthrough time. So any value calculated for before this time should be eliminated.

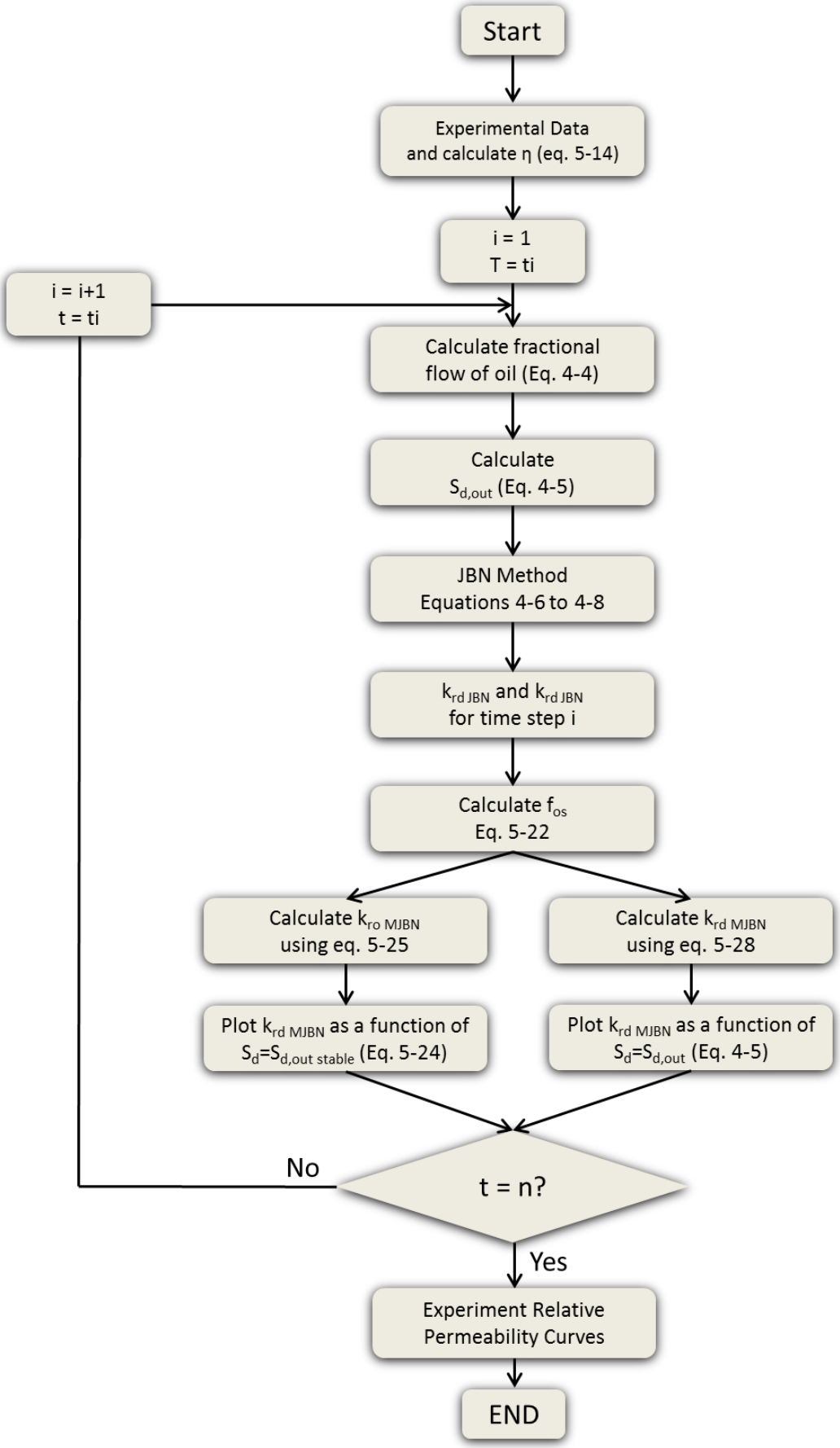

Figure 5-3: Methodology for application of MJBN to experimental SCAL data.

5.4.3.1 Practical Example

Numerical Coreflood data was created to use as examples for application of the MJBN method by following the algorithm presented in Figure 5-3. A set of 3 NCFEs was created with their beginning in a fairly stable displacement and incrementally imposing instability in successive displacements. The NCFEs represented experiments where gas is injected into an oil saturated core with some irreducible water. This was done by changing the viscosity ratio in the coreflood experiments. Gas viscosity was maintained constant at 0.05 mPa.s and the oil viscosity was varied from 0.25 to 2.5 and 35, resulting in viscosity ratios 5, 50 and 700, respectively.

The CMG – IMEX simulator was used to perform the 2D NCFEs. The core was the same for the three NCFEs and was defined as being 60.5 cm in length and 5.08 cm in diameter. The simulation used a quadratic representation of the cylindrical core, changing it to an equivalent prism with 60.5x4.5x4.5 (length, width and thickness) dimensions. Width and thickness were chosen keeping the same cross-sectional area as in the original cylindrical core. The core was rendered with 55,296 grid blocks distributed in 864x64x1: length, width and thickness respectively. To represent a coreflood experiment with rotating core (no gravity effect), the cores were created in XY Cartesian coordinate grid, X being the direction of the flow.

Gas injection was fixed at 0.375 cm^3/min for the cases with viscosity ratios of 5, 50 but at 0.1 cm^3/min for the viscosity ratio of 700 (the latter change was necessary because of convergence problems) and the initial pressure of the experiments was set at 12,000 kPa. The core was initially saturated with 82% oil and 18% of irreducible water and the average absolute permeability of the core was 65 mD. The permeability distribution used, was a Gaussian distribution with a variance of 42 and mean of 65 mD. This distribution was created within the software using a specific tool.

The relative permeability used in the NCFEs was created using Sigmund & McCaffery 1979 equations with parameters N_o = 2.5, N_g = 2.5, A = 0.01, B = 0.01, k_{ro}^0 = 0.6, k_{rg}^0 = 0.8, resulting in the relative permeability curves shown in Figure 5-4. The main core and fluid properties used in the NCFEs are presented in Table 5-1.

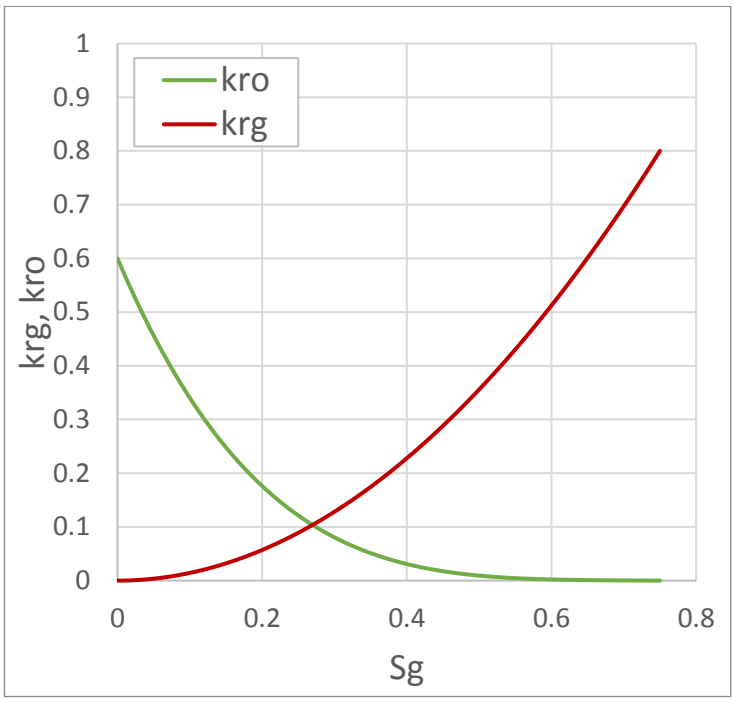

Figure 5-4:Relative Permeability used in the NCFEs.

Table 5-1: Core and Fluid Properties used in the Numerical Coreflood Experiments (NCFEs).

Parameter	***Value***	***Units***
S_{oi}	0.82	frac.
S_{wc}	0.18	frac.
Length	60.5	cm
Diameter	5.08	cm
Porosity	0.2	frac
Pore Volume	245	cm^3
Injection Rate	0.1 to 0.375	cm^3/min
Gas Viscosity	0.05	mPa.s
Pressure	12.000	kPa
Permeability	65	mD

To evaluate the fingering formation in different NCFEs, the gas saturation profile was gathered to see the gas fingering and stability of the oil-gas front, the results are presented in Figure 5-5 for the three values of viscosity ratio. Note that a dichromatic scheme was used with black for oil (parts of the core untouched by gas) and shades of grey for different values of gas saturation (lighter colour meaning more gas in that zone of the core). The colour scale was different between each of the NCFEs in order to highlight the differences

in the front. Also, the picture of the core length was cut, in the images, to show only the fingering zone more clearly, since the NCFEs were performed in a relatively long core. For low viscosity ratios there is a high saturation shock at the front, which is not seen for high viscosity ratios due to the difference in mobility (e.g. high viscosity ratio leads to lower mobility of the fluid and less sharp a saturation front inside the core). Therefore, it was decided to use a colour scale that would fit each experiment best. Every image was captured at a point where the front is fully visible but close to the gas breakthrough time. It is known that viscous fingers can coalesce into a few 'main' fingers while going through the total length of the core (Slobod & Thomas 1963; Zimmerman & Homsy 1991), so by capturing the front image near the breakthrough time, the effect of fingering in production is better captured, since that will be the final aspect of the fingering before leaving the core.

Viscosity Ratio	***Gas Saturation Profile***
5	
50	
700	

Figure 5-5: Gas saturation profiles inside the core for different viscosity ratios, using the core and fluid properties, showing differences in the frontal stability and formation of fingering for unfavourable viscosity ratios (Black = oil, different shades of grey correspond to different gas saturations).

NCFE with Viscosity Ratio = 5

The NCFE production data and differential pressure are presented in Table 5-2, where N_p is the cumulative oil production, G_i is the cumulative gas injected, ΔP is the differential pressure, V_p is the pore volume, Q_i is the cumulative water injection in pore volumes, $\overline{S_g}$ is the average gas saturation inside the core and S_{gi} is the initial gas saturation (which is 0 in this case). This table represents the above-mentioned Step 1 in the MJBN methodology workflow. The values are a small sample of data selected from a greater pool of numbers (more than 20,000 time steps) to demonstrate the procedure for this first example.

Table 5-2: Data for Calculation of Oil/Water Relative Permeability with MJBN for viscosity ratio = 5.

Time /min	**N_p /cm^3**	**G_i /cm^3**	**ΔP /kPa**	**Q_i = G_i/V_p**	**$\overline{Sg}$ = $S_{gi} + N_p/V_p$**
0.00	0.00	0.00	0.00	0.00	0.00
0.03	0.01	0.01	5.35	0.00	0.00
7.98	2.99	2.99	13.02	0.01	0.01
34.51	12.94	12.94	12.41	0.05	0.05
52.12	19.55	19.55	12.14	0.08	0.08
75.22	28.21	28.21	11.74	0.12	0.12
83.68	31.38	31.38	11.58	0.13	0.13
152.13	57.05	57.05	10.44	0.23	0.23
201.33	75.51	75.50	9.62	0.31	0.31
271.25	101.72	101.72	8.64	0.42	0.42
275.15	102.33	103.18	8.41	0.42	0.42
291.00	103.69	109.12	8.24	0.45	0.42
306.00	104.84	114.75	8.05	0.47	0.43
309.00	105.07	115.87	8.01	0.47	0.43
312.00	105.29	117.00	7.97	0.48	0.43
315.00	105.50	118.13	7.93	0.48	0.43
318.00	105.72	119.25	7.89	0.49	0.43
321.00	105.93	120.38	7.86	0.49	0.43
324.00	106.14	121.50	7.82	0.50	0.43
372.00	109.18	139.50	7.31	0.57	0.45
558.00	117.66	209.25	6.10	0.85	0.48
594.00	118.92	222.75	5.94	0.91	0.49
801.00	124.77	300.38	5.27	1.23	0.51
900.00	126.98	337.50	5.04	1.38	0.52
1251.00	133.03	469.13	4.49	1.91	0.54
1938.00	140.59	726.75	3.90	2.97	0.57
2673.00	145.77	1002.38	3.55	4.09	0.59
3276.00	148.86	1228.50	3.37	5.01	0.61
4257.00	152.64	1596.38	3.16	6.52	0.62
5760.00	156.69	2160.00	2.95	8.82	0.64
6744.00	158.67	2529.00	2.86	10.32	0.65
7647.00	160.18	2867.63	2.79	11.70	0.65
9087.00	162.16	3407.63	2.70	13.91	0.66
12960.00	165.90	4860.00	2.55	19.83	0.68

The η factor is calculated using equations 5-11 to 5-15, all the values necessary for its calculation are given in the experimental details. The residual oil saturation, S_{or}, had a value of 0.185. The value of η was calculated to be 1.00, meaning that in this case (i.e., at low viscosity ratio of 5) no instability was observed and the MJBN k_r curves will be equal to those calculated by the JBN method (pseudo relative permeability curves). This was to be expected from the gas saturation profiles in Figure 5-5, top. Using the JBN's standard equations 4-3 to 4-8 the pseudo relative permeabilities are estimated to oil and

water by the JBN method as it is presented in sequential order from left to right in Table 5-3.

Table 5-3: Calculation of pseudo relative permeabilities by JBN method.

f_o	S_{gout}	I_r	$A = 1/Q_i I_r$	$B = 1/Q_i$	$d(A)/d(B)$	k_{ro} JBN	k_{rg} JBN
-	-	-	-	-	-	-	-
1.00	0.00	2.43	8981.93	21814.90	-	-	-
1.00	0.00	1.00	81.96	81.87	0.41	1.47	0.00
1.00	0.00	1.05	18.08	18.94	1.02	0.59	0.00
1.00	0.00	1.07	11.71	12.54	0.99	0.60	0.00
1.00	0.00	1.11	7.84	8.69	1.01	0.60	0.00
1.00	0.00	1.12	6.96	7.81	1.01	0.60	0.00
1.00	0.00	1.24	3.45	4.30	1.00	0.60	0.00
1.00	0.00	1.35	2.40	3.25	1.00	0.60	0.00
1.00	0.00	1.50	1.60	2.41	0.96	0.63	0.00
0.42	0.24	1.55	1.54	2.37	1.88	0.13	0.04
0.23	0.32	1.58	1.42	2.25	0.88	0.16	0.11
0.21	0.33	1.61	1.32	2.14	0.92	0.13	0.10
0.20	0.34	1.62	1.30	2.11	0.93	0.13	0.10
0.19	0.34	1.63	1.28	2.09	0.92	0.13	0.10
0.19	0.34	1.64	1.27	2.07	0.93	0.12	0.10
0.19	0.34	1.65	1.25	2.05	0.93	0.12	0.10
0.19	0.34	1.65	1.23	2.04	0.92	0.12	0.11
0.19	0.34	1.66	1.21	2.02	0.91	0.12	0.11
0.17	0.35	1.78	0.99	1.76	0.87	0.12	0.12
0.12	0.38	2.13	0.55	1.17	0.75	0.10	0.14
0.09	0.40	2.19	0.50	1.10	0.66	0.09	0.17
0.08	0.42	2.47	0.33	0.82	0.60	0.07	0.18
0.06	0.44	2.58	0.28	0.73	0.55	0.07	0.21
0.05	0.45	2.90	0.18	0.52	0.50	0.06	0.23
0.03	0.49	3.33	0.10	0.34	0.43	0.04	0.27
0.02	0.52	3.66	0.07	0.24	0.37	0.03	0.32
0.01	0.54	3.86	0.05	0.20	0.34	0.02	0.35
0.01	0.56	4.12	0.04	0.15	0.31	0.02	0.38
0.01	0.58	4.40	0.03	0.11	0.29	0.02	0.41
0.01	0.59	4.55	0.02	0.10	0.27	0.01	0.44
0.00	0.60	4.66	0.02	0.09	0.26	0.01	0.46
0.00	0.61	4.81	0.01	0.07	0.25	0.01	0.48
0.00	0.63	5.09	0.01	0.05	0.24	0.01	0.51

These JBN's relative permeability values will be used in 5-22 to calculate the stable equivalent fractional flow of oil, f_{os}. Then, using equations 5-23, 5-24, and 5-27 the relative permeability curves for oil and gas from MJBN are estimated. This process is summarized in Table 5-4, showing the corrected relative permeability. However, for this

case, since η = 1, JBN and MJBN give the same results. The resulting relative permeability curves can be seen in Figure 5-6 for the valid saturation range.

Table 5-4: Calculation of relative permeabilities by MJBN method.

f_{os}	S_{gout} Stable	k_{ro} MJBN	k_{rg} MJBN
-	-	-	-
-	-	-	-
-	-	-	-
1.00	0.00	-	-
1.00	0.00	0.60	0.00
1.00	0.00	0.60	0.00
1.00	0.00	0.60	0.00
1.00	0.00	0.60	0.00
1.00	0.00	0.60	0.00
1.00	0.00	0.63	0.00
0.42	0.24	0.13	0.04
0.23	0.32	0.16	0.11
0.21	0.33	0.14	0.10
0.20	0.34	0.13	0.10
0.19	0.34	0.13	0.10
0.19	0.34	0.12	0.10
0.19	0.34	0.12	0.10
0.19	0.34	0.12	0.11
0.19	0.34	0.12	0.11
0.17	0.35	0.12	0.12
0.12	0.38	0.10	0.14
0.09	0.40	0.09	0.17
0.08	0.42	0.07	0.18
0.06	0.44	0.07	0.21
0.05	0.45	0.06	0.23
0.03	0.49	0.04	0.27
0.02	0.52	0.03	0.32
0.01	0.54	0.02	0.35
0.01	0.56	0.02	0.38
0.01	0.58	0.02	0.41
0.01	0.59	0.01	0.44
0.00	0.60	0.01	0.46
0.00	0.61	0.01	0.48
0.00	0.63	0.01	0.51

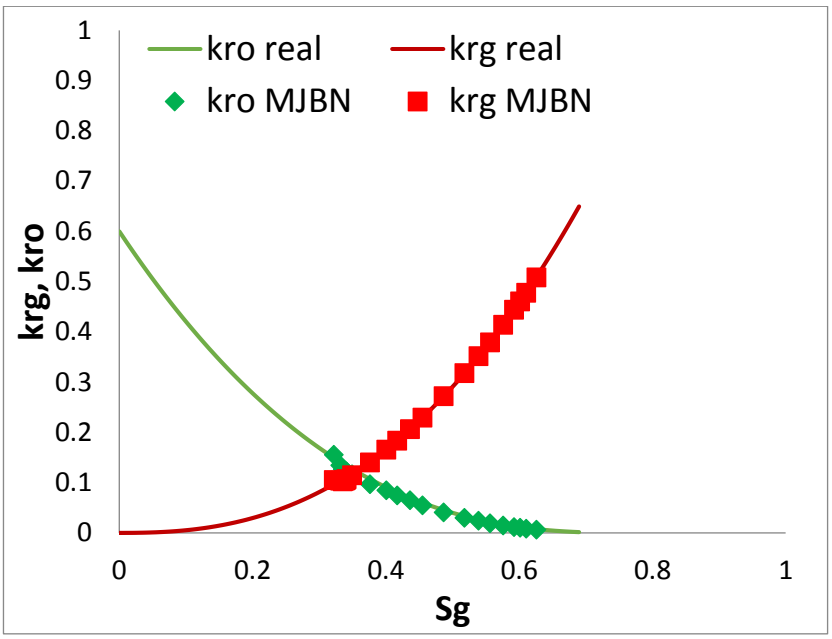

Figure 5-6:Relative Permeability Curves as calculated by MBJN versus the real kr curves for a NCFE with viscosity ratio = 5. Absence of viscous fingering has resulted in the kr curves to JBN and MJBN to be identical.

NCFE with Viscosity Ratio = 50

The procedure for this case was exactly the same as for the previous one, but here the results of all the time steps of the simulation used in the calculations are presented. The η factor was calculated to be 0.921 in this case (8.6% deviation from stability). Figure 5-7 and Figure 5-8 show, in points, the k_r values obtained for each time step using JBN and MJBN, respectively, with the corresponding fit using a relative permeability correlation. The correlation used to fit the point was the one developed by Sigmund & McCaffery 1979, which is based on the Corey correlation but has more degrees of freedom, so it allows a better matching. In these 2 figures is also visible what may seem as numerical dispersion for the last gas saturation range. This mismatch is due to the very small differences in the differential pressure, which are bound to happen at the end of the simulation, when almost no oil is being produced. The JBN method (and the MJBN) are very sensitive to these changes and this results in high error, typically that part of the curve should be ignored, but it was decided to be shown here as an example. For the correlation, the k_{ro} endpoints obtained were used shown as black dots on Figure 5-9. The correlation was fitted considering the density of points, meaning that the fitting curve is the result of the minimization of the error between the point and the curve. The saturation range presented is the valid saturation range for the experiment: the range of saturations between the breakthrough time and the end of the coreflood (when insignificant amount of oil is being produced). It should also be noted that, since these cases have viscous

fingering, the saturations at a time just immediately after breakthrough may have some error due to the fact that not all the outlet surface of the core is yet in 2-phase flow. This may result in some error at the first saturation points when gas fingers are still leaving the core. In order to compare the correction performed by MJBN onto the standard JBN, the fitted curves from both methods were plotted against the real k_r curves in Figure 5-9. From this Figure it is evident that there is some considerable error in k_{ro} when using JBN in this case. On the contrary, MJBN k_r curves match the real k_r curves very well.

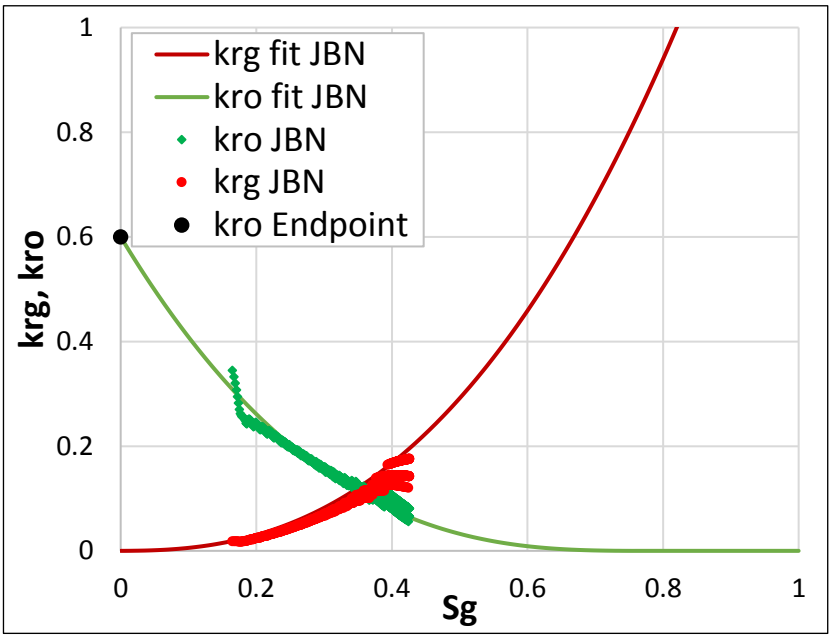

Figure 5-7: Relative permeability curves as calculated by JBN fitted by Sigmund & McCaffery 1979 correlation for viscosity ratio 50.

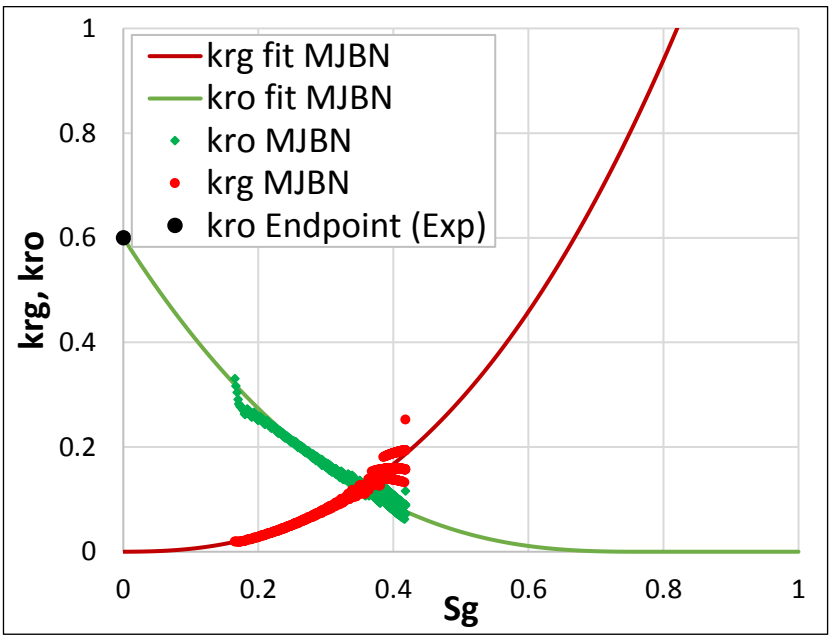

Figure 5-8: Relative permeability curves as calculated by MJBN fitted by Sigmund & McCaffery 1979 correlation for viscosity ratio 50.

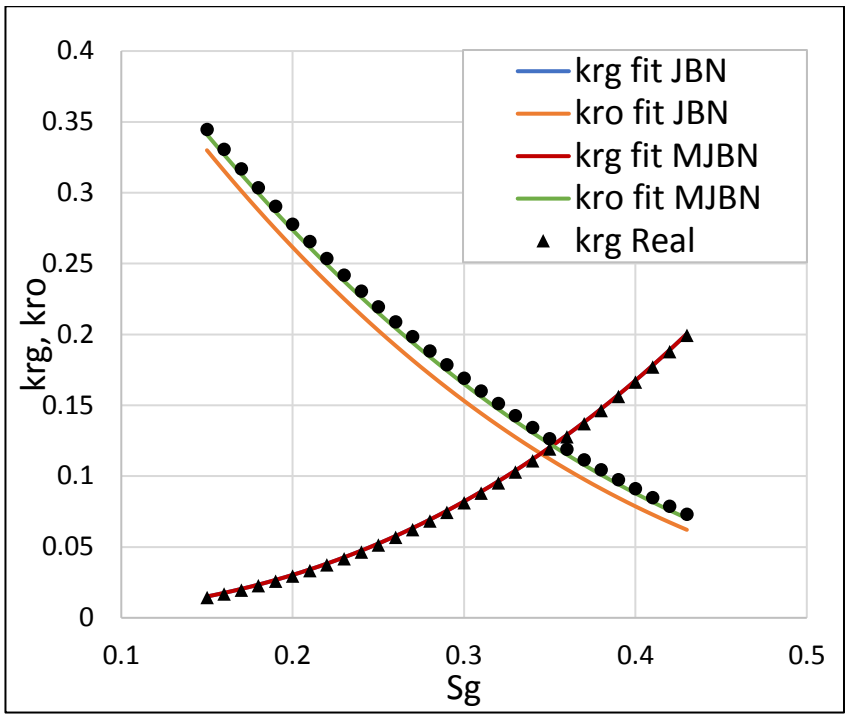

Figure 5-9: Comparison of the fitted relative permeability curves as calculated by JBN and MJBN versus the real k_r curves for viscosity ratio 50.

NCFE with Viscosity Ratio = 700

The procedure for estimating the k_r curves for this case was exactly the same as for the previous cases. The η factor was calculated to be 0.883 in this case (13.3% deviation from stability).

Comparison between the fitted curves of the JBN and MJBN results and the real k_r curves are presented for oil in Figure 5-10 and for gas in Figure 5-11. The JBN estimated k_{ro} curves are in considerable error, while the MJBN curves have good match with real k_r curves for both oil and gas. Since this case was the one with the highest viscosity ratio from the 3 simulations, it was expected for the error to increase in relation to the previous simulations. Also notice that the η factor changed accordingly with the error increased.

These three practical examples show how easy it is to apply the MJBN method to a numerical or laboratory coreflood experiment and, at the same time, show the type and magnitude of errors that can be avoided by using the modified MJBN method to account for fingering.

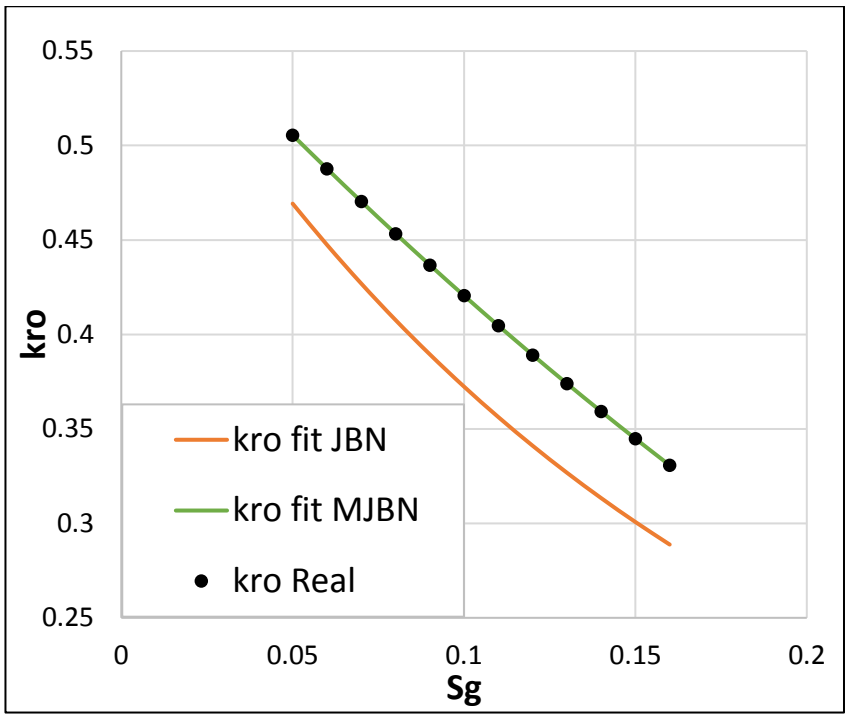

Figure 5-10: Comparison of the fitted relative permeability curves to oil as calculated by JBN and MJBN versus the real curves for viscosity ratio 700.

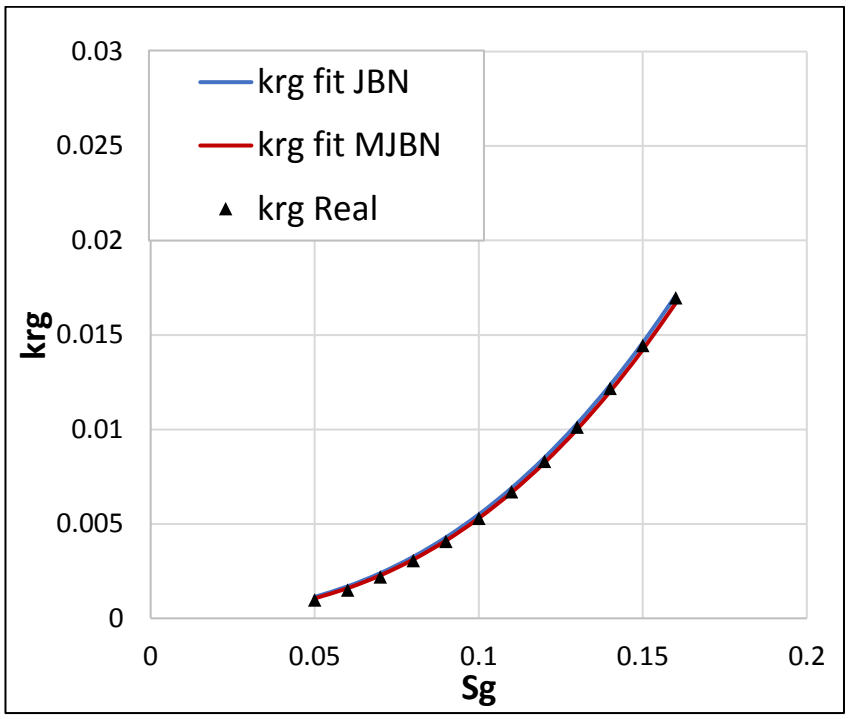

Figure 5-11: Comparison of the fitted relative permeability curves to gas as calculated by JBN and MJBN versus the real curves for viscosity ratio 700.

5.4.4 Limitations

The MJBN method is a modification of the standard JBN method so there are some limitations shared by both methods. Adding to those are also some limitations included in this list which are outside the scope of the current study. For example, heterogeneity influences the flow in similar way to viscous fingering, by acceleration of certain parts of the displacing fluid relative to others. It might be possible using η correction method in the same way to predict the influence of heterogeneity in k_r estimation, but such cases are out of the scope of this work. The properties of cases where the MJBN method can be applied are as follows:

- The displacement is immiscible.
- Compositional exchanges are negligible.
- The rock is relatively homogeneous.
- The capillary pressure (P_c) effects are negligible.
- The gravity effects can be ignored.

It must be borne in mind that viscous fingering is a very complicated phenomenon, and many factors may influence its formation. In this study it was decided that all simulations performed should be under immiscible conditions justifying the use of a Black-Oil model. Therefore, the MJBN method may not be accurate for use in miscible fluids or when compositional effects are present. It does not mean however that attempts cannot be made for those cases, but since it was not validated for them it would be unwise to use it without further checking.

The effect of P_c has been one of the major issues of the JBN method. In many, situations, especially at reservoir scale, the capillary pressure can be ignored, because the viscosity/mobility ratio has higher influence in the control of the flow and efficiency of the displacement than viscous effects (Deng et al. 2015; Dake 2008; Chuoke et al. 1959; Welge 1952). Although some authors have found a way to include P_c in semi-analytical methods (Civan & Donaldson 1987; Civan & Donaldson 1989), but an iterative method would be needed to find the optimal solution. The effect of P_c can be controlled in water injection coreflooding by increasing the injection rate (Li et al. 1994), However, for gas injection the effect of P_c may be difficult to avoid. Some of that effect can be reflected in the value of η when the MJBN method is used, particularly the effect of capillary pressure in fingering formation can be implicitly accounted for. It is known that Pc has a stabilizing effect in the flow of the displacing fluid, this will be translated in later breakthrough recovery, which, in the same way as in gravity, can be accounted for in the

velocity of the displacing fluid and therefore in η. Nevertheless, since Pc may change with the conditions of the experiment from MJBN it is not possible to obtain a relative permeability dissociated from P_c. For cases with considerable Pc it is suggested, if possible, the use of MJBN as first guess of a 2D/3D history matching (with saturation profile matching). This would immensely reduce the amount of time of a multidimensional history matching. Another possibility is the correction of 1D HM to account for viscous fingering.

5.4.5 MJBN Application

The MJBN method is a simple and fast way to assess the stability of a coreflood experiment and produce relative permeabilities that are more accurate than those produced by JBN method and could account for the effect of viscous fingering. In this section direct application of this method, from the perspective of a core analyst, will be presented.

When performing a coreflood experiment if viscous fingering is not suspected, i.e., the mobility ratio is near, or lower than, 1, viscosity ratio is low and breakthrough time is close to the expected value, then a 1D history matching can be performed to obtain the k_r curves. However, if viscous fingering is suspected, η (values from 0 to 1) should be calculated to access the degree of instability. If η value is close to 1, then 1D history matching can be performed to obtain the relative permeability curves. Though, if η is less than 1, that means that the flow is being influenced by viscous fingering and the use of MJBN method is necessary to avoid errors. From the MJBN method the relative permeability curves accounting for the fingering effect are obtained. These curves may be used directly for whatever end they are needed, or they may be used as the first estimate of the k_r curves to obtain more accurate curves by 2D or 3D history matching, thereby reducing the convergence time considerably and avoiding the non-uniqueness of the estimation problem. This will allow inclusion of the effect of Pc if significant. Figure 5-12 illustrates this methodology in a simple step-wise diagram.

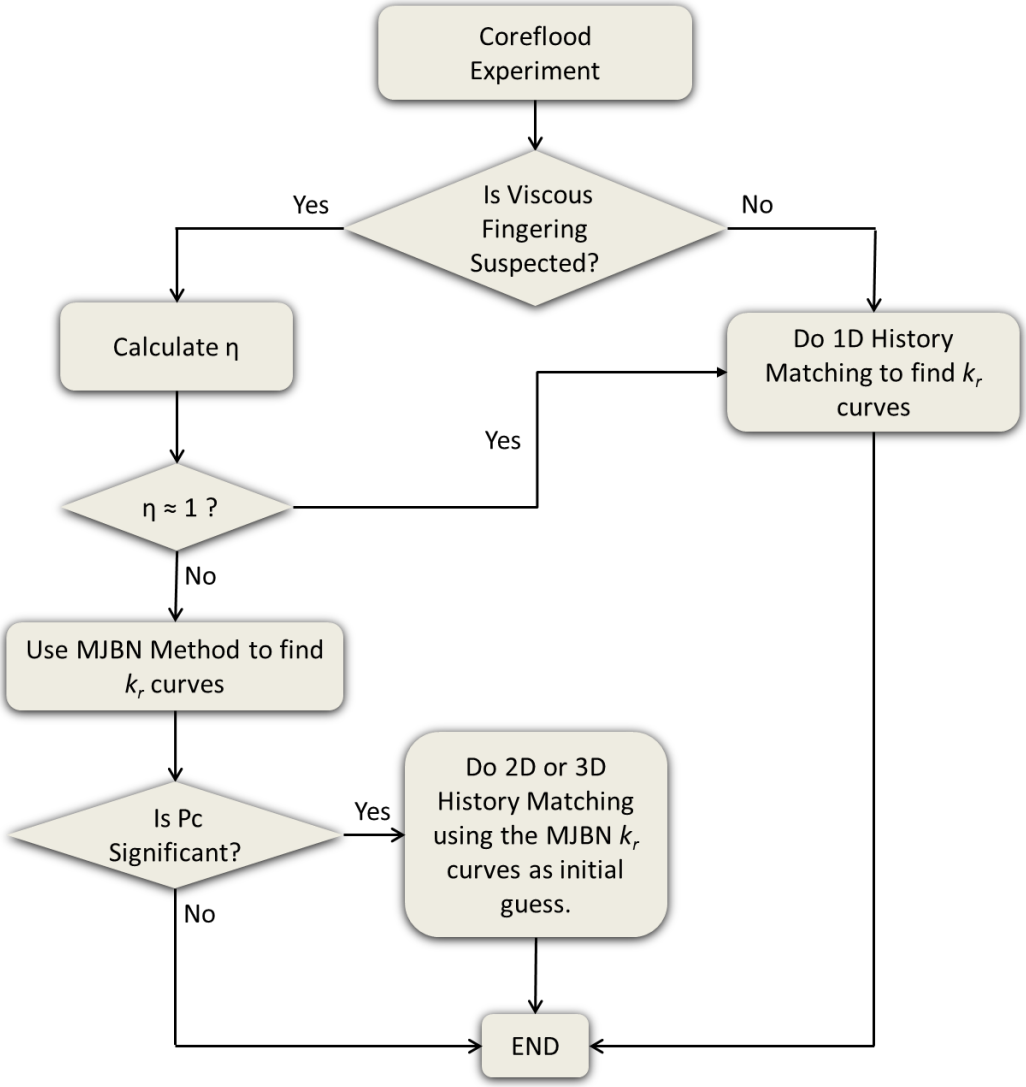

Figure 5-12: Methodology for the use of MJBN in SCAL measurements.

5.5 Modifying 1D History Matching to Account for Viscous Fingering

In Chapter 5, unstable numerical coreflood experiments relative permeability were estimated using 1D history matching to reveal considerable error when using this type of estimation method for flow with viscous fingering. In this section the stable equivalent model derived previously is going to be used to modify the 1D history matching method in order to account for viscous fingering, the newly developed method was called 'Stable Equivalent Matching' or 'SEM'.

5.5.1 Modification of the Flow Equations

1D history matching may be modified to account for viscous fingering in a similar manner to as JBN was modified to MJBN. From the stable equivalent model the flow equations

are presented by equations 5-7 and 5-9. Using these equations in the 1D simulator would result in a stable equivalent case to the unstable experiment.

Nevertheless, many users of 1D HM software don not have the means to change the actual code to apply these equations into the simulation. For those cases, it is proposed the following methodology.

Using the modified equation for the stable equivalent displacing fluid flow:

$$q_{ds} = \frac{-Kk_{rd}A}{\mu_d}\frac{dP_d}{dx}\eta \quad \text{..... 5-9}$$

It is possible to define the factor η as a reduction in the mobility of the displacing fluid, so that its velocity represents the velocity of the displacing fluid if fingering had not formed. Therefore, the factor η is closely related to the mobility $\left(\frac{k_{rd}}{\mu_d}\right)$ of the displacing fluid. Since k_{rd} is not known, a new constant called the stable equivalent displacing fluid viscosity is created as follows:

$$\mu_{ds} = \frac{\mu_d}{\eta} \quad \text{..... 5-28}$$

Where μ_{ds} is the stable equivalent gas viscosity. This modification is the same as aggregating the η factor to the viscosity of the gas. So, in a 1D history matching software, one only needs to change the viscosity ratio of the unstable experiment to the stable equivalent viscosity.

After this change, the 1D history matching may be run to calculate the relative permeability to oil accounting for viscous fingering:

$$k_{ro}(S_d) = k_{ro\,SEM}\left(S_{d,s}\right) \quad \text{..... 5-29}$$

The SEM will automatically present the relative permeabilities as a function of the stable equivalent saturation of the displacing fluid, $S_{d,s}$. However, as in the MJBN method, this approach only corrects the oil relative permeability estimation. A correction on the saturation must be done to correctly estimate the relative permeability of the displacing fluid.

5.5.2 Correction for the Displacing Fluid Relative Permeability

To estimate the displacing fluid relative permeability, the saturation must be corrected after the estimation. The correction of the saturation is similar to the one performed in the MJBN method.

To correct the stable equivalent saturation, $S_{d,s}$, into the corrected saturation, $S_{d,corr}$, it is necessary to calculate the corresponding fractional flow of oil. The factional flow of the unstable experiment is given by equation 4-4. Although this equation is used in JBN, it is correct to use it in the 1D HM method because the flow equations that rule both equations are the same and derive from the observations of Welge 1952 and Buckley & Leverett 1942. Likewise, the equation to calculate the saturation at the outlet for the unstable experiment is the same, equation 4-5. This saturation is equal to the corrected saturation needed for this method:

$$f_o = \frac{dS_{d,avg}}{dD_i} \quad \text{.....4-4}$$

$$S_{d,out} = S_{d,avg} - D_i \times f_o \quad \text{.....4-5}$$

$$S_{d,out} = S_{d,corr} \quad \text{.....5-30}$$

Nevertheless, it is only possible to estimate this saturation for each time step that was gathered from the unstable experiment. In 1D HM, because it is an implicit method, the relative permeability curves are calculated for how many saturation points desired. To solve this issue, it is necessary to calculate $S_{d,out}$ from $S_{d,s}$. This can be done by initially calculating the fractional flow of oil at the stable equivalent flow, f_{os}, from equation 5-22.

$$f_{os} = \frac{\frac{1}{\eta}}{\left(\frac{1}{\eta} + \frac{\mu_o}{\mu_d}\frac{k_{rd}}{k_{ro}}\right)} \quad \text{..... 5-22}$$

Unfortunately, it is not possible to calculate f_{os} without performing the standard JBN method for the unstable experiment, because k_{rd} and k_{ro} in equation 5-22 are the relative permeability curves calculated from JBN estimation. From equation 5-22 it is then possible to calculate the $S_{d,s}$ using equation 5-23. Here a question may arise: why cannot be used the relative permeabilities as calculated from the standard 1D HM method? The answer for this equation was explained before, JBN is an explicit method and therefore has more physical meaning that in 1D where the relative permeability curves are created

until one of them matches the experiment. Also, JBN method is very fast and easy to apply and take considerably less time to present a result of estimation.

From this procedure a value of $S_{d,s}$ and $S_{d,out}$ is calculated for each time the production results were registered. Then, the saturation $S_{d,out}$ plotted as a function of $S_{d,s}$, allowing to calculate the corrected saturation for any output saturation value given by the 1D HM estimation of relative permeability curves of the stable equivalent flow. Figure 5-13 shows an example of this process for NCFE_2.

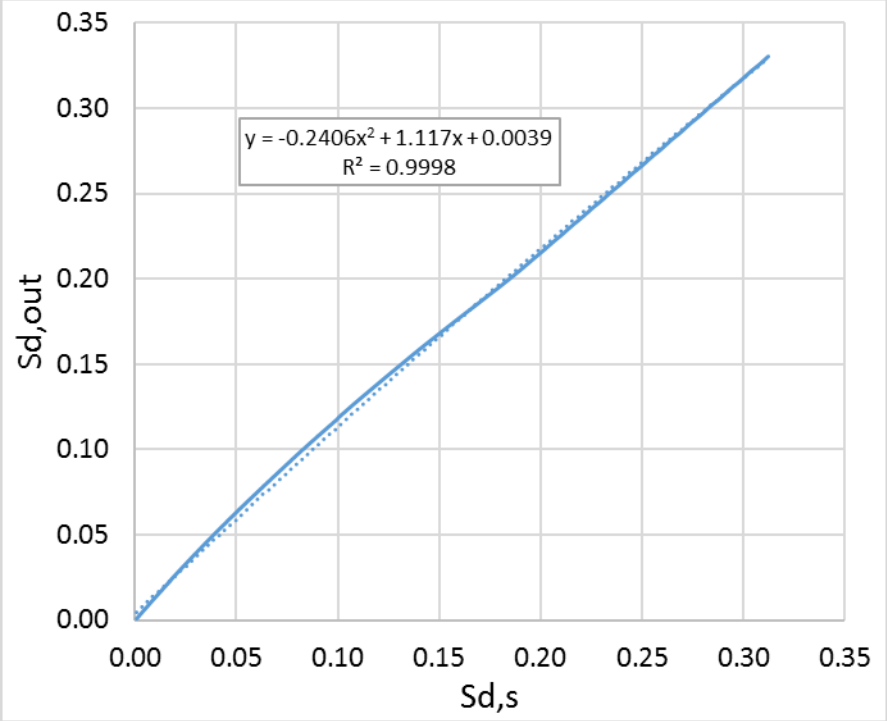

Figure 5-13: Sd,out as a function of Sd,s. Using a trendline it is possible to find a function that will give the value of Sd,out from the saturations resulted from the 1D HM.

Using a simple trend line, polynomial or a combination between linear and polynomial, it is possible to estimate an equation to calculate the $S_{d,out}$ (the corrected saturation) as a function of the saturation given by the 1D HM from the estimation of the *kr* curves in the stable equivalent method. For example, using Figure 5-13 function, the $S_{d,out}$ for that experiment would be equal to:

$$s_{s,out} = -0.2406 \times S_{d,s}^2 + 1.117 \times S_{d,s} + 0.0039 \quad \text{.....5-31}$$

After this correction, the relative permeability curves estimated by the SEM and, therefore, accounting for viscous fingering are:

$$k_{ro}(S_d) = k_{ro\,SEM}\left(S_{d,s}\right) \quad \text{.....5-29}$$

$$k_{rd}(S_d) = k_{rd\,SEM}\left(S_{d,out}\right) \quad \text{.....5-32}$$

5.5.3 Method Algorithm

After presenting the base equations for the Stable Equivalent Matching (SEM), an algorithm in a workflow form will be presented to easily understand the needed steps to use such tool.

1. Gather all the necessary experimental data, this includes the core and fluid data and, also, the production and differential pressure results.
2. With the experimental data, calculate η factor using equation 5-14, this factor is constant and specific for a certain experiment.
3. Use equation 5-28 and the previously estimated η factor, calculate the stable equivalent displacing fluid viscosity, μ_{ds}.
4. Use the experimental data with the stable equivalent displacing fluid viscosity in the 1D HM method.
5. Following these steps will give the relative permeability curves for oil and displacing fluid for the stable equivalent experiment, $k_{ro\ 1DHM\ corr}$ and $k_{rd\ 1DHM\ corr}$.
6. Use the experimental data to perform JBN and obtain the k_{ro} and k_{rd} by JBN.
7. In each time step (e.g. time interval when the production data was collected from the experiment), calculate the stable equivalent fractional flow of oil, f_{os}, using equation 5-22 and the relative permeabilities values from JBN method.
8. Calculate $S_{d,s}$ with equation 5-23, using f_{os} calculated in the previous step.
9. Use the experimental data to calculate the fractional flow of oil, f_o, equation 4-4.
10. Calculate $S_{d,out}$ with equation 4-5, using f_o calculated in the previous step.
11. Plot $S_{d,out}$ as a function of $S_{d,s}$ and find the equation that described the function: $S_{d,out} = f(S_{d,s})$.
12. Correct the saturation from $S_{d,s}$ to $S_{d,out}$ for the relative permeability of the displacing fluid from Step 5.
13. The relative permeabilities account for viscous fingering are found.

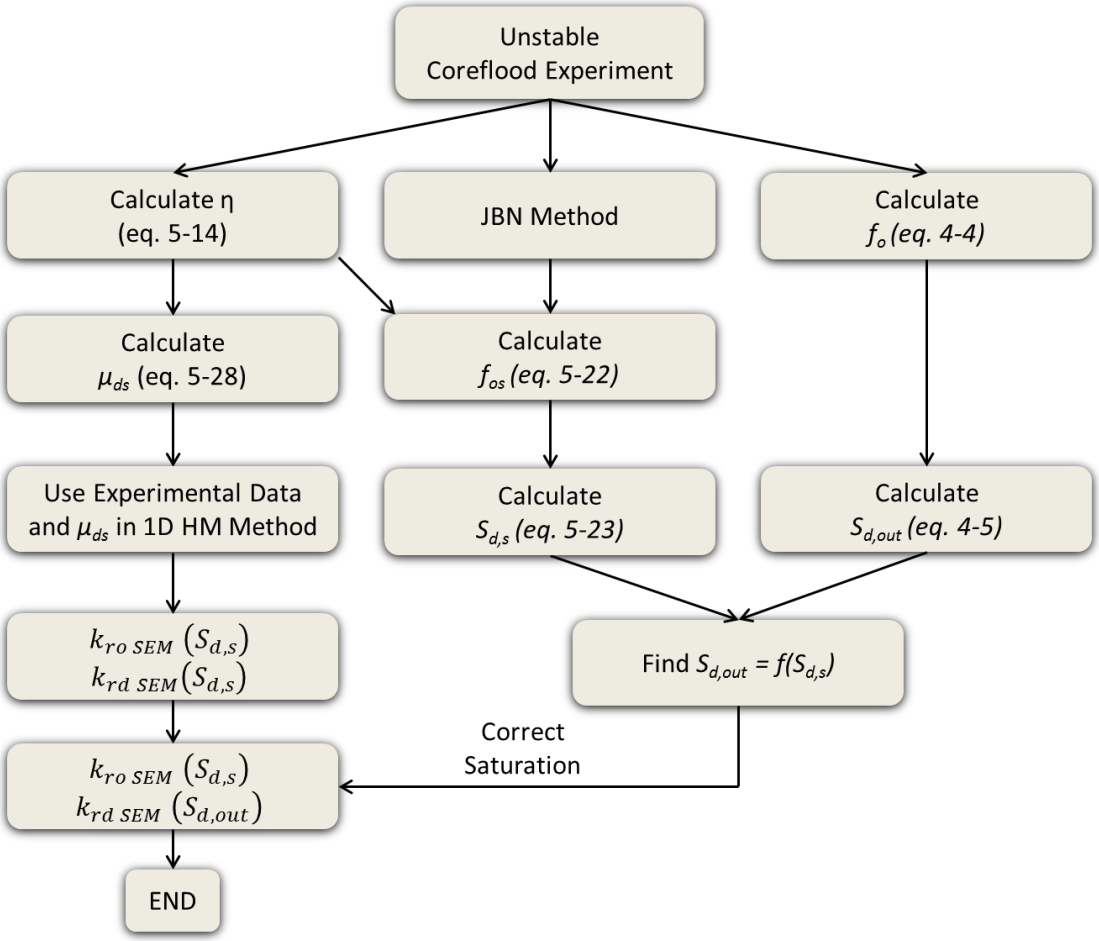

Figure 5-14: Methodology for application of SEM to experimental SCAL data.

5.6 Conclusions

The following conclusion may be drawn from accounting for viscous fingering in relative permeability estimation methods based in stability:

- A theory was proposed to explain the results from stable k_r estimation methods in presence of viscous fingering. This theory proposes that the displacing fluid flow follows methods based in stable flow, but the formation of fingering disrupts the flow of oil, because the oil can't handle the high mobility of the displacing fluid.
- From the proposed theory, a model, called Stable Equivalent, was developed to change an unstable experiment data so that k_r estimation methods (based on stability) can estimate relative permeability curves without error from viscous fingering. In this model, the velocity of the gas is reduced in order to revert the acceleration due to viscous fingering, allowing the oil to move at a velocity equivalent to the one it would move if viscous fingering had not formed. This velocity is changed in function of an adimensional factor called η. This change is

enough to guarantee the estimation of the oil relative permeability taking into account the viscous fingering. However, since the gas velocity was changed in relation to the original experiment, a correction in the saturation was proposed to account for this fact.

- The Stable Equivalent model was applied to the JBN and 1D history matching methods and a methodology workflow was present to allow the easily application of the methods to an experiment.
- The modified methods, MJBN and SEM, allow SCAL analysts to estimate the relative permeability for cases with viscous fingering quickly, without the need of complex 2D/3D history matching methods. MJBN may also be used to reduce the non-uniqueness if 2D and 3D HM and accelerate matching of this methods by providing a good first guess.

Chapter 6: Validation of MJBN and SEM as Relative Permeability Estimation Methods for Cases with Viscous Fingering

6.1 Introduction

The MJBN and SEM methods allow the user to rapidly obtain relative permeability curves more accurately than the standard JBN and 1D HM methods, by accounting for viscous instability in the process of core flooding. Up until now, MJBN and SEM was presented from a purely mathematical/conceptual point of view, but as logical as an idea may seem it would be useless without proper validation. A validation procedure will be proposed for these two methods using actual experimental data and numerical data and compare the predictions with what is seen in real data.

The AED from a report by Peters 1994 was used in this section. Peters has performed 2 experiments with unfavourable mobility and viscosity ratio of approximately 100. Both experiments are with immiscible fluids; in unconsolidated relatively homogeneous sand-packs. The production data and saturation profiles of these experiments were provided in their paper along with some matched relative permeabilities. This gives a unique opportunity to test the MJBN and SEM, because Peters' relative permeability curves were obtained by history matching the production data and the saturation profiles in 3D simulation, which means that they must be very close to the real k_r curves, i.e., those curves capture the physics in the experiment, because the saturation profile matching should reflect the fingering effects on relative permeability.

Unfortunately, there is a considerable lack of actual experimental data to be used for calibration of any method that attempts to reflect phenomena involving complex flow patterns. Not only experimental difficulties but also lack of the access to reliable measuring equipment may have contributed to this. Also, many times, all the data necessary to correctly simulate a specific case from literature is not available, for example, it is very rare to find, in the same article, saturation profiles, production data, and corresponding estimated k_r curves for an experiment. Moreover, there are some difficulties associated with the limitations of the MJBN method, for example not accounting for capillary pressure and gravity effects in the MJBN. However, in cases where such factors are not significant it is possible to use the method with satisfactory results. IFT is another problem, a lot of research is done in miscible conditions, both methods (MJBN and SEM) were developed for immiscible conditions and therefore the

experiments with miscible fluids are not usable for validating the method. In fact, such restrictions are very common in petroleum engineering. Many methods would be completely useless if the effect of one parameter like wettability was ignored. There is, however, a very powerful tool, numerical simulation, which is often overlooked and sometimes taken to be unreliable. Numerical simulation, if properly used, can adequately predict what happens inside a core or reservoir. Once again, the user must be aware of its limitations and the cases where it is or is not usable. Using numerical simulation, it may be possible to examine the limitations of the method. Benefitting from the power of simulation, a series of different NCFE's were developed with the objective of validating the method. Such NCFEs will use a given set of known kr curves, allowing determination of the errors between them and the ones estimated using the two methods. Unstable flooding will be produced using permeability distributions and high viscosity ratios resulting in different scenarios and patterns of viscous fingering. The NCFEs will be treated as experiments, accounting for as many as practicable of the physical phenomena. The resulting data will then be used in MJBN and SEM in the same way as it would if a physical experiment was being used.

6.2 Validation Using Numerical Simulation

As referred before, NCFEs have the advantage of allowing the user to define with certainty the properties of the core and the fluids under the study. This is essential for this work, where a parameter that is 'virtual' in the sense that it cannot be measured directly by definition and is always product of an estimation, this parameter is the relative permeability. In this section of the work, NCFEs will be used to develop and validate the MJBN and SEM methods.

To reach this goal, each NCFE will be treated as a separate experiment, with its own properties and fluid characteristics, while all simulations will be maintained with reasonable values of core and fluid properties; the values that resemble closely standard laboratory corefloods. Each of these numerical experiments will also utilize a set of relative permeabilities generated by Sigmund and McCaffery correlation. These kr curves will be treated as the 'real' curves for the corresponding NCFE.

6.2.1 Independent NCFEs

6.2.1.1 Calculation of η Factor

Before applying MJBN or SEM methods, the value of the η factor had to be calculated for each one the NCFEs in study. The necessary values for its calculation resulted from the simulation results of this numerical experiments, the values of such parameters and η are present in Table 6-1 for NCFE_1 to NCFE_9.

Table 6-1: Values of the necessary parameters for η calculation in each NCFE.

*NCFE_*	**1**	**2**	**3**	**4**	**5**	**6**	**7**	**8**	**9**
Φ (frac.)	0.2	0.2	0.19	0.15	0.15	0.4	0.18	0.4	0.15
S_{wi} *(frac.)*	0.18	0.05	0.2	0.15	0.15	0.3	0.15	0.126	0
S_{or} *(frac.)*	0.66	0.41	0.46	0.59	0.34	0.46	0.45	0.52	0.72
L (cm)	60.5	30.25	60.5	60.5	30.25	30.25	60.5	30.25	30.25
M (adim.)	933	3333	407	125	475	1667	429	220	500
$v_{ad\ ex}$ *(cm/min)*	0.362	0.378	0.385	0.637	0.344	0.336	0.297	0.128	0.776
η (adim.)	**0.847**	**0.726**	**0.784**	**0.779**	**0.738**	**0.907**	**0.915**	**0.977**	**0.914**

The η factor is a measurement of how much the displacing fluid velocity increased due to viscous fingering. When the factor is close to 1, the velocity is the same, meaning that viscous fingering didn't form in the core and the no correction is needed. In this case methods like MJBN or SEM result in the same estimation k_r curves as JBN and 1D HM. When the facto is far from 1, then the conventional methods will have an error that is proportional to this factor deviation from 1. Then it is no surprise that the calculated value of these factor is in agreement with the error seen in JBN estimations for the same NCFEs.

Figure 6-1 shows the values of η factor as a function of the NCFE. For NCFE_8, for example, Figure 4-24 shows that the error of estimation is low. This was explained by the fact that in this experiment no fingering was formed as it was verified by the saturation profiles. In Figure 6-1 the η factor is very close to 1, reflecting this same conclusion, that viscous fingering would have little influence in the relative permeability estimation.

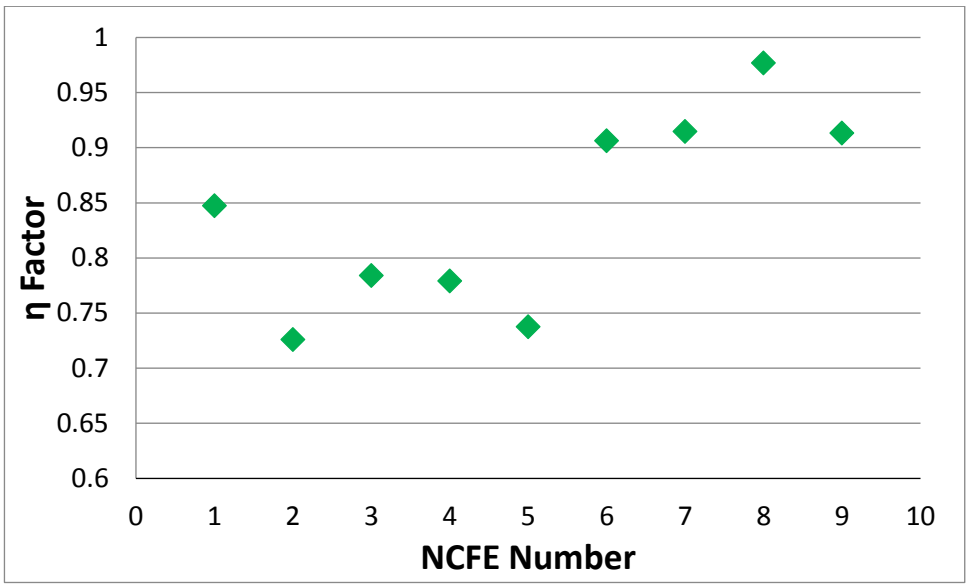

Figure 6-1: Calculated values of η for each of the NCFEs (NCFE_1 to NCFE_9).

The independent NCFEs cannot be compared with one another and serve only as a validation safeguard against case specific issues. So, perhaps, the most important analysis of the η factor may be drawn from the NCFE_1_VR and NCFE_2_VR sets. In these sets, each numerical coreflood experiment has an incremental increase in viscosity ratio, maintaining the same exact core and fluid properties, including the relative permeability curves. Figure 6-2 shows the value of η for different viscosity ratios corresponding to each one of the simulations from NCFE_1_VR set, Figure 6-3 is a zoom for the smaller range of viscosity ratios of Figure 6-2. In these two figures, η values go from 1 (stable flow) to 0.83, but the most important observation is the way it changes from value to value. Firstly, it is observed a stable zone exists, it starts in this example in viscosity ratio of 5, but it means that any viscosity ratio lower than 5 is also stable. This stable zone extends up until viscosity ratio of 10, where the factor value is 0.995, so it is still considered stable. Although, after this point, the value of the factor starts to drop drastically from viscosity of 10 up until to 300 (in this case), this zone can be called transition zone. It goes from the stable flow to a point where the viscous fingering is fully formed. After viscosity ratio of 300, there is no much change in the value of η, a pseudo stable zone is reached, where the flow will not increase its instability any further. This description is very similar to the one made by Sarma & Bentsen 1987. These author have proposed these 3 zones based on the change in the breakthrough recovery with stability: stable zone, transition zone and pseudo-stable zone.

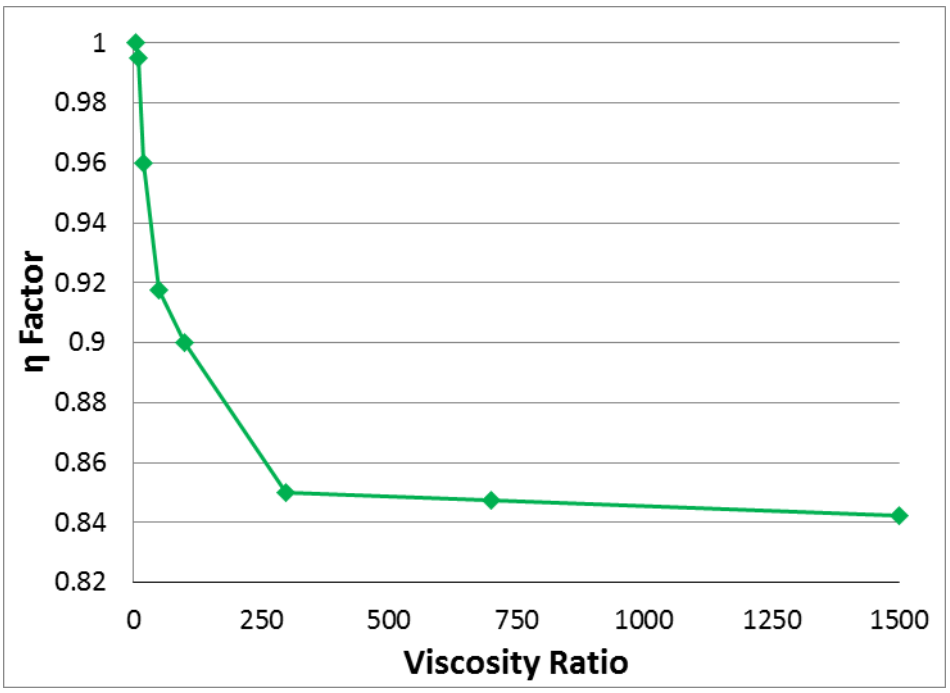

Figure 6-2: Calculated values of η factor for the simulation of NCFE_1_VR set, from viscosity ratio of 5 to 1500.

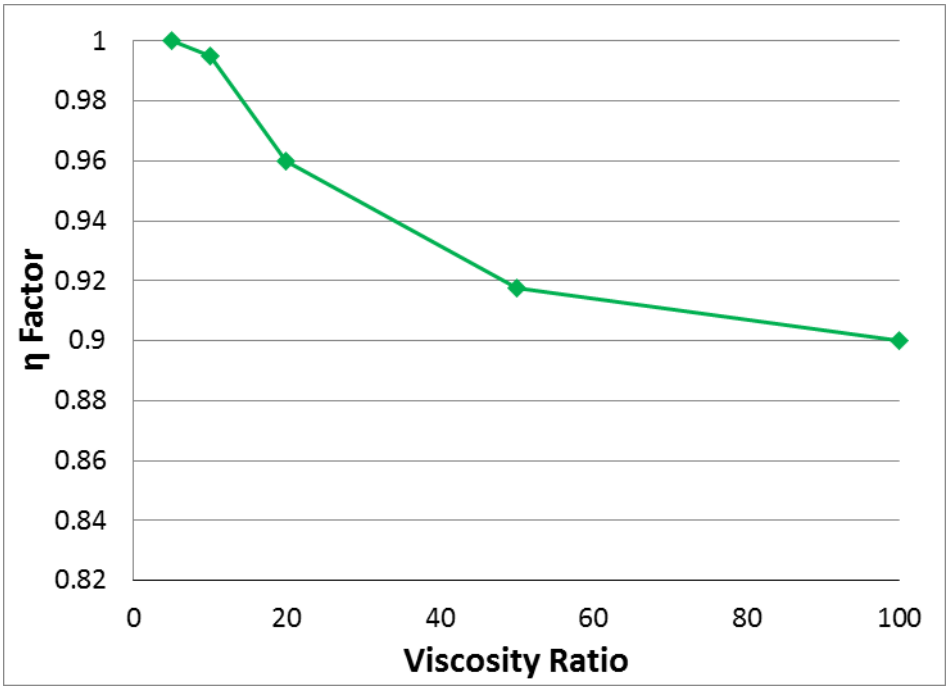

Figure 6-3: Calculated values of η factor for the simulation of NCFE_1_VR set, from viscosity ratio of 5 to 100.

The factor η predicts these 3 zones very well, but it is also consistent with the saturation profiles of these experiments, Figure 3-11. From these saturation profiles, the viscous fingering formations start at viscosity ratio of 10, as it is predicted from the η value, and get progressively more unstable in terms of 'fingering zone length' up until 300. After

that point the length of the core that is in fingering does not change much, although fingers may become different in pattern.

Another important conclusion is that the way a coreflood becomes progressively more unstable is case dependent and it is not possible to create a correlation based only on the mobility difference of each experiment. Figure 6-4 shows the values of η for the NCFEs from the NCFE_2_VR set. In this set, the 'curvature' of the change of η values with the viscosity ratio is completely different from the NCFE_1_VR set and the stable, transition and pseudo-stable zones happen at different periods. Although, once again, the calculated value of η, translates very well the saturation patterns seen in Figure 3-12.

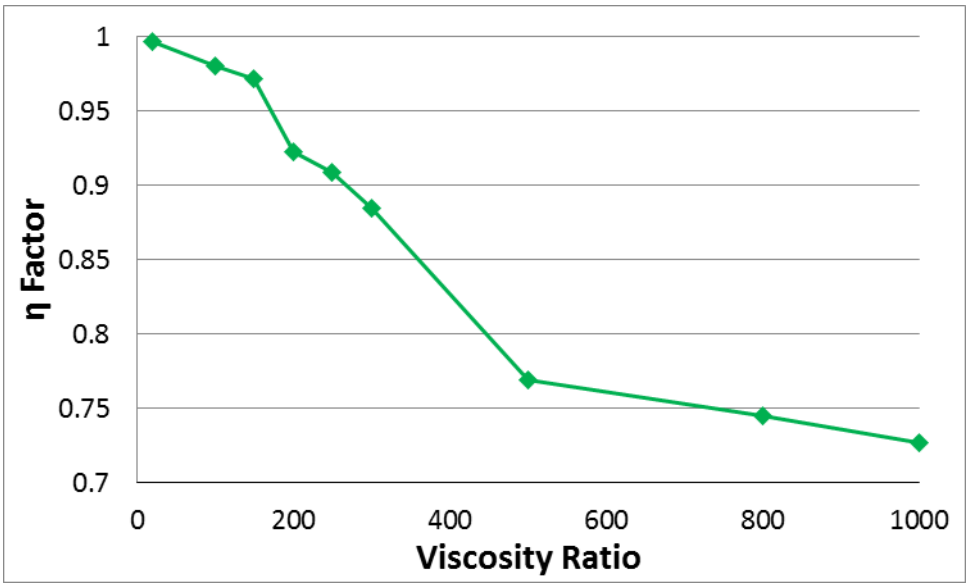

Figure 6-4: Calculated values of η factor for the simulation of NCFE_2_VR set.

The calculation of η factor has shown a very good relation with the stability of the different NCFEs, giving a good likelihood that the developed model is accurately taking into account viscous fingering. Although the importance of this factor is its inclusion in stable models in order to correct them for viscous fingering scenarios, so in the next sections MJBN and SEM are going to be used to evaluate this same NCFEs.

6.2.1.2 MJBN

The MJBN method as present in Chapter 5 was used in this section to estimate the relative permeability of unstable NCFEs namely NCFE_1 to NCFE_9. The NCFE_1 to NCFE_9 results from 2D high resolution simulation with permeability distribution as triggering method for viscous fingering, presented in Chapter 3, were used for this purpose. Oil production and differential pressure, along with some pertinent core and fluid data, were gathered and used in MJBN methodology as descripted in Figure 5-3. The relative

permeability curves estimated by MJBN were compared with the relative permeabilities used originally in the NCFEs simulation with the mean average percentage error, equation 4-2, in a procedure equal to the one presented in Figure 4-1. The results from MJBN estimation are given in points so a fitting method (Sigmund & McCaffery 1979) was used to fit the points into a smooth curvature.

The relative permeability curves resulted from MJBN and JBN methods were plotted against the real curves in Figure 6-5 to Figure 6-22, for each phase and NCFE. These results show the clear advantage of MJBN into predicting the real oil relative permeability curves for the cases where JBN had high error. In this cases, it was used the saturation correction, instead of simply use the relative permeability to gas as predicted from JBN (explained in the previous Chapter). This was done for validation purposes: to prove that the saturation correction is correctly developed. The prediction of the displacing fluid relative permeability was the same either by using MJBN or JBN method, being in accordance with the model developed, where it is assumed that the displacing fluid flow is perfectly described by the stability models, validating the saturation correction proposed.

In addition to the relative permeability visual comparison, the error was calculated so that MJBN could be numerically compared with JBN in term of precision. Figure 6-23 shows the errors of prediction from MJBN and JBN for the 9 independent NCFEs.

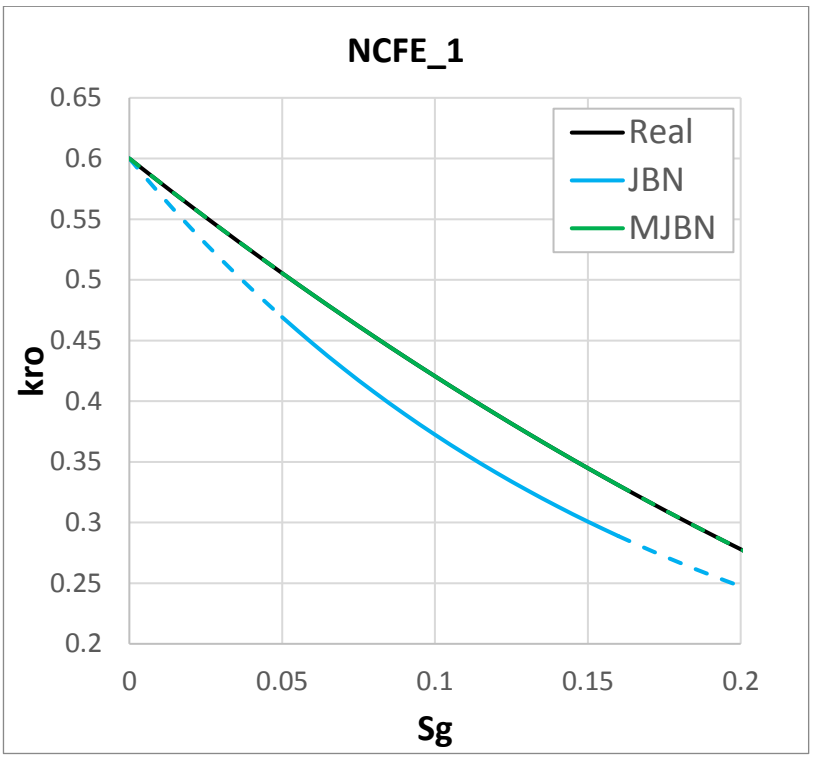

Figure 6-5: Relative permeability to oil as estimated by JBN and MJBN compared with the real relative permeability for NCFE_1, the solid lines represent the valid saturation range.

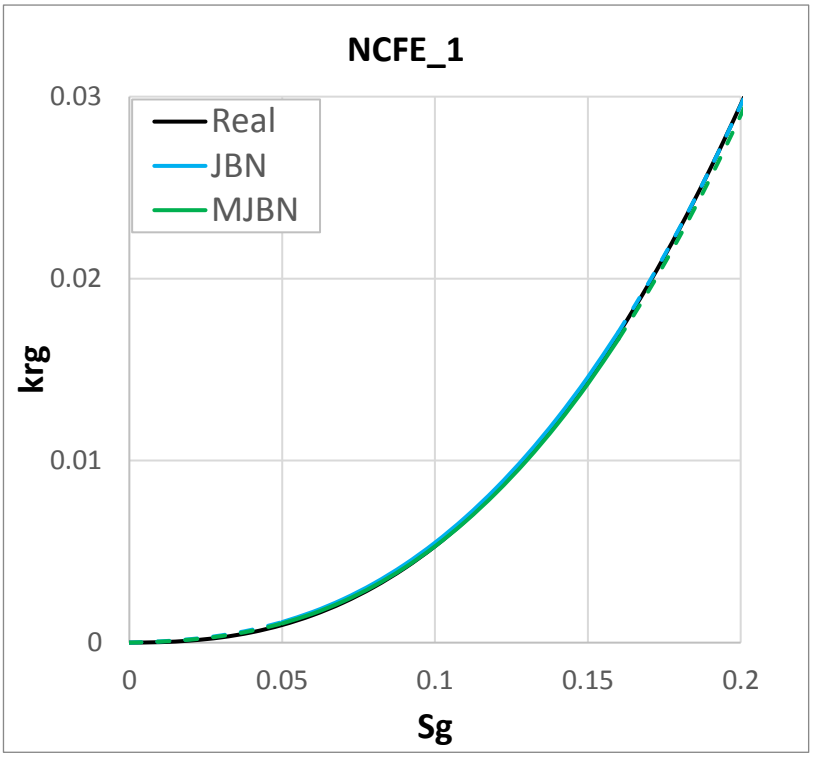

Figure 6-6: Relative permeability to gas as estimated by JBN and MJBN compared with the real relative permeability for NCFE_1, the solid lines represent the valid saturation range.

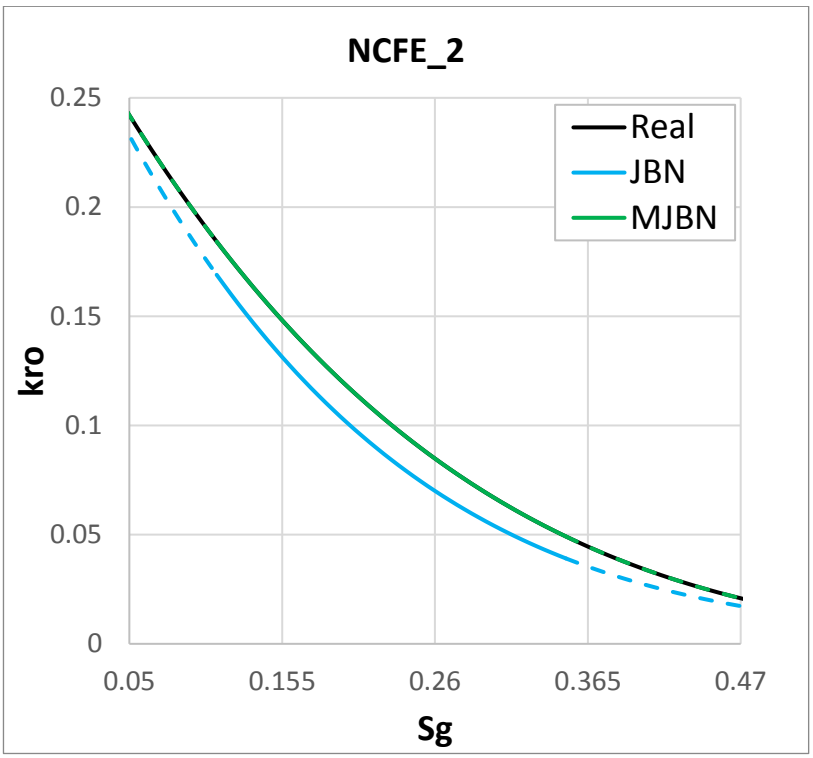

Figure 6-7: Relative permeability to oil as estimated by JBN and MJBN compared with the real relative permeability for NCFE_2, the solid lines represent the valid saturation range.

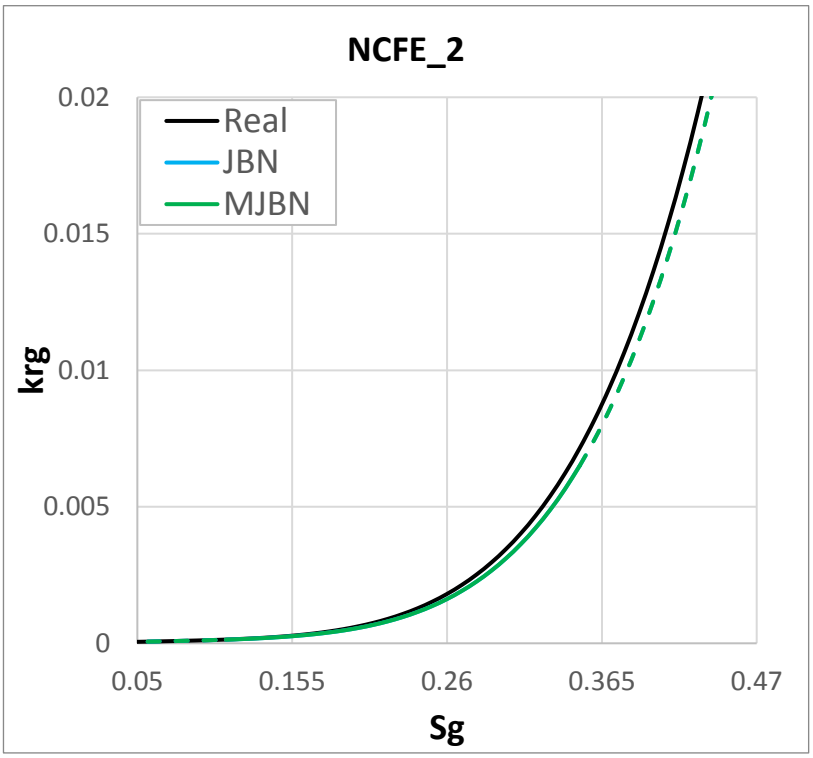

Figure 6-8: Relative permeability to gas as estimated by JBN and MJBN compared with the real relative permeability for NCFE_2, the solid lines represent the valid saturation range.

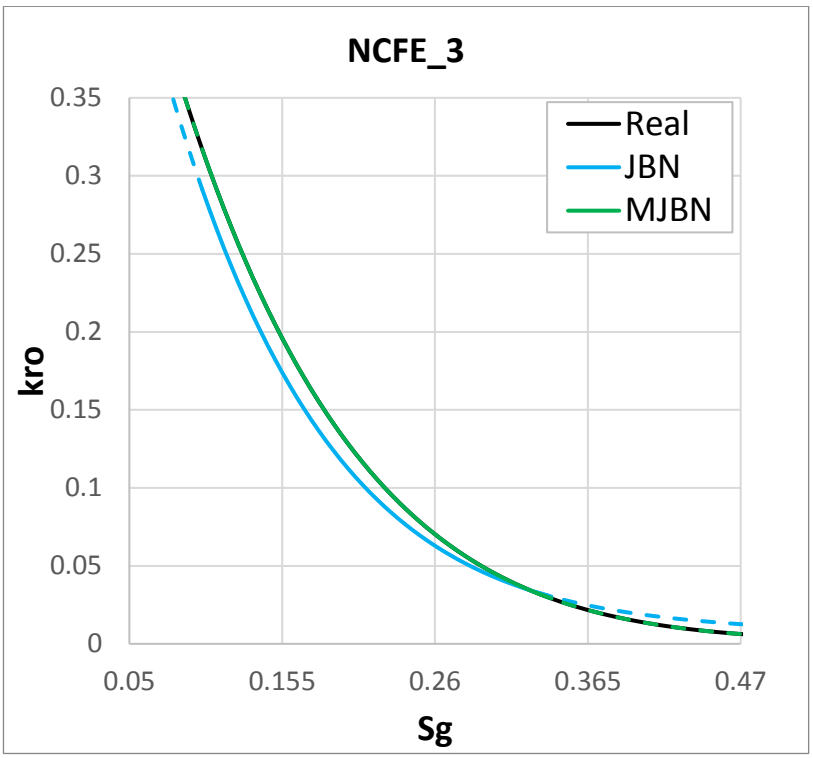

Figure 6-9: Relative permeability to oil as estimated by JBN and MJBN compared with the real relative permeability for NCFE_3, the solid lines represent the valid saturation range.

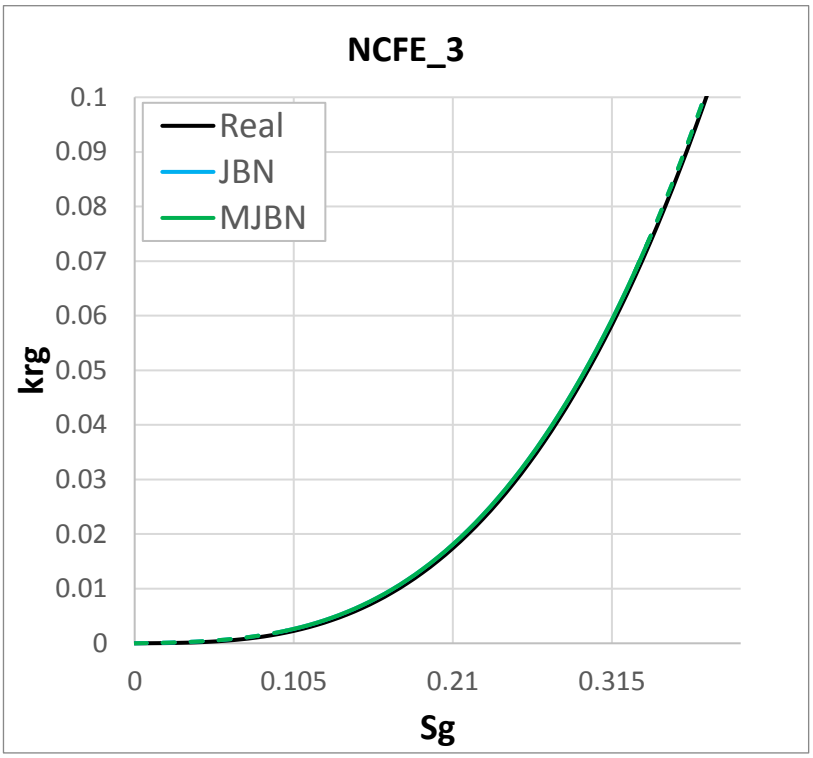

Figure 6-10: Relative permeability to gas as estimated by JBN and MJBN compared with the real relative permeability for NCFE_3, the solid lines represent the valid saturation range.

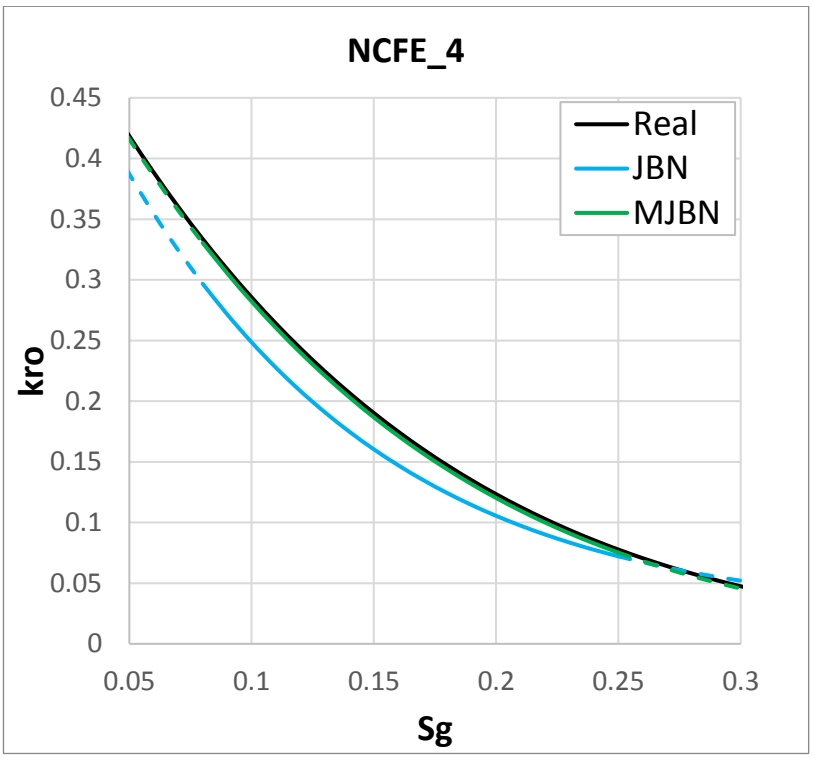

Figure 6-11: Relative permeability to oil as estimated by JBN and MJBN compared with the real relative permeability for NCFE_4, the solid lines represent the valid saturation range.

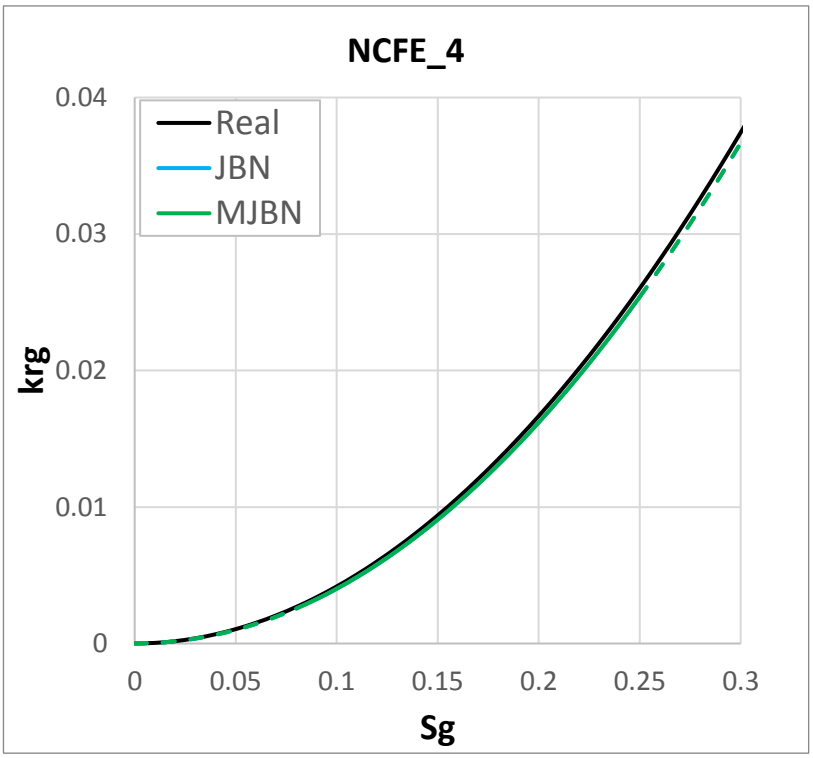

Figure 6-12: Relative permeability to gas as estimated by JBN and MJBN compared with the real relative permeability for NCFE_4, the solid lines represent the valid saturation range.

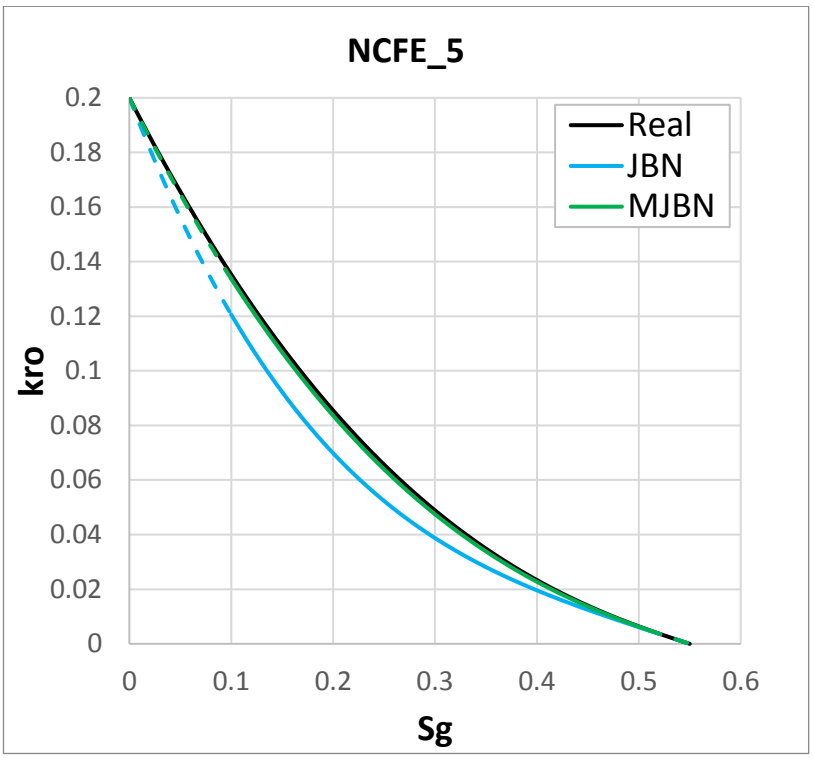

Figure 6-13: Relative permeability to oil as estimated by JBN and MJBN compared with the real relative permeability for NCFE_5, the solid lines represent the valid saturation range.

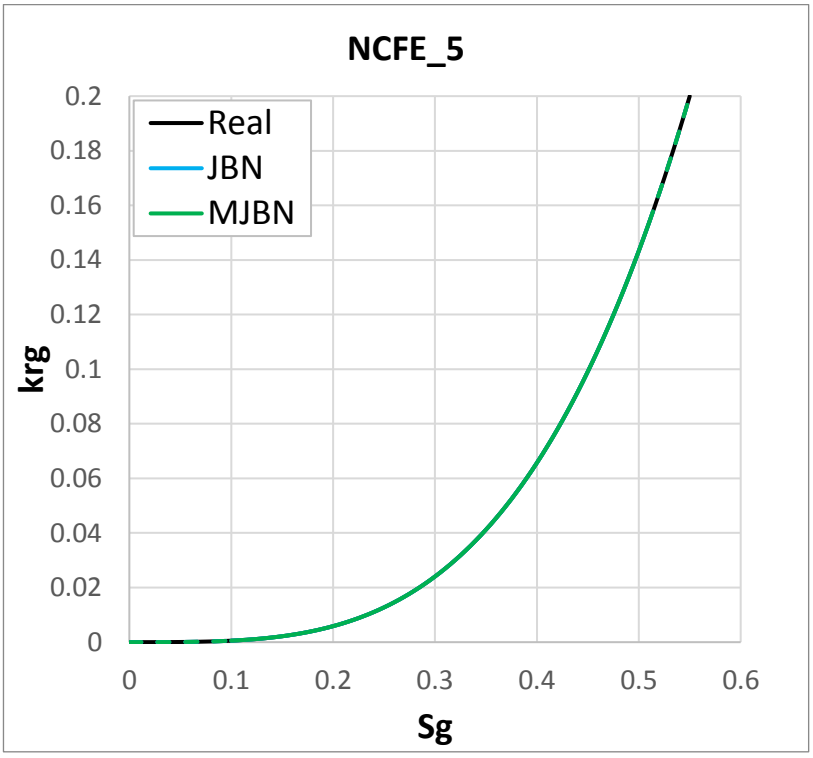

Figure 6-14: Relative permeability to gas as estimated by JBN and MJBN compared with the real relative permeability for NCFE_5, the solid lines represent the valid saturation range.

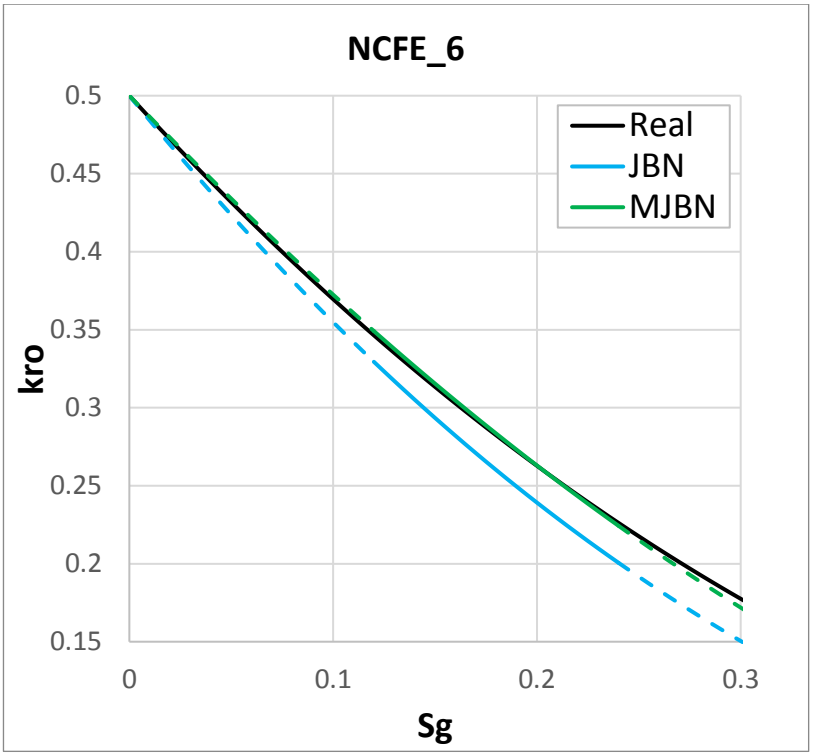

Figure 6-15: Relative permeability to oil as estimated by JBN and MJBN compared with the real relative permeability for NCFE_6, the solid lines represent the valid saturation range.

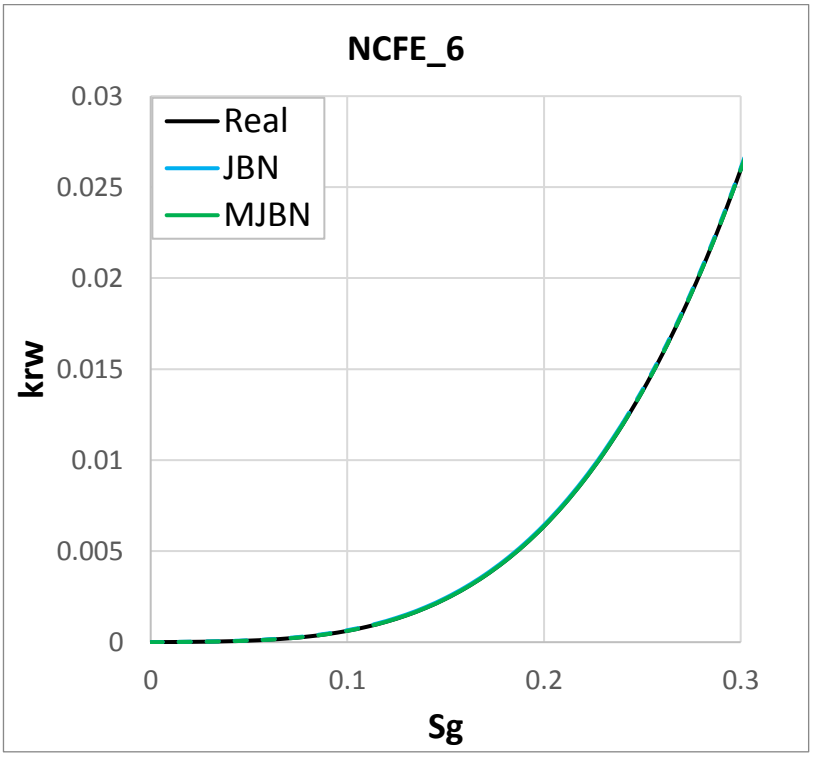

Figure 6-16: Relative permeability to gas as estimated by JBN and MJBN compared with the real relative permeability for NCFE_6, the solid lines represent the valid saturation range.

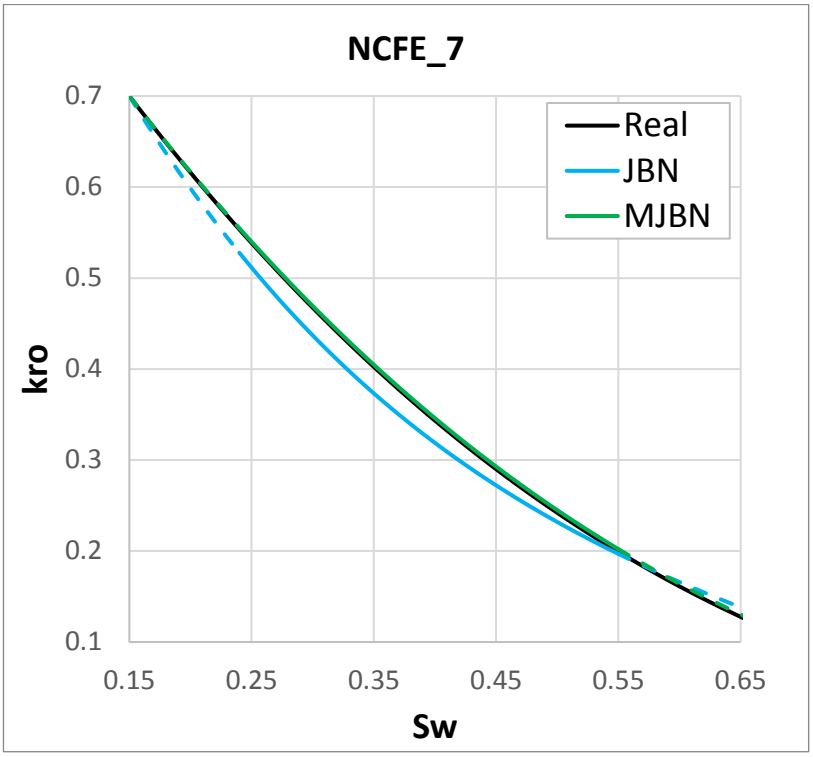

Figure 6-17: Relative permeability to oil as estimated by JBN and MJBN compared with the real relative permeability for NCFE_7, the solid lines represent the valid saturation range.

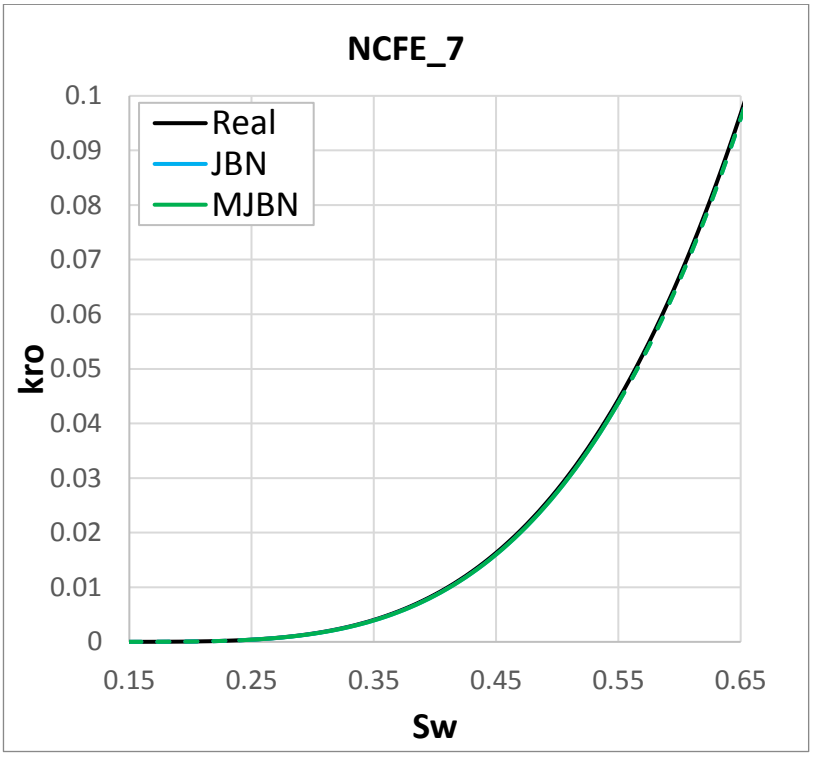

Figure 6-18: Relative permeability to gas as estimated by JBN and MJBN compared with the real relative permeability for NCFE_7, the solid lines represent the valid saturation range.

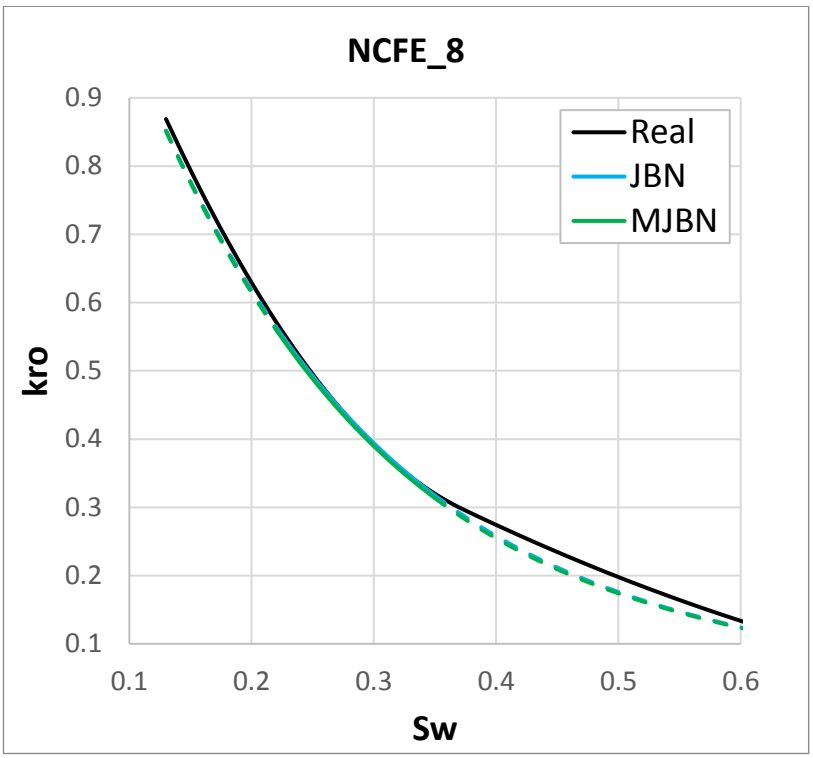

Figure 6-19: Relative permeability to oil as estimated by JBN and MJBN compared with the real relative permeability for NCFE_8, the solid lines represent the valid saturation range.

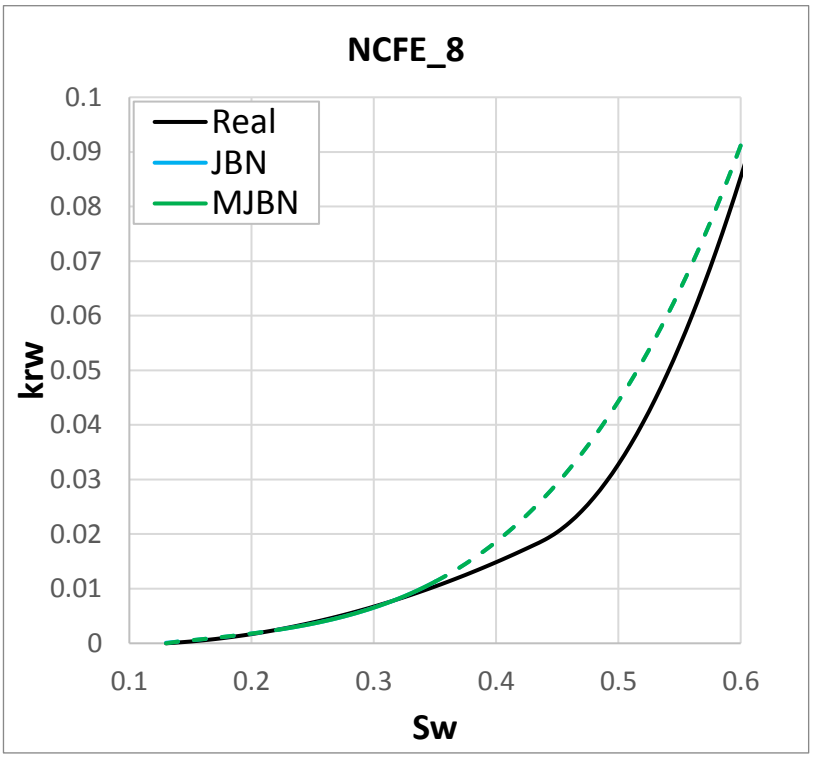

Figure 6-20: Relative permeability to gas as estimated by JBN and MJBN compared with the real relative permeability for NCFE_8, the solid lines represent the valid saturation range.

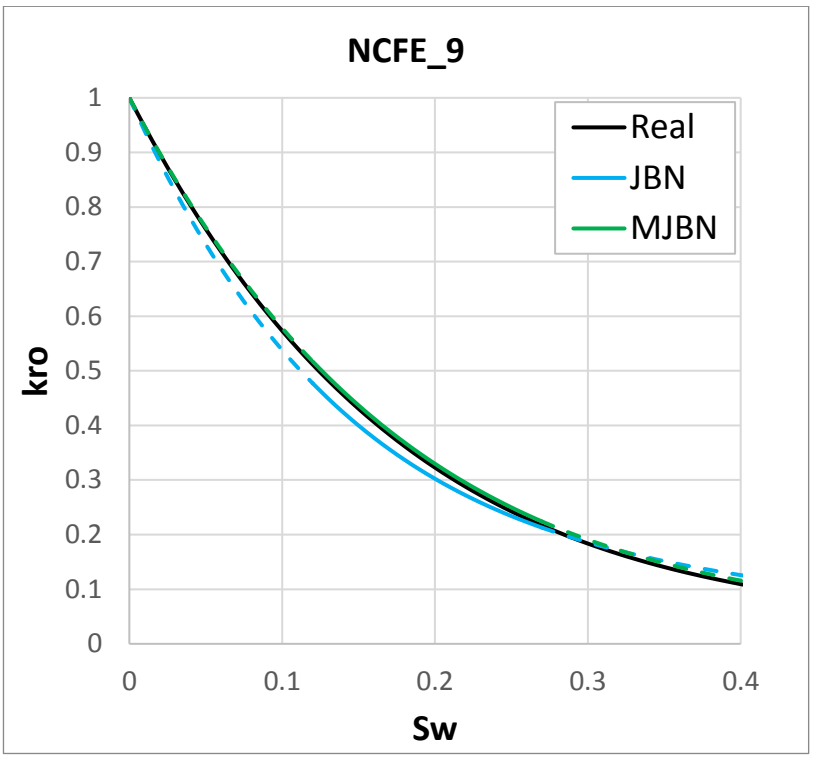

Figure 6-21: Relative permeability to oil as estimated by JBN and MJBN compared with the real relative permeability for NCFE_9, the solid lines represent the valid saturation range.

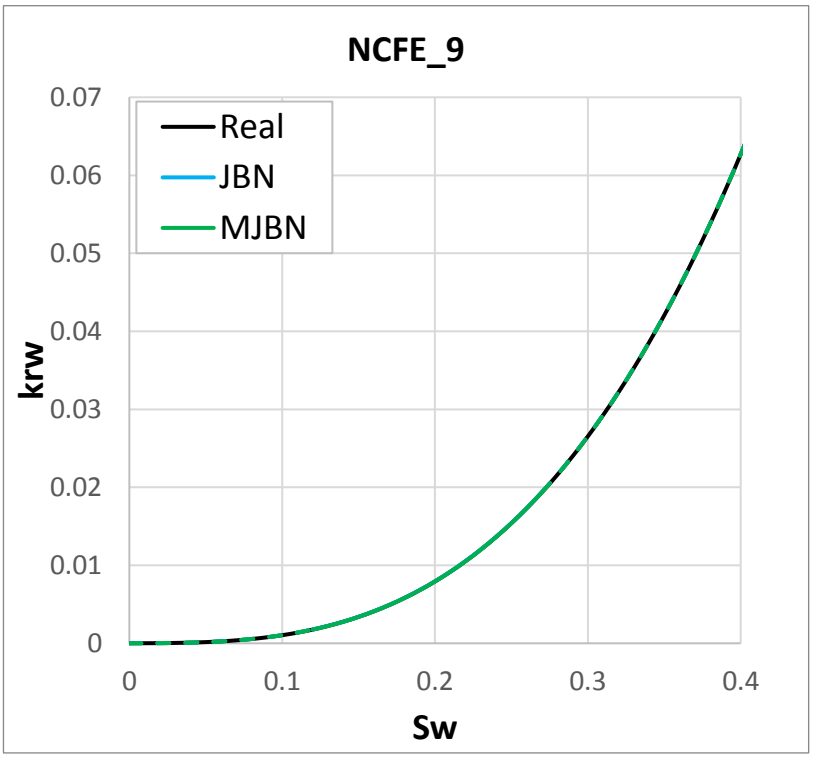

Figure 6-22: Relative permeability to gas as estimated by JBN and MJBN compared with the real relative permeability for NCFE_9, the solid lines represent the valid saturation range.

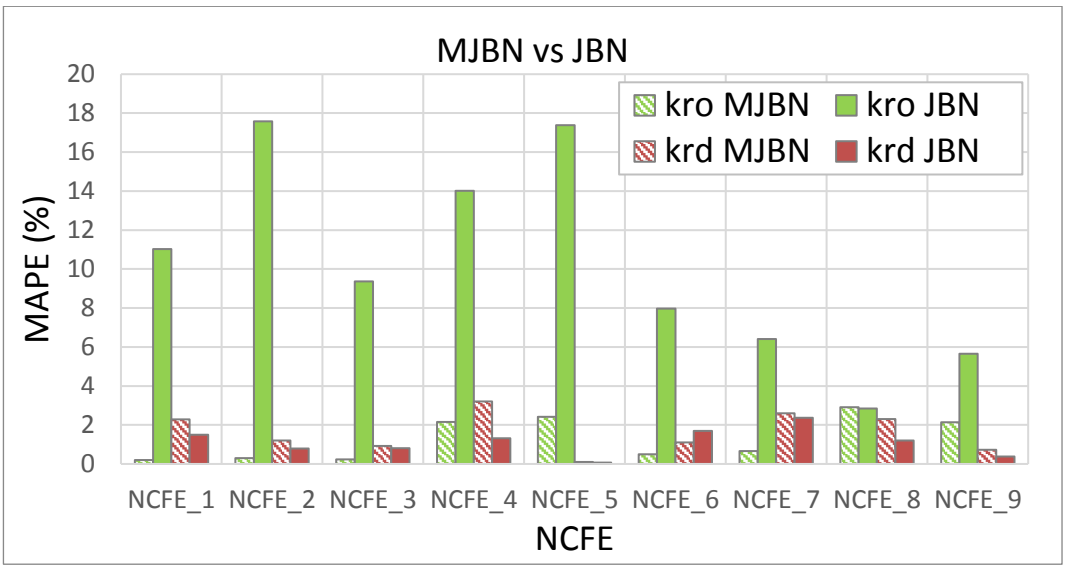

Figure 6-23: Error comparison between JBN and MJBN relative permeability estimations for NCFE_1 to NCFE_9, showing a clear reduction in error when using MJBN for the oil relative permeability.

From Figure 6-23 it is possible to conclude that the application of MJBN has considerably reduced the error of estimation from JBN method in stable experiment. It is also important to notice that for NCFE_8 the error of MJBN and JBN is approximately the same and below 3%. The reason for this is because viscous fingering did not develop in that coreflood, which resulted in low error on the original JBN method. This also serves as validation of MJBN in stable scenarios, showing that MJBN is not only applicable in cases with viscous fingering but also in stable cases, becoming an improvement in all aspects against the traditional method. In fact, the calculated values of η predicted this results very well, Figure 6-1.

6.2.1.3 SEM

The modified 1D history matching accounting for viscous fingering presented in Chapter 5, named 'Stable Equivalent Matching' or 'SEM', was used in this section to estimate the relative permeability of unstable NCFEs. The NCFE_1 to NCFE_9 results from 2D high resolution simulation with permeability distribution as triggering method for viscous fingering, presented in Chapter 3, were used for this purpose. Oil production and differential pressure, along with some pertinent core and fluid data, were gathered and used in SEM methodology as described in Figure 5-14. The relative permeability curves estimated by SEM were compared with the relative permeabilities used originally in the NCFEs simulation with the mean average percentage error, equation 4-2, in a procedure equal to the one presented in Figure 4-1. The results from MJBN estimation are given in

points so a fitting method (Sigmund & McCaffery 1979) was used to fit the points into a smooth curvature.

The relative permeability curves that resulted from SEM and the original 1D HM method were plotted against the real curves in Figure 6-24 to Figure 6-41, for each phase and NCFE. These results show a clear improvement from the traditional 1D HM by the use of the developed method, SEM. The error between SEM's estimation and the real curves is considerably reduced when compared with 1D HM. In addition to the quantitative reduction in error, the curvature of the relative permeability seems to have more similarities with the real curve when SEM is used instead of 1D HM, especially for NCFE_1, NCFE_3, NCFE_4 and NCFE_5. 1D HM had considerable errors for the displacing fluid's relative permeability, but the correction of the saturation showed to be appropriate to account for the error, translating to much less error in all the SEM estimations.

In addition to the relative permeability visual comparison, the error was calculated so that SEM could be numerically compared with 1D HM in terms of precision. Figure 6-42 shows the errors of prediction from SEM and 1D HM for the 9 independent NCFEs. For the exception of NCFE_8 and NCFE_9 (in which the flow is very close to stability), SEM shows considerable reduction in the value of error in the NCFEs. Notably for NCFE_5, where the error for the relative permeability to gas was around 42% using 1D HM, the use of SEM resulted in only 8%, more than 5 times less than the original method. These results validate SEM as an improvement to 1D HM when viscous fingering is present in coreflood displacements.

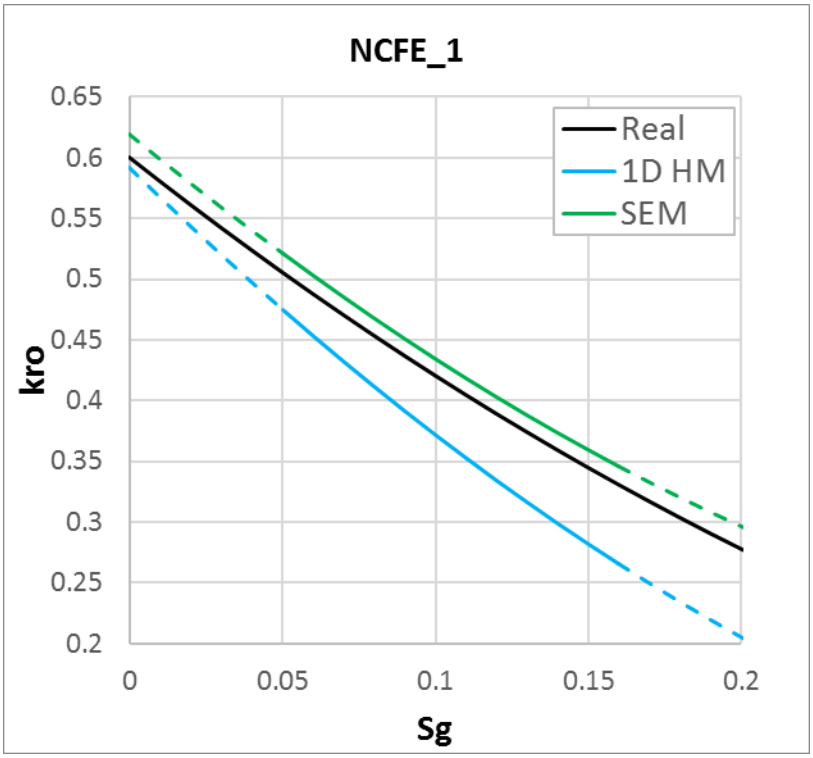

Figure 6-24: Relative permeability to oil as estimated by 1D HM and SEM compared with the real relative permeability for NCFE_1, the solid lines represent the valid saturation range.

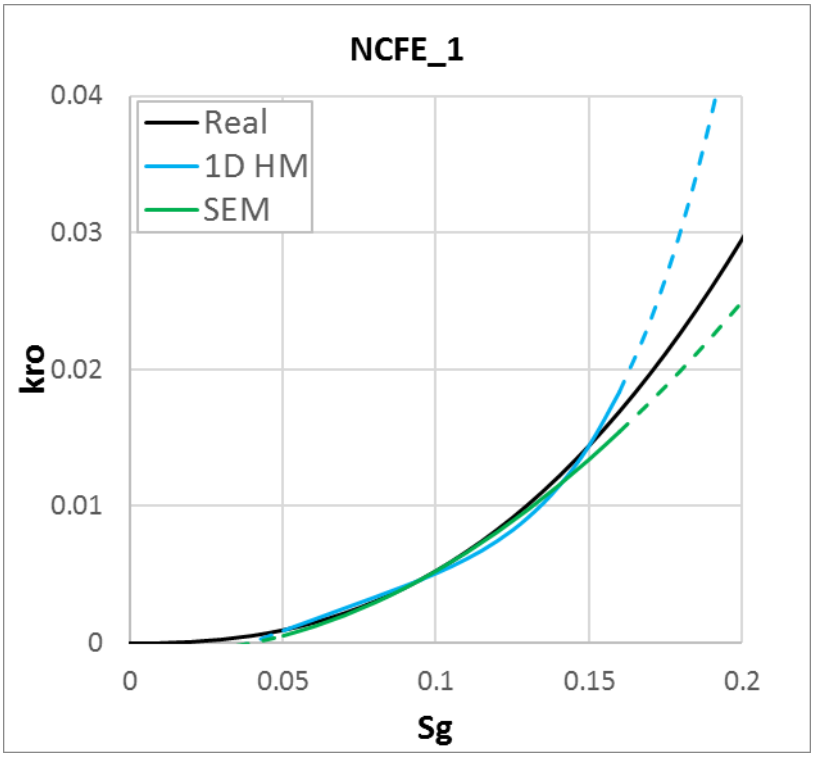

Figure 6-25: Relative permeability to gas as estimated by 1D HM and SEM compared with the real relative permeability for NCFE_1, the solid lines represent the valid saturation range.

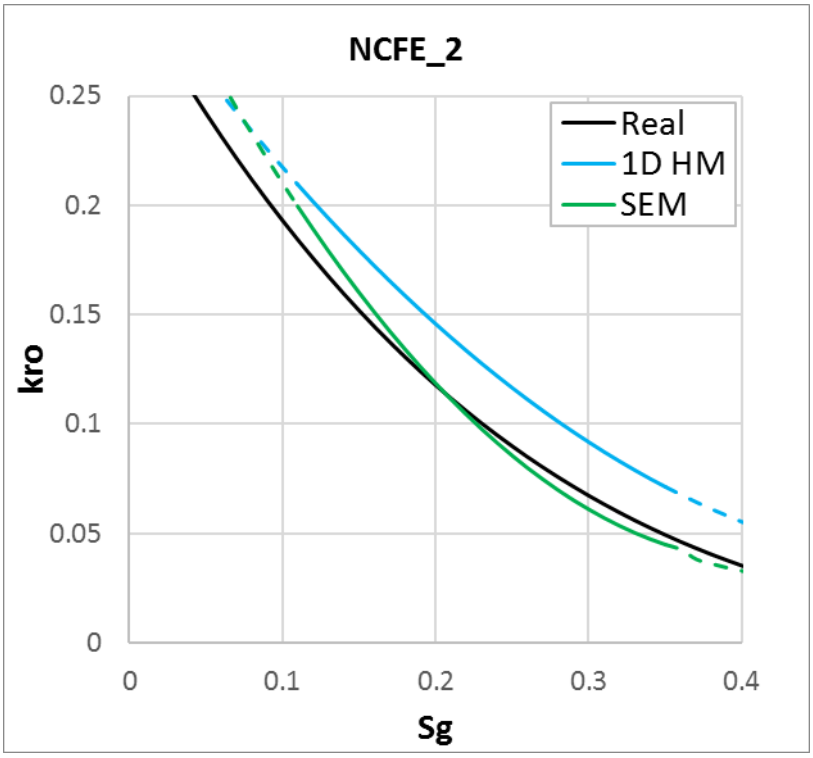

Figure 6-26: Relative permeability to oil as estimated by 1D HM and SEM compared with the real relative permeability for NCFE_2, the solid lines represent the valid saturation range.

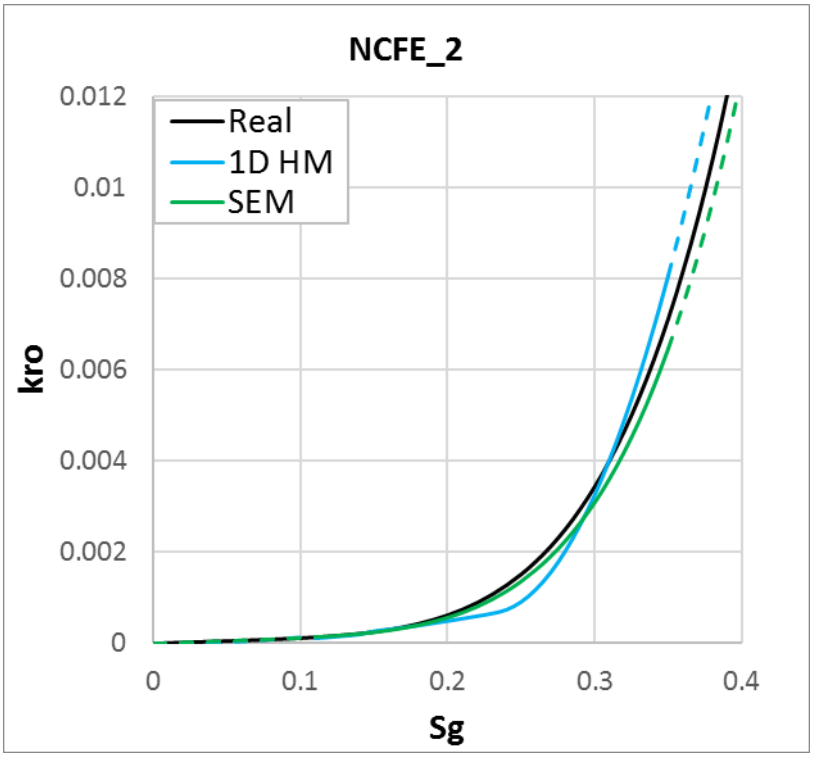

Figure 6-27: Relative permeability to gas as estimated by 1D HM and SEM compared with the real relative permeability for NCFE_2, the solid lines represent the valid saturation range.

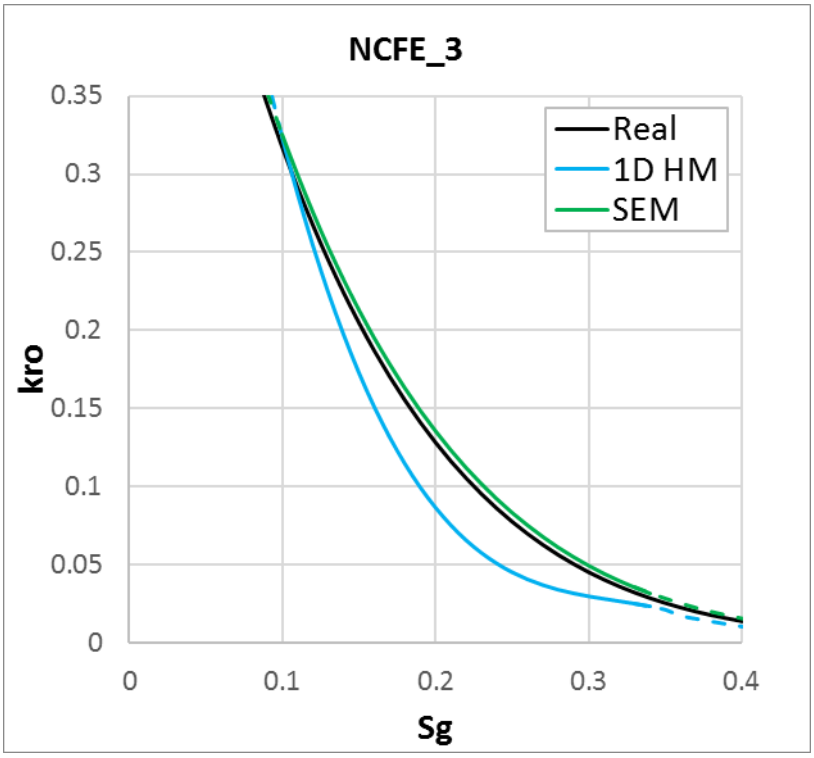

Figure 6-28: Relative permeability to oil as estimated by 1D HM and SEM compared with the real relative permeability for NCFE_3, the solid lines represent the valid saturation range.

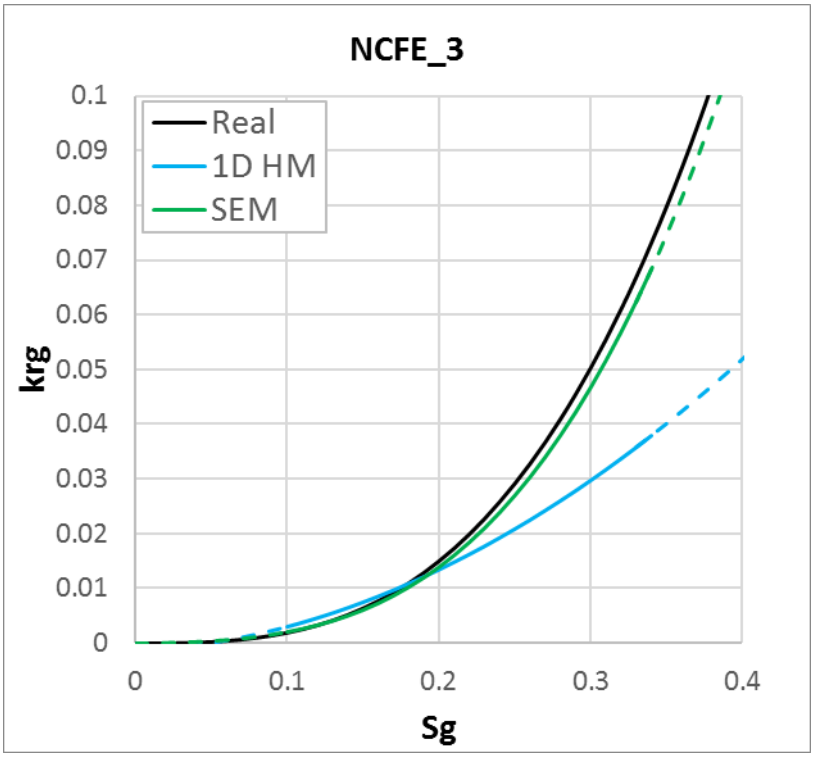

Figure 6-29: Relative permeability to gas as estimated by 1D HM and SEM compared with the real relative permeability for NCFE_3, the solid lines represent the valid saturation range.

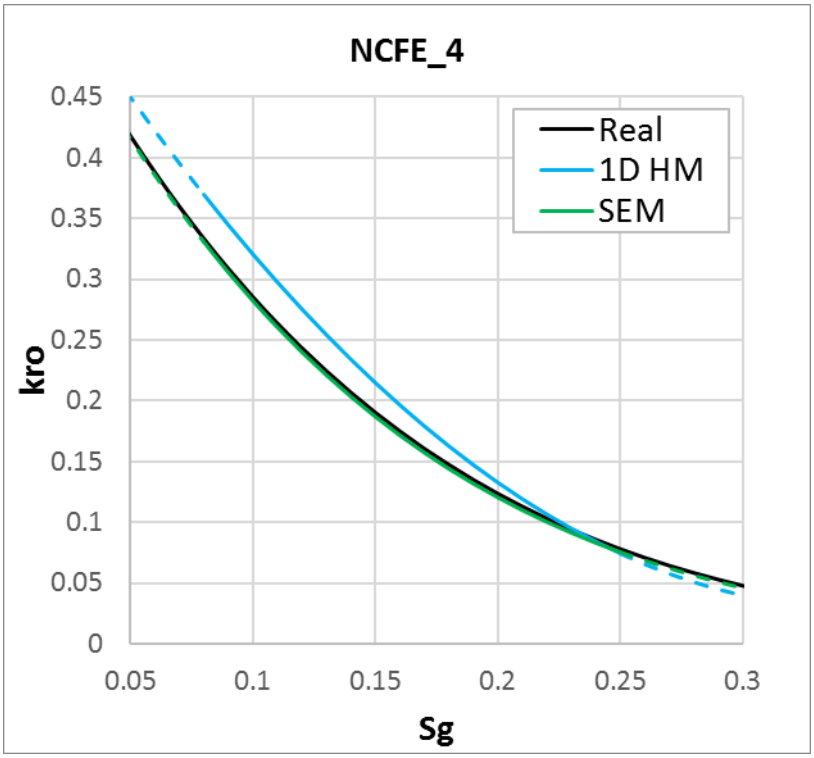

Figure 6-30: Relative permeability to oil as estimated by 1D HM and SEM compared with the real relative permeability for NCFE_4, the solid lines represent the valid saturation range.

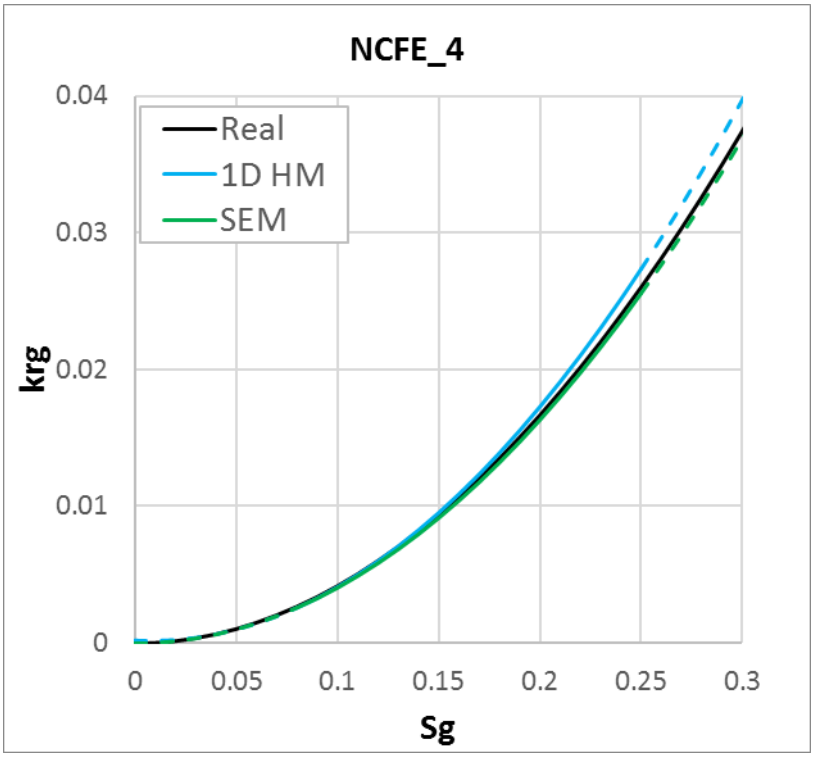

Figure 6-31: Relative permeability to gas as estimated by 1D HM and SEM compared with the real relative permeability for NCFE_4, the solid lines represent the valid saturation range.

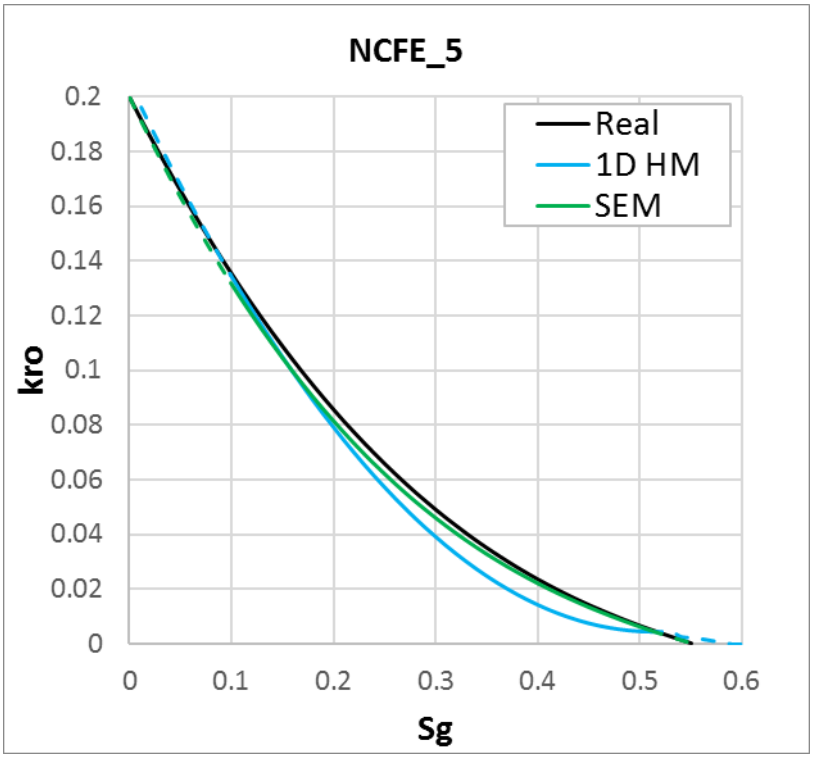

Figure 6-32: Relative permeability to oil as estimated by 1D HM and SEM compared with the real relative permeability for NCFE_5, the solid lines represent the valid saturation range.

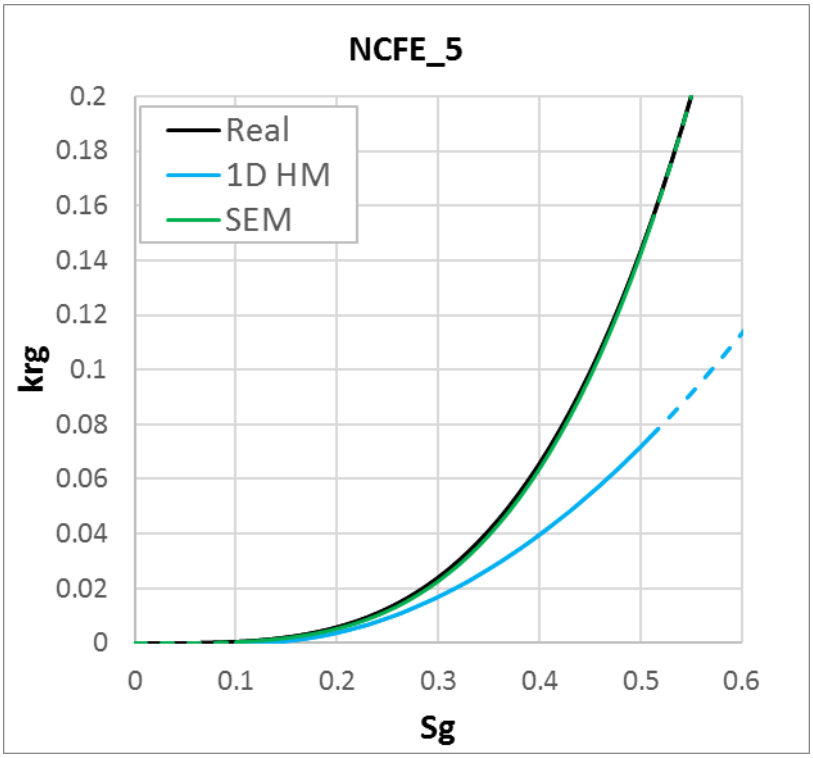

Figure 6-33: Relative permeability to gas as estimated by 1D HM and SEM compared with the real relative permeability for NCFE_5, the solid lines represent the valid saturation range.

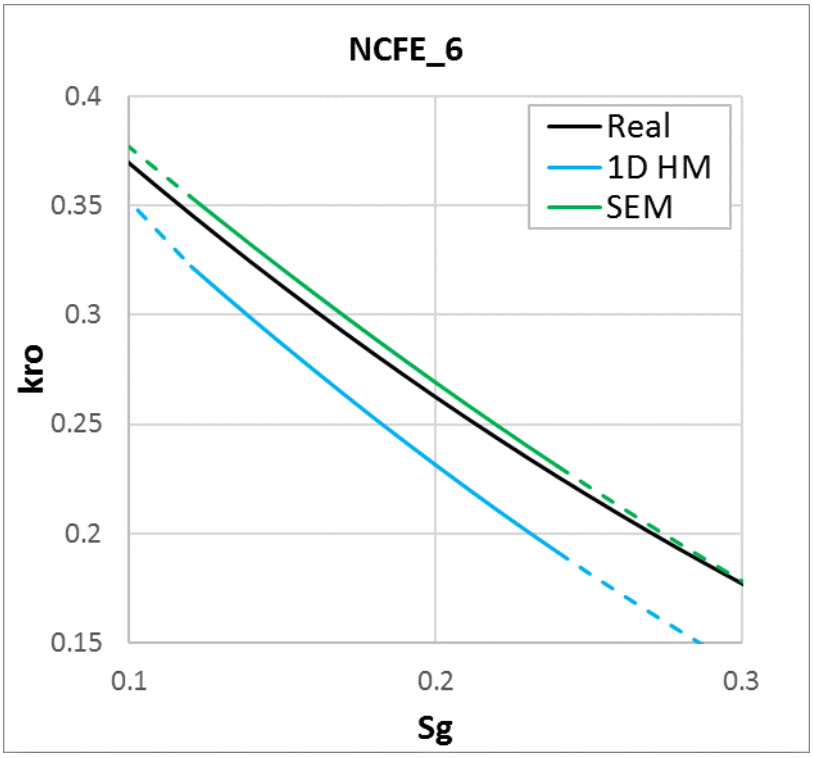

Figure 6-34: Relative permeability to oil as estimated by 1D HM and SEM compared with the real relative permeability for NCFE_6, the solid lines represent the valid saturation range.

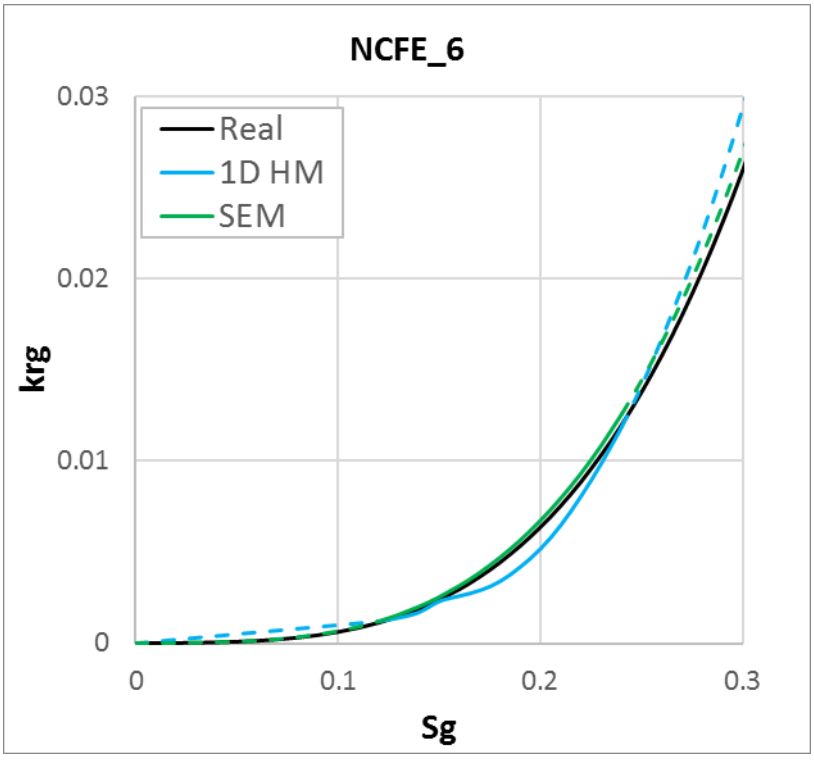

Figure 6-35: Relative permeability to gas as estimated by 1D HM and SEM compared with the real relative permeability for NCFE_6, the solid lines represent the valid saturation range.

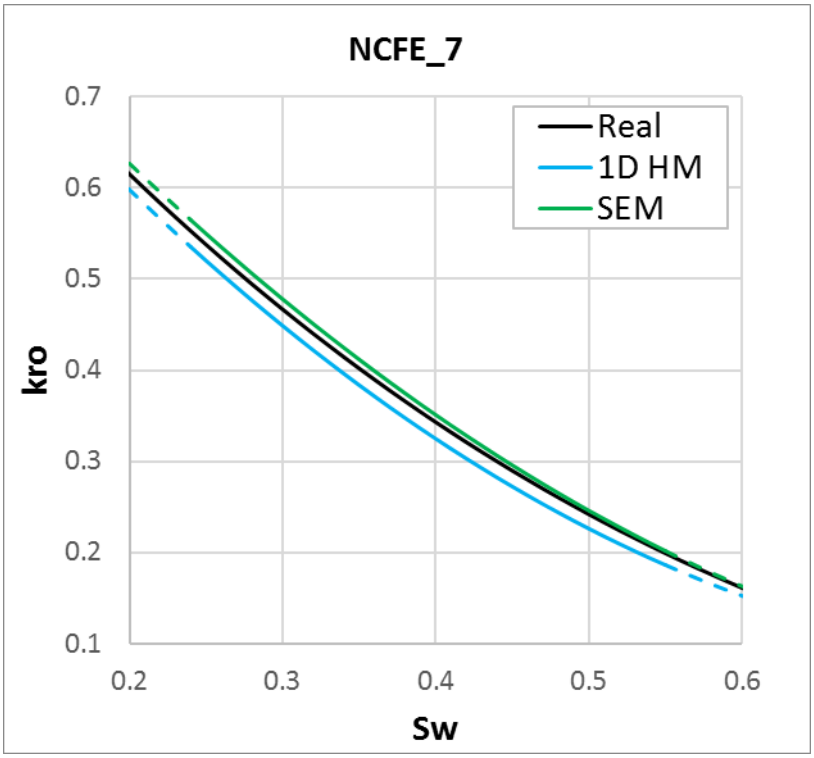

Figure 6-36: Relative permeability to oil as estimated by 1D HM and SEM compared with the real relative permeability for NCFE_7, the solid lines represent the valid saturation range.

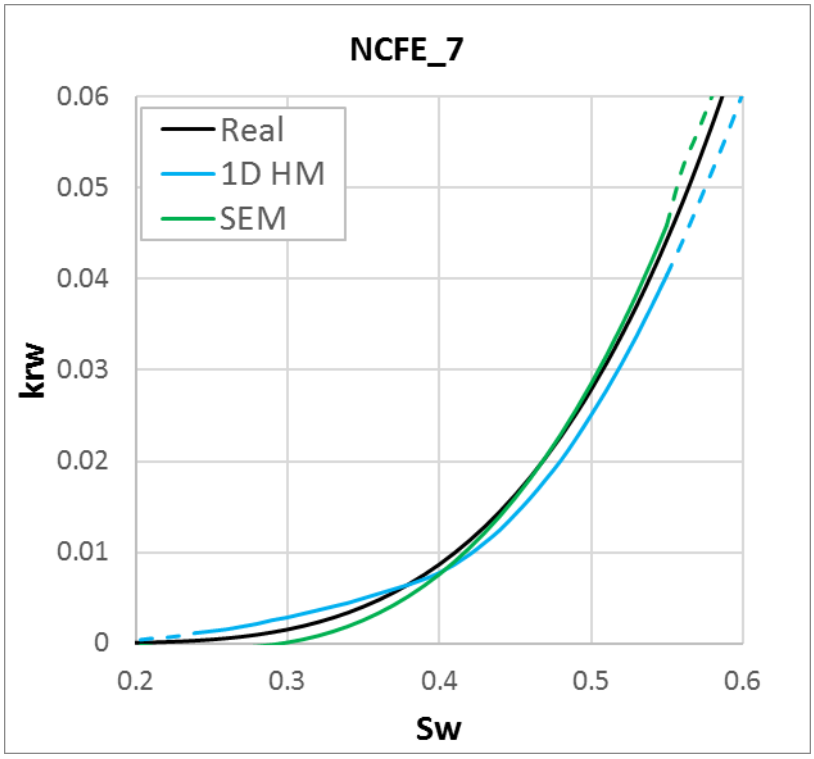

Figure 6-37: Relative permeability to water as estimated by 1D HM and SEM compared with the real relative permeability for NCFE_7, the solid lines represent the valid saturation range.

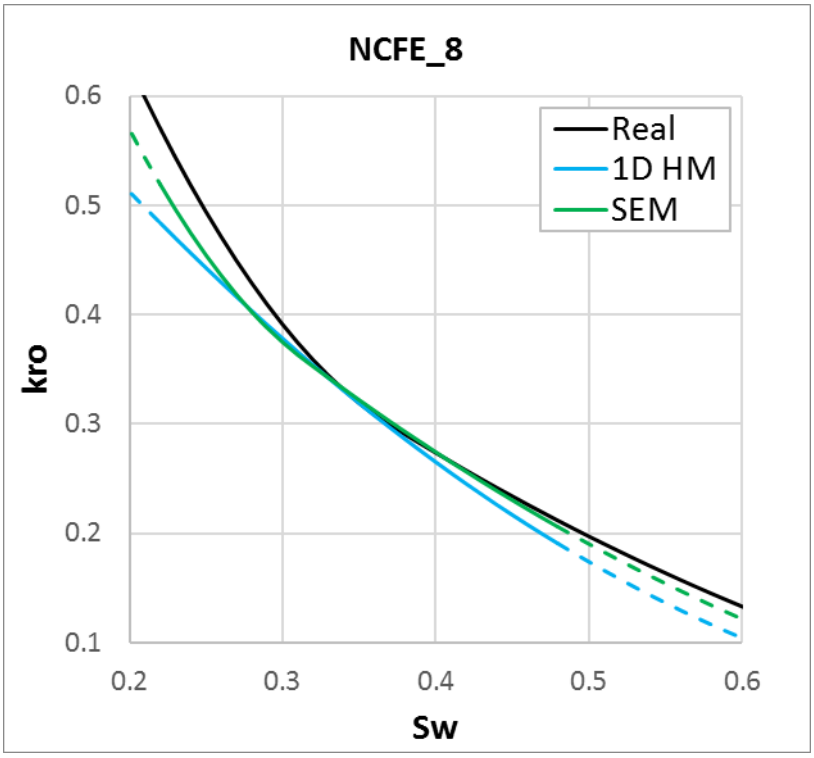

Figure 6-38: Relative permeability to oil as estimated by 1D HM and SEM compared with the real relative permeability for NCFE_8, the solid lines represent the valid saturation range.

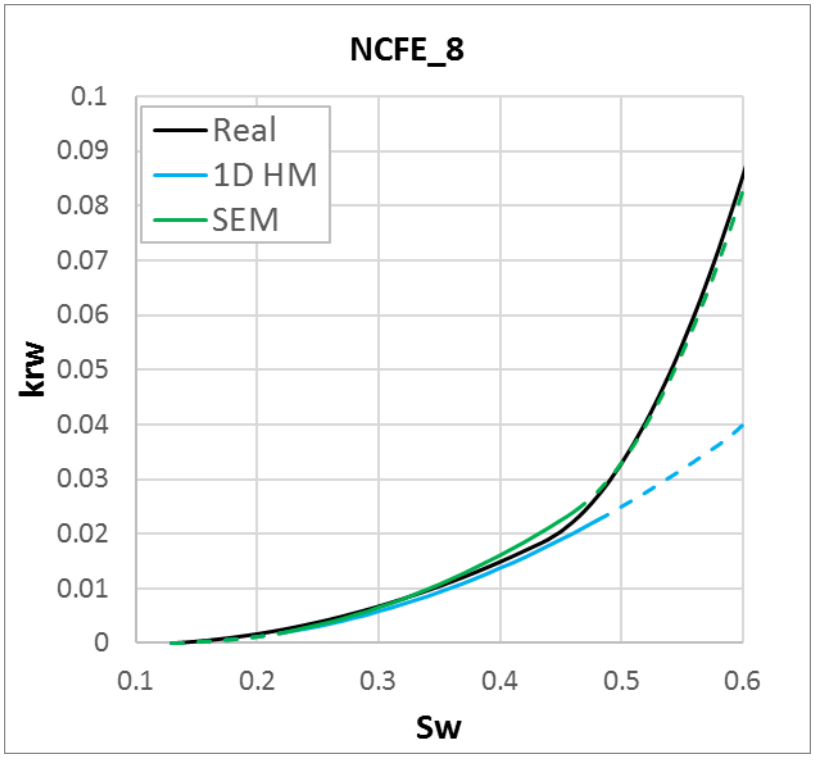

Figure 6-39: Relative permeability to water as estimated by 1D HM and SEM compared with the real relative permeability for NCFE_8, the solid lines represent the valid saturation range.

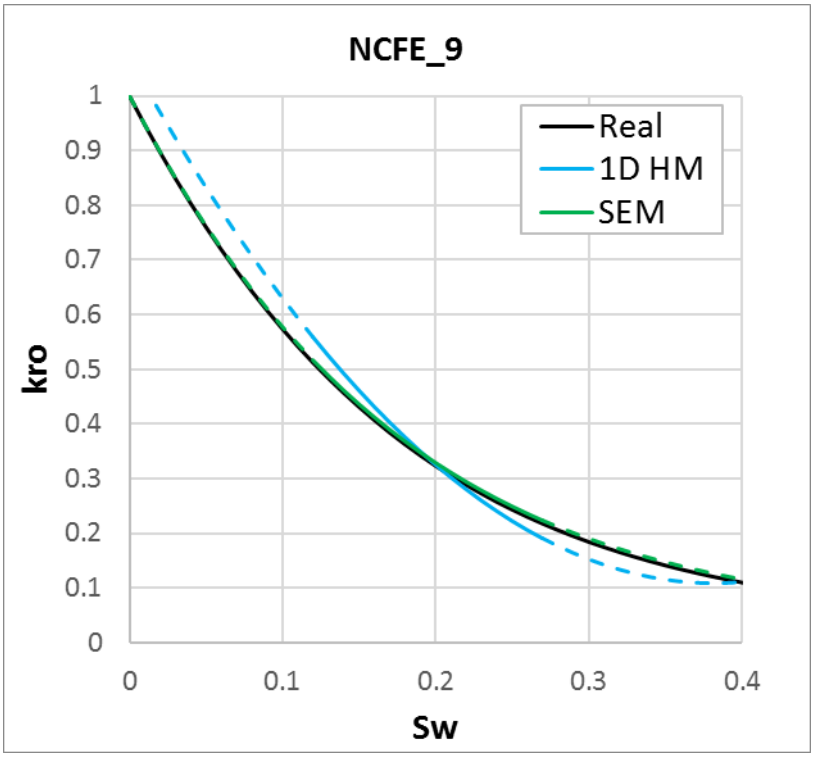

Figure 6-40: Relative permeability to oil as estimated by 1D HM and SEM compared with the real relative permeability for NCFE_9, the solid lines represent the valid saturation range.

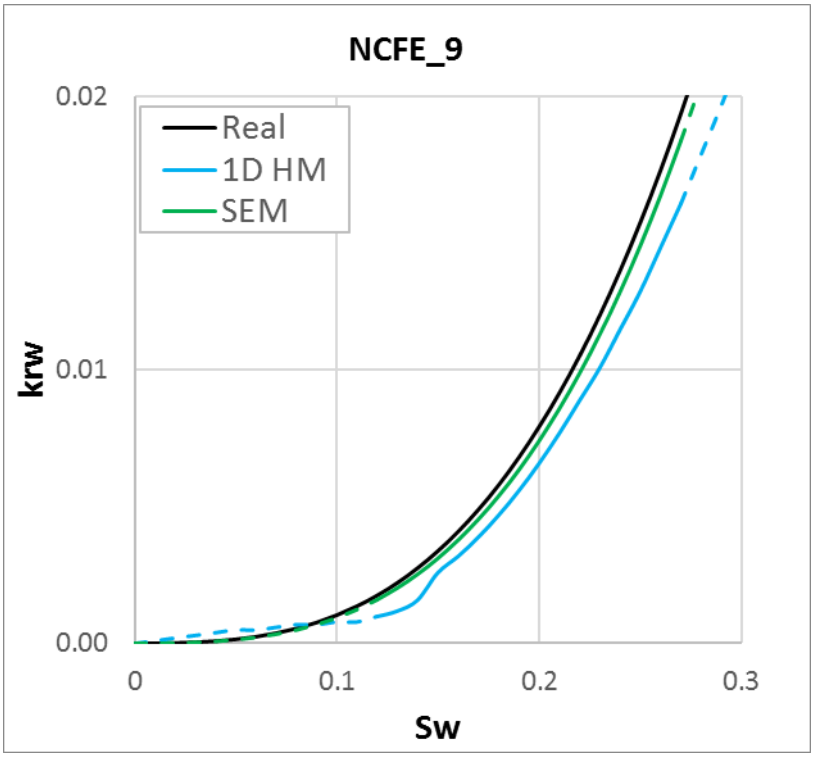

Figure 6-41: Relative permeability to water as estimated by 1D HM and SEM compared with the real relative permeability for NCFE_9, the solid lines represent the valid saturation range.

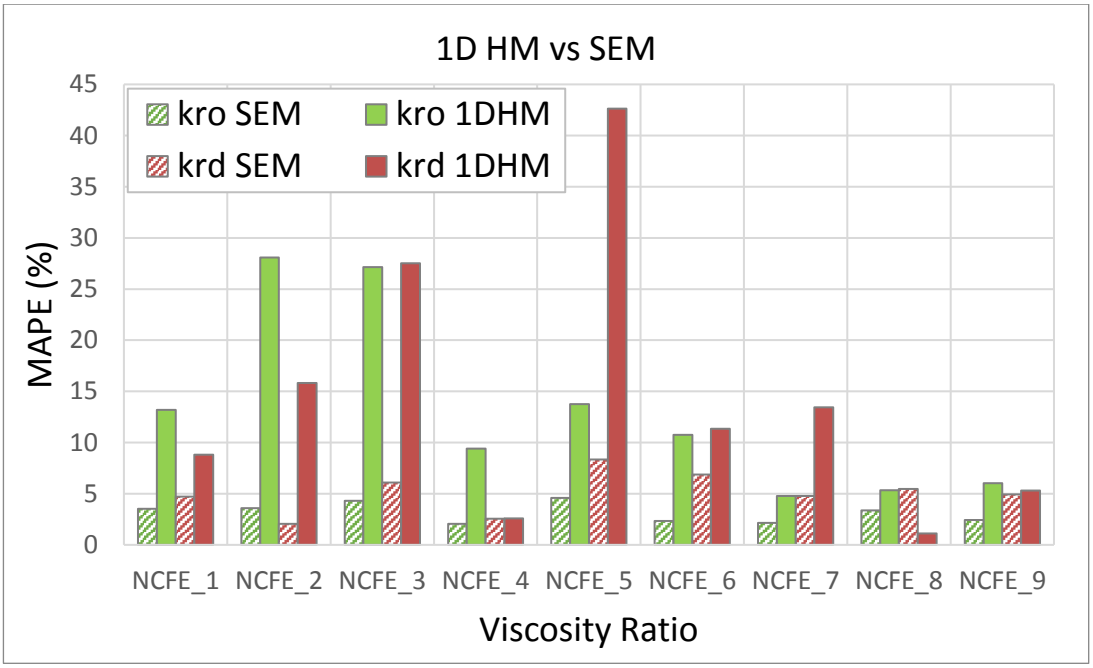

Figure 6-42: Error comparison between 1D HM and SEM relative permeability estimations for NCFE_1 to NCFE_9, showing a clear reduction in error when using SEM for the relative permeability curves estimations.

6.2.1.4 Production Data Analysis

The relative permeability is one of the most important parameters in fluid flow simulation through porous medium, so the error observed in relative permeability curves will affect the predictions of coreflood simulations. In NCFEs 1 to 9 it was seen that the different methods of estimation resulted in different amounts of error in the relative permeability curves. However, depending on the case, this error may have a big or small impact in the production data of each NCFE.

One of the main objectives of this thesis is to understand the amount of error related to the viscous fingering phenomenon in SCAL analysis, so it is important to understand how the relative permeability errors seen in the previous section affect the production data results if those relative permeability curves were to be used in simulation (for example, to predict the performance of similar cores in a SCAL analysis). In this section, the results are presented for oil production data, differential pressure and saturation profile for each of the NCFEs (NCFE_1 to NCFE_9) using MJBN, SEM and 1D HM compared with the real production data. Since 1D HM is probably the most used relative permeability estimation method it was important to evaluate the amount of error in production data

resulting from using this method not fitted for viscous fingering against SEM and MJBN, which were created to deal with this instability.

The methodology to generate the production data resultant from the use of each method (MJBN, SEM and 1D HM) estimated relative permeability was to substitute the k_r curves from the original NCFE simulation data file (Real) with the method relative permeability. All other parameters remained the same and the alteration of the relative permeability was performed in the same data file as the original NCFE in order to avoid errors. The data file was then used in a CMG high resolution simulation. The production data was gathered and compared.

For simplicity, when a method is referred to (MJBN, SEM or 1D HM) in this section, it is always referring to the results obtained from the use of the relative permeability as estimated from those methods. So, for example, saying that more error was observed in the 1D HM case, it does not mean that a 1D case is being compared with the 2D NCFE, instead, the relative permeability produced by a 1D history matching is being used in a 2D NCFE and the results are being compared against the original values of that specific NCFE (e.g. NCFE_1). Also, when it is said 'real NCFE' it is referring to the NCFE base with the relative permeability presented in Chapter 3, in the same manner as in the previous sections to calculate the error.

NCFE_1

The oil production data for NCFE_1 is shown in Figure 6-43. The relative permeability resultant from MJBN and SEM methods predicted with good precision the real cumulative oil production. The 1D HM's relative permeability however resulted in an early breakthrough and less recovery throughout the injection. The differential pressure shows similar results, Figure 6-44, where both MJBN and SEM outperform the traditional 1D HM method. Nevertheless, it can be said that the general amount of error is small for the cumulative oil production and differential pressure, at least taking into account that the error in the relative permeability estimation for the 1D HM method was of around 13% for the oil k_r and 9% for the gas k_r.

Many relative permeability estimation methods rely on the cumulative oil production and the differential pressure to access the precision of estimation, however, it is more accurate if one can add the saturation profile along the core. Such a parameter may be difficult to obtain experimentally, normally requiring CT imaging of the core at different points of injection. In the NCFEs, though, it is simple to retrieve this information and compare the resulting profiles. Figure 6-45 and Figure 6-46 show the average cross-section gas

saturation for different points throughout the core length at different moments of injection (36, 87, 132, 165, 210, 294, 502 and 1200 minutes of injection).

The saturation profiles show considerable mismatch between the real saturations in comparison with the saturation produced using 1D HM's relative permeability, while SEM and MJBN k_r curves predict the real results well. This considerable mismatch is caused by the relative permeability error from the viscous fingering formation. In this case it would be very unreliable to evaluate the precision of 1D HM by only evaluation of the oil cumulative production data and differential pressure, where the error seemed to be small. Also, the fact that the saturation patterns changed so much with the relative permeability may suggest that a much bigger impact in the production could be seen if this relative permeability was used for scale-up (reservoir simulation).

In addition to the numerical values of the saturation profiles, the 'visual' patterns were gathered in order to understand the implication of the flow changes inside the core, Figure 6-47. The flow pattern from the 1D HM's k_r show a longer fingering zone (total length of the core where viscous fingering is occurring) than the real case, this is responsible for the reduced oil recovery in this case. In contrast, SEM and MJBN show a fingering zone with almost the same length as the real case and the fingering patterns are much similar to real than the case using 1D HM's k_r.

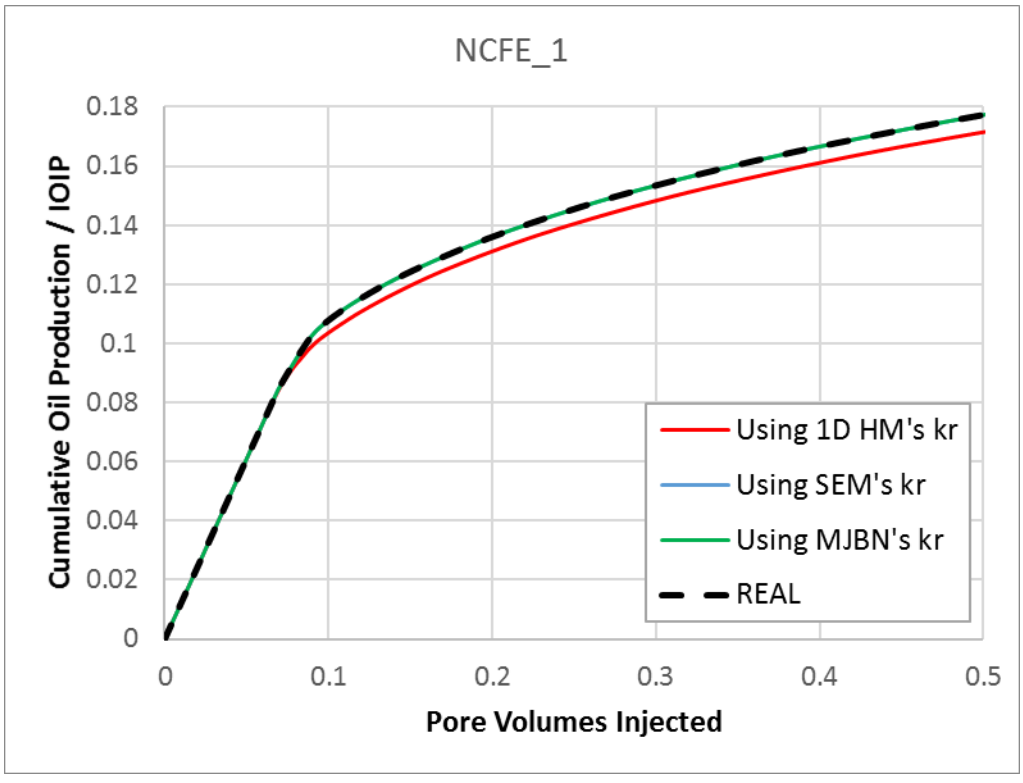

Figure 6-43:Cumulative Oil Production (fraction of initial oil in place) as a function of PVI for NCFE_1 using relative permeability curves obtained by 1D HM, SEM and MJBN, compared with the real data.

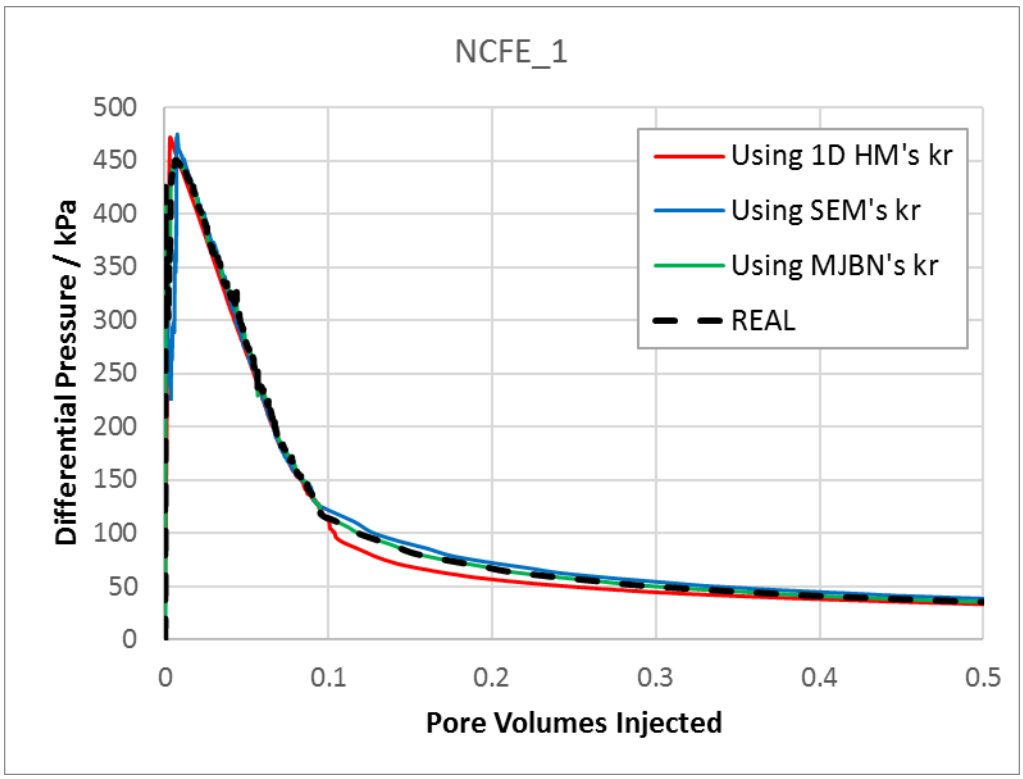

Figure 6-44: Differential Pressure as a function of PVI for NCFE_1 using relative permeability curves obtained by 1D HM, SEM and MJBN, compared with the real data.

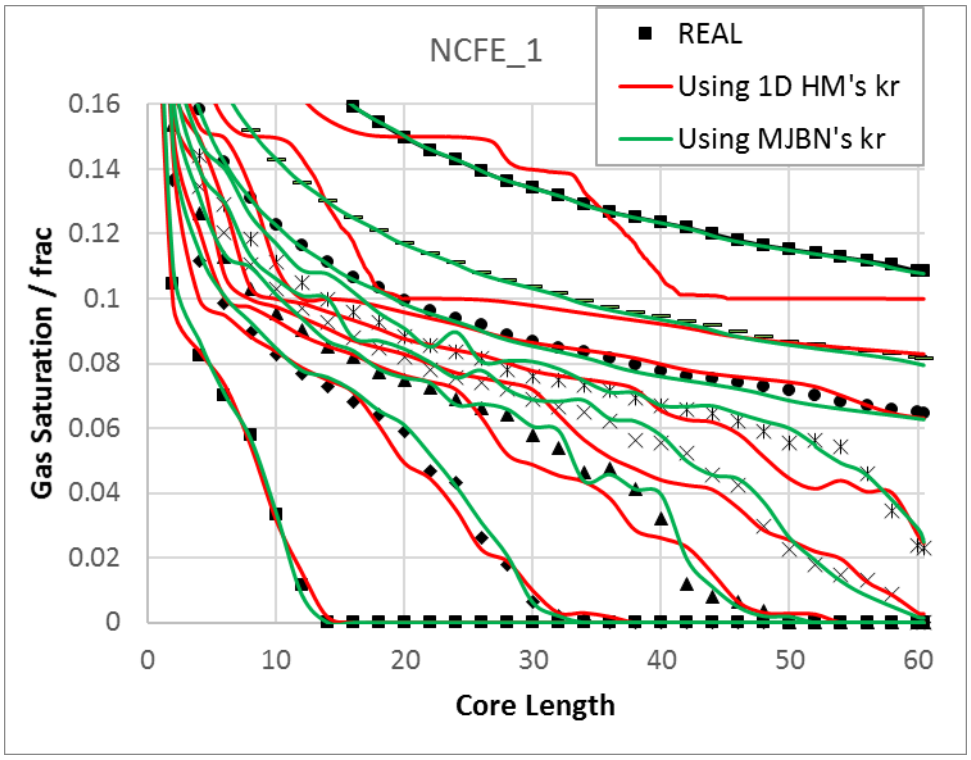

Figure 6-45:Values of average gas saturation for different positions (in the axis horizontal to the flow) inside the core and at different times of injection resultant of the use of the k_r curves of 1D HM, MJBN and the real curves in NCFE_1. In black are the real saturation values, each black symbol (square, triangle, diamond, etc) represents a different injection time.

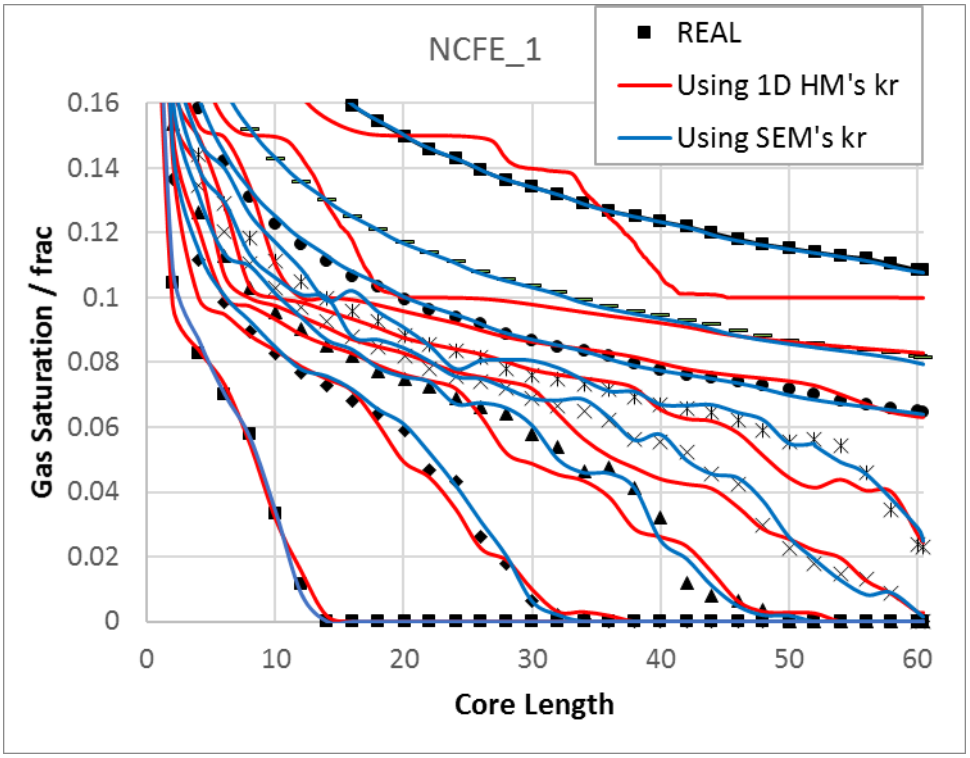

Figure 6-46: Values of average gas saturation for different positions (in the axis horizontal to the flow) inside the core and at different times of injection resultant of the use of the k_r curves of 1D HM, SEM and the real curves in NCFE_1. In black are the real saturation values, each black symbol (square, triangle, diamond, etc) represents a different injection time.

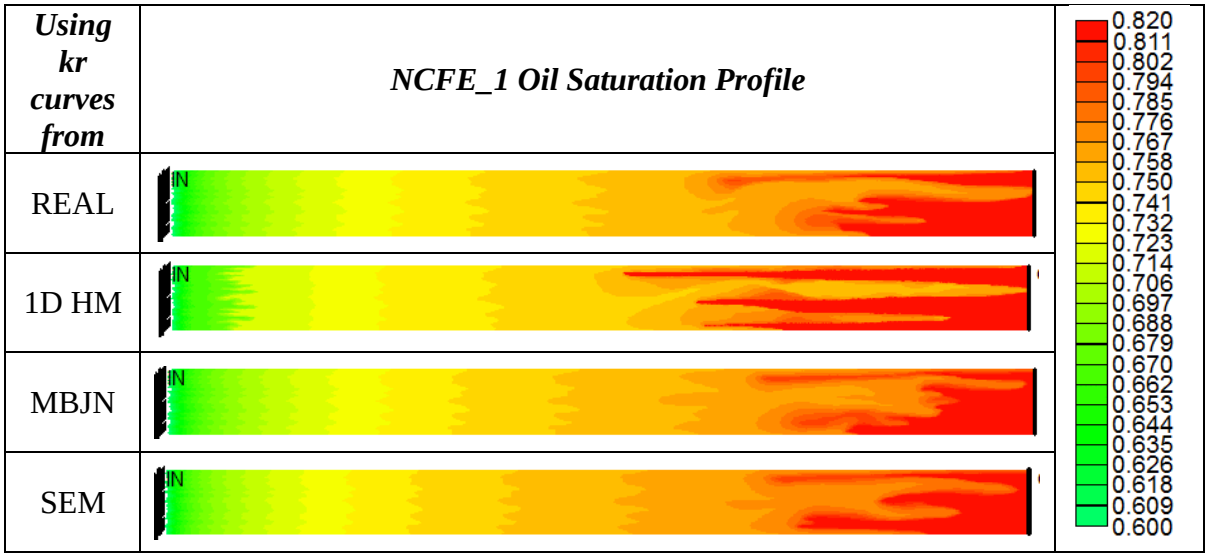

Figure 6-47: Average gas saturations inside the core near the breakthrough time, resultant of the use of the k_r curves of 1D HM, SEM and MJBN in NCFE_1; in comparison with the real gas saturation.

NCFE_2

The cumulative oil production as a fraction of initial oil in place and the differential pressure resulting from using the relative permeability curves estimated by 1D HM, SEM and MJBN are presented against the real values in Figure 6-48 and Figure 6-49,

respectively. SEM and MJBN's relative permeability curves result in good matches with the real values. On the contrary, using 1D HM's relative permeability leads to considerable error in both oil production and differential pressure. The error observed in this 2 parameters is considerable higher than the one observed in NCFE_1, but, since the error of k_r estimation is also higher (Figure 6-42) this was to be expected.

The saturation profiles obtained from each method are presented in Figure 6-50 and Figure 6-51. These figure further confirm SEM and MJBN as superior estimation methods than the traditional 1D HM. The traditional method presents considerable differences in saturation along the core. This fact is consolidated by the images from Figure 6-52, where it is visible that the fingering pattern is completely different in the 1D HM's k_r scenario. SEM and MJBN, however, show very good match for the saturation images of the real case, with similar number of fingers and the same mostly the same pattern.

In NCFE_1 it was observed that most of the error was in the saturation profiles and that the oil production and differential pressure had little error. NCFE_2 shows different conclusions, showing considerable error is all the parameters. It is possible that this is a result of a poorer precision of 1D HM for this case (since the error in the relative permeability estimation is higher), but it may also indicate that differences in the relative permeability may have influence in different parameters depending of other parameters of the coreflood.

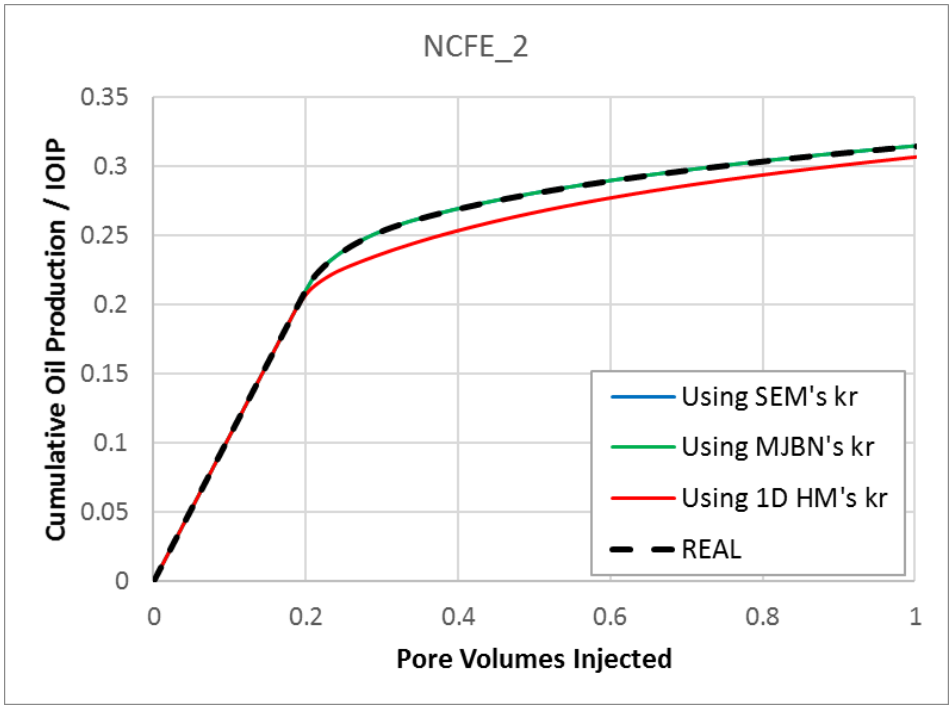

Figure 6-48: Cumulative Oil Production (fraction of initial oil in place) as a function of PVI for NCFE_2 using relative permeability curves obtained by 1D HM, SEM and MJBN, compared with the real data.

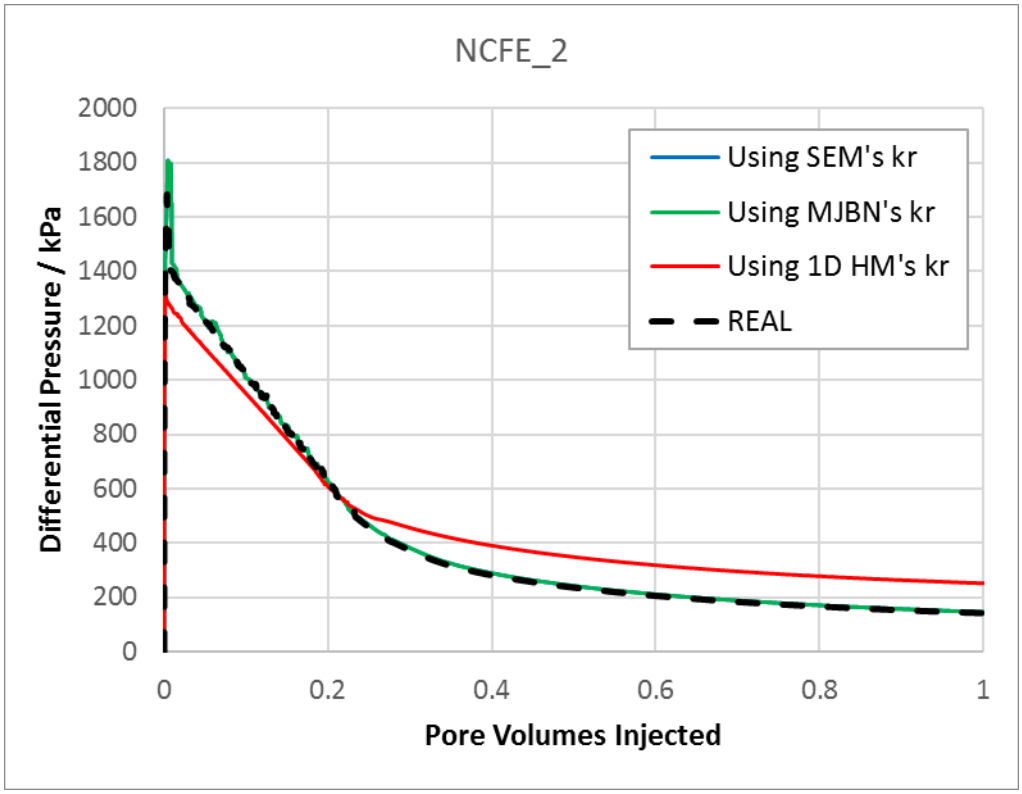

Figure 6-49: Differential Pressure as a function of PVI for NCFE_2 using relative permeability curves obtained by 1D HM, SEM and MJBN, compared with the real data.

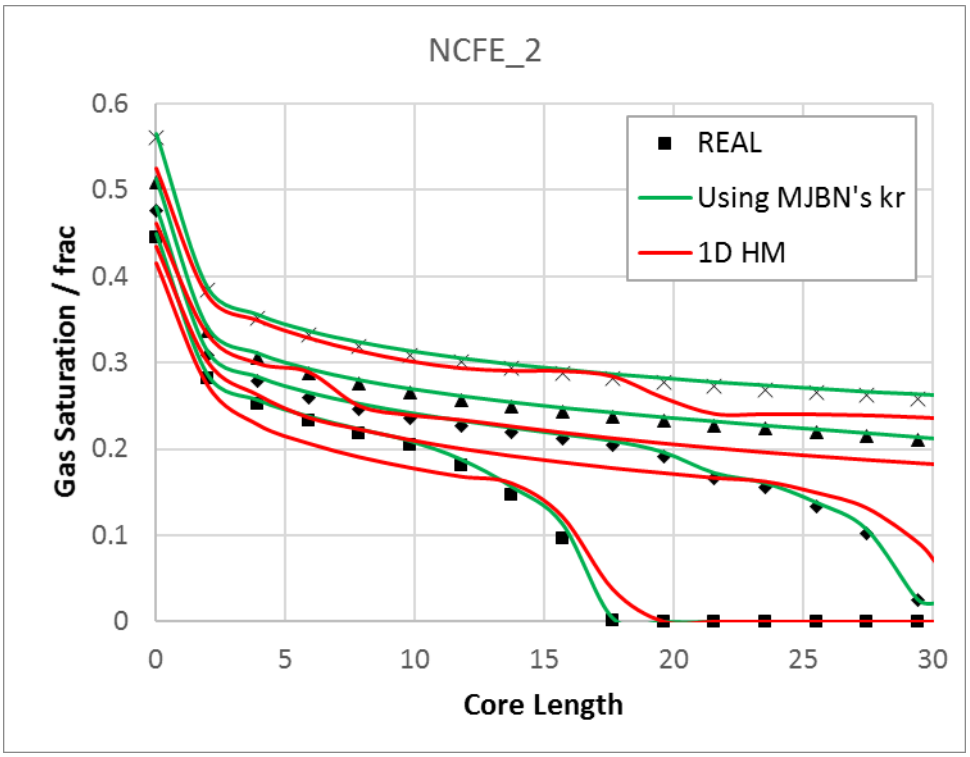

Figure 6-50: Values of average gas saturation for different positions (in the axis horizontal to the flow) inside the core and at different times of injection resultant of the use of the k_r curves of 1D HM, MJBN and the real curves in NCFE_2. In black are the real saturation values, each black symbol (square, triangle, diamond, etc) represents a different injection time.

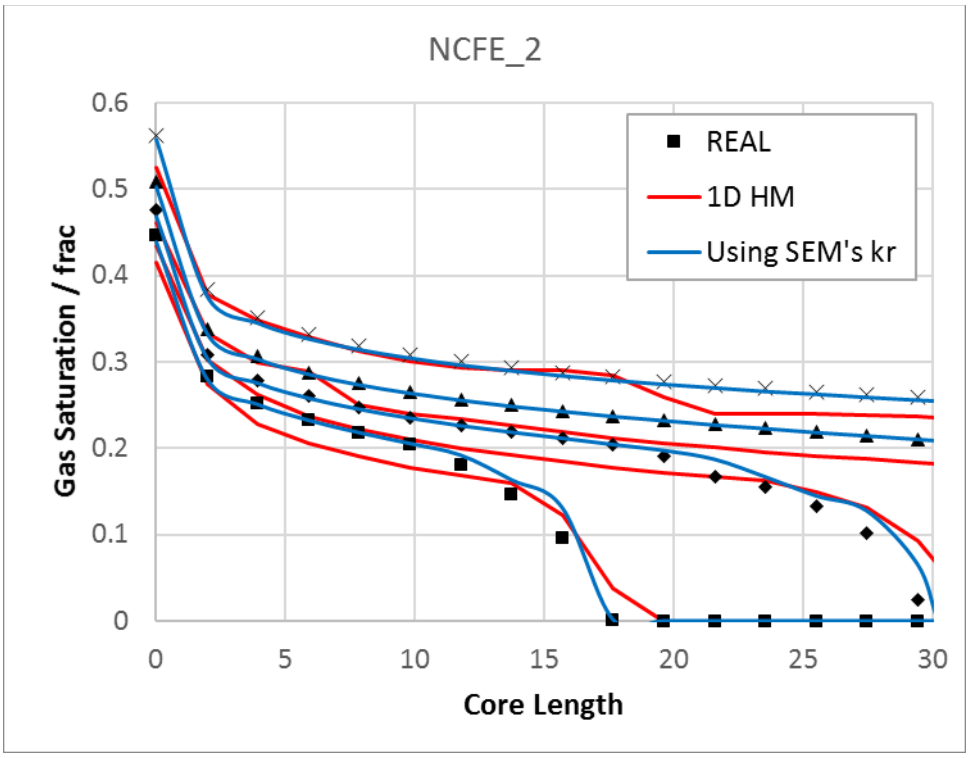

Figure 6-51: Values of average gas saturation for different positions (in the axis horizontal to the flow) inside the core and at different times of injection resultant of the use of the k_r curves of 1D HM, SEM and the real curves in NCFE_2. In black are the real saturation values, each black symbol (square, triangle, diamond, etc) represents a different injection time.

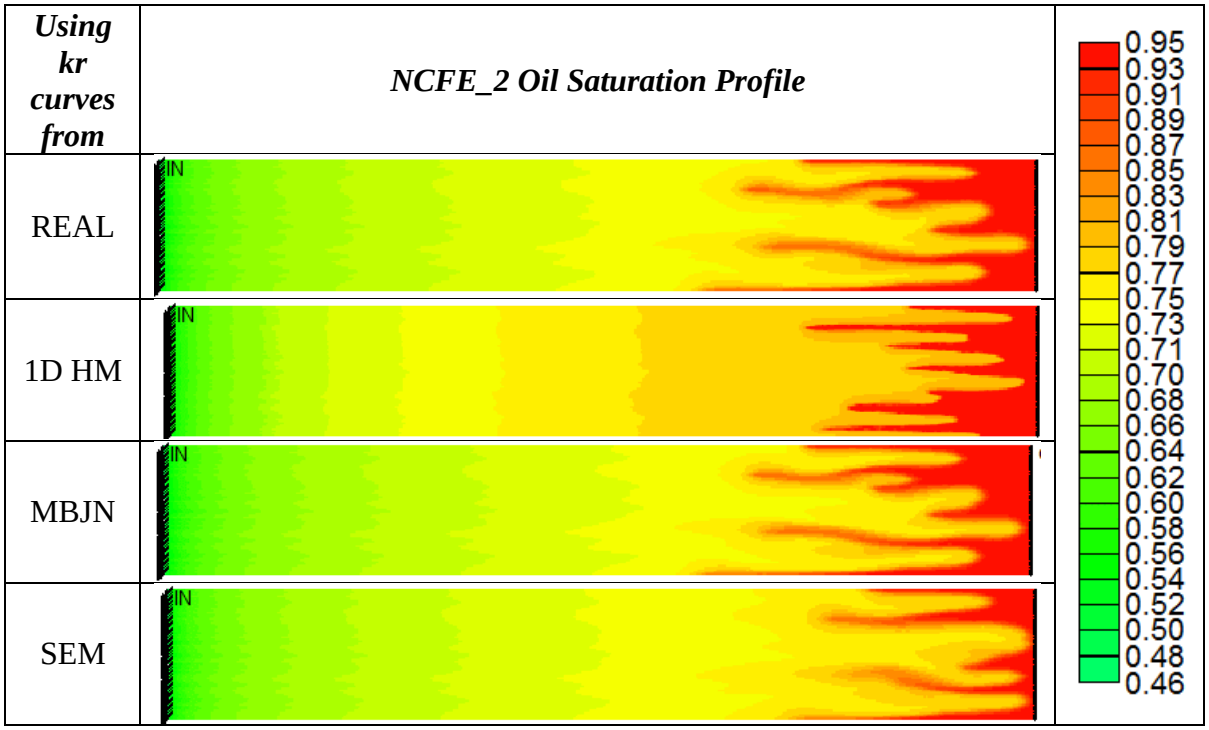

Figure 6-52: Average gas saturations inside the core near the breakthrough time, resultant of the use of the k_r curves of 1D HM, SEM and MJBN in NCFE_2; in comparison with the real gas saturation.

NCFE_3

The oil cumulative production and differential pressure for NCFE_3 are presented in Figure 6-53 and Figure 6-54, respectively. For this case the 1D HM error is more evident in the differential pressure than the cumulative oil production. Similarly, to the previous cases, SEM and MJBN have matched the real results well.

The saturation profiles obtained by the use of different methods on NCFE_3 data are presented in Figure 6-55, Figure 6-56 and Figure 6-57. In these figures only 1D HM shows a bad matching against the real data. Also, the fingering patterns shown in Figure 6-57 emphasize this error by showing a completely different pattern than in the real case.

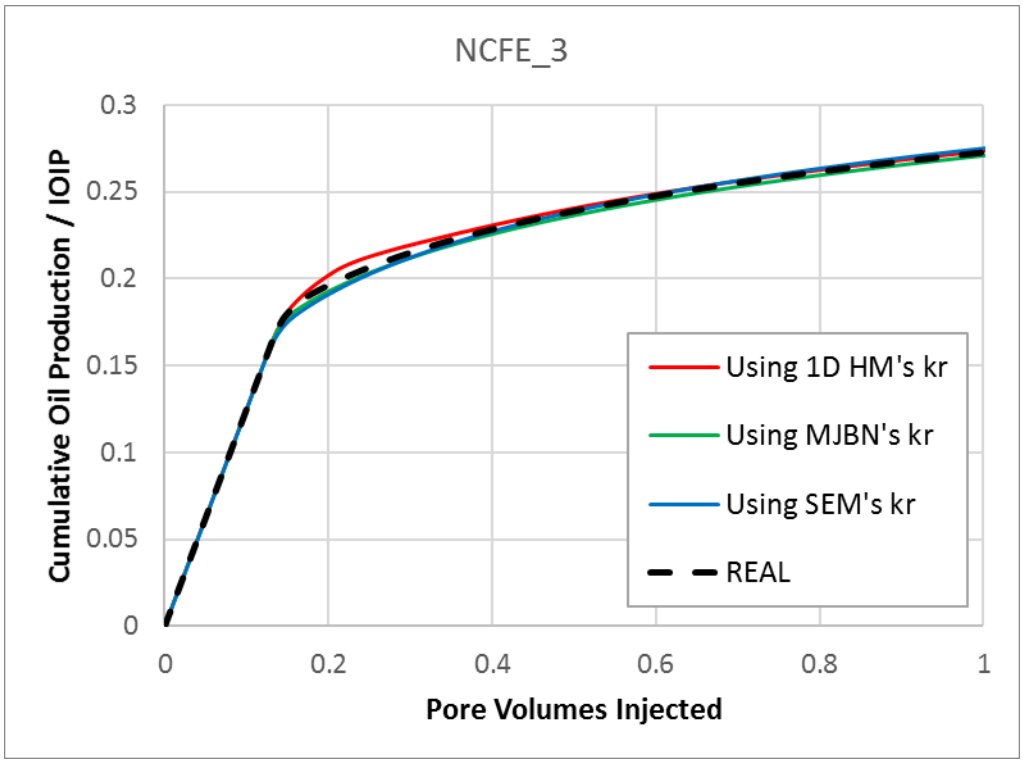

Figure 6-53: Cumulative Oil Production (fraction of initial oil in place) as a function of PVI for NCFE_3 using relative permeability curves obtained by 1D HM, SEM and MJBN, compared with the real data.

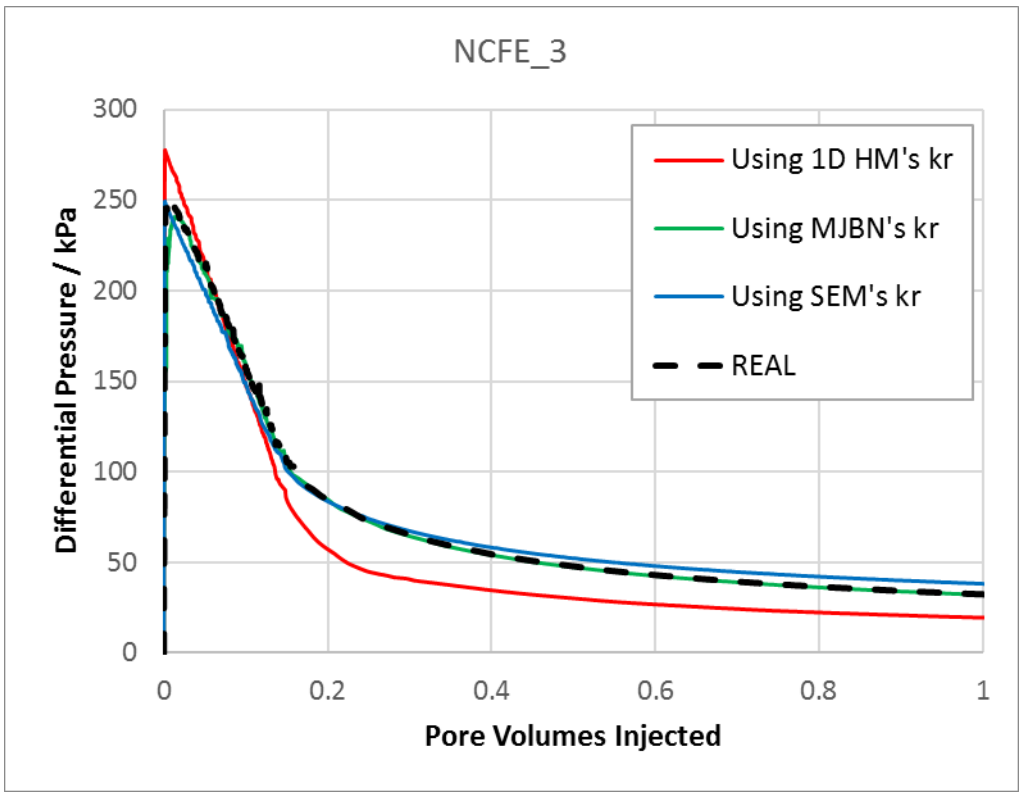

Figure 6-54: Differential Pressure as a function of PVI for NCFE_3 using relative permeability curves obtained by 1D HM, SEM and MJBN, compared with the real data.

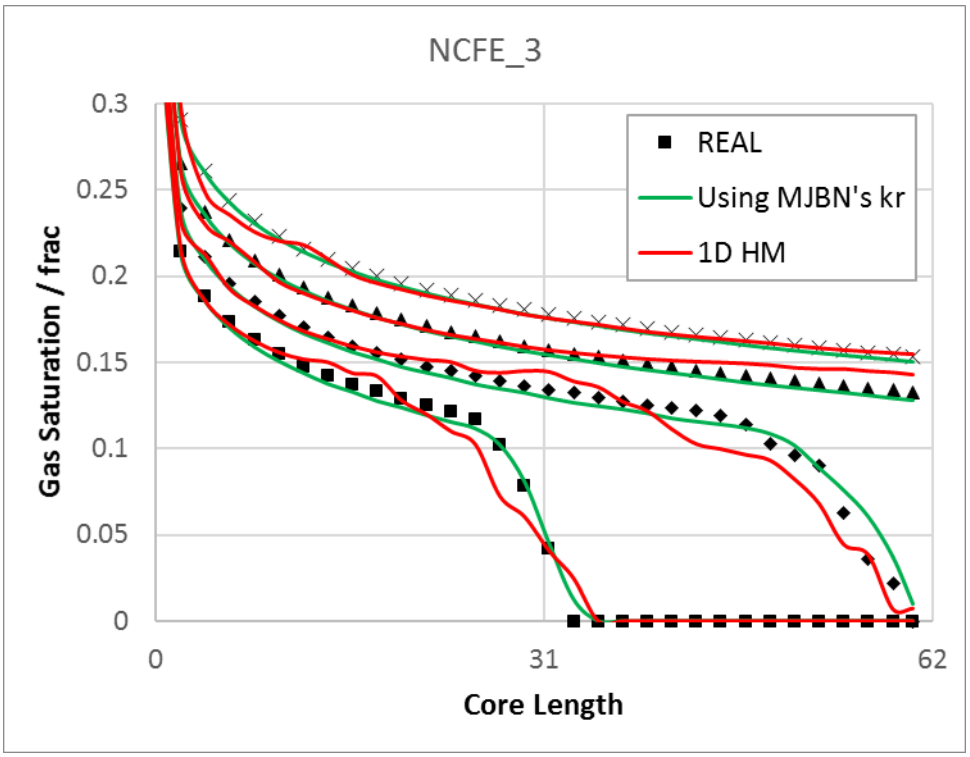

Figure 6-55: Values of average gas saturation for different positions (in the axis horizontal to the flow) inside the core and at different times of injection resultant of the use of the k_r curves of 1D HM, MJBN and the real curves in NCFE_3. In black are the real saturation values, each black symbol (square, triangle, diamond, etc) represents a different injection time.

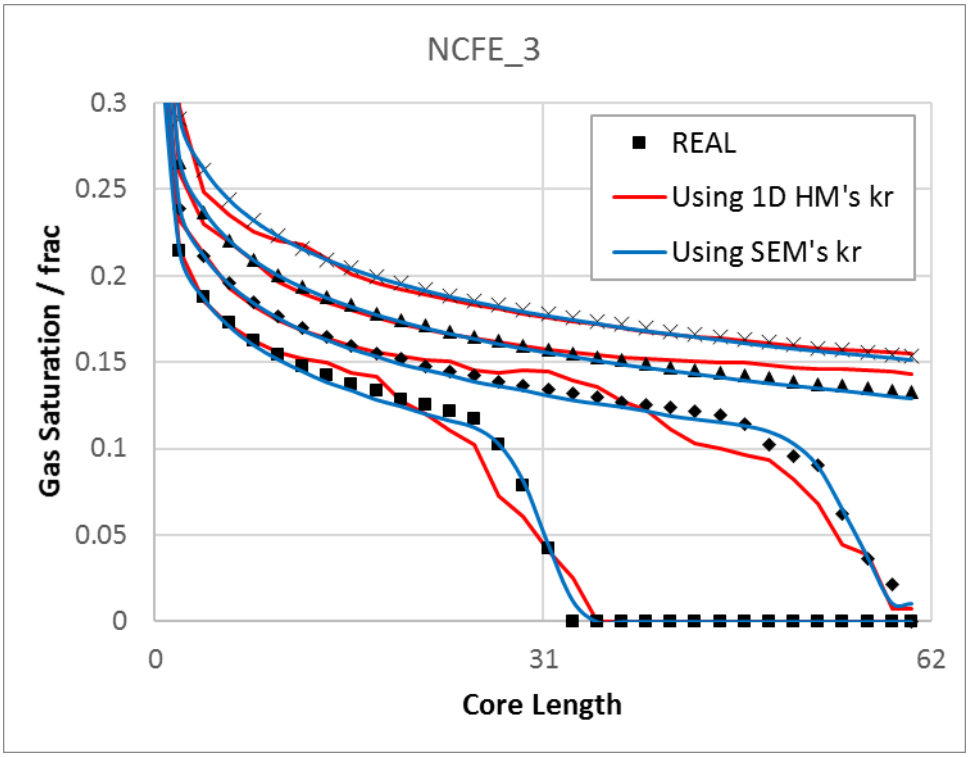

Figure 6-56: Values of average gas saturation for different positions (in the axis horizontal to the flow) inside the core and at different times of injection resultant of the use of the k_r curves of 1D HM, SEM and the real curves in NCFE_3. In black are the real saturation values, each black symbol (square, triangle, diamond, etc) represents a different injection time.

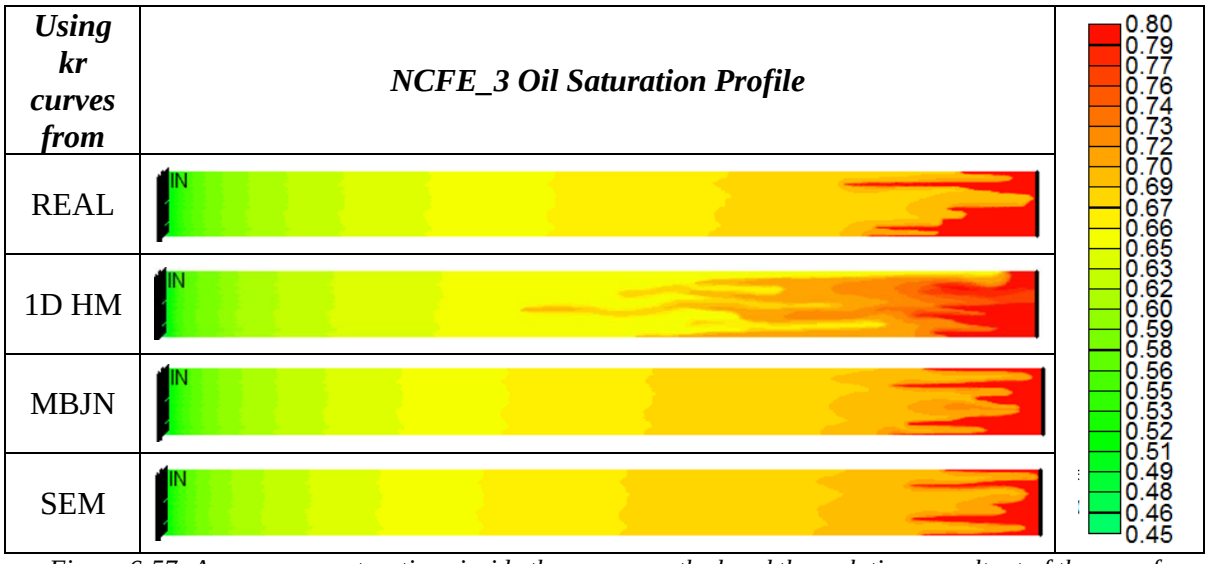

Figure 6-57: Average gas saturations inside the core near the breakthrough time, resultant of the use of the k_r curves of 1D HM, SEM and MJBN in NCFE_3; in comparison with the real gas saturation.

NCFE_4

The oil cumulative production and differential pressure for NCFE_3 are presented in Figure 6-58 and Figure 6-59, respectively. For this case, all methods have good matching with the exception of 1D HM for the first values of differential pressure. Nevertheless,

when comparing this error with the previous case (NCFE_3) it fairly small. This was expected since NCFE_4 resulted in less error on the 1D HM's relative permeability estimation, Figure 6-42.

In the saturation profiles, Figure 6-60, Figure 6-61 and Figure 6-62, using SEM and MJBN's relative permeability resulted in good match with the real results, but considerable error, when using 1D HM.

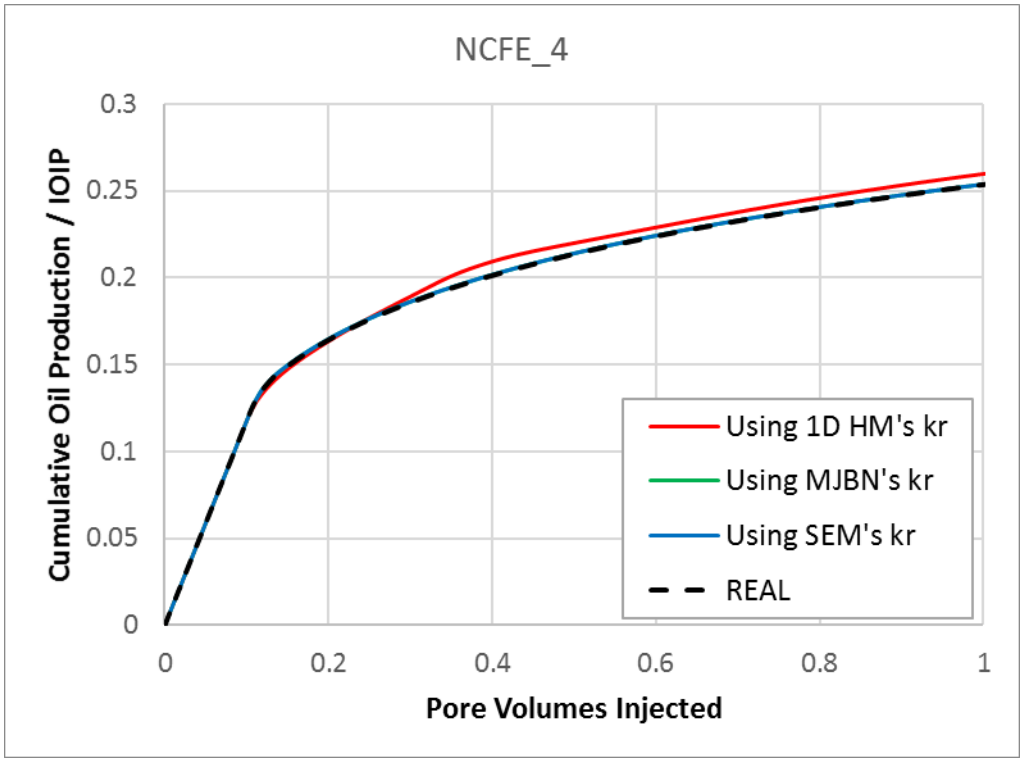

Figure 6-58: Cumulative Oil Production (fraction of initial oil in place) as a function of PVI for NCFE_4 using relative permeability curves obtained by 1D HM, SEM and MJBN, compared with the real data.

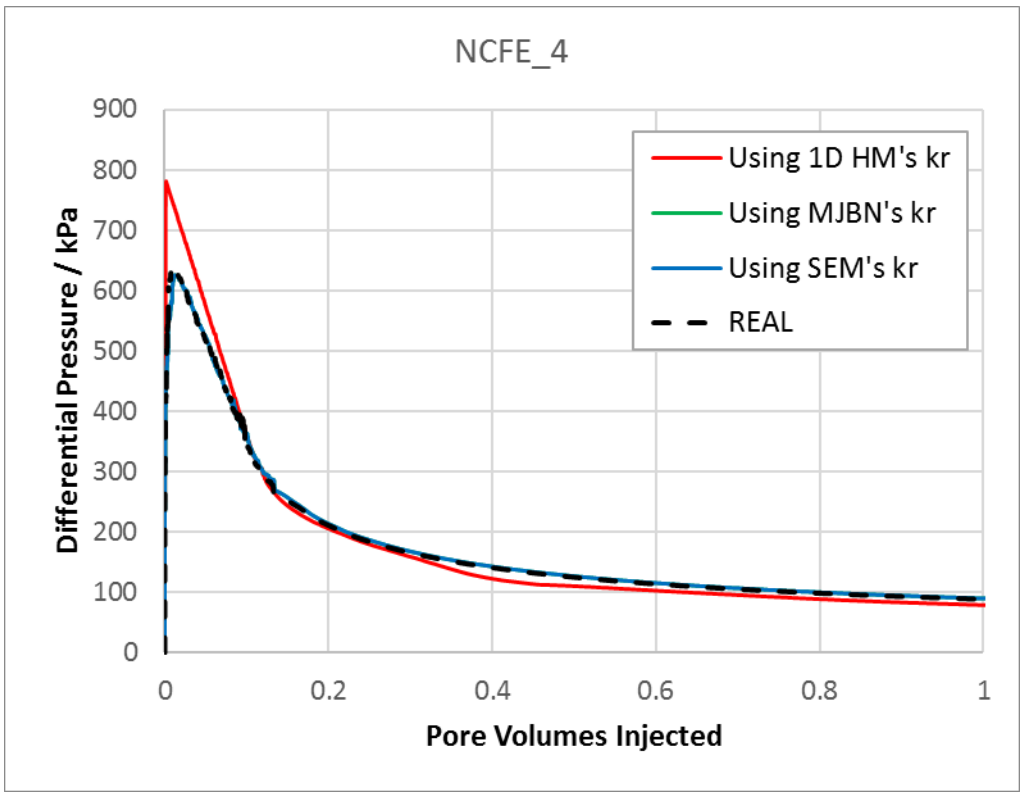

Figure 6-59: Differential Pressure as a function of PVI for NCFE_4 using relative permeability curves obtained by 1D HM, SEM and MJBN, compared with the real data.

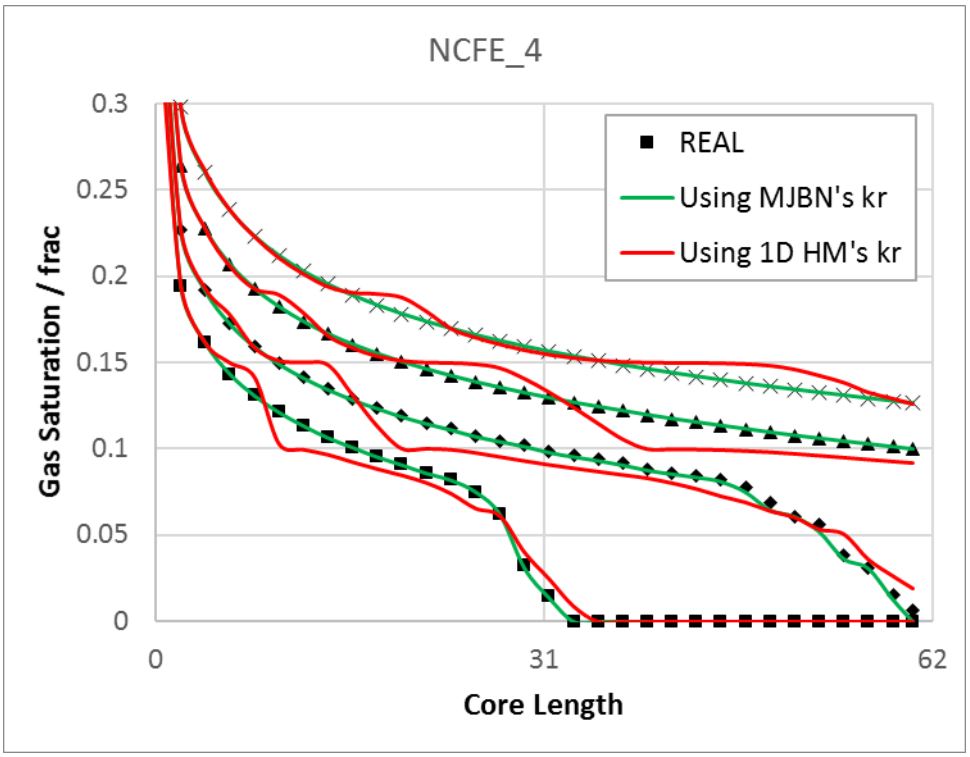

Figure 6-60: Values of average gas saturation for different positions (in the axis horizontal to the flow) inside the core and at different times of injection resultant of the use of the k_r curves of 1D HM, MJBN and the real curves in NCFE_4. In black are the real saturation values, each black symbol (square, triangle, diamond, etc) represents a different injection time.

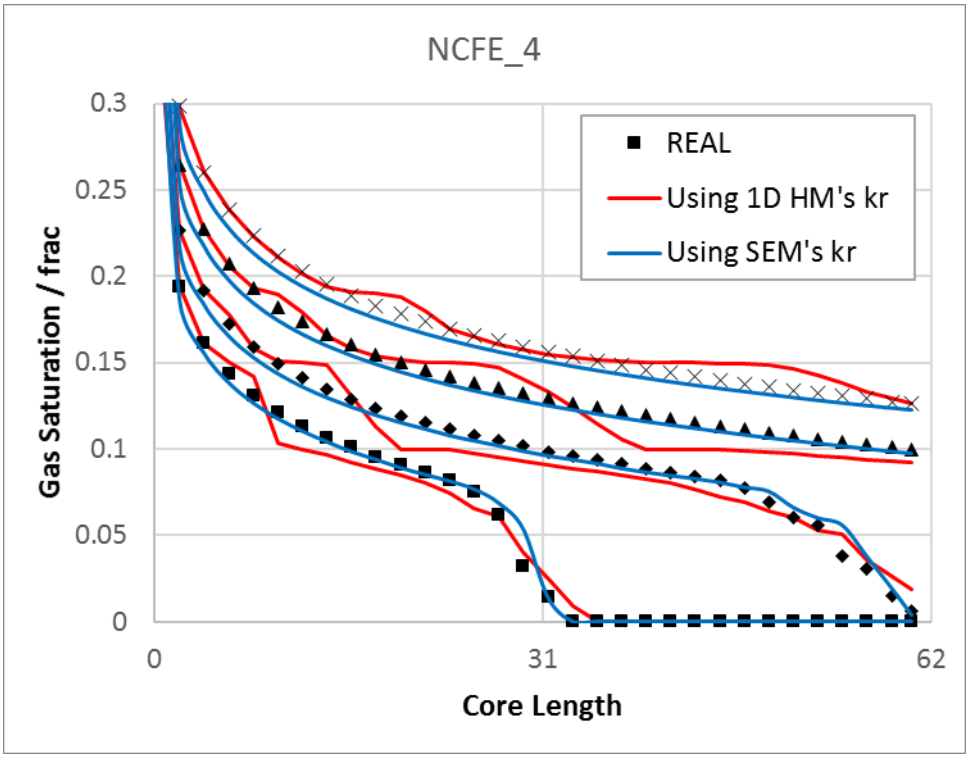

Figure 6-61: Values of average gas saturation for different positions (in the axis horizontal to the flow) inside the core and at different times of injection resultant of the use of the k_r curves of 1D HM, SEM and the real curves in NCFE_4. In black are the real saturation values, each black symbol (square, triangle, diamond, etc) represents a different injection time.

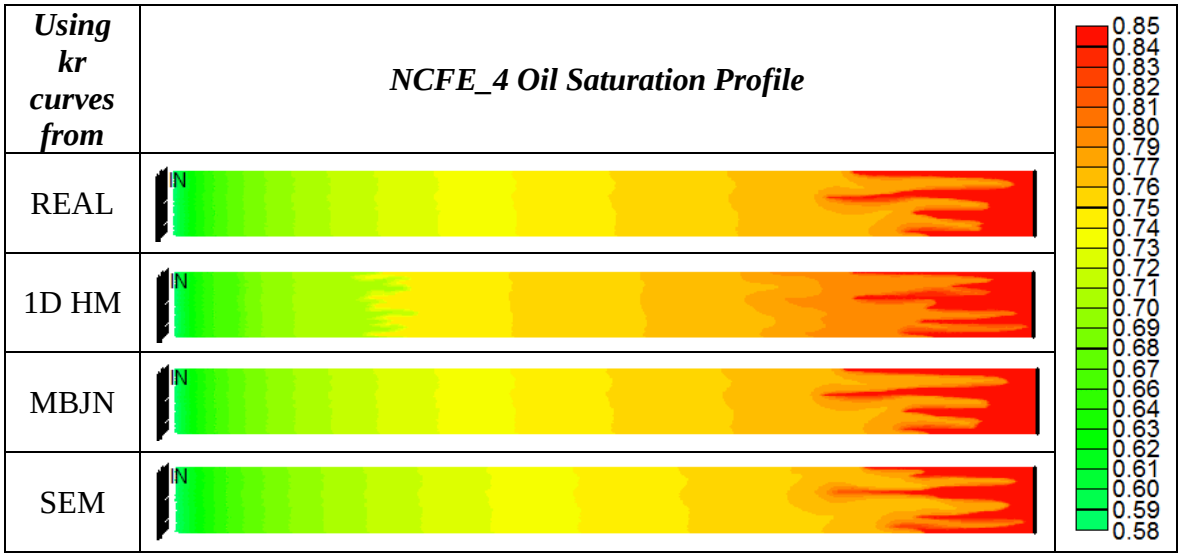

Figure 6-62: Average gas saturations inside the core near the breakthrough time, resultant of the use of the k_r curves of 1D HM, SEM and MJBN in NCFE_4; in comparison with the real gas saturation.

NCFE_5

The cumulative oil production, differential pressure and saturation profiles obtained with the different methods for NCFE_5 are present at Figure 6-63, Figure 6-64, Figure 6-65,

Figure 6-66 and Figure 6-67. In this case, SEM, MJBN and 1D HM have acceptable match with the real values for both the cumulative production of oil and the differential pressure, although 1D HM has a slight error in this results. Nevertheless, in the saturation profiles SEM and MJBN are clearly superior to 1D HM.

It's interesting to notice that using 1D HM to estimate the relative permeability of NCFE_5 resulted in the higher error of estimation for the k_{rg} of all the independent NCFEs, Figure 6-42. However, this high error only had a meaningful impact on the saturation profiles. This fact emphasizes the uniqueness of each experiment, in other words, different degrees of error in the relative permeability may result in different amounts of error in the production data and affect different parameters. As in this case, where the saturation profile was the parameters mostly affected by the error in the relative permeability.

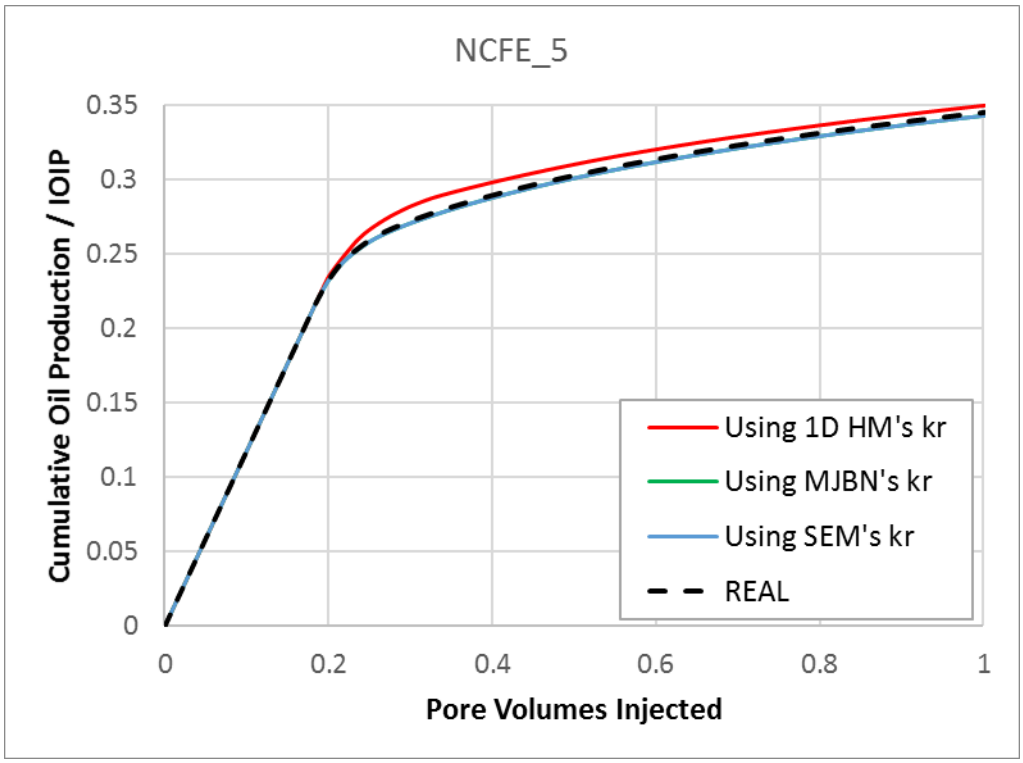

Figure 6-63: Cumulative Oil Production (fraction of initial oil in place) as a function of PVI for NCFE_5 using relative permeability curves obtained by 1D HM, SEM and MJBN, compared with the real data.

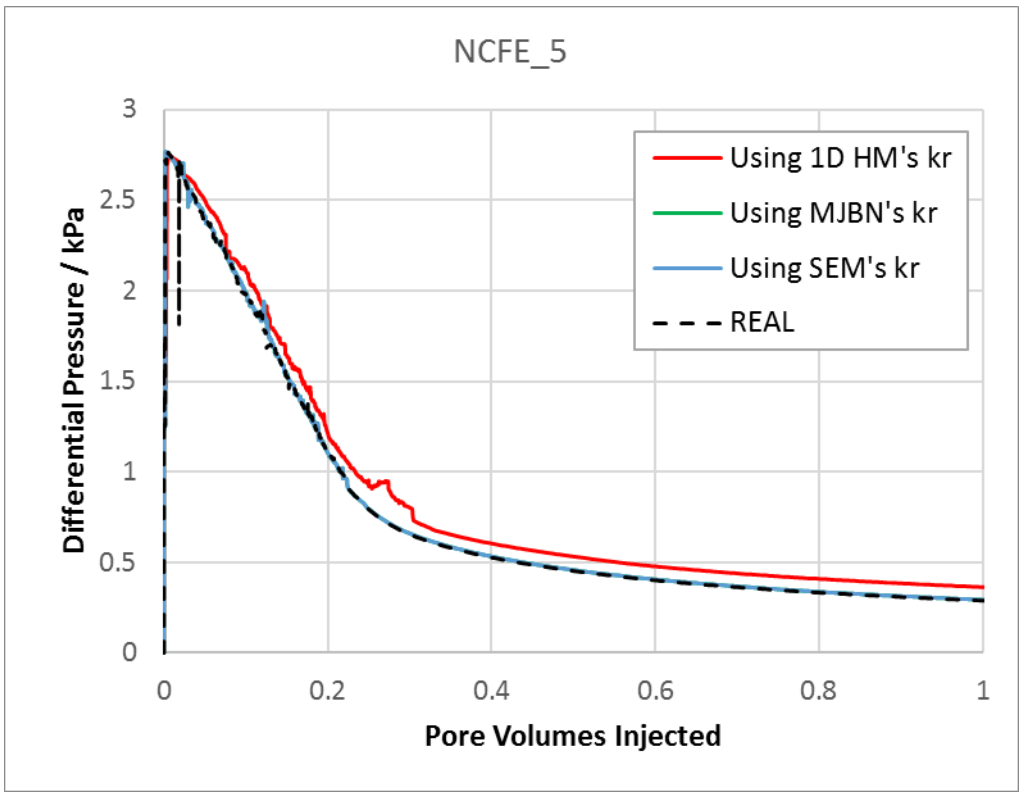

Figure 6-64: Differential Pressure as a function of PVI for NCFE_5 using relative permeability curves obtained by 1D HM, SEM and MJBN, compared with the real data.

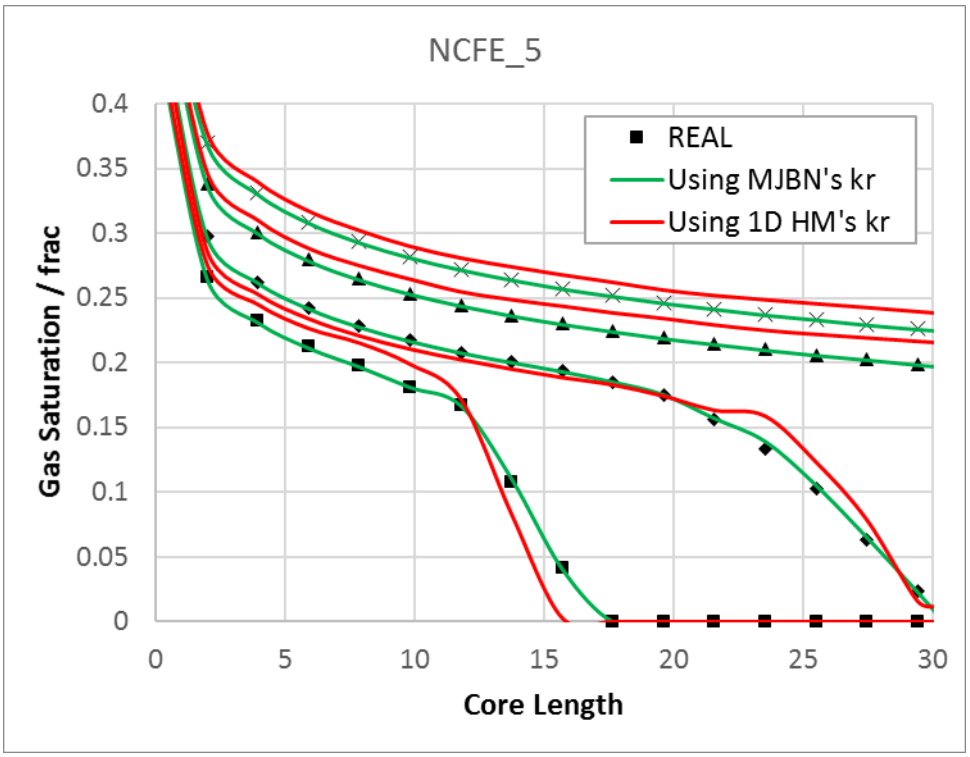

Figure 6-65: Values of average gas saturation for different positions (in the axis horizontal to the flow) inside the core and at different times of injection resultant of the use of the k_r curves of 1D HM, MJBN and the real curves in NCFE_5. In black are the real saturation values, each black symbol (square, triangle, diamond, etc) represents a different injection time.

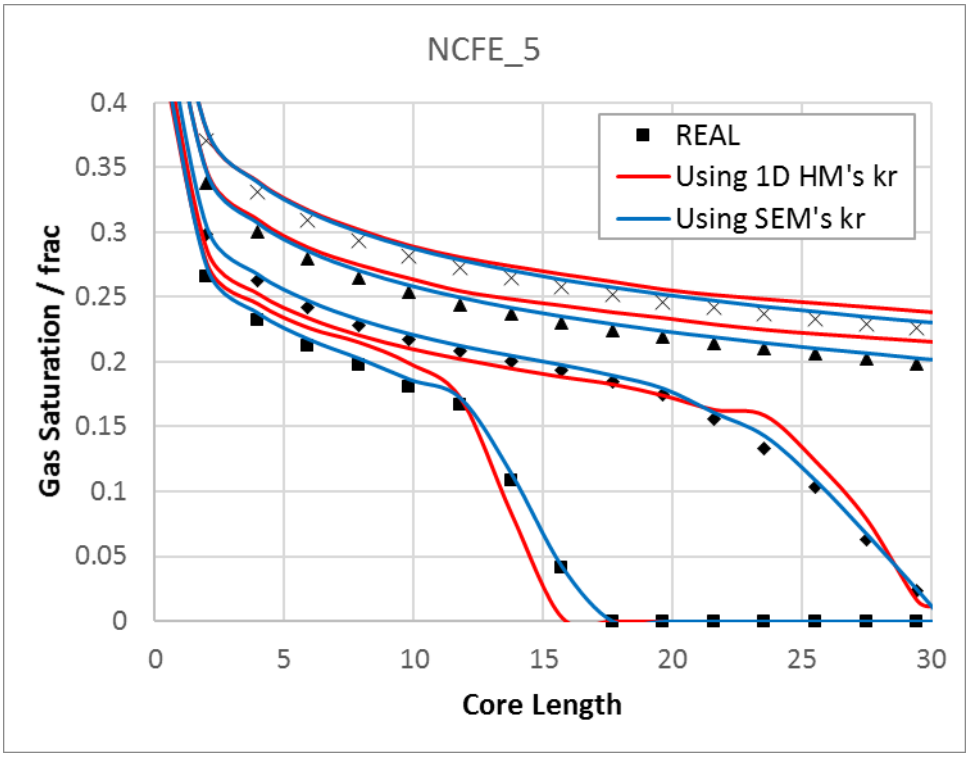

Figure 6-66: Values of average gas saturation for different positions (in the axis horizontal to the flow) inside the core and at different times of injection resultant of the use of the k_r curves of 1D HM, SEM and the real curves in NCFE_5. In black are the real saturation values, each black symbol (square, triangle, diamond, etc) represents a different injection time.

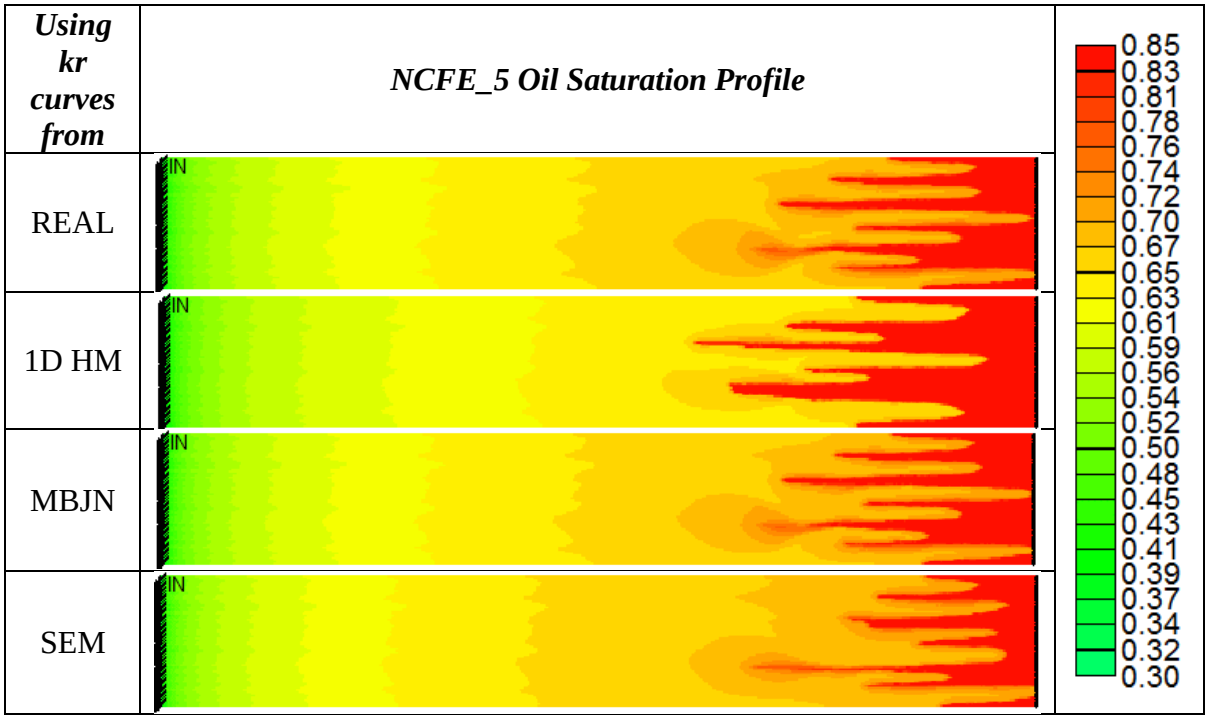

Figure 6-67: Average gas saturations inside the core near the breakthrough time, resultant of the use of the k_r curves of 1D HM, SEM and MJBN in NCFE_5; in comparison with the real gas saturation.

NCFE_6

For all parameters of NCFE_6, SEM and MJBN match the real values. 1D HM, however, show considerable difference in the oil cumulative production, Figure 6-68. Using 1D HM's relative permeability the breakthrough time was much sooner than the real NCFE. Obviously this resulted in considerable differences in the saturation profiles Figure 6-70, Figure 6-71 and Figure 6-72. The error of this method for the differential pressure much smaller than for the other parameters.

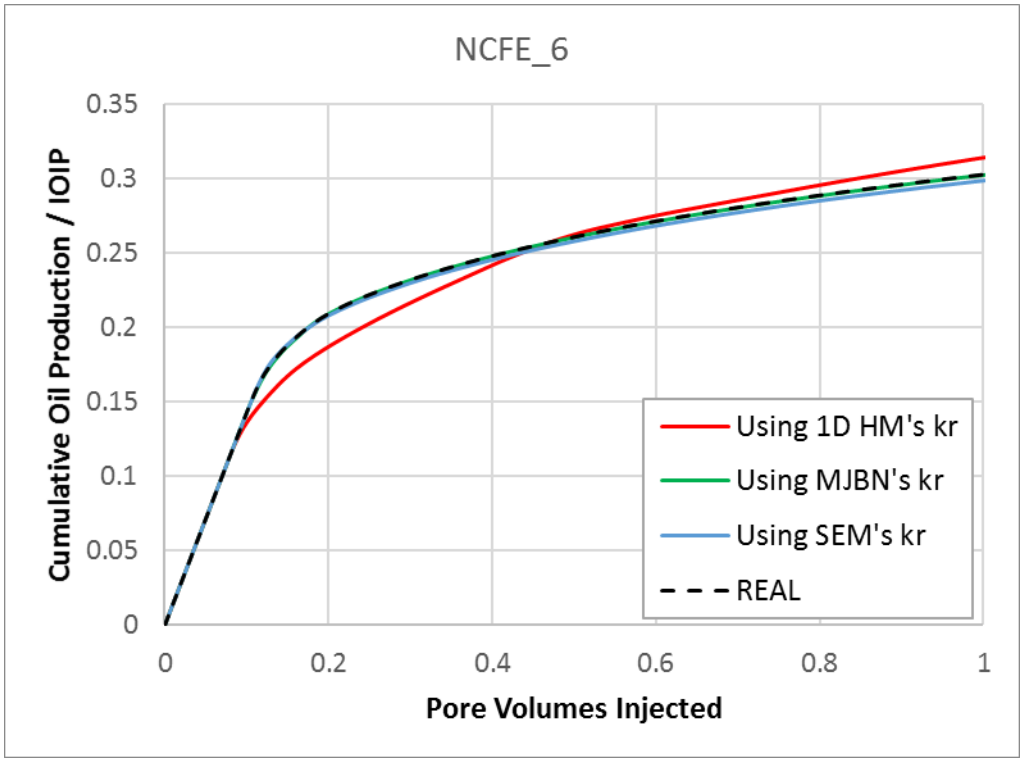

Figure 6-68: Cumulative Oil Production (fraction of initial oil in place) as a function of PVI for NCFE_6 using relative permeability curves obtained by 1D HM, SEM and MJBN, compared with the real data.

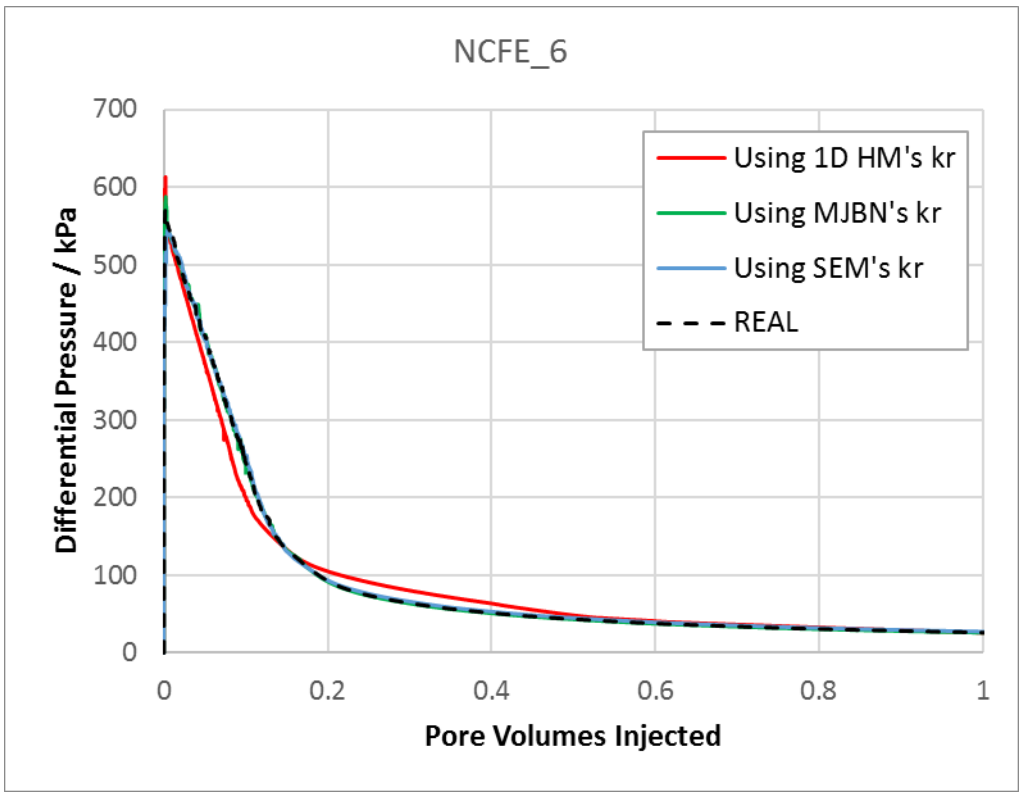

Figure 6-69: Differential Pressure as a function of PVI for NCFE_6 using relative permeability curves obtained by 1D HM, SEM and MJBN, compared with the real data.

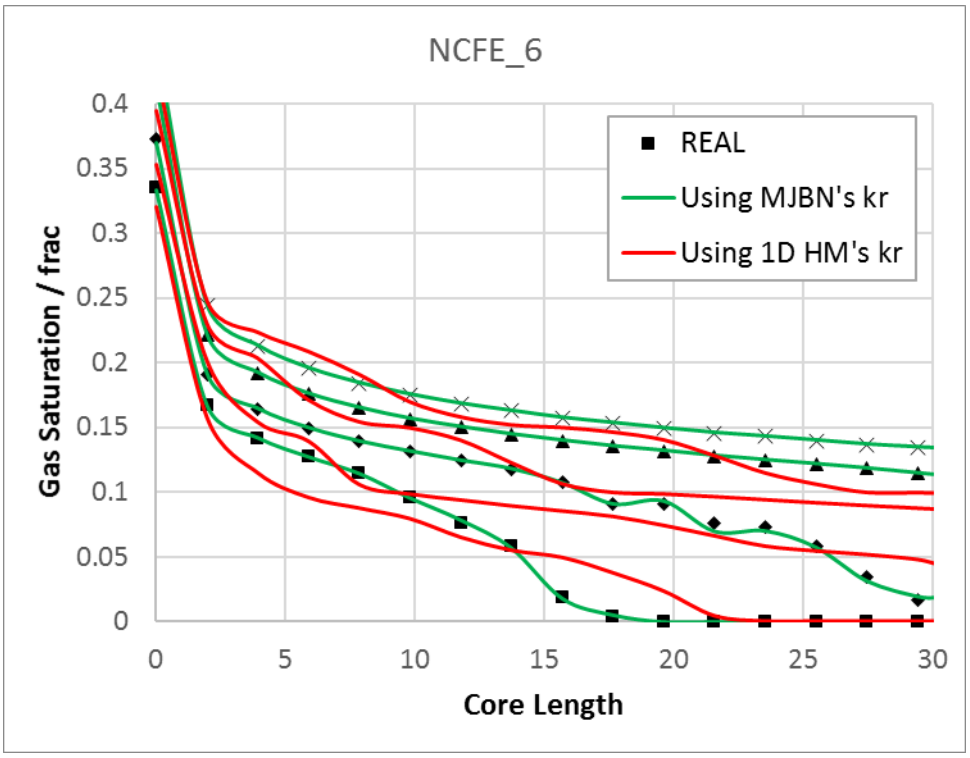

Figure 6-70: Values of average gas saturation for different positions (in the axis horizontal to the flow) inside the core and at different times of injection resultant of the use of the k_r curves of 1D HM, MJBN and the real curves in NCFE_6. In black are the real saturation values, each black symbol (square, triangle, diamond, etc) represents a different injection time.

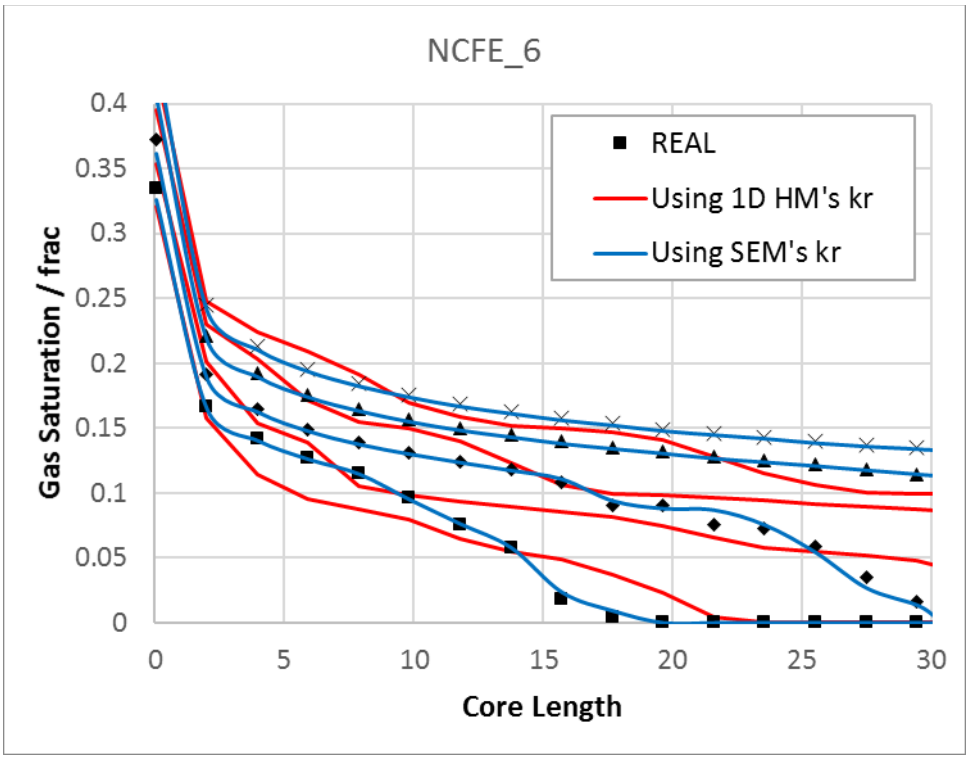

Figure 6-71: Values of average gas saturation for different positions (in the axis horizontal to the flow) inside the core and at different times of injection resultant of the use of the k_r curves of 1D HM, SEM and the real curves in NCFE_6. In black are the real saturation values, each black symbol (square, triangle, diamond, etc) represents a different injection time.

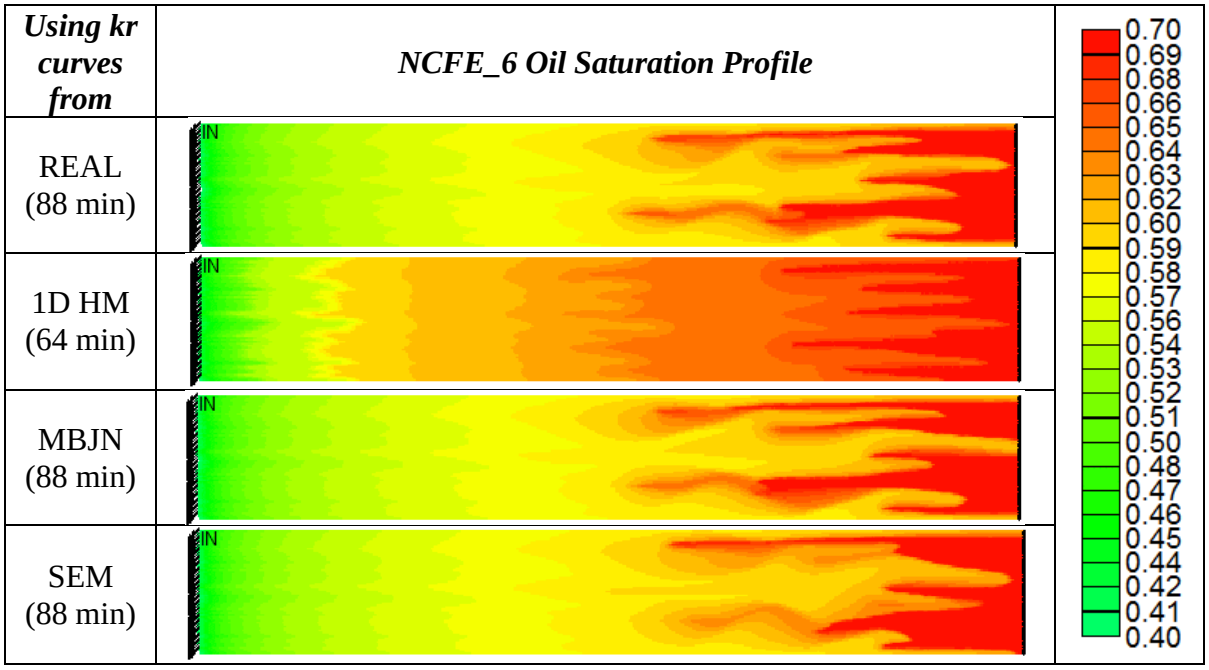

Figure 6-72: Average gas saturations inside the core near the breakthrough time, resultant of the use of the k_r curves of 1D HM, SEM and MJBN in NCFE_6; in comparison with the real gas saturation.

NCFE_7

As in the previous cases SEM and MJBN estimated relative permeability shows to match perfectly the real values of cumulative oil production, differential pressure and saturation profiles, as presented in Figure 6-73, Figure 6-74, Figure 6-75, Figure 6-76 and Figure 6-77. 1D HM's relative permeability, however, resulted in considerable error in the oil production and saturation profiles.

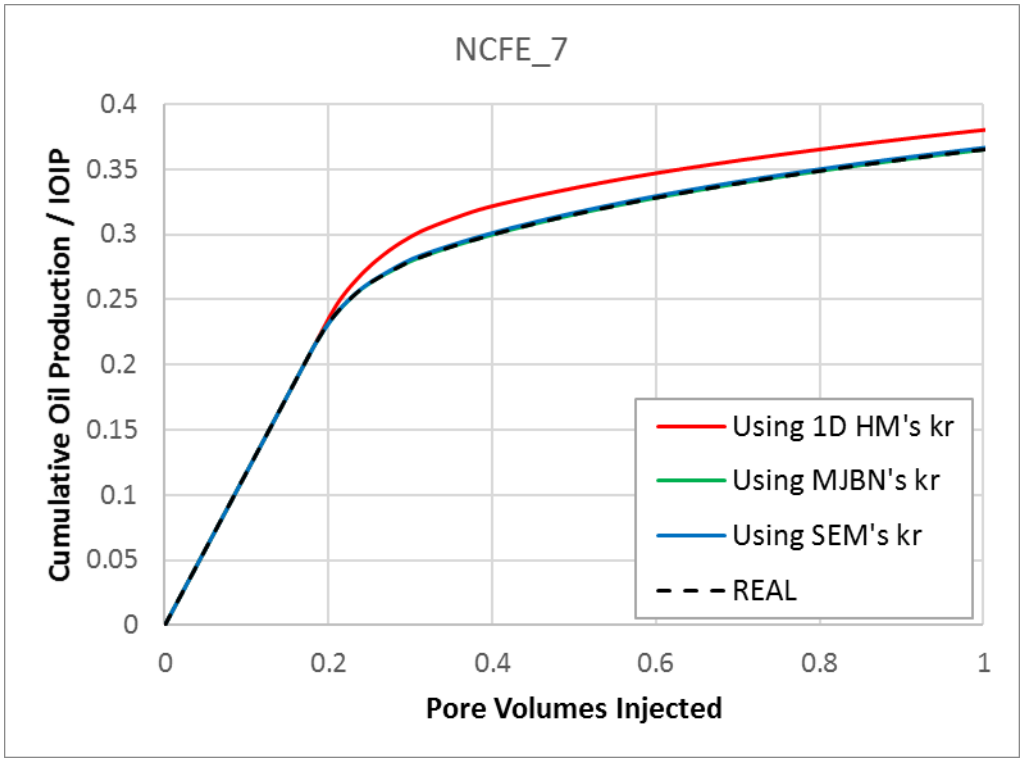

Figure 6-73: Cumulative Oil Production (fraction of initial oil in place) as a function of PVI for NCFE_7 using relative permeability curves obtained by 1D HM, SEM and MJBN, compared with the real data.

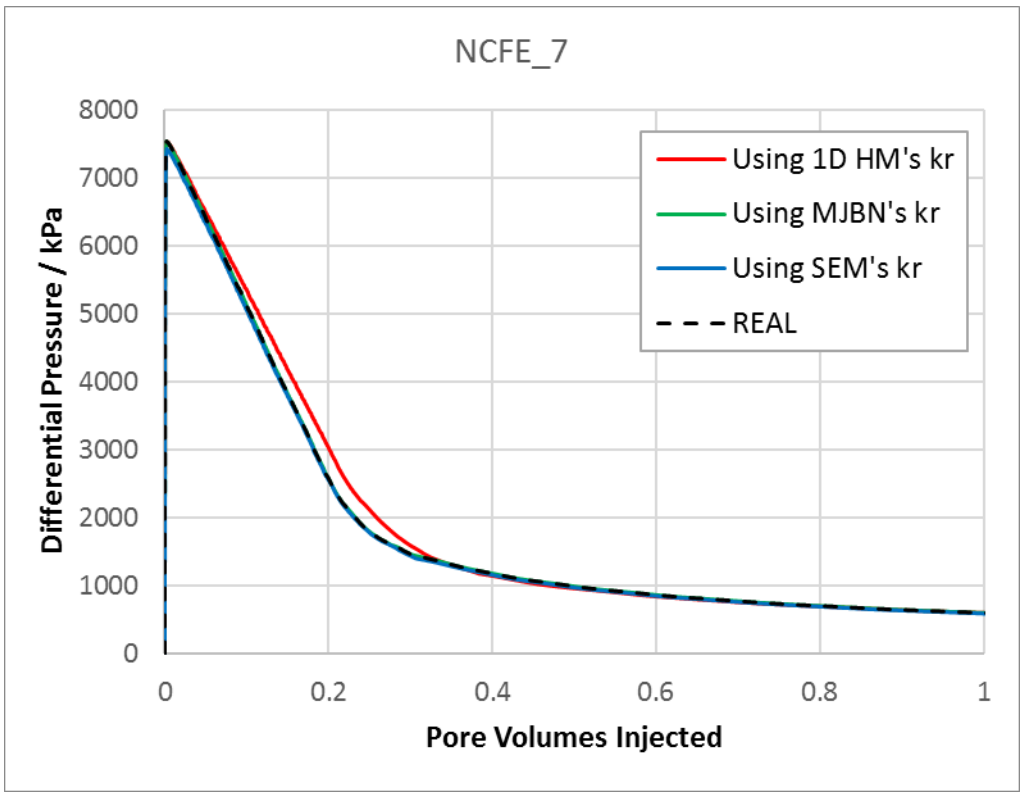

Figure 6-74: Differential Pressure as a function of PVI for NCFE_7 using relative permeability curves obtained by 1D HM, SEM and MJBN, compared with the real data.

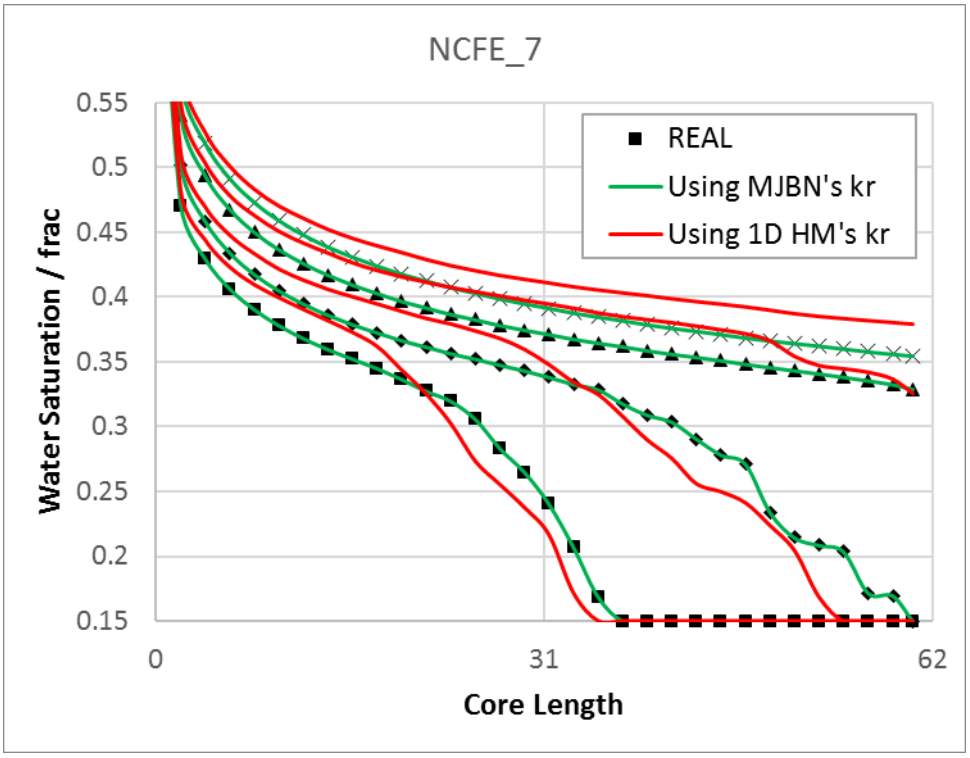

Figure 6-75: Values of average gas saturation for different positions (in the axis horizontal to the flow) inside the core and at different times of injection resultant of the use of the k_r curves of 1D HM, MJBN and the real curves in NCFE_7. In black are the real saturation values, each black symbol (square, triangle, diamond, etc) represents a different injection time.

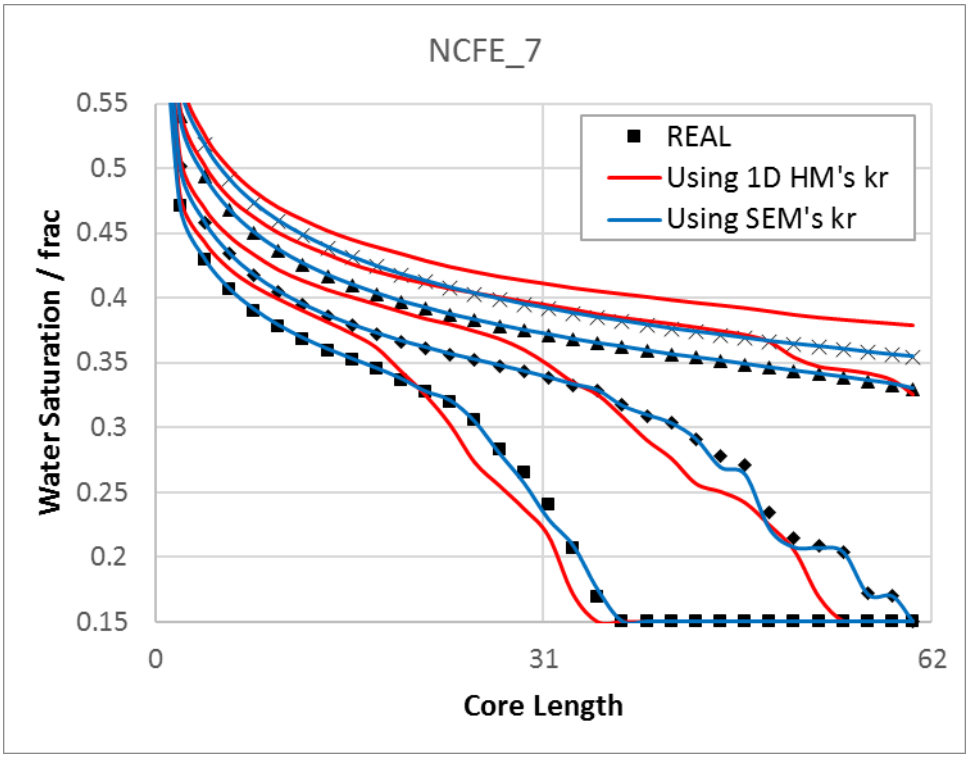

Figure 6-76: Values of average gas saturation for different positions (in the axis horizontal to the flow) inside the core and at different times of injection resultant of the use of the k_r curves of 1D HM, SEM and the real curves in NCFE_7. In black are the real saturation values, each black symbol (square, triangle, diamond, etc) represents a different injection time.

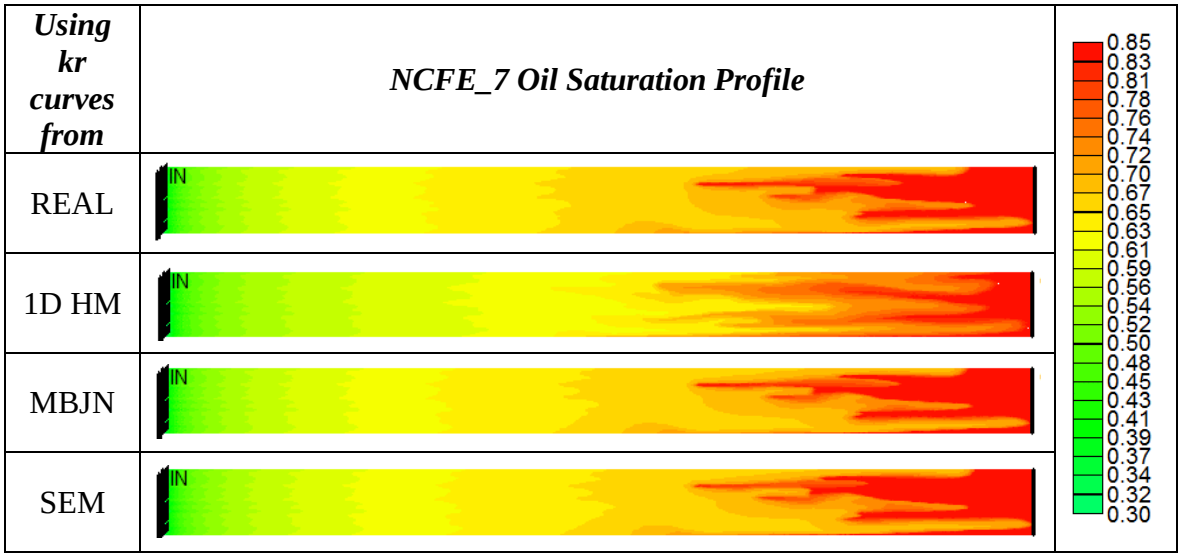

Figure 6-77: Average gas saturations inside the core near the breakthrough time, resultant of the use of the k_r curves of 1D HM, SEM and MJBN in NCFE_7; in comparison with the real gas saturation.

NCFE_8 and NCFE_9

As seen previously, Figure 6-42, the 1D HM k_r estimation error for NCFE_8 and NCFE_9 was very small, meaning that viscous fingering had very low influence in the relative permeability estimation. This fact is supported by the production data of these two NCFE. The cumulative oil production, differential pressure and saturation profiles of NCFE_8, Figure 6-78, Figure 6-79, Figure 6-80, Figure 6-81 and Figure 6-82, respectively show a perfect match for all the methods in study. The same is true for NCFE_9's cumulative oil production, differential pressure and saturation profiles Figure 6-83, Figure 6-84, Figure 6-85, Figure 6-86 and Figure 6-87, respectively.

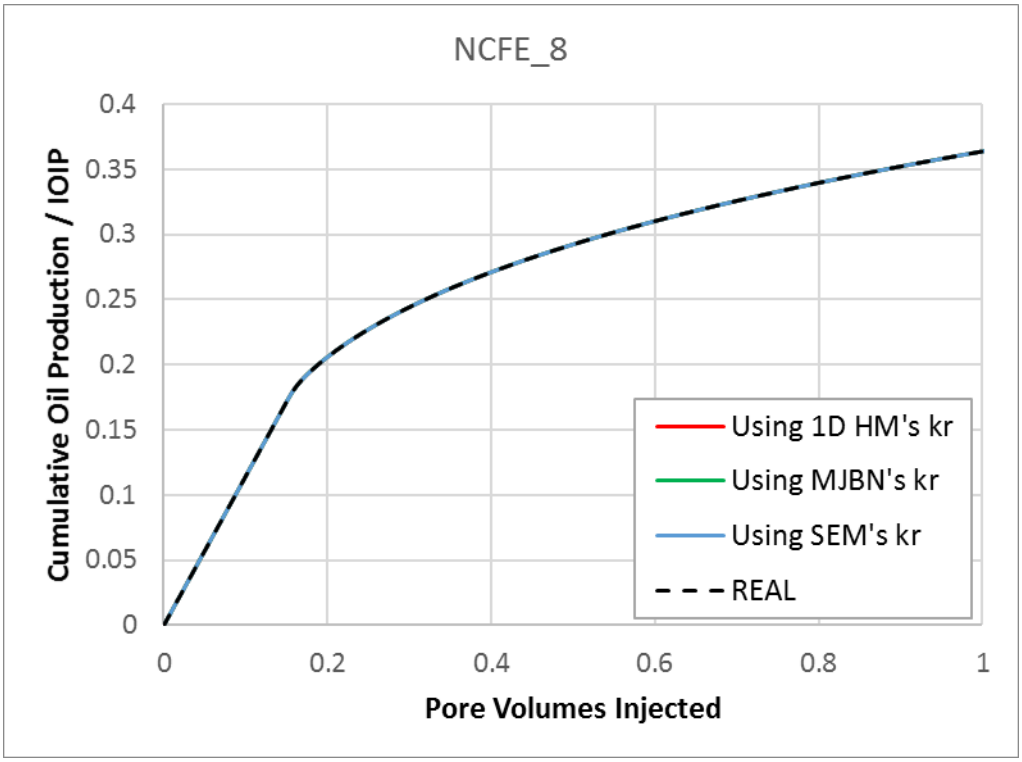

Figure 6-78: Cumulative Oil Production (fraction of initial oil in place) as a function of PVI for NCFE_8 using relative permeability curves obtained by 1D HM, SEM and MJBN, compared with the real data.

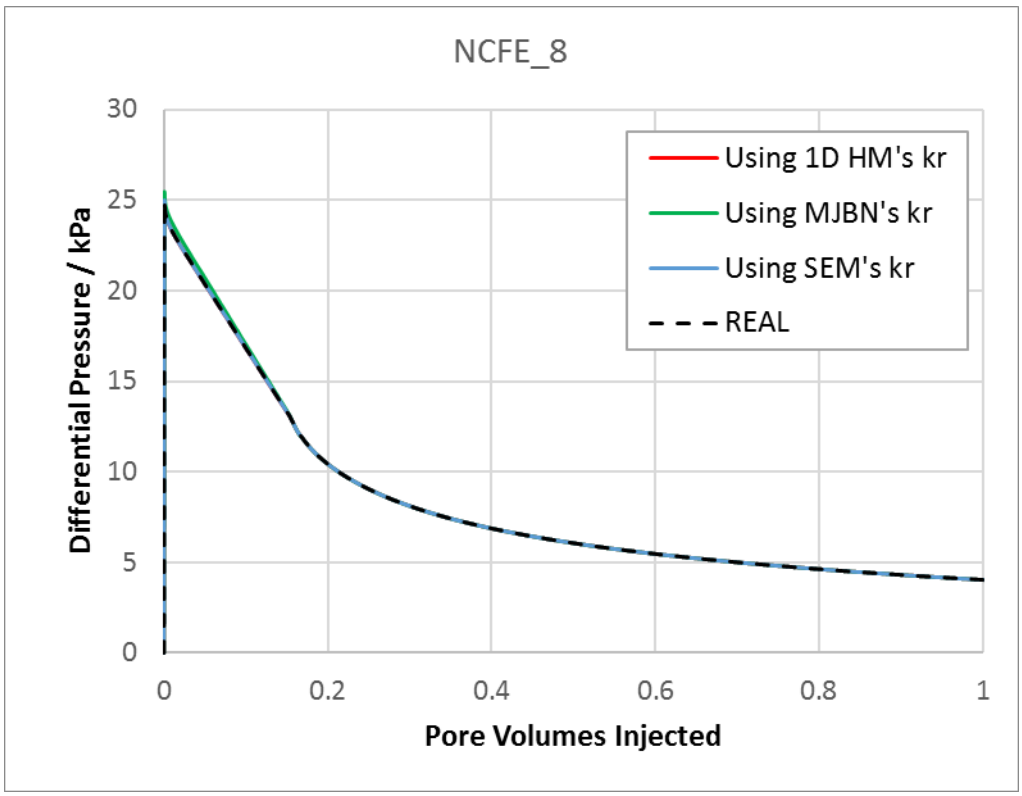

Figure 6-79: Differential Pressure as a function of PVI for NCFE_8 using relative permeability curves obtained by 1D HM, SEM and MJBN, compared with the real data.

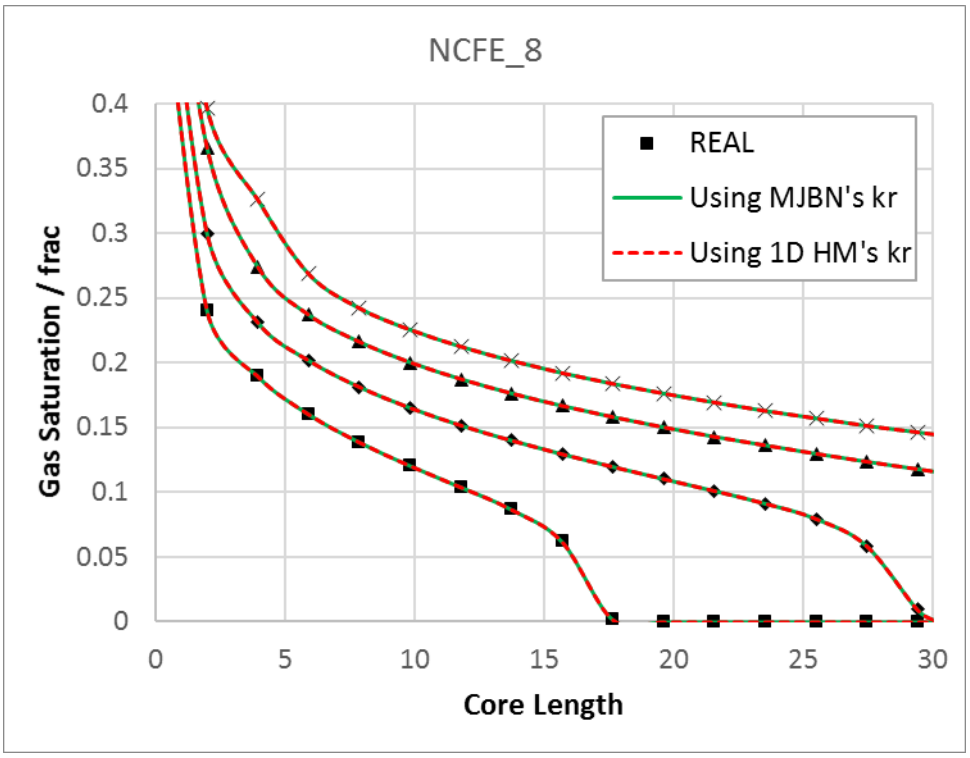

Figure 6-80: Values of average gas saturation for different positions (in the axis horizontal to the flow) inside the core and at different times of injection resultant of the use of the k_r curves of 1D HM, MJBN and the real curves in NCFE_8. In black are the real saturation values, each black symbol (square, triangle, diamond, etc) represents a different injection time.

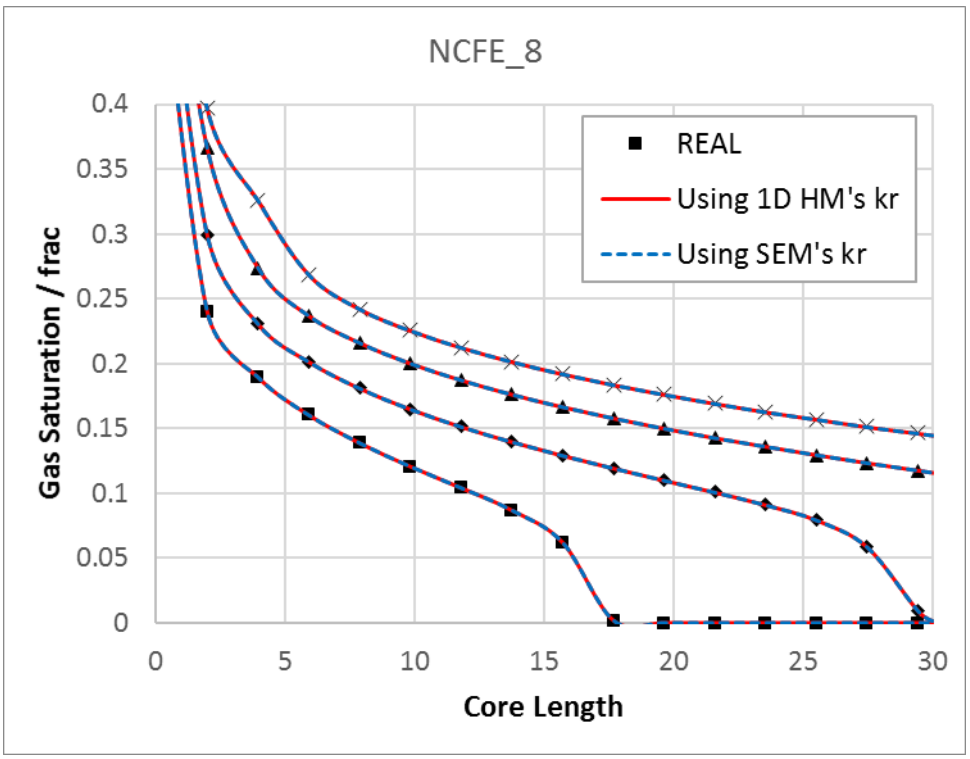

Figure 6-81: Values of average gas saturation for different positions (in the axis horizontal to the flow) inside the core and at different times of injection resultant of the use of the k_r curves of 1D HM, SEM and the real curves in NCFE_8. In black are the real saturation values, each black symbol (square, triangle, diamond, etc) represents a different injection time.

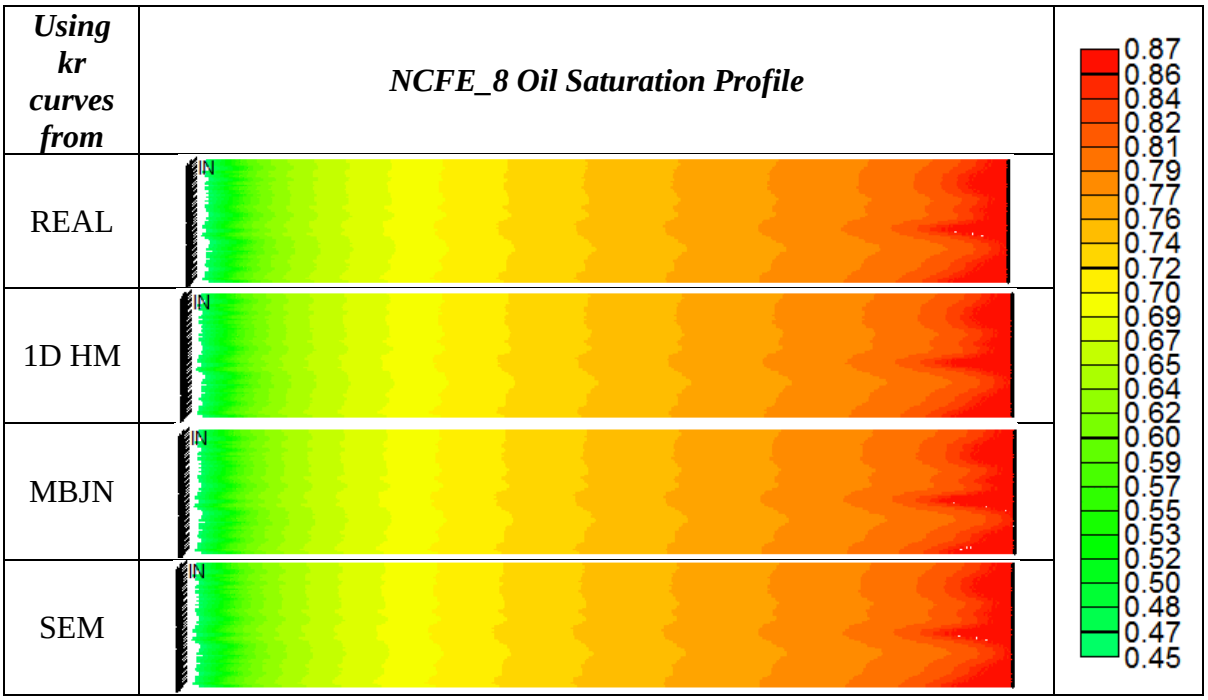

Figure 6-82: Average gas saturations inside the core near the breakthrough time, resultant of the use of the k_r curves of 1D HM, SEM and MJBN in NCFE_8; in comparison with the real gas saturation.

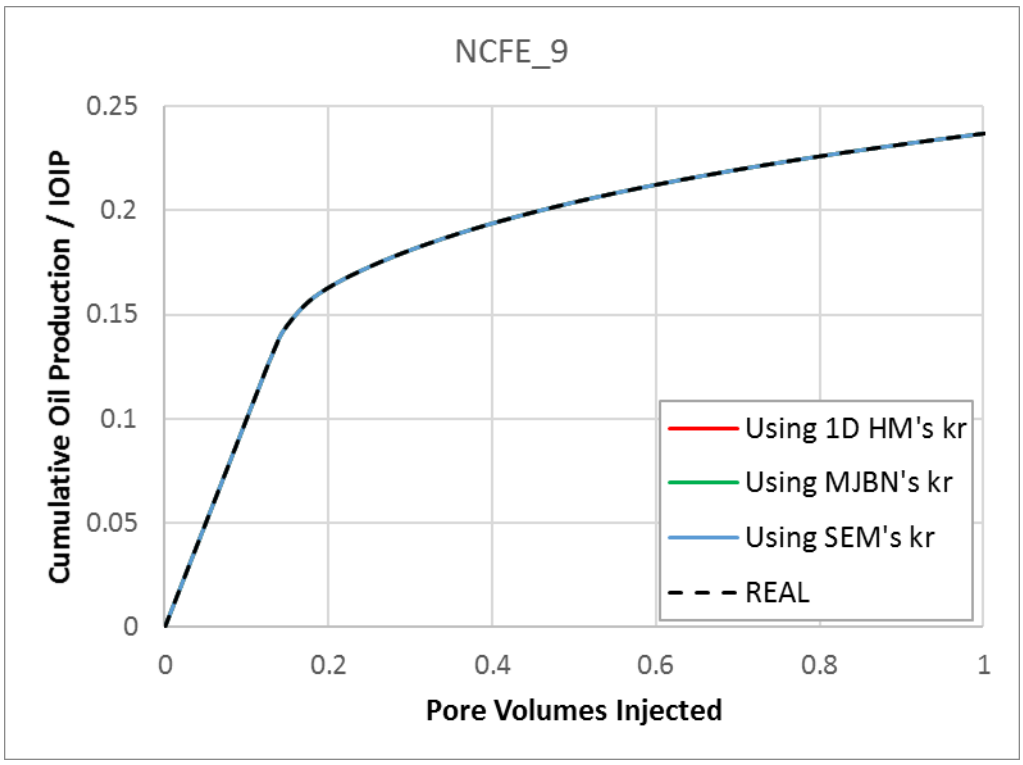

Figure 6-83: Cumulative Oil Production (fraction of initial oil in place) as a function of PVI for NCFE_9 using relative permeability curves obtained by 1D HM, SEM and MJBN, compared with the real data.

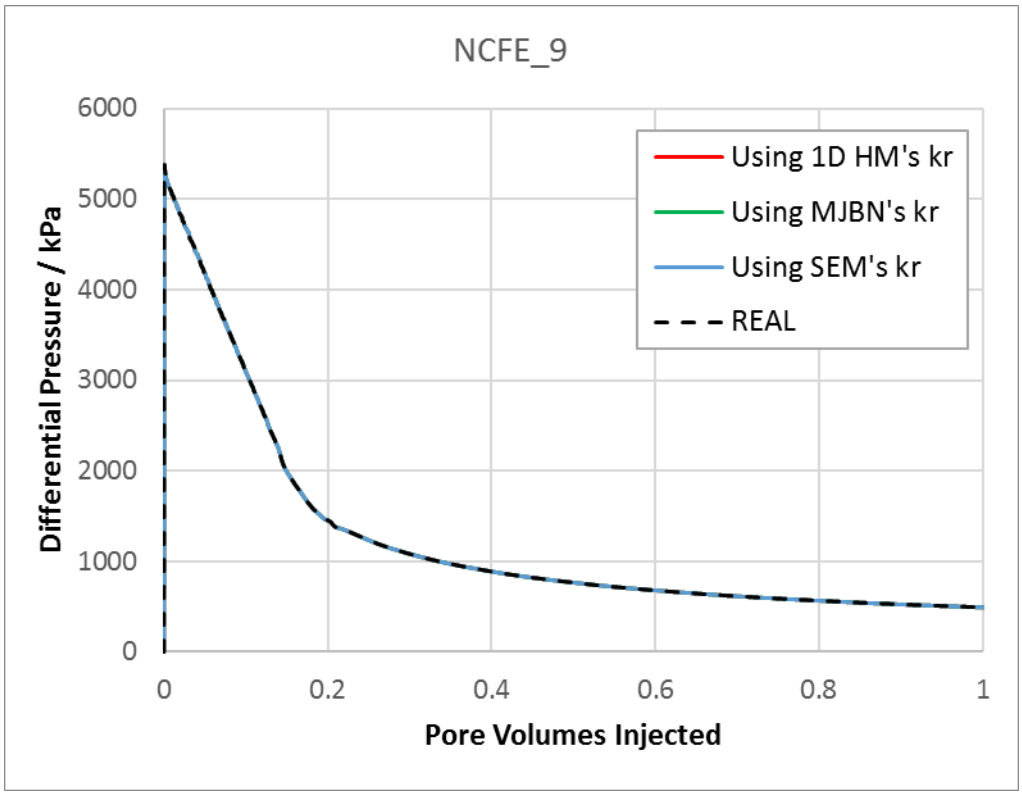

Figure 6-84: Differential Pressure as a function of PVI for NCFE_9 using relative permeability curves obtained by 1D HM, SEM and MJBN, compared with the real data.

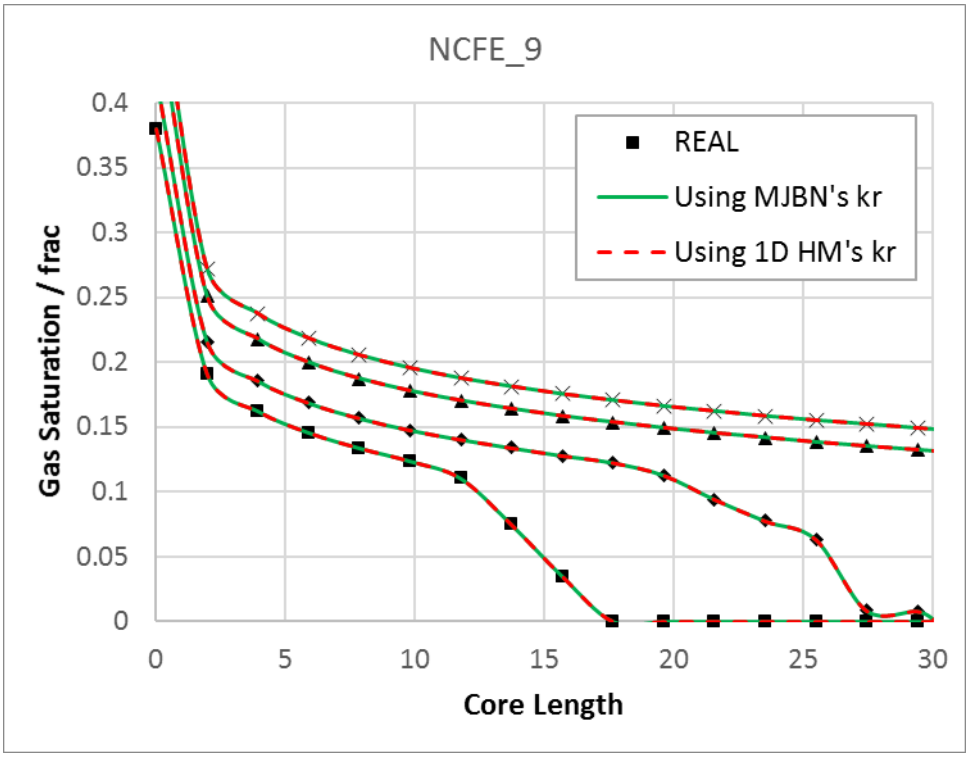

Figure 6-85: Values of average gas saturation for different positions (in the axis horizontal to the flow) inside the core and at different times of injection resultant of the use of the k_r curves of 1D HM, MJBN and the real curves in NCFE_9. In black are the real saturation values, each black symbol (square, triangle, diamond, etc) represents a different injection time.

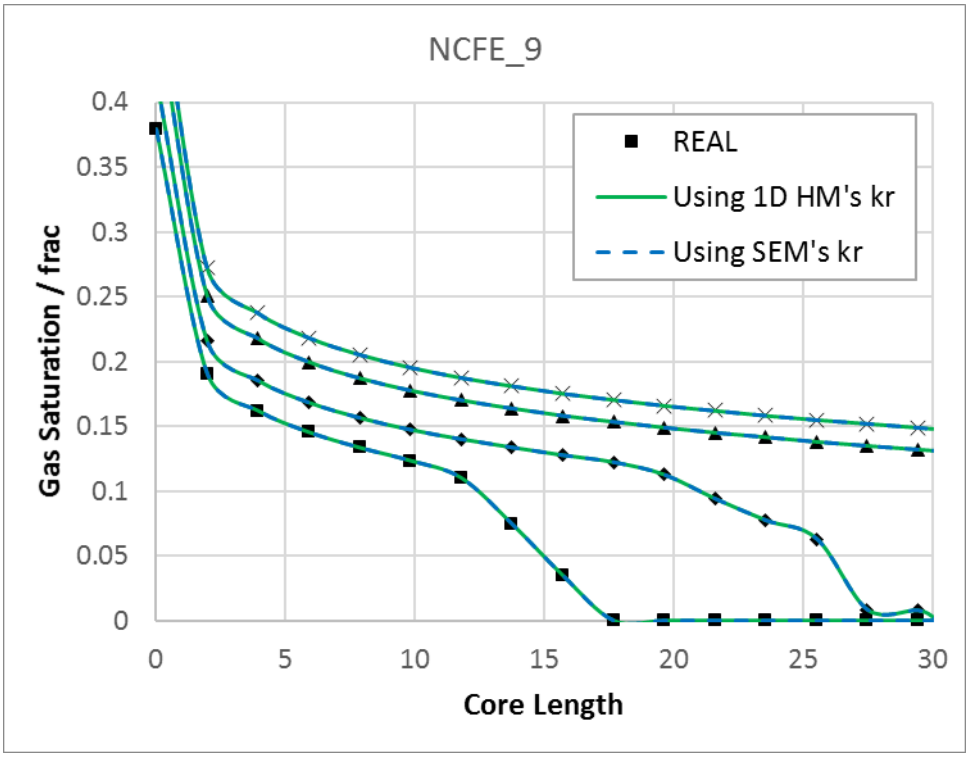

Figure 6-86: Values of average gas saturation for different positions (in the axis horizontal to the flow) inside the core and at different times of injection resultant of the use of the k_r curves of 1D HM, SEM and the real curves in NCFE_9. In black are the real saturation values, each black symbol (square, triangle, diamond, etc) represents a different injection time.

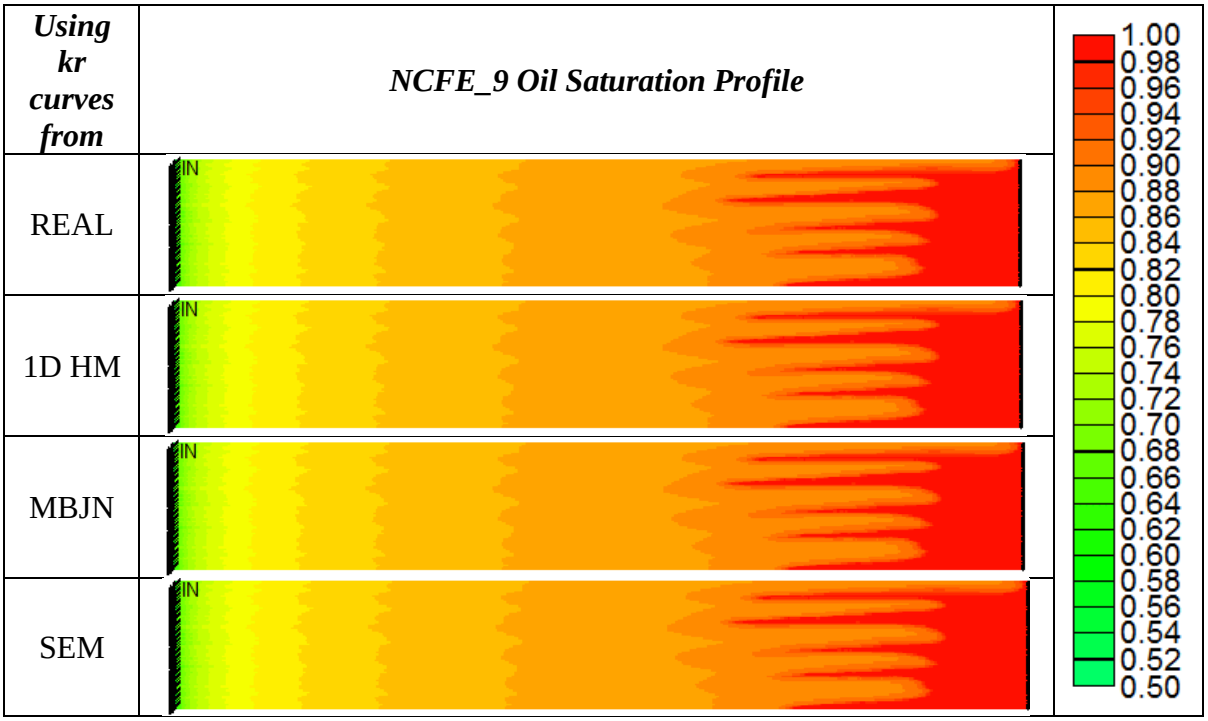

Figure 6-87: Average gas saturations inside the core near the breakthrough time, resultant of the use of the k_r curves of 1D HM, SEM and MJBN in NCFE_9; in comparison with the real gas saturation.

Discussion

The relative permeability as estimated by the different methods, SEM, MJBN and 1D HM, was evaluated in terms of production data. Error of estimation in the relative permeabilities may lead to considerable error in terms of production data. This error is not directly proportional to the error in the relative permeability estimation itself, but it depends on each case. Small errors in the relative permeability estimation may result in considerable differences in production depending on the case that is in study, as it is the case of NCFE_6, where the 1D HM relative permeability resulted in high error on the oil production and saturation profiles, even higher than NCFE_5 which had considerable more error in the relative permeability estimation as seen in Figure 6-42.

6.2.2 NCFE Sets

6.2.2.1 MJBN

The MJBN method was also used in the simulations of NCFE_1_VR and NCFE_2_VR sets. Figure 6-88 and Figure 6-89 show the estimation errors of MJBN and JBN versus the experimental relative permeability. These images show that while JBN error decreases with the decrease of viscosity ratio (the flow is getting more stable), MJBN has

low error (within the base error range defined previously for JBN method) for all the NCFEs within the set. Also for the higher viscosity ratios the error reaches almost four times more than the maximum base error observed in this work (3%).

The analysis of these numerical coreflood experiments are clear in concluding that using MJBN to estimate the relative permeability curves of viscous fingering flows translates into a substantial decrease in the error in comparison with the standard JBN method.

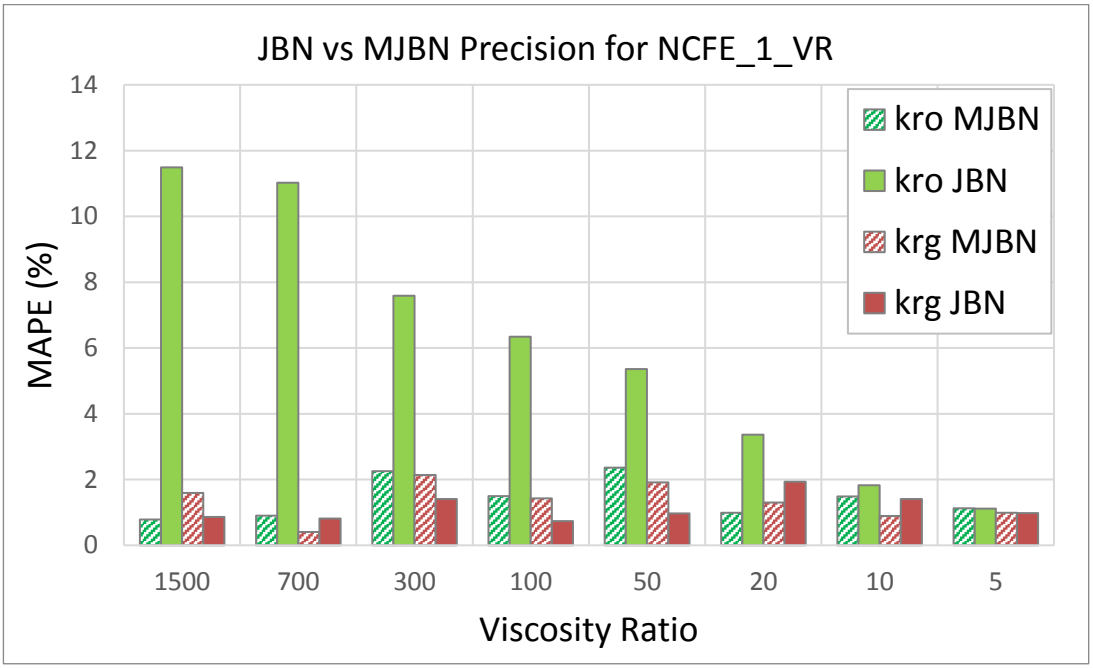

Figure 6-88: Error comparison between JBN and MJBN relative permeability estimations for NCFE_1_VR set, showing a clear reduction in error when using MJBN for the oil relative permeability.

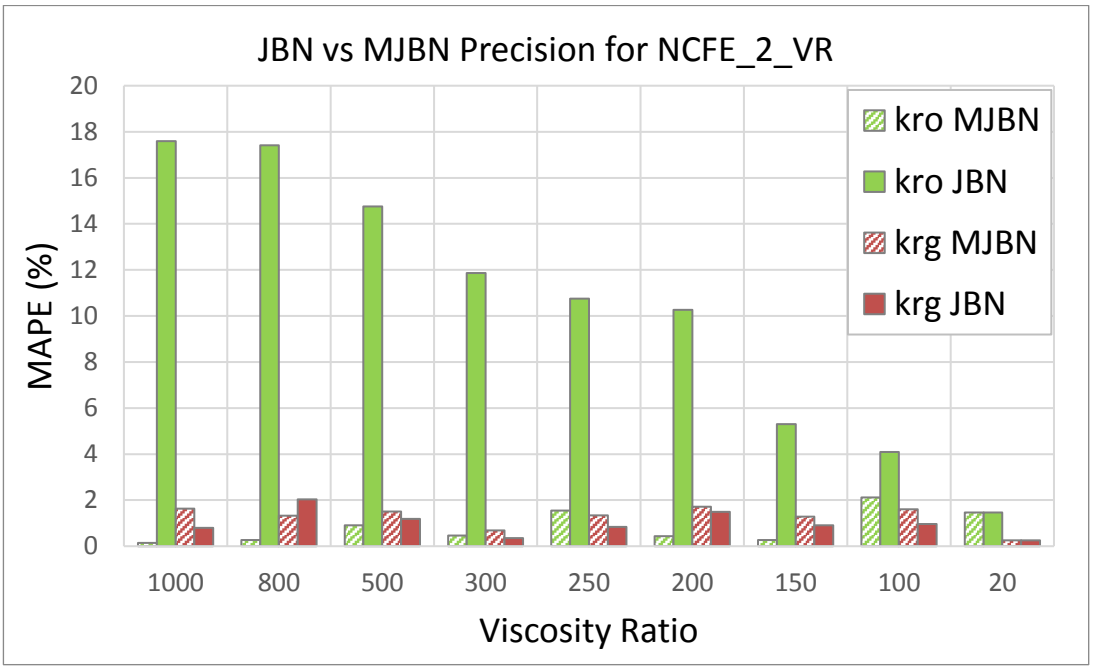

Figure 6-89: Error comparison between JBN and MJBN relative permeability estimations for NCFE_2_VR set, showing a clear reduction in error when using MJBN for the oil relative permeability.

6.2.2.2 SEM

In the previous section, SEM was validated for a for independent NCFEs, meaning that each NCFE was considered as a separate experiment and comparison between different NCFEs was, in this manner, impossible. In this section, SEM will be used in a series of NCFEs presented and detailed explored in previous chapters NCFE_1_VR and NCFE_2_VR. Each one of these series have fixed parameters except for the oil viscosity, which allows to have different degrees of viscous fingering instability with the variation of this parameter.

Figure 6-90 and Figure 6-91 show the estimation errors of SEM and 1D HM versus the real relative permeability. In these images 1D HM error decreases in function of the viscosity ratio: the error decreases as the flow becomes more stable (lower viscosity ratio value), showing that 1D HM is being influenced by the presence of viscous fingering in the flow. SEM's results, however, don't present such a trend and the error is variable around 3%, which is consistent with the base error for this history matching seen in Chapter 4.

These results further validate the SEM method as an improvement in relation to the tradition 1D HM for cases with viscous fingering formation.

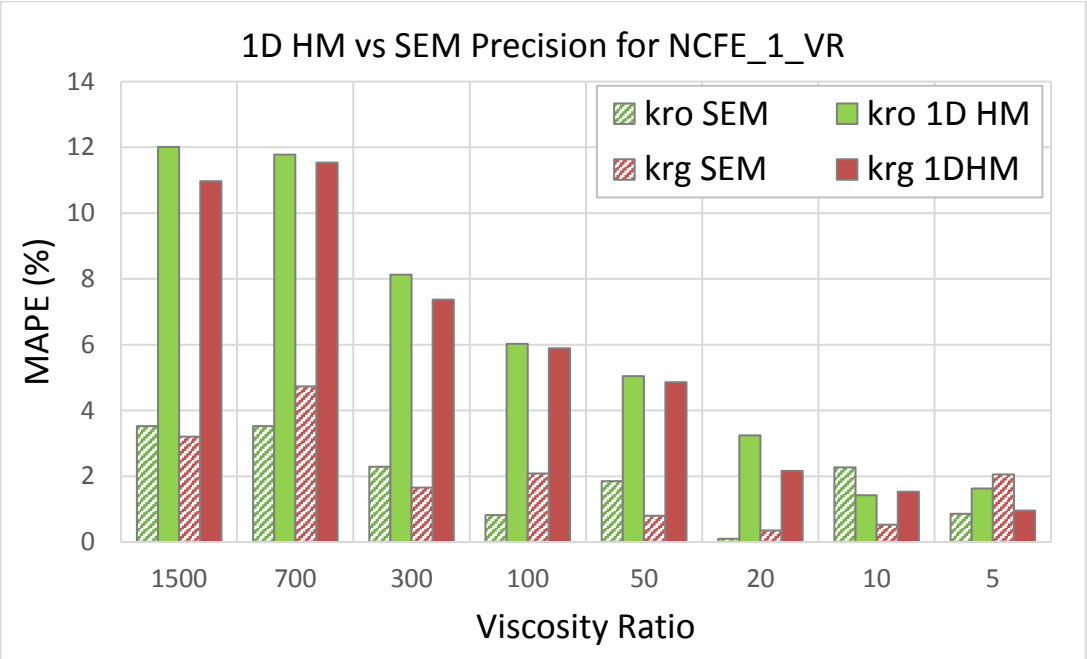

Figure 6-90: Error comparison between 1D HM and SEM relative permeability estimations for NCFE_1_VR set, showing a clear reduction in error when using SEM for the relative permeability estimation.

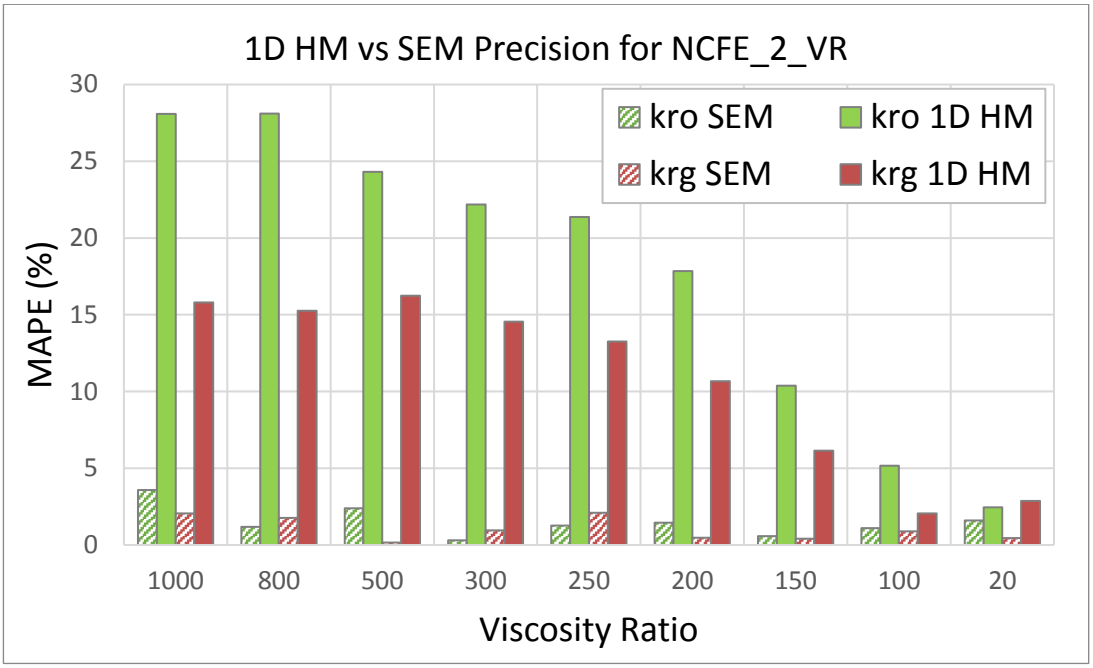

Figure 6-91: Error comparison between 1D HM and SEM relative permeability estimations for NCFE_2_VR set, showing a clear reduction in error when using SEM for the relative permeability estimation.

6.3 Validation Using Actual Experimental Data

In addition to the numerical experiments, actual experimental data was used to serve as validation for MJBN and SEM methods as more accurate alternatives than JBN and 1D HM in cases with viscous fingering formation.

The actual experimental data (AED) in this section was collected from Peters 1994 report. Peters has performed 2 water injection coreflood experiments. Experiment 1, or Exp 1, was performed in an oil-wet core, while Experiment 2, or Exp 2, in a water-wet core. The author has used unconsolidated sand pack cores and the fluids used were immiscible. Table 6-2 and Table 6-3 present the properties for both experiments. Both experiments were performed with the cores in horizontal orientation.

Table 6-2: General Coreflood Properties of Peters (1994) report

Experiment	***Length / cm***	***Diameter / cm***	***Porosity / %***	***Permeability / D***	S_{oi} ***/ frac***	S_{wi} ***/ frac***	S_{wirr} ***/ frac***
Exp 1	54.08	4.83	31.5	10.4	1.00	0.00	-
Exp 2	54.53		30.9	9.3	0.85	0.15	0.15

Table 6-3: Fluid Properties.

Experiment	***IFT /mNm^{-1}***	***μ_o /mPa.s***	***μ_{water} /mPa.s***	***ρ_{oil} /g.cm^{-3}***	***ρ_{water} /g.cm^{-3}***
Exp 1	26.7	103.4	1.138	1.088	0.966
Exp 2			1.128		

Exp 1 CT scans, of the water saturation, and the corresponding simulation results, obtained by the author, are presented in Figure 6-92 (top) for the experimental CT scan results and (bottom) for the simulation. Due to the quality of the document, it was not possible to obtain the simulation result image Figure 6-92 (bottom) in colour, so the images were digitally coloured. The experimental CT images were collected from another publication by the author (Peters 2012), where he presented the results for the same experiment but in more perceptive colour version. For the high viscosity contrast (almost 100 to 1) of Exp 1, it is expected to see clearly displayed fingering in the scanned image, Figure 6-92 (top). The author has described this experiment as unstable, but in this case gravity has a very big influence in the flow, by pushing the water to travel under the oil. The observation of the experiment images seems to suggest some gravity segregation, might have reduced the formation of fingering. The author also suggests that most of the oil left behind (clearly seen in the image by the red colour 'bits' in the middle of the core) is due to wettability, the oil wet medium makes water channels form in large pores leaving considerable amount of oil in the small pores. However, in their simulation, Figure 6-92 (bottom) a fingering profile is observed. Although the simulation profiles approximately reflect the CT scanned values, the differences are rather significant. This experiment is not an ideal case for the study of MJBN, because most of the observed instability is probably provoked by gravity segregation (one of the limitations of MJBN). However, it will be interesting to see how the MJBN method responds to this type of unstable flow.

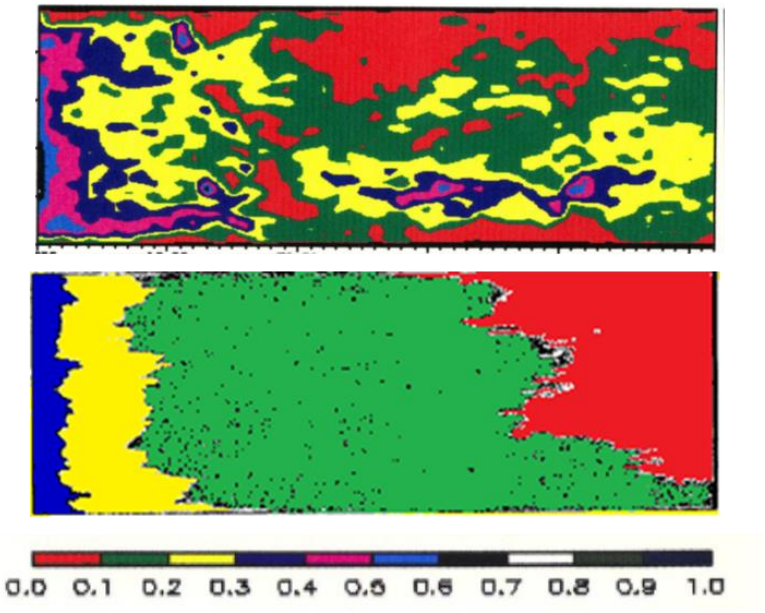

Figure 6-92: Water saturation profile for experiment 1 from CT scans of the core (top) and from simulation results (bottom).

The cumulative oil production and saturation profiles for Exp 1 can be seen in Figure 6-93. The author was able to obtain good matches in simulation for both oil production and saturation profiles.

The CT scans for Exp 2 are presented in Figure 6-94 (top) for the experimental results and (bottom) for the simulation results. Due to the quality of the document, it was not possible to obtain the original simulation result image, Figure 6-94 (bottom), in colours, therefore they were digitally coloured. The experimental CT images were collected from another publication by the same author (Peters 2012), where he presented the results for the same experiment but in more perceptive colour version. The unstable front in the experimental results was contained in a small length of the core. In other words, 2 fingers are formed with considerable widths and they progress just a bit faster than the rest of the front, therefore, this case is assumed to reflect a mildly unstable flow. Their simulation results, Figure 6-94 (bottom), show a higher number of fingers, but it reflects, in my opinion, the general trend of the flow, with two main fingers dominating the flow pattern. The cumulative oil production and saturation profiles for Exp 2 are shown in Figure 6-95. The author was able to obtain good matches in the saturation profiles; however, the oil production was slightly over predicted.

The author performed the history matching, by matching oil production and saturation profiles together, using their in-house software, for both experiments. The resulting k_r curves are presented in Figure 6-96.

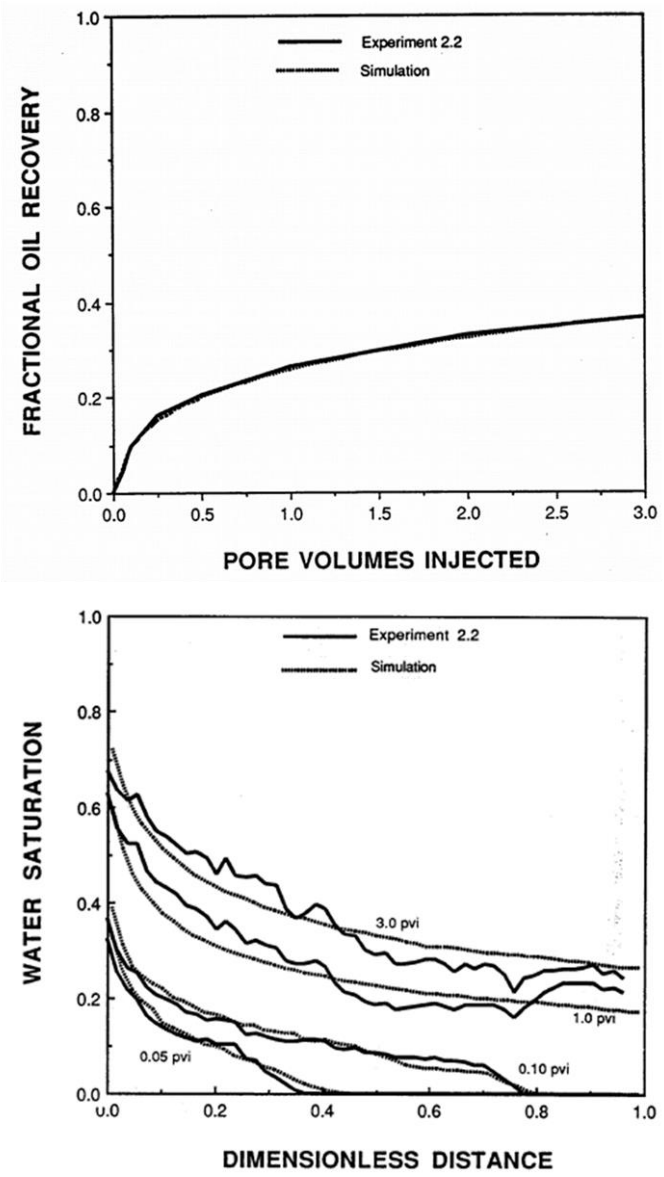

Figure 6-93: Peters (1994) experimental and simulation results for fractional oil recovery (top) and water saturation profiles (bottom) of Exp 1 (experiment 2.2 in the original paper), showing a good match between CT scanned experimental and simulation results.

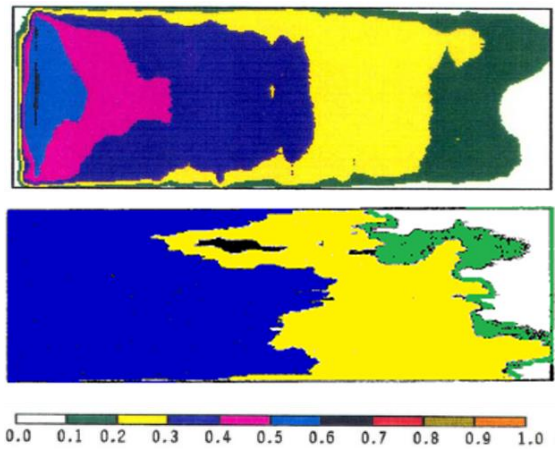

Figure 6-94: Water saturation profile for experiment 2 from CT scans of the core (top) and from simulation results (bottom).

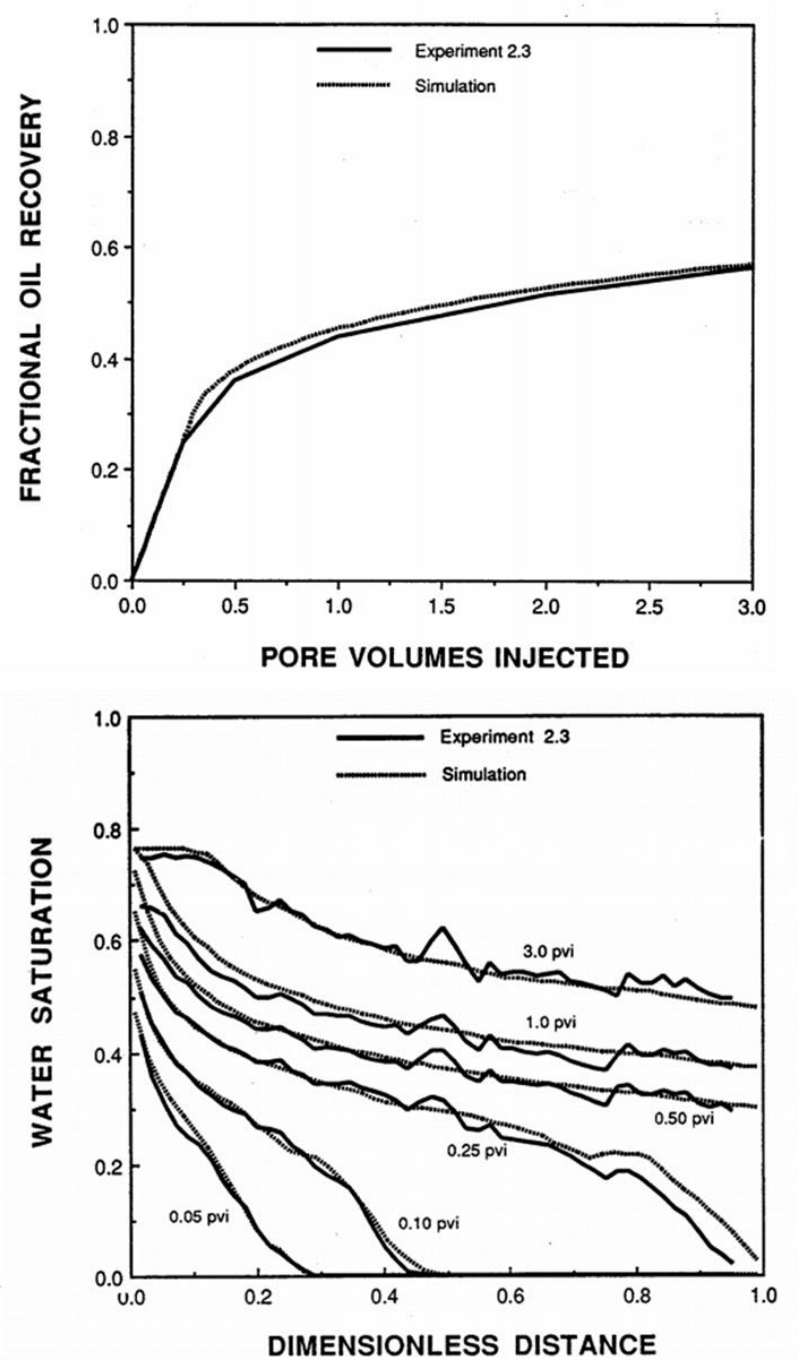

Figure 6-95: Peters (1994) experimental and simulation results for fractional oil recovery (top) and water saturation profiles (bottom) of Exp 2 (experiment 2.3 in the original paper), showing a good match between experimental and simulation results.

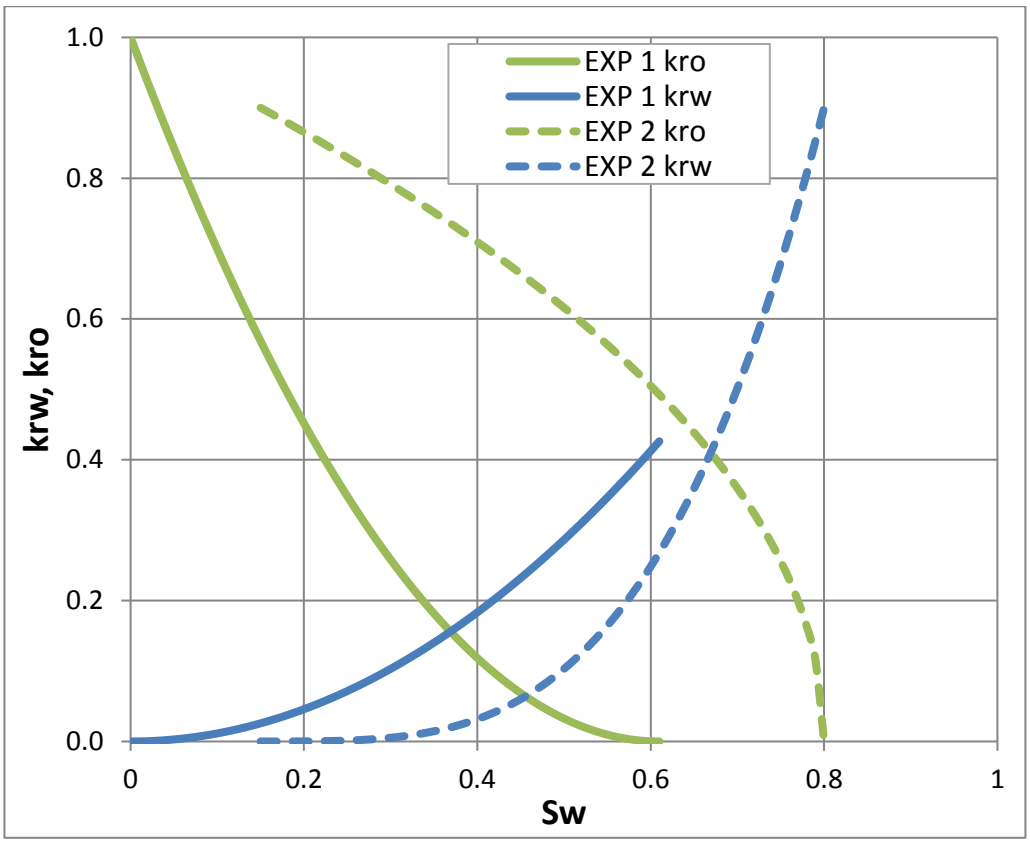

Figure 6-96: Matched relative permeability curves for experiments 1 and 2 obtained by Peters (1994).

6.3.1 Standard Relative Permeability Estimation Methods

Peters (1994) refers to Exp 1 and Exp 2 as unstable immiscible water injections with formation of viscous fingering. Under such conditions the standard JBN and 1D HM methods shouldn't be able to estimate the correct relative permeability, since these methods are based on stability. In this section, JBN and 1D HM methods are used in Peters' unstable experiments, in order to evaluate their precision. Later, these results will be used to show the advantage of using MJBN or SEM in cases with viscous fingering formation, instead of the standard ones.

The core and fluid data presented in Table 6-2 and Table 6-3 is necessary in order to estimate the relative permeability curves with JBN and 1D HM, using the methodology presented in Chapter 4. In addition to these, the production data was also collected from Peters (1994). The 1D HM was performed in an in-house optimization software that uses the ECLIPSE simulator software to perform the simulation runs.

Figure 6-97 and Figure 6-98 show the relative permeability as estimated by JBN and 1D HM, respectively, against Peters estimation. The valid water saturation range (water saturation range observed during the unsteady-state injection) in Exp 1 is 0.05 to 0.28 and in Exp 2 0.15 to 0.55, meaning that every relative permeability value outside this ranges

isn't valid and, therefore, should not be considered to evaluate the precision. Peters has used a complex history matching to account for viscous fingering in a multidimensional simulation scenario, resulting in a very accurate relative permeability, corroborated by the production data matching presented in the previous section. It is, then, natural that the standard methods that do not account for fingering can't predict the relative permeabilities with the same accuracy. For Exp 1, Figure 6-97 and Figure 6-98 show that using JBN and 1D HM result in considerable error, especially 1D HM. For Exp 2, the conclusions are the same as for Exp 1, but in this case JBN and 1D HM results are very close to each other with just a slight higher error in the k_{ro} from 1D HM.

The results are clearly indicating that both methods can't tackle the instability present in Peters' experiments. This allows to measure how much MJBN and SEM can improve the results in contrast with their counterparts (JBN and 1D HM, respectively).

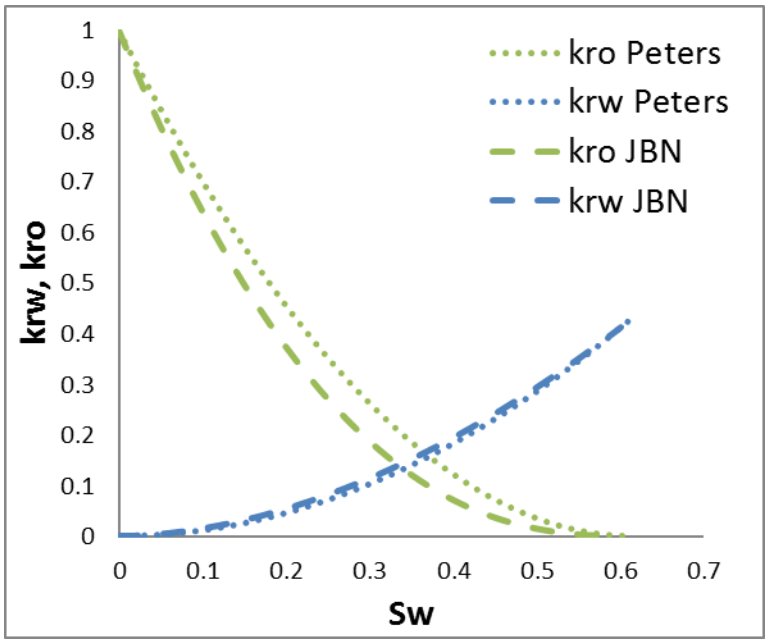

Figure 6-97: Relative Permeability estimated by JBN method for Exp 1 against the ones estimated by Peters (1994).

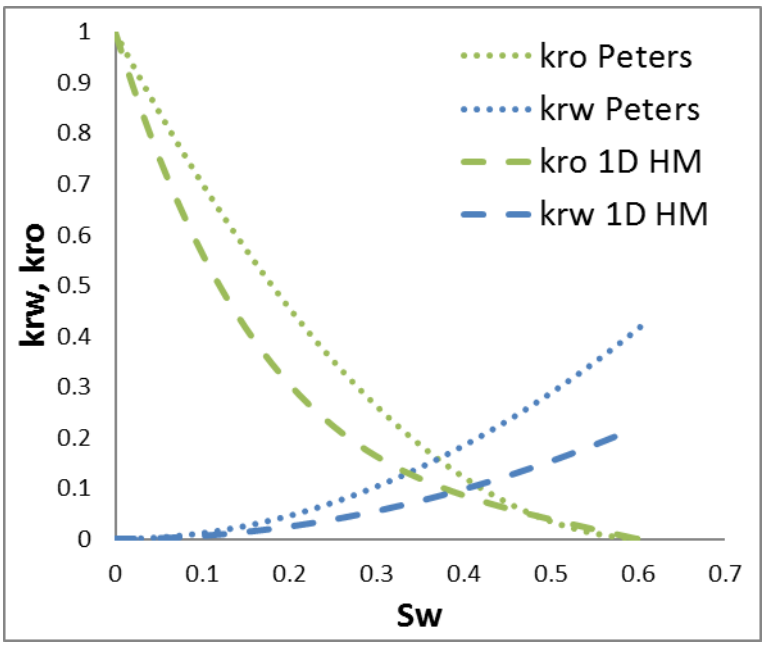

Figure 6-98: Relative Permeability estimated by 1D HM method for Exp 1 against the ones estimated by Peters (1994).

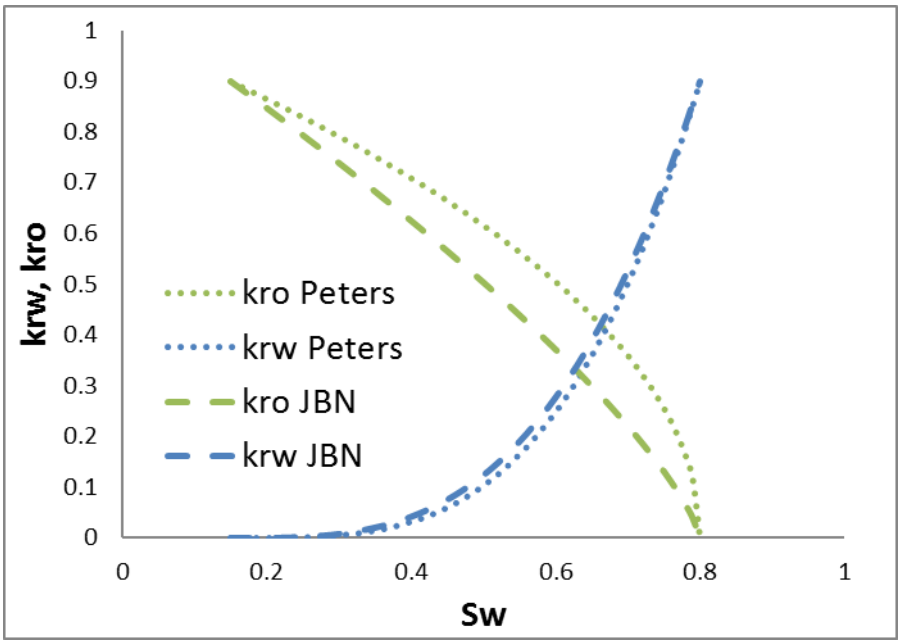

Figure 6-99: Relative Permeability estimated by JBN method for Exp 2 against the ones estimated by Peters (1994).

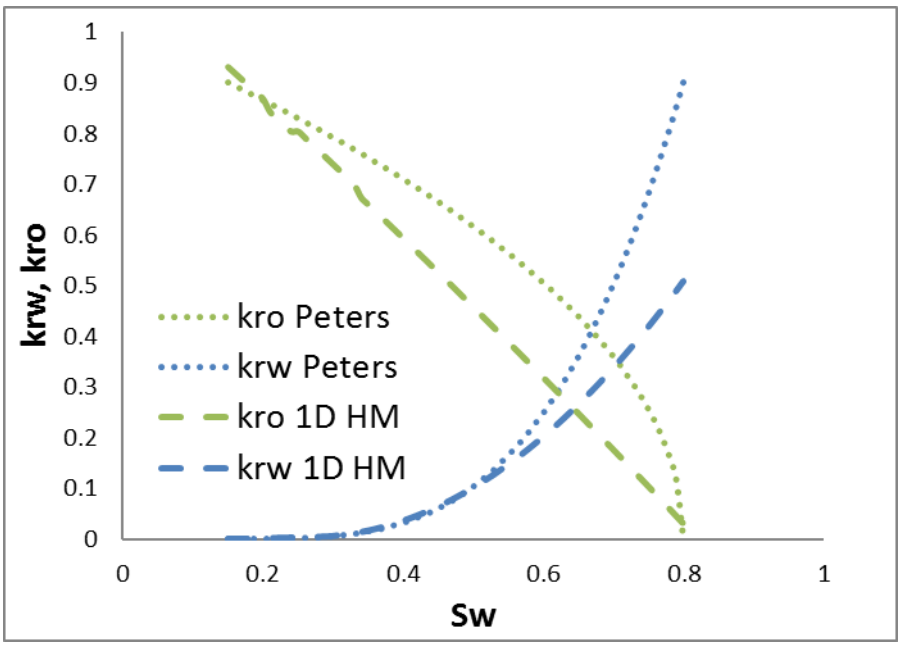

Figure 6-100: Relative Permeability estimated by 1D HM method for Exp 2 against the ones estimated by Peters (1994).

6.3.2 Modified JBN Method

In the previous section is was shown that the standard JBN method can't tackle the viscous fingering present in Peters' experiments resulting in estimation error. In this section the proposed MJBN will be used in the same experiments in order to show the advantage of using this method instead of the standard JBN.

6.3.2.1 kr Estimation Results

Using the experimental data provided by Peters (1994), the methodology enunciated in Figure 5-3 was followed, to obtain the estimated relative permeabilities by the MJBN method. Figure 6-101 and Figure 6-102 present the relative permeability curves estimated by MJBN against Peters' simulation and experimental results for Exp 1 and Exp 2, respectively. For these Figures, it was decided to show the raw estimation (point by point) results from MJBN. Later, the same results will be fitted into a Corey model for use in simulation. Also, please note that the saturation range calculated by MJBN is the saturation range of the experiment (after breakthrough at the outlet surface, in accordance with unsteady-state relative permeability estimation), any point presented in Peters' estimation after S_w = 0.28 in Exp 1 and S_w = 0.55 in Exp 2 is extrapolation fitted with a Corey Model.

For both experiments the MJBN estimation of the relative permeability curves was very close to those obtained from the 3D high resolution history matching by Peters. As it was

mentioned before, the *kr* curves obtained by Peters were expected to be very accurate in terms of accounting for viscous fingering in these experiments, mainly because they could match not only the production data but also the saturation profiles using multi-dimensional high resolution simulation. Therefore, Peters estimations are very accurate and capable to account for viscous fingering.

There are some differences between MJBN results and the Peters' estimated curves, not only due to natural dispersion due to MJBN being very sensitive to small production variations. To carry a better evaluation of the results, the points were matched into the Corey model, capturing the closest possible fit for those points. The Corey correlations are used by several authors, the equations describing them are:

$$k_{row}(S_w) = k_{row}^0(1 - S_{wn})^{N_o} \quad 6\text{-}1$$

$$k_{rw}(S_w) = k_{rw}^0 {S_{wn}}^{N_w} \quad 6\text{-}2$$

$$S_{wn}(S_w) = \frac{S_w - S_{wi}}{1 - S_{wi} - S_{or}} \quad 6\text{-}3$$

Where:

k_{row} = relative permeability of oil to water,

k_{rw} = relative permeability of water,

k_{row}^0 = endpoint oil relative permeability,

k_{rw}^0 = endpoint water relative permeability,

S_w = water saturation,

S_{wi} = initial water saturation,

S_{or} = residual oil saturation.

The results of the fitting are presented in Figure 6-103 for Exp 1 and Figure 6-104 for Exp 2.

The results from MJBN are surprisingly good in terms of accuracy (in comparison with Peters' estimation of relative permeability), even considering that these experiments had influence from Pc and gravity. Additionally, Peters' estimation was done using a complex 3D history matching methodology, while MJBN was performed in a simple excel sheet. The fact that MJBN can correctly predict these curves in a much simpler and fast methodology is one of the major advantages of this method against other methods from literature (like Peters' method).

Nevertheless, since Peters has presented comprehensible data in terms of saturation profiles, it was possible to compare the MJBN results with the experimental saturation profiles. To do this, the fitted MJBN curves were used into a high resolution 2D simulation with permeability distribution to trigger viscous fingering (following the methodology presented before in this thesis) and see how significant these changes were in comparison to Peters' results. The reason to use 2D simulation instead of 3D simulation is the considerable less computational time of the simulation, which, in this high resolution simulations, is very high. Also, it has been concluded elsewhere (Tchelepi & Jr. 1994) that in viscous fingering simulations, 2D and 3D simulation have very similar results, except when the gravity segregation is very important. In this case, the gravity segregation was small, because the difference between water and oil densities small.

All the variables reported in Peters' work were maintained the same, as much as possible, in these simulations. Gravity effects (even if small) and the Peters' suggested Pc curves were used in each simulation. The only value used by Peters' that wasn't used in these simulations was the Dykstra Parsons Coefficient. The Dykstra Parsons Coefficient is a value that evaluates the heterogeneity of a core, by looking to the Gaussian permeability distribution and the bigger this value is, the more heterogeneous a core is, Willhite (1986), Figure 6-105. The way Peters' have history matched the experimental results was by changing k_r, P_c and the heterogeneity of the core. Changing the heterogeneity of the core may change the fingering formation and therefore their pattern and acts like a triggering methodology for fingering. Based on the previous works in fingering simulation, e.g., Christie (1989), when using permeability distribution to generate viscous fingering, the variability must be low to ensure that heterogeneity isn't the main factor that influences the instability. Normally Dykstra Parsons Coefficient values between 0.01 and 0.03 are used this work simulations, to ensure that the permeability anisotropy is very low and is only used to initiate the fingering. Peters' simulations have a Dykstra Parsons Coefficient of 0.576 for Exp 1 and 0.050 for Exp 2. The value used in Exp 1 is considered to be high and most probably representing a heterogeneous core. The cores used in the experiments were constructed using unconsolidated sand-packs, and the author considers them to be fairly homogenous. Then, using a low Dykstra Parsons Coefficient is more in line with the experimental conditions.

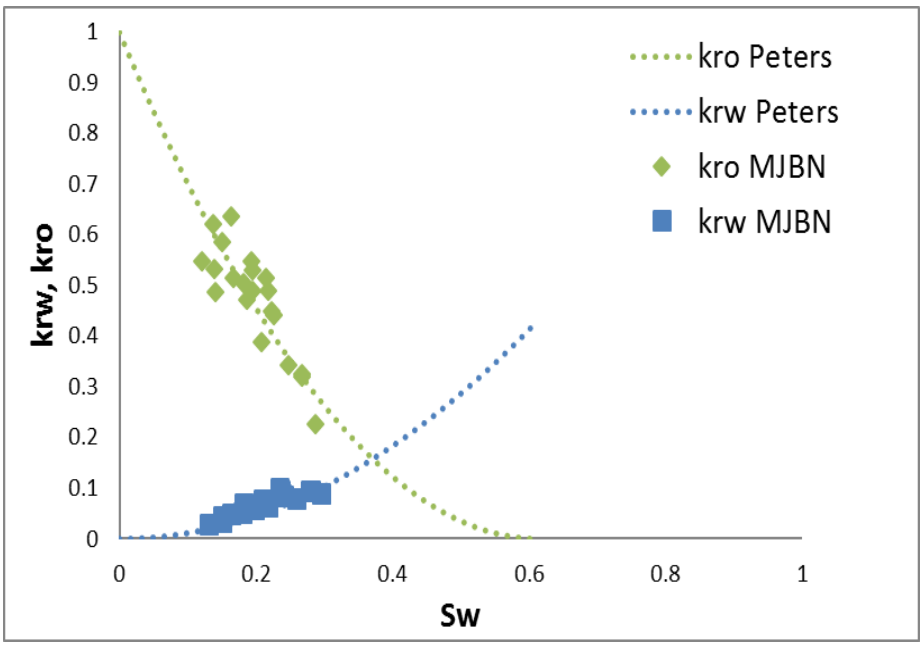

Figure 6-101: Relative permeability estimated for Exp 1 using MJBN compared with those of Peters' estimation (raw dot by dot result) for the experimental saturation range.

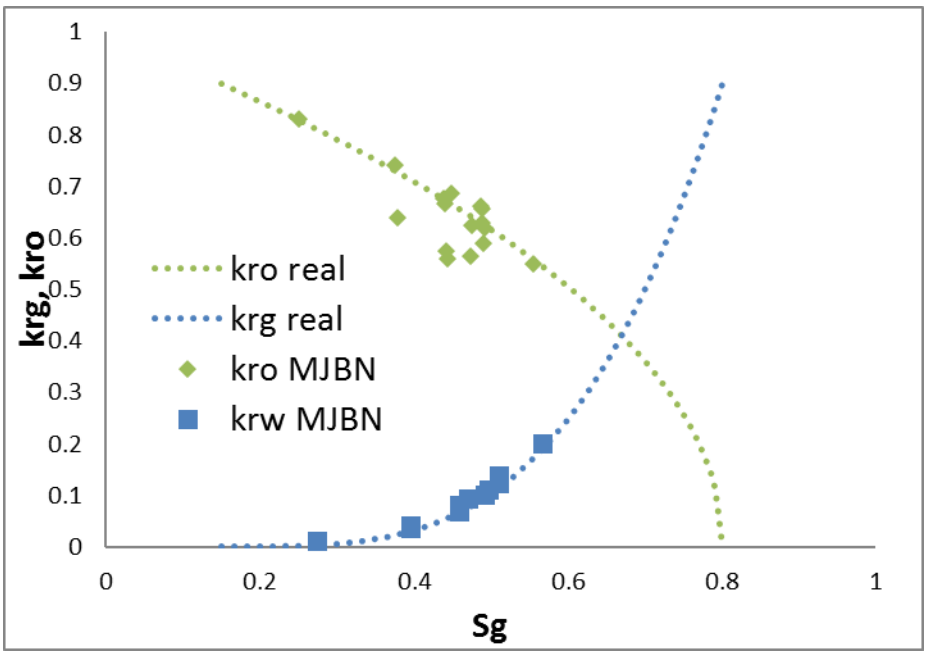

Figure 6-102: Relative permeability estimated for Exp 2 using MJBN against Peters' estimation (raw dot by dot result) for the experimental saturation range.

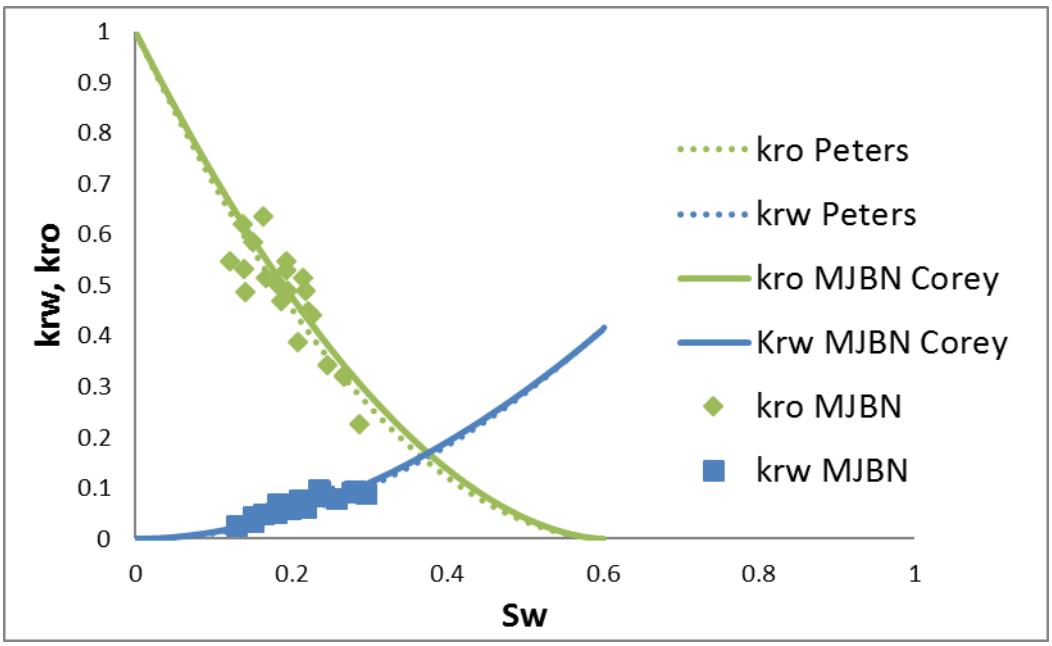

Figure 6-103: Corey match for MJBN kr estimation points in Exp 1.

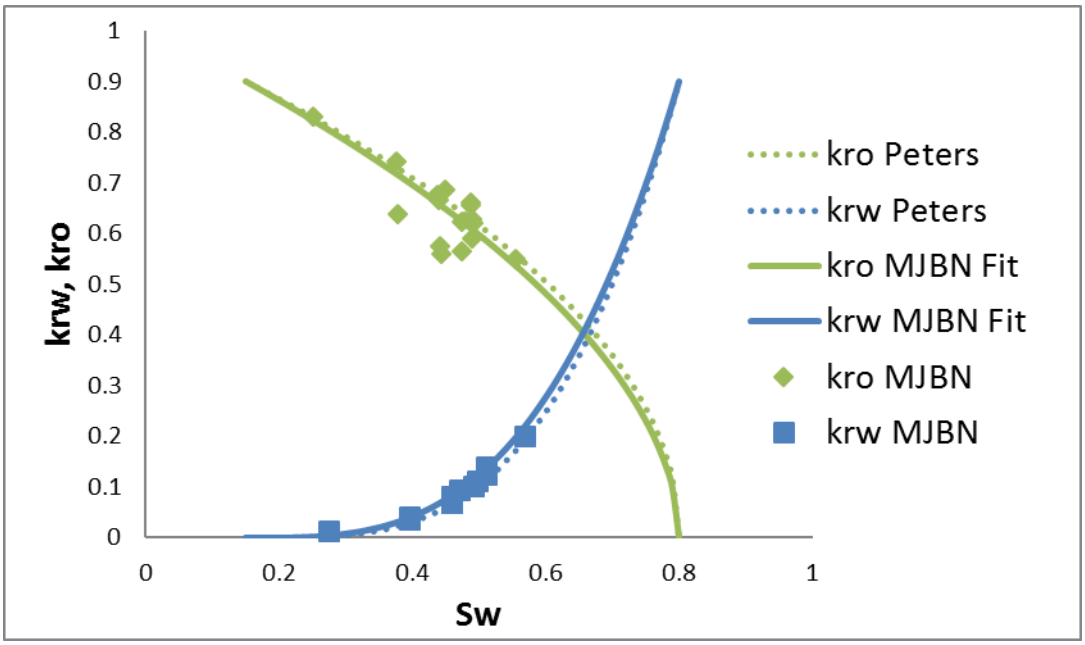

Figure 6-104: Corey match for MJBN kr estimation points in Exp 2.

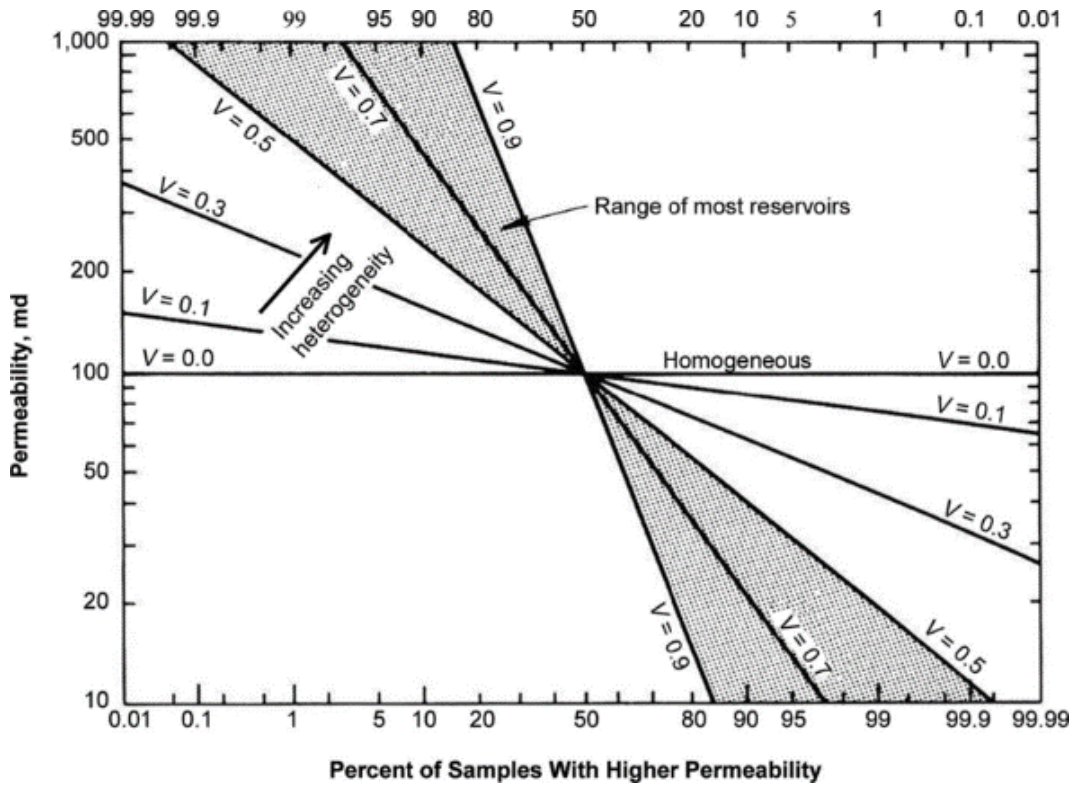

Figure 6-105: Dykstra Parsons Coefficient, V, in relation to core heterogeneity.

6.3.2.2 Production Results - Experiment 1

Using the previous assumptions, the MJBN method estimated k_r curves were used within a 2D high resolution model of Exp 1, the oil production data resulted from this simulation versus the experimental data for Exp 1 is presented in Figure 6-106. Simulation results were superimposed in the original image by Peters (1994), so that it could be better compared. The results are very close to the experimental data with only very small variations in few points, although the whole trend of the curve is well fitted, especially regarding the points just after breakthrough, where fingering tends to influence. The simulated water saturation profiles curves for Exp 1 were checked against the experimental results in Figure 6-107. A good match for all saturation values is seen, except for those at 0.05 and 0.1 PVI at near the interface water-oil. Regarding the saturation values at 0.1 PVI, there is an inconsistency in the experimental values, when comparing the saturation profiles with the fractional oil recovery. In Figure 6-106, the breakthrough can be seen to be somewhere around 0.1 PVI, although in Figure 6-107 the saturation profiles show that for 0.1 PVI the water is still at 80% of the total core length. It's not known if this has to do with some technical issue with CT scan, or whether there is a limit in the saturation range by CT images that didn't allowed to see a water profile close to the end of the core at 0.1 PVI (e.g. different saturations can only be distinguish

from 0.05 fraction and above). Nevertheless, when probing the data from Peters (1994) image, Figure 6-93 (top), the breakthrough point was around 0.11 PVI and that information was used in the MJBN estimation, so is natural that the simulation would represent the same breakthrough point. Due to these reasons, it's assumed that these variations as not significant, especially because the very good match obtained for all the other saturation points.

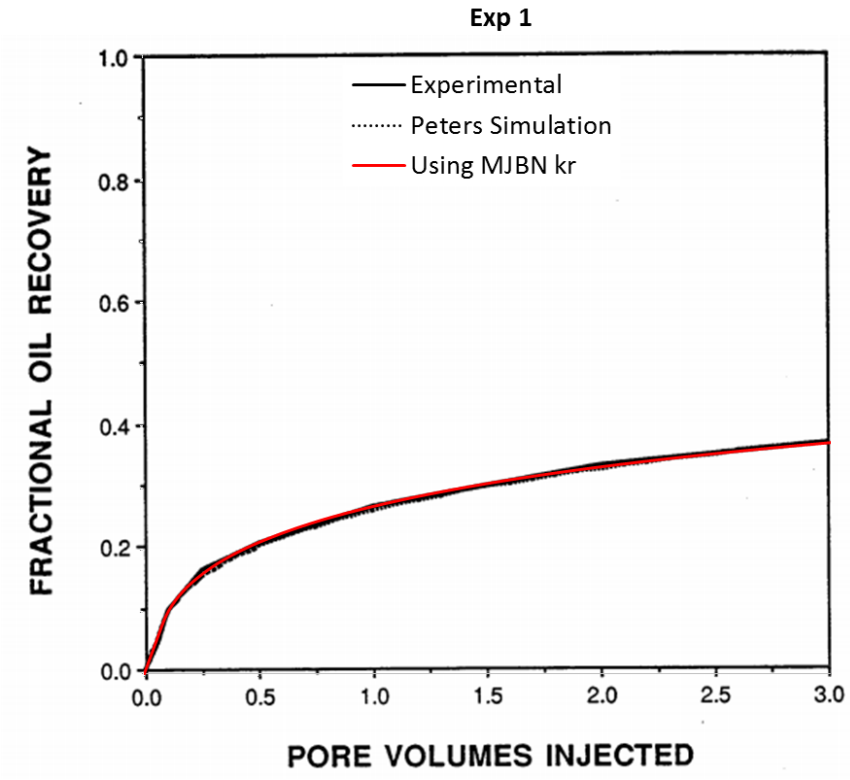

Figure 6-106: Fractional oil recovery versus the pore volumes injected for Exp 1 using MJBN estimated kr against experimental results. This work simulation results were superimposed in the original Peters (1994) image. Showing a good match along the whole curve.

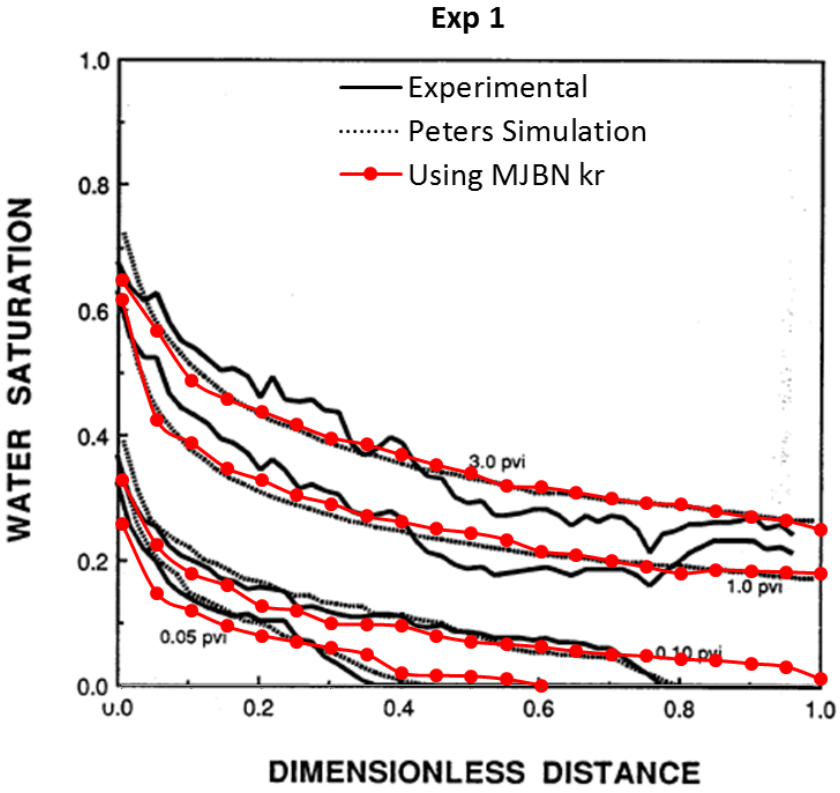

Figure 6-107: Water saturation profiles vs. dimensionless distance for Exp 1. This work simulation results were superimposed upon the original Peters' (1994) image. They show a good trend match for all saturation values, with some differences between 0.05 and 0.1 PVI.

6.3.2.3 Production Results - Experiment 2

Following the same procedure as for Exp 1, the fractional oil recovery data and water saturation profiles for Exp 2 were generated, using the k_r curves estimated by MJBN in a 2D high resolution simulation. The fractional oil recovery was superimposed over the original results of Peters' (1994) in Figure 6-108.

Using the MJBN's k_r, a very good match with experimental results was obtained, in fact less error was achieved than in Peters Simulation results. From Figure 6-95 it may seem that both this work's simulation and Peters' have failed to predict the breakthrough point, although that may not be true. In Figure 6-95 the experimental points seem to be connected using straight lines between each sequential pair of points, so without more information, it is impossible to know if the breakthrough happened at 0.25 PVI or somewhere between 0.25 and 0.5 PVI. This hypothesis gains strength when analysing the saturation profiles next. The water saturation profiles are shown in Figure 6-109. In general, there is a very good agreement between this work simulation, Peters' simulation, and the experimental results.

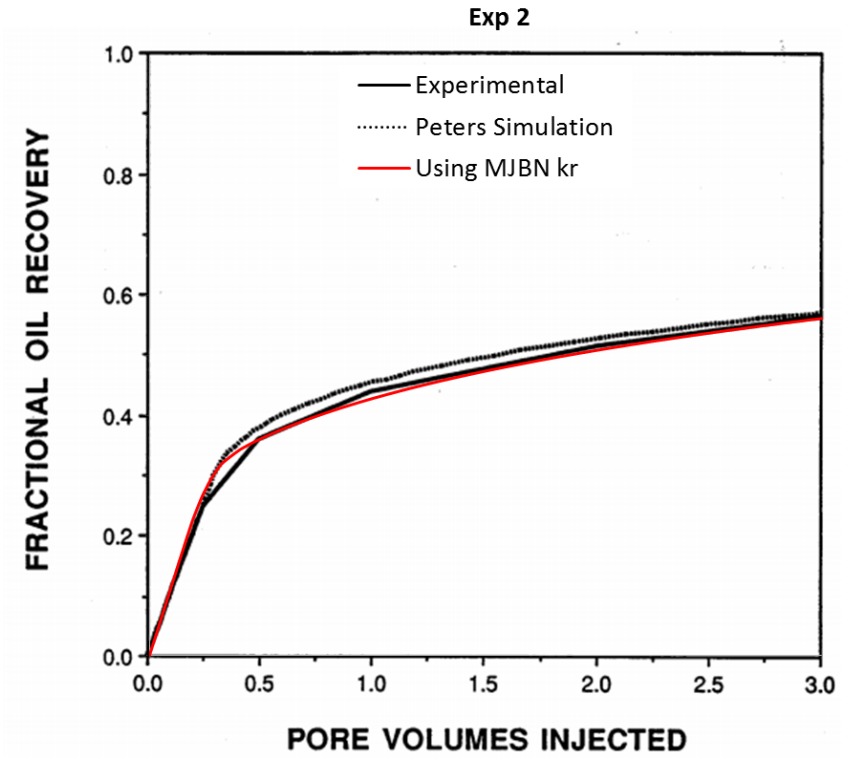

Figure 6-108: Fractional oil recovery versus pore volumes injected for Exp 2 using MJBN estimated kr against experimental results. This work's simulation results were superimposed over the original Peters (1994) image. Showing a better match than Peters' simulation.

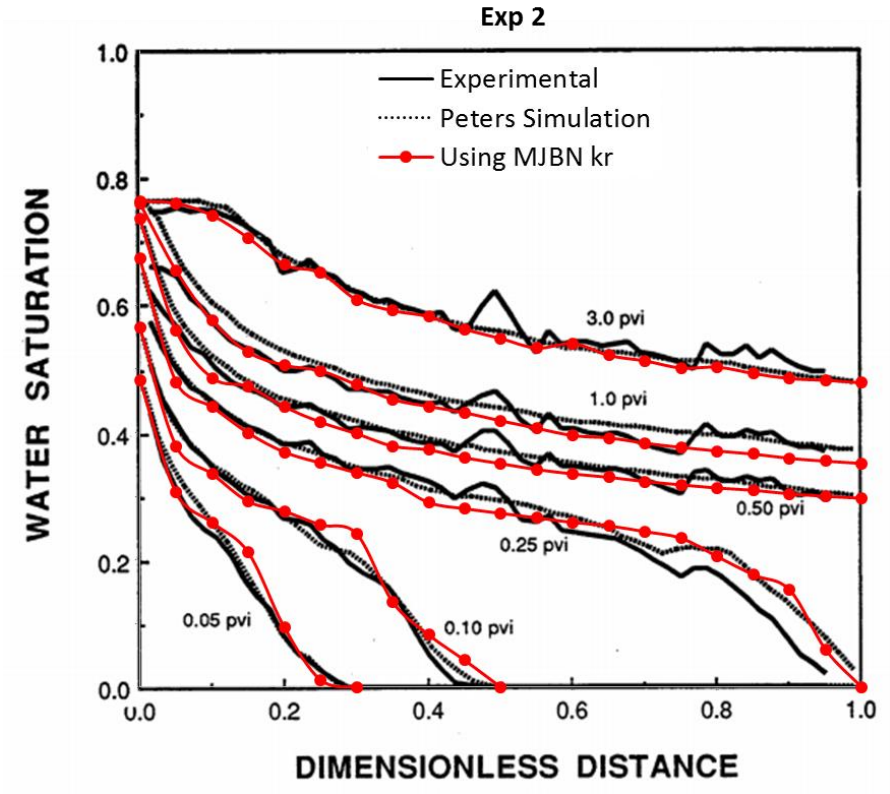

Figure 6-109: Water saturation vs. dimensionless distance for Exp 2. This work's simulation results were superimposed upon the original Peters' (1994) image. Showing a reasonable match for all saturation values.

6.3.3 SEM

Peters (1994) experiments were performed under unstable conditions and viscous fingering has formed during the injection. In section 6.3.1 it is concluded that 1D HM is an unsuitable method to estimate the relative permeability in these experiments due to the viscous fingering. The proposed SEM method is an improved 1D HM method to tackle the influence of viscous fingering in relative permeability estimation. In this section, SEM will be used in Peters experiments, in order to evaluate how much improvement, it represents, in comparison with the traditional 1D HM.

6.3.3.1 kr Estimation Results

Using the experimental data provided by Peters (1994), the methodology enunciated in Figure 5-14 was followed, to obtain the estimated relative permeabilities by the SEM method. Figure 6-101 and Figure 6-102 present the relative permeability curves estimated by SEM against those by Peters' for Exp 1 and Exp 2, respectively. Please note that the saturation range calculated by MJBN is the saturation range of the experiment (after breakthrough at the outlet surface, in accordance with unsteady-state relative permeability estimation), any point presented in Peters' estimation after $S_w = 0.28$ in Exp 1 and $S_w = 0.55$ in Exp 2 is extrapolation fitted with a Corey Model. The same may be said from the SEM results, all the values outside the valid saturation range are considered invalid for precision evaluation purposes.

SEM results show a very good accuracy with Peters' estimation results. It is important to notice that Peters' history matching consists in a complex 3D high definition history matching with saturation profile matching, which the author achieved by changing the permeability of the rock in the matching process. SEM is a much simpler method and is basically a 1D history matching with a few alterations, but that benefits of the same speed and simplicity. Additionally, SEM may be used by the end user of a history matching software, because it is possible (as enunciated in Chapter 5) to modify the 1D HM by changing the viscosity ratio and correct the saturation of the displacing fluid.

The estimated relative permeability curves from SEM were then used in a 2D Simulation of the 2 Peters' experiments. This simulation uses high resolution and permeability distribution to trigger fingering. The objective is to compare the production results from using SEM's k_r curves against the experimental observed production data.

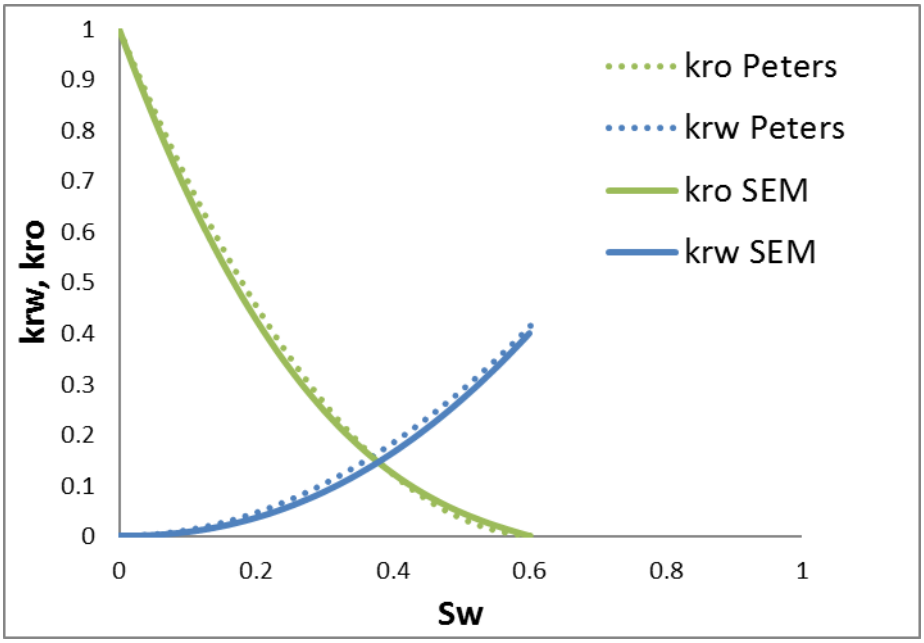

Figure 6-110: Relative permeability estimated for Exp 1 using SEM compared with those of Peters' estimation for the experimental saturation range.

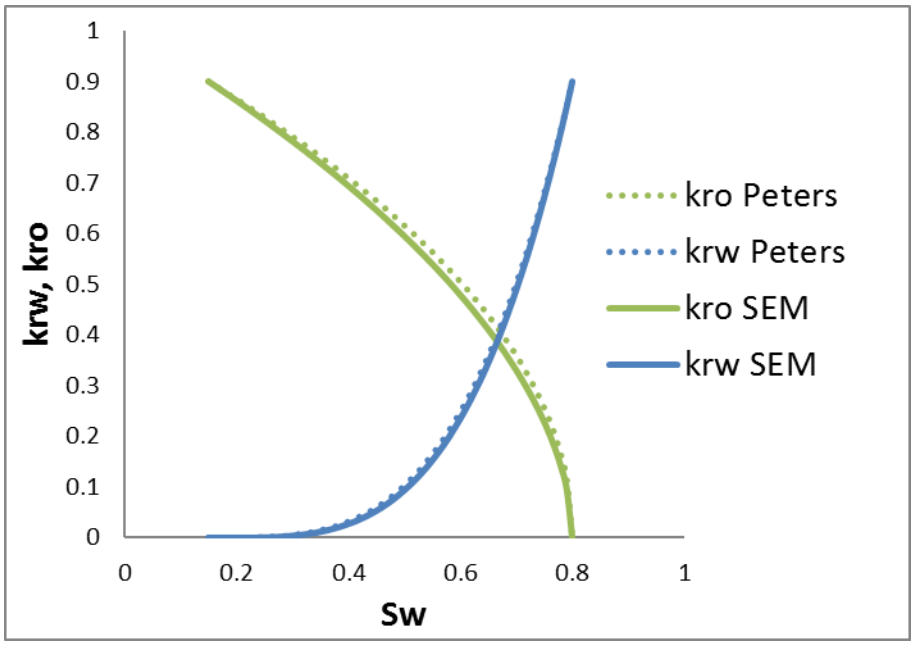

Figure 6-111: Relative permeability estimated for Exp 2 using SEM compared with those of Peters' estimation for the experimental saturation range.

6.3.3.2 Production Results - Experiment 1

The results of using SEM's relative permeability in a numerical simulation of Exp 1 are presented in Figure 6-112 for the fractional oil recovery and Figure 6-113 for the saturation profiles. The results are in perfect agreement with the experimental values for the exception of the near outlet water saturation values in 0.1 pore volumes injected (PVI). This difference is due to the same reasons explained in the MJBN's results for the same experiment (section 6.3.2.2). Due to these reasons, it's assumed that these variations as not significant, especially because the very good match obtained for all the other saturation points.

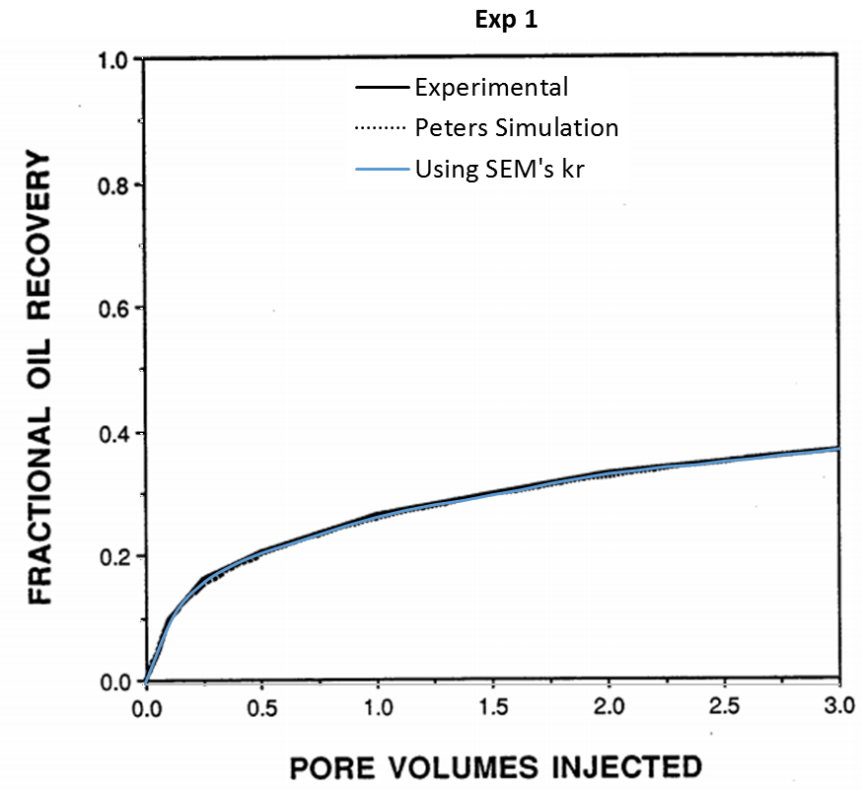

Figure 6-112: Fractional oil recovery versus pore volumes injected for Exp 1 using SEM estimated kr against experimental results. This work's simulation results were superimposed over the original Peters (1994) image. Showing a better match than Peters' simulation.

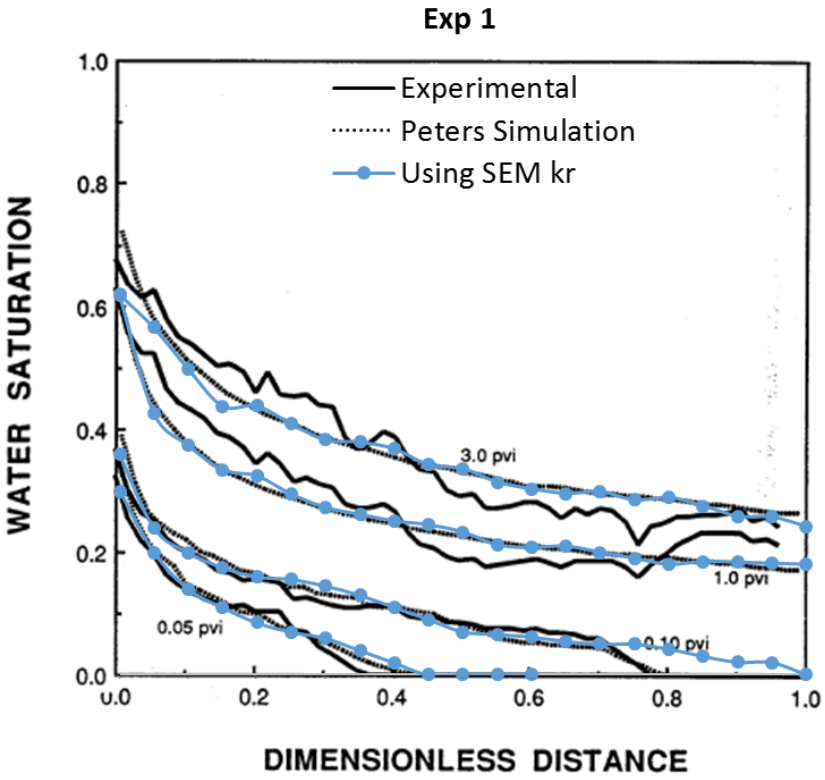

Figure 6-113: Water saturation vs. dimensionless distance for Exp 1. This work's simulation results were superimposed upon the original Peters' (1994) image. Showing a reasonable match for all saturation values.

6.3.3.3 Production Results - Experiment 2

The results of using SEM's relative permeability in a numerical simulation of Exp 2 are presented in Figure 6-114 for the fractional oil recovery and Figure 6-115 for the saturation profiles. The results are in perfect agreement with the experimental values for the exception of the zone just after the breakthrough point, in the fractional oil production. As explained before, the experimental data was collected in 0.25 PVI steps and the dots were linearly connected, so the difference is due to fitting. Also, the breakthrough point was correctly estimated. For this experiment, SEM's results were slightly better than Peters' simulation at matching the fractional oil recovery, which is impressive since SEM is a 1D history matching and Peters used a complex 3D history matching. Clearly, this is evidence of the utility of this method as a relative permeability estimation process.

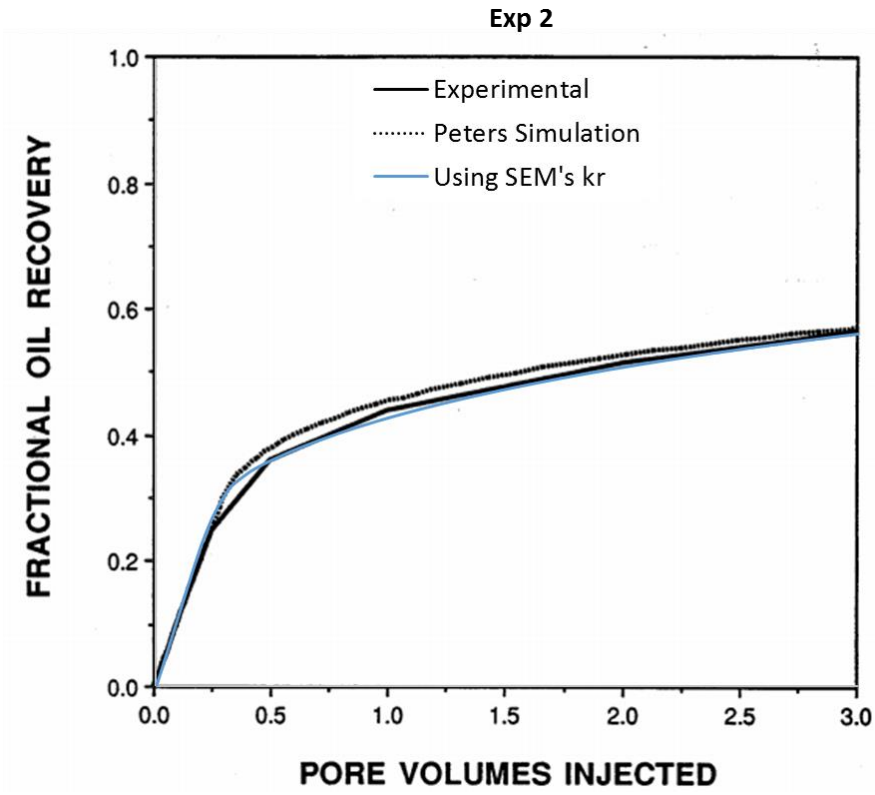

Figure 6-114: Fractional oil recovery versus pore volumes injected for Exp 2 using SEM estimated kr against experimental results. This work's simulation results were superimposed over the original Peters (1994) image. Showing a better match than Peters' simulation.

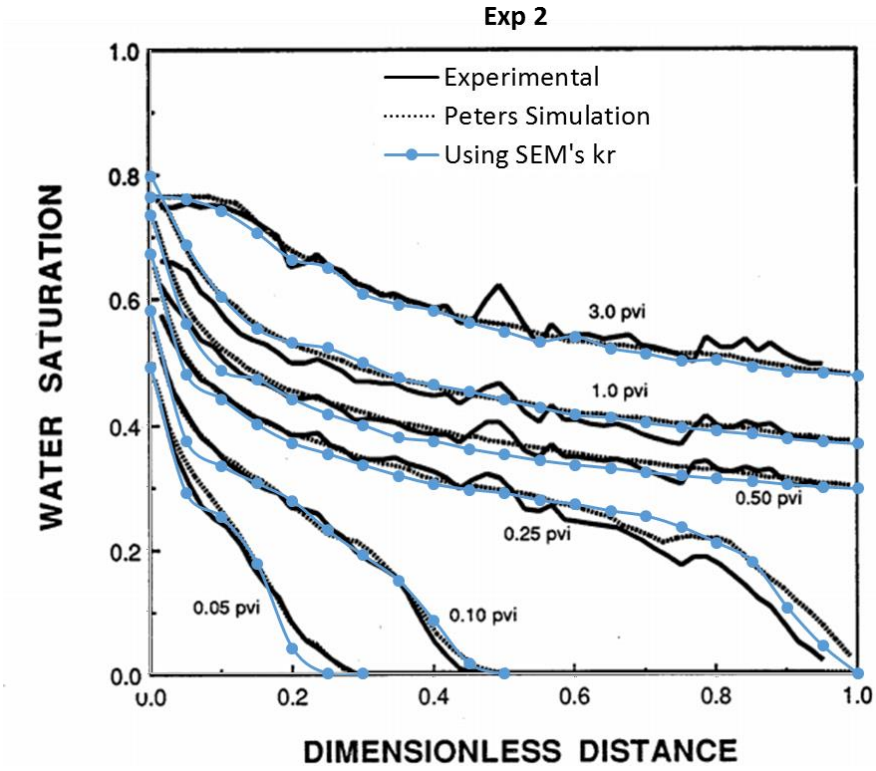

Figure 6-115: Water saturation vs. dimensionless distance for Exp 2. This work's simulation results were superimposed upon the original Peters' (1994) image. Showing a reasonable match for all saturation values.

6.3.4 Discussion

The estimation of the relative permeability in unstable experiments was evaluated using the traditional JBN and 1D HM against the proposed MJBN and SEM methodologies. The accuracy of the proposed methods was far superior than the traditional methods, showing a clear advantage in using these modified versions to account for viscous fingering. These modifications to the traditional methods not only increased the precision of the estimation of the relative permeability, but they resulted in very close values of k_r to the ones proposed by Peters. Peters used a complex 3D history matching with saturation pattern matching using a variable permeability field in the core. The fact that these 'simple' and fast methods could result in relative permeability curves with practically the same accuracy highlights the usefulness of MJBN and SEM. Also, the computational time that is necessary to reach a good k_r estimation is considerably lower. Peters in his paper, doesn't refer how much time each history matching took, but in 1D history matching, these unstable cases, may take 6-8 hours. In 3D history matching it would take much more, probably weeks. MJBN and SEM are clearly an advantage in terms of time.

6.4 Conclusions

The following conclusion may be drawn from Validation of MJBN and SEM Methods as Relative Permeability Estimation Methods for Cases with Viscous Fingering:

- The validation of MJBN and SEM methods as k_r estimation methods for coreflood experiments with viscous fingering formation was performed with the use of numerical and actual experiments, by comparison of the estimated relative permeabilities versus the real ones. The numerical experiments allow to objectively analyse the precision of MJBN and SEM, since the real relative permeability is known (k_r is an input value). However, the actual experiments it is impossible to know with absolute certainty the real relative permeability, however the experiments chosen for the validation were matched in literature with a complex 3D history matching with saturation profile matching that allow the prediction of relative permeability curves to be very close to the real., enabling the determination of the precision of MJBN and SEM from experimental data.
- The NCFEs used for validation were divided into independent and sets. Independent NCFEs refer to 'stand-alone' simulation where many parameters

change between each different NCFE. This allowed the study of the precision of MJBN and SEM in different scenarios in order to prove that these methods aren't case dependent and that can have accurate parameters in a number of scenarios. Sets, however, use the exact same parameters but changing the oil viscosity in order to obtain a gradient of instability from one simulation to another. This allows to study k_r estimation precision as a function of instability.

- In the independent NCFEs, using MJBN and SEM resulted in excellent match with the real k_r curves. Both MJBN and SEM performed better than their standard counter parts, JBN and 1D HM. The influence of the k_r curves precision in the results of coreflood experiments was evaluated by using the different methods (MJBN, SEM and 1D HM) in high resolution simulation. This evaluation clearly showed that the influence of the error of estimation of the relative permeability is not linearly correlated with the production error. Therefore, it was concluded that in one experiment the relative permeability error may be higher than another but the error in production doesn't necessarily follow this pattern, because the influence of the change in the relative permeability value is case dependent.
- The NCFEs Sets allowed to evaluate MJBN and SEM against a gradual increase of instability. It was concluded that MJBN and SEM error of precision doesn't increase with the increase of instability, meaning that the methods are correctly accounting for viscous fingering 'severity'. This conclusion was reinforced by the fact that both 1D HM and JBN methods had more error for cases with higher instability.
- Unstable experimental data, with viscous fingering, collected from literature was used to validate the relative permeability estimation method, this experimental data was accompanied with relative permeability curves estimated by complex 3D history matching by the author (Peters 1994). These relative permeability curves, were assumed to be the real relative permeability curves. JBN and 1D HM were used to estimate the relative permeability from the experimental data. This relative permeability was shown to have considerable error in comparison with the real relative permeability for both Exp 1 and Exp 2, concluding that these experiments have considerable fingering formation and that the standard methods can't account for it.
- MJBN and SEM's estimated relative permeability had higher precision than any of the standard methods. This fact was further proven by the use of the estimated

relative permeabilities to predict the experimental production results. The experimental production results obtained from the use of MJBN and SEM's k_r were in perfect agreement with the results observed by Peters (1994).

Chapter 7: Conclusions and Recommendations

7.1 Conclusions

A summary of the work and the main conclusions derived from each chapter are as follows:

Chapter 2: Viscous Fingering Simulation

In this chapter, the methodology used to create viscous fingering in numerical simulation was presented, along with the sensitivity analysis for the parameters used. The main conclusions of this chapter are:

- In this thesis, Numerical Coreflood Experiments (NCFEs) were defined as coreflood experiments numerically generated using commercial simulators, using similar input data as the one used in the Centre for Enhanced Oil Recovery & CO_2 Solutions at Heriot-Watt University. These NCFEs have a big advantage against laboratory experiments, because it is possible to precisely define the uncertain parameters like relative permeability or capillary pressure, allowing the user to study the direct effect of these parameters in the production results. Also, NCFEs enable the production of a high amount of synthetic coreflood data in minimal time in comparison with laboratory corefloods that may take months to complete.
- Typical commercial simulators are not able to generate viscous fingering even in unfavourable mobility conditions. Triggering methods are, then, used to create enough differences between each grid block in order to generate viscous fingering. In this thesis permeability distribution was used in order to trigger the fingering formation. Permeability distribution methodology consists in assigning a different value of absolute permeability to each grid block in the simulation following a Gaussian distribution. The degree of variance is very important to be able to generate viscous fingering while avoiding heterogeneity effects (which are undesirable because they would mask the viscous fingering influence in the flow). It was found that using a coefficient of variation of 10% is sufficient to generate viscous fingering and low enough to ensure homogeneity.
- Viscous fingering simulation result in very complex patterns. These patterns can only be fully captured using a high number of grid blocks (high resolution

simulation) to avoid the effect of dispersion. Using a higher number of grids may result in more fingers generated, especially for very unstable flows. Nevertheless, there is a limit where the use of more grid blocks will not have significant impact in the production results, meaning that increasing the number of block after this limit only results in a higher simulation time. It was concluded that the optimal number of grid blocks was around 20.31 blocks/cm^2, so in all simulations performed throughout this thesis the number of grid blocks is always bigger than this value.

- The viscous fingering patterns generated by simulation were compared with those from experimental observation made by other authors. The simulation results present some of the main mechanisms of viscous fingering in coreflood: shielding, spreading, coalescence and tip splitting, representing well observation made by other authors. Some of this mechanism only happen when the mobility is very unfavourable, being completely inexistent in low viscosity ratio cases. This behaviour means that the physics of the fingering formation is being correctly captured by using the permeability distribution triggering method. Also the patterns generated in simulation were compared with patterns captured by core imaging in literature, concluding that they were very similar. In conclusion, using the methodology presented to generate fingering (with the appropriate triggering and simulation parameters like high resolution gridding) allows to closely represent the complex patterns in simulation.
- Viscous fingering generation was evaluated to realise if the instability was being generated only in cases where the conditions were favourable for their formation. Using a stability model from literature called stability number, I_{sr}, developed by Sarma & Bentsen 1987, it was proved that fingering only forms, in this work simulations, if the value of I_{sr} is beyond the stability threshold, obeying their stability model. This gives validity to the methodology used to simulate viscous fingering, proving that viscous fingering will only form if the conditions are just right.

Chapter 3: Created Unstable Numerical Coreflood Experiments

The numerical coreflood experiments (NCFEs) to be used throughout this thesis were created. The NCFEs were performed using commercially available software from

Computer Modelling Group, CMG. All results were produced using either CMG-IMEX (black-oil simulator) or CMOST (history matching tool). IMEX was used to produce all the NCFEs, while CMOST was used to produce 2D history matching. The propose of this exercise was to create numerical corefloods that resemble as much as possible real experiments. The use of NCFEs allows to know the real parameters of that experiment, like the true relative permeability.

Chapter 4: Evaluation of Existing Relative Permeability Estimation Methods for Unfavourable Mobility Corefloods

In this chapter NCFEs were used to evaluate the precision of existing relative permeability estimation methods. Using this numerical experiments, analytical JBN and 1D history matching were evaluated against the 'real' relative permeability curves, giving insight on the amount of error instabilities may produce in the standard methods. The conclusions drawn from this chapter are as following:

- Unsteady-state relative permeability estimation methods are commonly used to estimate the relative permeability of coreflood experiments. One dimensional history matching and JBN method are arguably the mostly used methods to estimate the relative permeability curves, probably because of their simplicity and fast results. These methods have been widely used and their results are considered good estimations for the typical stable coreflood experiments, especially if capillary pressure and gravity have small influence in the flow. However, no published data was found to access their validity in a conclusiveness manner towards flows with viscous fingering formation. In this chapter, a novel methodology was proposed to evaluate the precision of 1D HM and JBN method in coreflood experiments with viscous fingering. The methodology uses numerical coreflood experiments (NCFEs) in other to allow a precise definition of the relative permeability curves, so that the estimation methods' results could be conclusively compared. These NCFEs were treated as real laboratory experiments and the relative permeability used as the real curves for that experiment. The error of each method could be easily calculated by comparison of the estimated k_r and the real k_r curves.

- Three sets of NCFEs were used in JBN and 1D HM method to evaluate the methods precision, one set of independent NCFEs and two sets using one experiment each at different viscosity ratios. These 3 set of NCFEs were simulated in 1D simulation and 2D simulation, the first corresponding to a stable version of the NCFEs and the second a realistic version with viscous fingering formation.
- JBN method exhibited good precision on the stable version of the NCFEs, with all errors below 3%, deeming the method appropriate for relative permeability estimation of stable corefloods. For the unstable version of the NCFEs, JBN estimation of k_{ro} showed to be highly dependent on the viscous fingering severity. Differently, for k_{rd}, the results didn't reveal any correlation with the instability of the flow and all errors were within the range of the error observed in the stable version of the NCFEs. This fact allows to imply that JBN is correctly capturing the physics of flow for the displacing fluid but not the displaced fluid.
- One dimensional history matching had similar results to JBN method in the stable version of the NCFEs, with all the errors below 3%. For unstable version of the NCFEs, 1D HM estimation resulted in high error for both oil and displacing fluid relative permeability curves. The precision of the method followed a good correlation with viscous fingering formation, resulting in much higher errors than the ones observed in the stable version of these corefloods.
- This chapter results allow to declare 1D HM and JBN methods as unfit for the estimation of relative permeability curves of unstable coreflood experiments. Both methods showed a great dependency on the stability of the flow. Nevertheless, from these results, JBN seems to be a better choice to deal with instability when gravity and capillary pressure are ignorable, since the method showed good precision for the displacing fluid relative permeability. It is also possible to advice the caution of the industry when using any of these method to estimate the relative permeability for potentially unfavourable coreflood experiments.

Chapter 5: Accounting for Viscous Fingering in Relative Permeability Estimation Methods Based in Stability

In this chapter two new methods based in the standard JBN and 1D HM methods, were proposed in order to account for the viscous fingering in unstable coreflood experiments. The major conclusions of this chapter are:

- A theory was proposed to explain the results from stable k_r estimation methods in presence of viscous fingering. This theory proposes that the displacing fluid flow follows methods based in stable flow, but the formation of fingering disrupts the flow of oil, because the oil can't handle the high mobility of the displacing fluid.
- From the proposed theory, a model, called Stable Equivalent, was developed to change an unstable experiment data so that k_r estimation methods (based in stability) can estimate relative permeability curves without error from viscous fingering. In this model, the velocity of the gas is reduced in order to revert the acceleration due to viscous fingering, allowing the oil to move at a velocity equivalent to the one it would move if viscous fingering hadn't form. This velocity is changed in function of an adimensional factor called η. This change is enough to guaranty the estimation of the oil relative permeability taking into account the viscous fingering. However, since the gas velocity was changed in relation to the original experiment, a correction in the saturation was proposed to account for this fact.
- The Stable Equivalent model was applied to the JBN and 1D history matching methods and a methodology workflow was present to allow the easily application of the methods to an experiment.
- The modified methods, MJBN and SEM, allow SCAL analysts to estimate the relative permeability for cases with viscous fingering quickly, without the need of complex 2D/3D history matching methods. MJBN may also be used to reduce the non-uniqueness if 2D and 3D HM and accelerate matching of this methods by providing a good first guess.

Chapter 6: Validation of MJBN and SEM as Relative Permeability Estimation Methods for Cases with Viscous Fingering

In this chapter, MJBN and SEM methods were validated, using both numerical and laboratory experiments. The conclusions drawn from this chapter are as following:

- The validation of MJBN and SEM methods as k_r estimation methods for coreflood experiments with viscous fingering formation was performed with the use of numerical and actual experiments, by comparison of the estimated relative permeabilities versus the real ones. The numerical experiments allow to objectively analyse the precision of MJBN and SEM, since the real relative permeability is known (k_r is an input value). However, the actual experiments it is impossible to know with absolute certainty the real relative permeability, however the experiments chosen for the validation were matched in literature with a complex 3D history matching with saturation profile matching that allow the prediction of relative permeability curves to be very close to the real., enabling the determination of the precision of MJBN and SEM from experimental data.
- The NCFEs used for validation were divided into independent and sets. Independent NCFEs refer to 'stand-alone' simulation where many parameters change between each different NCFE. This allowed the study of the precision of MJBN and SEM in different scenarios in order to prove that these methods aren't case dependent and that can have accurate parameters in a number of scenarios. Sets, however, use the exact same parameters but changing the oil viscosity in order to obtain a gradient of instability from one simulation to another. This allows to study k_r estimation precision as a function of instability.
- In the independent NCFEs, using MJBN and SEM resulted in excellent match with the real k_r curves. Both MJBN and SEM performed better than their standard counter parts, JBN and 1D HM. The influence of the k_r curves precision in the results of coreflood experiments was evaluated by using the different methods (MJBN, SEM and 1D HM) in high resolution simulation. This evaluation clearly showed that the influence of the error of estimation of the relative permeability is not linearly correlated with the production error. Therefore, it was concluded that in one experiment the relative permeability error may be higher than another but the error in production doesn't necessarily follow this pattern, because the influence of the change in the relative permeability value is case dependent.
- The NCFEs Sets allowed to evaluate MJBN and SEM against a gradual increase of instability. It was concluded that MJBN and SEM error of precision doesn't increase with the increase of instability, meaning that the methods are correctly accounting for viscous fingering 'severity'. This conclusion was reinforced by

the fact that both 1D HM and JBN methods had more error for cases with higher instability.

- Unstable experimental data, with viscous fingering, collected from literature was used to validate the relative permeability estimation method, this experimental data was accompanied with relative permeability curves estimated by complex 3D history matching by the author (Peters 1994). These relative permeability curves, were assumed to be the real relative permeability curves. JBN and 1D HM were used to estimate the relative permeability from the experimental data. This relative permeability was shown to have considerable error in comparison with the real relative permeability for both Exp 1 and Exp 2, concluding that these experiments have considerable fingering formation and that the standard methods can't account for it.
- MJBN and SEM's estimated relative permeability had higher precision than any of the standard methods. This fact was further proven by the use of the estimated relative permeabilities to predict the experimental production results. The experimental production results obtained from the use of MJBN and SEM's k_r were in perfect agreement with the results observed by Peters (1994).

7.2 Recommendations

- From this work it is clear that the traditional methods based in Buckley & Leverett (1942) should not be used to estimate the relative permeability of cases where viscous instabilities take place. JBN and 1D HM, being the mostly used for SCAL measurements, may result in considerable error. It's not recommended to use any of this methods without properly access the level of instability.
- MJBN and SEM were validated in immiscible NCFEs and experimental corefloods. It is possible that they are not valid for other types of displacements, especially the MJBN, since it is based on JBN and, therefore, it shares its limitations. SEM has the possibility to be used for certain cases that MJBN can't, like the capillary pressure is important. However, proper validation for this cases wasn't performed since it was outside the scope of this thesis. It is recommended a validation before using these methods for cases that are outside their limitations.

7.3 References

Abaci, S., Edwards, J.S. & Whittaker, B.N., 1992. Relative permeability measurements for two phase flow in unconsolidated sands. *Mine Water and the Environment*, 11(2), pp.11–26.

Araktingi, U.G. & Orr Jr, F.., 1993. Viscous fingering in heterogeneous porous media. *SPE Advanced Technology Series*, 1(01), pp.71–80.

Bacri, J.-C. et al., 1992. Miscible viscous fingering: Experiments versus continuum approach. *Phys. Fluids A*, 4(8), pp.1611–1619.

Bard, Y., 1974. *Nonlinear Parameter Estimation*,

Bentsen, R.G., 1985. A New Approach to Instability Theory in Porous Media. *Society of Petroleum Engineers Journal*, 25(5).

Blackwell, R.J. & Pozzi, A.L., 1963. Design of Laboratory Models for Study of Miscible Displacement. *SPE Journal*, (3), pp.28–40.

Blackwell, R.J., Ryne, J.R. & Terry, W.M., 1959. Factors Influencing the Efficiency of Miscible Displacement. *Spe J.*, 216(1), pp.1–8.

Blunt, M. & Christie, M., 1994. Theory of viscous fingering in two phase, three component flow. *SPE Advanced Technology Series*, 2(2), pp.52–60.

Brock, D. & Orr Jr, F., 1991. Flow visualization of viscous fingering in heterogeneous porous media. *SPE Annual Technical Conference and …*.

Brooks, R.H. & Corey, a. T., 1966. Properties of Porous Media Affecting Fluid Flow. *Journal of the Irrigation and Drainage Division*, June, pp.61–88.

Buckley, S. & Leverett, M., 1942. Mechanism of fluid displacement in sands. *Trans. AIME*, 146(1337), pp.107–116.

Chandrasekhar, S., 1981. Hydrodynamic and hydromagnetic stability. *Physics Uspekhi*, 179, p.652.

Chen, C.Y. & Meiburg, E., 1998. Miscible porous media displacements in the quarter five- spot configuration. Part 1. The homogeneous case. *J. Fluid Mech.*, 371, pp.233–268.

Chen, Z. & Ewing, R.E., 2002. *Fluid Flow and Transport in Porous Media, Mathematical and Numerical Treatment: Proceedings of an AMS-IMS-SIAM Joint Summer Research Conference on Fluid Flow and Transport in Porous Media, Mathematical and Numerical Treatment*, American Mathematical Soc.

Christie, M. a, Culverwell, I.D. & Mansfield, M., 1993. Compositional Reservoir Simulation With a Predictive Model for Viscous Fingering.

Christie, M. a., 1989. High-Resolution Simulation of Unstable Flows in Porous Media. *SPE Reservoir Engineering*, 4(3), pp.297–303.

Christie, M. a. & Jones, A.D.W., 1987. Comparison between laboratory experiments and detailed simulation of miscible viscous fingerin. *Fourth European Symposium on Enhanced Oil Recovery*.

Christie, M. a., Muggeridge, a. H. & Barley, J.J., 1993. 3D Simulation of Viscous Fingering and WAG Schemes. *SPE Reservoir Engineering*, 8.

Chuoke, R.L., van Meurs, P. & van der Poel, C., 1959. The instability of slow, immiscible, viscous liquid-liquid displacements in permeable media. *Petroleum Transactions, AIME*, 216, pp.188–194.

Civan, F. & Donaldson, E.C., 1989. Relative Permeability From Unsteady-State Displacements With Capillary Pressure Included. *SPE Formation Evaluation*, 53(9), pp.1689–1699.

Civan, F. & Donaldson, E.C., 1987. Relative Permeability From Unsteady-State Displacements: An Analytical Interpretation. *SPE Production Operations Symposium, 8-10 March, Oklahoma City, Oklahoma*.

Claridge, E.L., 1972. Discussion of the Use of Capillary Tube Networks in Reservoir Performance Studies. *SPE Journal*, 53, pp.352–361.

Coskuner, G. & Bentsen, R.G., 1985. An Experimental Study of a New Approach to Instability Theory in Porous Media. *36th Annual Technical Meeting, Pet. Soc. of CIM*, 85(36), p.3.

Craig, F.. et al., 1957. A Laboratory Study of Gravity Segregation in Frontal Drives. In *Aime*. pp. 275–282.

Craig, F.F., 1993. *The Reservoir Engineering Aspects Of Waterflooding*, SPE Monograph Series Vol. 3.

Cuthiell, D. et al., 2001. Investigation of the Vapex Process Using CT Scanning and Numerical Simulation. , 42(2), pp.41–49.

Cuthiell, D. et al., 2006. Viscous fingering effects in solvent displacement of heavy oil. *Journal of Canadian Petroleum Technology*, 45(7), pp.29–38.

Dake, L.P., 1978. *Fundamentals of Reservoir Engineering*, Elsevier.

Dake, L.P., 2008. Fundamentals of Reservoir Engineering. *Environmental science technology*, 42, pp.2742–7.

Dandekar, A.Y., 2013. *Petroleum Reservoir Rock and Fluid Properties, Second Edition*, CRC Press.

Deng, L., King, M.J. & Texas, a, 2015. Capillary Corrections to Buckley-Leverett Flow. , (September), pp.28–30.

Djabbarov, S. et al., 2016. Experimental and Numerical Studies of First Contact Miscible Injection in a. , (Christensen 2001).

Dominguez, G.C. & V, F.S., 1992. *Carbonate Reservoir Characterization: A Geologic-Engineering Analysis, Part 1*, Elsevier.

Dou, Z. & Zhou, Z.-F., 2013. Numerical study of non-uniqueness of the factors influencing relative permeability in heterogeneous porous media by lattice Boltzmann method. *International Journal of Heat and Fluid Flow*, 42, pp.23–32.

Drazin, P. & Crepeau, J., 2003. Introduction to Hydrodynamic Stability. *Applied Mechanics Reviews*, 56(3), p.B43.

Engelberts, W.F. & Klinkenberg, L.J., 1951. Laboratory Experiments on the Displacement of Oil by Water From Packs of Granular Material. *Proceedings 3rd W.P.C., Section II*.

Firoozabadi, a. & Aziz, K., 1991. Relative Permeabilities From Centrifuge Data. *The Journal of Canadian Petroleum Technology*, 30(5).

Funk, E.E., 1956. Effect of Production Restrictions on Water-flood Recovery. *Presented at the API Meeeting, Wichita, Kan.*

Hagoort, J., 1974. Displacement Stability of Water Drives in Water-Wet Connate-Water-Bearing Reservoirs. *Society of Petroleum Engineers Journal*, 14(1), pp.63–74.

Hele-Shaw, H.J.S., 1898. The flow of water. *Nature*, 58(34).

Hill, S., 1952. Channeling in packed columns. *Chem. Eng. Sci.*, 1(6), pp.247–253.

Ho, C.K. & Webb, S.W., 2006. *Gas Transport in Porous Media*, Springer Science & Business Media.

Homsy, G.M., 1987. Viscous Fingering in Porous Media. *Annual Review of Fluid Mechanics*, 19(1), pp.271–311.

Honarpour, M., Koederitz, L. & Harvey, a H., 1986. *Relative Permeability of Reservoirs Petroleum*,

Johnson, E.F., Bossler, D.P. & Naumann, V.O., 1959. Calculation of relative permeability from Displacement Experiments. *Petroleum Transactions, AIME*, pp.370–372.

Jones, S.C. & Roszelle, W.O., 1978. Graphical Techniques for Determining Relative Permeability From Displacement Experiments. *Journal of Petroleum Technology*, 30(5), pp.1–11.

Juanes, R. & Blunt, M.J., 2006. Analytical solutions to multiphase first-contact miscible models with viscous fingering. *Transport in Porous Media*, 64(3), pp.339–373.

Kerig, P.D. & Watson, a. T., 1986. Relative-Permeability Estimation From Displacement Experiments: An Error Analysis. *SPE Reservoir Engineering*, 1(March), pp.175–182.

Koval, E.J., 1963. A Method for Predicting the Performance of Unstable Miscible Displacement in Heterogeneous Media. *Society of Petroleum Engineers Journal*, 3(2), pp.145–154.

Kumar, M. et al., 2008. High-Mobility-Ratio Waterflood Performance Prediction: Challenges and New Insights. *SPE Reservoir Evaluation & Engineering*, 11(1), pp.5–6.

Li, H., Maini, B. & Azaiez, J., 2006. Experimental and Numerical Analysis of the Viscous Fingering Instability of Shear-Thinning Fluids. , 84(February), pp.52–62.

Li, K., Shen, P. & Qing, T., 1994. A New Method for Calculating Oil-Water Relative Permeabilities with Consideration of Capillary Pressure. *Institute of Petroleum*, (2), pp.46–52.

Lucia, F.J., 2007. *Carbonate Reservoir Characterization: An Integrated Approach*, Springer Science & Business Media.

Maher, J. V., 1985. Development of Viscous Fingering Patterns. *Physical Review Letters*, 54(14), pp.1498–1501.

Maini, B., Coskuner, G. & Jha, K., 1990. A comparison of steady-state and unsteady-state relative permeabilities of viscous oil and water in Ottawa sand. *Journal of Canadian Petroleum Technology*, 29(2), pp.72–77.

Malhotra, S., Sharma, M.M. & Lehman, E.R., 2015. Experimental study of the growth of mixing zone in miscible viscous fingering. *Physics of Fluids*, 27(1).

Manickam, O. & Homsy, G., 1994. Simulation of viscous fingering in miscible displacements with nonmonotonic viscosity profiles. *Physics of Fluids (1994-present)*, 95(1994), pp.95–107.

Manickam, O. & Homsy, G., 1993. Stability of miscible displacements in porous media with nonmonotonic viscosity profiles. *Physics of Fluids (1994-present)*, 1356(1993), pp.95–107.

Manickam, O. & Homsy, G.M., 1995. Fingering instabilities in vertical miscible displacement flows in porous media. *Journal of Fluid Mechanics*, 288(-1), p.75.

Van Meurs, P. & van der Poel, C., 1958. A Theoretical Description of Water-Drive Processes Involving Viscous Fingering. *Petroleum Transactions*, 213, pp.103–112.

Mohammed A. Mian, 1992. *Petroleum Engineering Handbook for the Practicing Engineer, Volume 1*, PennWell Books.

Moortgat, J., 2016. Viscous and gravitational fingering in multiphase compositional and compressible flow. *Advances in Water Resources*, 89, pp.53–66.

Outmans, H.D., 1962. Nonlinear Theory for Frontal Stability and Viscous Fingering in Porous Media. *Society of Petroleum Engineers Journal*, 2(02), pp.165–176.

Palaz, I. & Marfurt, K.J., 1997. *Carbonate Seismology*, SEG Books.

Paterson, L., 1985. Fingering with miscible fluids in a Hele Shaw cell. *Physics of Fluids*, 28(1), pp.26–30.

Pavone, D., 1992. Observations and Correlations for Immiscible Viscous-Fingering Experiments. *SPE Reservoir Engineering*, 7(2), pp.187–194.

Peaceman, D.W. & Rachford Jr, H.H., 1962. Numerical calculation of multidimensional miscible displacement. *Society of Petroleum Engineers Journal*, 2(04), pp.327–339.

Pereira, B.M.F., Shahverdi, H. & Sohrabi, M., 2014. Refinement of Relative Permeability Measurements by Accounting for Viscous Fingering in Coreflood Experiments. *SPE Annual Technical Conference and Exhibition Proceedings*.

Peters, E.J., 1994. *A Novel Approach to Modeling Unstable EOR Displacement*,

Peters, E.J., 2012. *Advanced Petrophysics: Volume 2: Dispersion, Interfacial Phenomena/Wettability, Capillarity/Capillary Pressure, Relative Permeability*, Live Oak Book Company.

Peters, E.J. & Flock, D.L., 1979. The Onset of Instability During Two-Phase Immiscible Displacement in Porous Media. *54th Annual Fall Technical Conference and Exhibition of SPE*, (April), p.11.

Rachford, H.H., 1964. Instability in Water Flooding Oil from Water -Wet Porous Media Containing Connate Water. *Society of Petroleum Engineers Journal*, 4(2), pp.133–148.

Ruith, M. & Meiburg, E., 2000. Miscible rectilinear displacements with gravity override. Part 1. Homogeneous porous medium. *J. Fluid Mech.*, 420, pp.225–257.

Saffman, P.G. & Taylor, G., 1958. The Penetration of a Fluid into a Porous Medium or Hele-Shaw Cell Containing a More Viscous Liquid. *Proceedings of the Royal Society of London. Series A, Mathematical and Physical Sciences*, 245(1242), pp.312–329.

Sarma, H.K. & Bentsen, R.G., 1987. EXPERIMENTAL VERIFICATION OF A MODIFIED INSTABILITY THEORY FOR IMMISCIBLE DISPLACEMENTS IN POROUS MEDIA. *Journal of Canadian Petroleum Technology*, 26(4), pp.88–99.

Scheidegger, a E. & Limited, I.O., 1960. General Spectral Theory For The Onset of Instabilities in Displacement Processes. *AIME*.

Scheidegger, A.E., 1960. Growth of Instabilities on Displacement Fronts in Porous Media. *The American Institute of Physics*, 3(1), pp.94–104.

Scott, E.Z. & Read, D.L., 1959. A Study of Variables in Linear Miscible Displacements. In *Regional Fall Meeting of the Los Angles Basin, San Joaquin Valley and Coastal Sections of SPE of AIM*. Pasadena, CA, USA.

Sesini, P. a, de Souza, D. a F. & Coutinho, A.L.G. a, 2010. Finite Element Simulation of Viscous Fingering in Miscible Displacements at High Mobility-Ratios. *Journal Of The Brazilian Society Of Mechanical Sciences & Engineering*, 32(3), pp.292–299.

Shahverdi, H., 2012. *Characterization of Three-phase Flow and WAG Injection in Oil Reservoirs*. Department of Petroleum Engineering Heriot-Watt University.

Sigmund, P.M. & McCaffery, F.G., 1979. An Improved Unsteady-State Procedure for Determining the Relative-Permeability Characteristics of Heterogeneous Porous Media. *Society of Petroleum Engineers Journal*, 19(1), pp.15–28.

Slobod, R.L. & Thomas, R. a., 1963. Effect of Transverse Diffusion on Fingering In Miscible-Phase Displacement. *Society of Petroleum Engineers Journal*, 3(1), pp.9–13.

Speight, J.G., 2013. *Heavy Oil Production Processes*, Gulf Professional Publishing.

Spivak, A., 1974. Gravity Segregation in Two-Phase Displacement Processes. *Society of Petroleum Engineers Journal*, 14(6), pp.619–632.

Stalkup, F.I., Lo, L.L. & Dean, R.H., 1990. Sensitivity to Gridding of Miscible Flood Predictions Made With Upstream Differenced Simulators. In *SPE/DOE Seventh Symposium on Enhanced Oil Recovery*. Tulsa, Oklahoma, pp. 59–70.

Tan, C.T. & Homsy, G.M., 1988. Simulation of nonlinear viscous fingering in miscible displacemen. *Phys. Fluids*, 6, pp.1330–1338.

Tchelepi, H. a. & Jr., F.M., 1994. Interaction of Viscous Fingering, Permeability Heterogeneity, and Gravity Segregation in Three Dimensions. *SPE Reservoir Engineering*, 9(4).

Tchelepi, H.A. & Orr Jr, F., 1994. Interaction of viscous fingering, permeability hetero- geneity and gravity segregation in three dimensions. *SPE Reservoir Engineering*, 9(4), pp.266–271.

Tsakiroglou, C.D., Avraam, D.G. & Payatakes, a. C., 2007. Transient and steady-state relative permeabilities from two-phase flow experiments in planar pore networks. *Advances in Water Resources*, 30(9), pp.1981–1992.

Vicsek, T., 1992. *Fractal Growth Phenomena*, World Scientific.

Virnovsky, A., Skjaweland, S.M. & Norge, E., 1995. Steady-State Relative Permeability Measurements Corrected for Capillary Effects. *SPE Annual Teohnioal Conferenoe & Exhibition held in Dallas, U.S.A*, (2), pp.85–95.

Welge, H.J., 1952. A simplified method for computing oil recovery by gas or water drive. *Journal of Petroleum Technology*, 4(04), pp.91–98.

Willhite, G.P., 1986. *Waterflooding, Vol. 3*, Texas: Textbook Series.

Wooding, R. a., 1969. Growth of fingers at an unstable diffusing interface in a porous medium or Hele-Shaw cell. *Journal of Fluid Mechanics*, 39(03), p.477.

Wyckoff, R.D., Botset, H.G. & Muskat, M., 1932. The Mechanics of Porous Flow Applied to Water-flooding Problems. *Trans. AIME*, (204), p.7.

Xu, J., 1997. *Interfacial wave theory of pattern formation: selection of dendritic growth and viscous fingering in Hele-Shaw Flow*,

Zimmerman, W.B. & Homsy, G.M., 1991. Nonlinear viscous fingering in miscible displacement with anisotropic dispersion. *Physics of Fluids A: Fluid Dynamics*, 3(8), p.1859.